Imagination is more important than knowledge.
—Albert Einstein

Peace of mind is a truth to heed,
Piece of rind begins with a seed.
—Marc Schostek

University of Alberta

Design and Use of Servo-Driven Actuators for Spanwise-Varying Control of a Backward-Facing Step Flow

by

Marc A. Schostek

A thesis submitted to the Faculty of Graduate Studies and Research in partial fulfillment of the requirements for the degree of **Master of Science**.

Department of Mechanical Engineering

Spring 2012
Edmonton, Alberta

Dedicated for more awesomeness,
and less selfishness in our world.
(shellfish may remain selfish if they themselves so do wish.)

Abstract

An experimental study was conducted of a forced backward-facing step water flow, and the design of 16 actuators for creating the perturbations used to force the flow. The 16 actuators allowed for variant forcing in the spanwise direction with a resolution of 0.5 times the step height h. They are capable of producing unique perturbation waveforms of forcing velocity amplitudes $0 < u'/U_\infty \leq 2$ and either single or multiple forcing Strouhal numbers in the range $0 < St_h \leq 1.0$. These forcing amplitudes are larger than ever used in any previous forced backward-facing step flow experiments. For measurement of the reattachment length in the wake of the backward-facing step, a novel hydro-tuft was designed which can indicate flow direction for local flow velocities less than 5 cm/s. A set of images taken of an array of hydro-tufts was computationally processed using a MATLAB program to calculate a time-averaged reattachment line. The effect of spanwise-invariant forcing for amplitudes $0 < u'/U_\infty \leq 2$ and forcing Strouhal numbers $0 < St_h \leq 0.5$ was investigated. The results show an optimal St_h which shifts to a lower value with increasing forcing amplitude, and a non-monotonic shortening of the reattachment length. As a function of forcing amplitude, reattachment reaches a pronounced minimum at $u'/U_\infty \approx 0.3 - 0.4$, and then rises to a peak at $u'/U_\infty \approx 0.5 - 0.6$. Any further increase in forcing amplitudes up to our maximum at $u'/U_\infty = 2$ results in more shortening. None of these behaviours have been previously noted in the literature.

Acknowledgements

Wow! This is fantastic! This work was conducted on the basis of finding truth. Truth provides fulfilment and peace to the mind. I am proud to have contributed, however slightly, toward this goal. Similarly to as Sir Isaac Newton gracefully gave forth: my work could not have been done without the support on the top of shoulders of giants. My giants have lifted me into a deeper insight and understanding of life I could never have reached on my own. They are great in number, the ones I give special thanks to are only a handful of them.

First to the VfDL staff. My adviser, Dr. Lorenz Sigurdson, who allowed my mind to roam free and allowed me to come to my own conclusions instead of constraining my process. To a premature student this can at times seem unnecessarily difficult: why doesn't he just give me the answer? However, it turns out this promotes exponential gain in wisdom for all. Thanks man. As well to Andrew Coward, Dory Parsonage, Stuart Gilbert, David Breakey, and Aaron Baugh for their invaluable contributions to the cause.

To my family. Like my adviser, they are advocates of the "let him roam" paradigm of learning. Without the support of my parents I would never had the opportunity to be here. My brother Kevin, whose out of the box thinking rubs off on me. My brother David, who enlightens with his philosophical knowing. Cassandra for her love and beauty, and to Dede and Nightly who gave me company while I was writing.

From the Mechanical Engineering department staff, over and over again I received their acceptant support. Bernie Falkner with his expertise, excitement and wonderful stories. Tuula Hilvo who would run six flights of stairs just to help me unlock a door. Rick Conrad for sharing 130% of his electronics lab and time. Andrew Campbell, David Waege, Daniel Mooney, Rick Bubenko, and Roger Marchand for their support in the shop.

An honourable mention goes out to many others. The Florence brothers who trained me from a young age to become one with the eagle. The Pittmans for their friendship and wisdom over the years. As well to four lifelong friends gained over my years at the UofA of unmistakable character. Dylan and Kayle who both share the same taste for crazy shenanigans as I. And Gillian and Aaron who taught me to think, drink, and stink like a Grad Student. All my giants have made my life an order of magnitude more enjoyable. Thank you all!

Contents

List of Tables

List of Figures

Chapter 1

Introduction

The complex nature of separating and reattaching shear flows has been a forefront subject of fundamental fluid dynamic research for over half a century. There exists a vast amount of geometries which give rise to flows forming an assemblage of separating and reattaching shear flows. A prominent geometry, and the one to be currently studied, is the flow in the wake of a backward-facing step (BFS). Its applications span many engineering fields: control of the flow over a stalled airfoil, increasing diffuser efficiency, reducing drag, or increasing mixing within a combustion chamber or chemical reactor. The backward-facing step is prominent for studying this type of flow because of its simple geometry with a well defined separation point. This helps reduce ambiguity between independent experiments, promoting collaboration of work between researchers.

This work was performed in the Vortex Fluid Dynamics lab of Professor Lorenz Sigurdson at the University of Alberta, Mechanical Engineering building. Professor Sigurdson has an abundance of experience with separating and reattaching flows. In the past he has largely dealt with forward-facing step configurations. Sigurdson and Roshko (1984) discussed and published an abstract about three-dimensional structures within reattaching flows for a forward-facing step flow along the blunt leading edge of a plate. They observed the initial free-shear layer structures to be primarily two-dimensional which evolved into three-dimensional structures as they neared reattachment. In 1985 Sigurdson and Roshko published a paper on the effect of a periodic velocity perturbation on the flow over a blunt faced cylinder aligned coaxially with the free stream. They observed that the velocity perturbations increased entrainment in the early part of the free shear layer, resulting in shorter reattachment lengths. Further work was carried out by Sigurdson (1986) for his PhD thesis on this flow and then refined in his 1995 paper.

These previous experiments examined the effect of forcing uniformly along the axis of separation. Because the flow is known to be three-dimensional, the long term

research question is whether variant forcing along the axis of separation will improve the control of a separating and reattaching flow. This was the inspiration for the present research program. The transition to the study of a backward-facing step flow was largely due to a numerical BFS study performed by Kang and Choi (2002), and that a water tunnel facility existed in the Mechanical Engineering building which was well suited for a BFS flow. Kang's and Choi's BFS numerical study examined the effect of spanwise-varying actuation. The current apparatus is intended to provide a physical manifestation of Kang's and Choi's study to which results can be compared.

After the recommission of the water tunnel by Professor Sigurdson and Andrew Coward (2004), design of the BFS apparatus was underway. Stuart Gilbert designed the step insert which would be positioned inside the water tunnel test section. Gilbert had also begun work on designing the prototype actuator used for creating the velocity perturbations needed for the experiment. Aaron Baugh (2010) then refined their design and constructed the actuators and used them in experiment. Throughout their use, faults in their performance arose. This led up to the current study, where the flow actuators were redesigned to improve performance and then used in further experiment.

1.1 Literature Review on the Forced Backward-Facing Step Flow

The reattachment length is one of the most commonly used measurements for describing the characteristics of the flow. It has become an index representing mixing behind the backward-facing step (Kang & Choi 2002) and pressure loss across the step region. The instantaneous reattachment line is defined by the line of zero wall shear stress, given by equation 1.1 for an isotropic, incompressible flow (Henning & King 2007). This occurs only when $\frac{\partial u}{\partial y}|_{y=0}$ is equal to zero, which is satisfied in the case of stagnation.

$$\text{Instantaneous Reattachment} \equiv \mu \frac{\partial u}{\partial y}\Big|_{y=0} = 0 \tag{1.1}$$

Many researchers have observed that the instantaneous reattachment line fluctuates with time (e.g., Eaton & Johnston). For this reason, the time-averaged reattachment line is often reported and used as the index of the flow. Eaton and Johnston (1980) defined a time-averaged reattachment location measurement as the point at which the flow, close to the wall along which reattachment occurs, fluctuates between upstream and downstream direction 50% of the time. This statement is only valid if the reattachment line distribution forms a symmetrical distribution.

Eaton and Johnston showed that this is true and used the 50% method for all their reattachment location measurements.

Methods used to control reattachment length can be broken down into two main categories; passive control and active control. Passive control methods are those where no energy is input into the flow from an external source. It usually involves modifying geometry for the purpose of perturbing the separating boundary layer. Examples of passive methods used on a backward facing step are using a tripping wire and cavity (Isomoto & Honami 1989), and positioning vortex generating tabs upstream of the step (Westphal, Johnston & Eaton 1984).

Active control of the reattaching flow involves energy input from an external source. The input energy is in the form of a perturbation. Introducing perturbations into the flow is often called "forcing" the flow in the literature. Active control can be further broken into two sub-groups, open loop and closed loop. Open loop control uses a predefined flow actuation which remains constant throughout an experiment. Whereas closed loop control uses feedback; the effect of input actuation on the flow is measured and processed to determine how to modify actuation for optimizing the measured flow characteristic. Open loop control is more commonly used because it is reduces the complexity of the experiment, making it easier to use. Common methods used for active control are inputting sound energy (e.g., Battecharjee, Scheelke & Troutt 1986; Kim, Choi & Yoo 2007; Hasan 1992; Yoshioka, Obi & Masuda 2001), perturbing the flow using a flap mechanism (e.g., Roos & Kegelman 1986, Lai; Yue, Platzer 2002), or using suction/blowing type actuation (e.g., Chun & Sung 1998; Sakakibara & Anzai 2001). Suction/blowing and sound energy type actuations are similar in nature. Suction/blowing refers to actuation produced for an experiment in water where the actuation frequencies tend to be low, allowing the individual actuation cycle to be observable by human perception. Whereas the actuation frequencies tend to be much higher in air. This gives rise to the distinction of *suction/blowing* and *sound energy* actuation.

In most actively controlled backward-facing step experiments, perturbations are introduced into the boundary layer just before or at separation. This location is often chosen since it has been shown by many that the status of incoming boundary layer has a significant influence on the evolution of shear layers (e.g., Oster & Wygnanski 1982; Eaton & Johnston 1980). There are a few exceptions such as Uruba, Jonáš, and Mazur (2007) who used suction/blowing type actuation at the step base, and Lai, Yue, and Platzer (2002) who used a flapping foil within the recirculation zone.

Early belief was that the flow behind a backward-facing step was of two-dimensional nature and many experiments addressed a centre-plane reattachment (Yanase, Kawahara,& Kiyama 2001). However, it is now well known that the backward-facing step flow is in fact strongly three-dimensional (3D) (Yanase et al. 2001). Armaly, Durst,

Pereira, & Schönung (1983) observed that the flow for BFS exhibited strong 3D nature using laser-Doppler measurements. As well, Sigurdson and Roshko (1984) observed three-dimensional structures within reattaching flows for a forward-facing step flow over a plate with a square leading edge. Thus it is becoming of more interest the effect of spanwise-varying forcing on the BFS flow to determine whether it interacts differently with the 3D aspects of the flow. Some examples of spanwise varying forcing are Chun & Sung (1999) and Henning & King (2007). Chun & Sung produced their spanwise variance by periodically blocking the port from which their perturbation would issue. This method of would allow the forcing to be either on or off at a particular spanwise location. Henning & King took this another step further and divided their spanwise forcing into four regions of 4.5 times their step height in width. This allowed them to create unique forcing waveforms for each of the four spanwise sections. The current experiment is designed to give a even higher spanwise resolution using sixteen individual actuators to give a spanwise resolution of 0.5 times our step height.

In deciding which frequencies with which to perturb the flow, understanding of the instabilities within the flow is helpful. For wall-free shear flows, it is now well known that the shear layer grows by successive pairings of spanwise vortical structures (Brown & Roshko 1974; Winant & Brown 1974), in which the process is initiated by the Kelvin-Helmholtz instability. This behaviour has also been witnessed as the pairing of shear layer vortices in a backward-facing step flow (Eaton & Jonston 1980; Roos & Kegelman 1986), and for a forward-facing step flow (Sigurdson & Roshko 1985; Sigurdson 1995). Thus, forcing the flow at frequencies comparable with the Kelvin-Helmholtz frequency inherent of the unperturbed flow is a good starting point.

Besides the Kelvin-Helmholtz instability, there has been reported in the literature of reattaching shear flows a second mode of instability. This second mode of instability has been observed by Sigurdson and Roshko (1985), and Sigurdson (1986; 1995) for forward-facing step flows, and later by Hasan (1992) for backward-facing step flows. It is often referred to as *shedding-type* or *step-mode* instability. It is analogous to the Kármán vortex shedding instability in the wake of a bluff body and "preferred frequency" in the early axisymmetric jet, and consists of the interaction of the vortices and their images due to the presence of the wall (Sigurdson 1995). In backward-facing step flow, the two modes of instability are commonly referred to as the *shear-layer* and *step* modes. The former refers to the Kelvin-Helmholtz instability, and the later the shedding instability.

When referring to the frequencies of these instabilities, a nondimensional frequency, the Strouhal number, is often used. For the shear-layer mode the Strouhal number is nondimensionalized using the momentum thickness of the separating

Table 1.1: *Optimum Strouhal numbers from various authors. A comparison of St_θ with St_h.*

Author	$\boldsymbol{St_\theta}$	$\boldsymbol{St_h}$
Roos & Kegelman 1986	n/a [1]	0.22
Battacharjee et al. 1986	n/a	0.2-0.4
Hasan 1992	0.012	0.185
Chun & Sung 1996	0.009-0.011	0.25-0.275
Yoshioka et al. 1999	n/a	0.18-0.22
Henning & King 2007	0.017	0.3

[1]Author does not present Strouhal number scaled with δ_θ

boundary layer (δ_θ) and a reference velocity often equal to the free-stream velocity (U_∞), $St_\theta = \frac{f\delta_\theta}{U_\infty}$. The step-mode is correspondingly nondimensionalized using the step height and free-stream velocity, $St_h = \frac{fh}{U_\infty}$. One of the objectives of many forced backward-facing step experiments is to discover the optimal forcing frequency at which the reattachment length is reduced by the most. Table 1.1 lists some of the optimal Strouhal numbers discovered by various authors.

There has historically been disagreement between authors as to which mode is of instability is more correct. Kim, Choi, & Yoo (2007) found instabilities in the shear layer behind a backward-facing step corresponding with $St_\theta = 0.011 - 0.013$ and $St_h = 0.48 - 0.77$. From these results Kim et al. concluded that natural instability scaled better with momentum thickness than with step height. It was not explicitly stated why they concluded such, but it can be presumed that it was due to the smaller absolute difference between the St_θ limits relative to the St_h limits. It is an unfair comparison to use absolute values, as St_θ is scaled with the momentum thickness, which is often smaller than step height, and in their particular experiment 60 times smaller than the step height. If one compares the percent difference of two frequency limits with respect to the mean value, the difference for St_h is 5% less than for St_θ.

It is believed in the present study that there is no one mode of instability which scales better for the backward-facing step flow, but that the two always exist. Which one of the two is dominant is of question. It could be that the dominance of the two modes is a function of the non-dimensional ratio of boundary layer momentum thickness and step height $\frac{\delta_\theta}{h}$. If the momentum thickness is larger than the step height, the shear-layer mode would be more dominant and vice versa.

Another important forcing characteristic is perturbation amplitude. In the literature, there has not been as much research on the influence of perturbation am-

Table 1.2: *Forcing amplitudes used by various authors. u'/U_∞ is the ratio of peak perturbation velocity amplitude to the free-stream velocity. If no range is given for excitation amplitude, author kept amplitude constant throughout experiments.*

Author	**Forcing Amplitude**
Kim et al. 2007	$u'/U_\infty = 0.04$
Hasan 1992	$u'/U_\infty \approx 0.025$
Henning & King 2007	$u'/U_\infty \approx 0 - 0.14$
Yoshioka et al. 2001	$u'/U_\infty \approx 0.3$
Chun & Sung 1996[1]	$u'/U_\infty \approx 0.04 - 0.1$

[1]Perturbation amplitudes of Chun & Sung converted to u'/U_∞ form. See page 93

plitude on the flow as there has been for perturbation frequency. Table 1.2 presents forcing amplitudes used by various authors. Henning & King examined the effect of perturbation amplitude on reattachment length for their optimal $St_h = 0.3$. They observed a monotonic reduction in time-averaged reattachment length for increasing perturbation amplitude with a maximum reduction at their largest amplitude $u'/U_\infty = 0.14$. The highest observed sensitivity of reattachment length as a function of amplitude was in the range of $0 \leq u'/U_\infty \leq 0.05$, and for $u'/U_\infty > 0.05$ little further reduction in reattachment length was achieved. Yoshioka et al. (2001) found that the effect of perturbation increased linearly to the amplitude up to 30% of U_∞, and saturated for larger amplitudes.

1.2 Objectives and Layout of Thesis

The present study has two main foci: the design of a flow actuator which is capable of large amplitude actuation and variation of the actuation in the spanwise direction, and a more in-depth investigation on the effect of forcing amplitude on the BFS flow compared with previous BFS experiments in the literature. The purpose for spanwise-varying actuation is to determine whether it interacts differently with the three-dimensional aspects of the BFS flow than conventional spanwise-invariant forcing, as it is expected that the flow in the wake of the BFS has strong three-dimensional nature.

Although the design of the flow actuator allows for spanwise varying actuation, all of the experiments of the current study used spanwise-invariant forcing. It is intended that future work using the apparatus will delve into the realm of spanwise-variant forcing.

Due to the diversity between the actuator design and the experimental study, this thesis has been divided into two parts. The first part gives description of the

actuator. It starts off with the objectives for creating such a versatile actuator. Detail on the actuator design and performance will be given. Part II begins with the objectives of the current experiments and a detailed theoretical analysis of the boundary layer properties at the point of separation. It then focuses on the experimental setup, methodology, and results for the forced BFS experiments performed.

Part I

Design of Servo-Driven Actuators for Flow Control

Chapter 2

Part I Objectives and Overview

Flow control was initiated by introducing velocity fluctuations (perturbations) into the separating flow near the step edge. In the literature, the introduction of velocity fluctuations into the flow has also been called "forcing" the flow. The introduced forcing reacts with the flow to enhance shear layer entrainment, altering reattachment length and mixing in the wake of the backward-facing step.

For the purpose of controlling the flow behind a backward-facing step in water, the design of servo-driven actuators will be discussed. One of the main design criterion was the ability to vary the perturbations along the span of our backward-facing step. This was of importance as there is an increasing interest of the effect of spanwise variance in the actuation on the BFS flow. An example of a computational study on the effect of spanwise variance is the work of Kang and Choi (2002). They observed an optimal spanwise sinusoidal wavelength for reducing reattachment of four times the step height. More experimental works are required to support the computational findings, which is the intent of the current actuator design.

Two actuator designs will be discussed; the Alpha actuator and Beta actuator. The Alpha design was the original design of Stuart Gilbert (2007), and refined, constructed, and used in experiment by Aaron Baugh (2010). Stuart Gilbert's design was based on a similar design used by Sakakibara and Anzai (2001) for their experiment of a plane laminar jet in water with introduced suction-blowing type perturbations. Their perturbations, like ours, were created using computer controlled servo-motors which each would drive one of sixteen glass syringe plungers. This motion of the syringe plunger would displace water creating the desired perturbation. This allowed for variance of perturbations in the spanwise direction. The conjoined actuator design of Gilbert and Baugh allowed for excellent spanwise resolution and could produce unique perturbations at each spanwise location. However, through experimental use by Baugh (2010), and the current investigation, flaws have been revealed through a lack of performance of the initial Alpha design. It is essential for

a well posed experiment that the actuators are performing as expected and creating the desired velocity fluctuations. This led to the current detailed investigation of the actuator performance, areas lacking performance, and modifications which have come about to improve performance resulting in the Beta actuator.

The following chapter begins Part I with a review of pulse width modulation reference signal controlled servomotor operation. This chapter is intended to update the reader on PWM signal theory and how it is used for servomotor control. The main matter for Part I starts with a description of the Alpha actuator. For a more detailed description see Gilbert (2007) and Baugh (2010). Next the performance of the Alpha actuator is discussed. An objective of the performance analysis is to determine at which actuation cases the Alpha actuator performed its best. This will help determine limits for which the experimental results of Baugh (2010) have the least errors due to actuation error. Another objective of the performance analysis is to gain insight into the areas needing improvement. The Alpha performance analysis is followed with the improvements made resulting in the Beta actuator design, and its performance analysis. Then a comparison of the Alpha and Beta performance, outlining the areas of most improvement.

Chapter 3

Review of Pulse Width Modulation Controlled Servomotor Operation

This chapter gives a review of servomotor theory. It is meant to be a brief description on the operation principals of pule-width modulation (PWM) signal controlled servomotors. If the reader has an understanding of this topic, this chapter may be skipped.

All actively controlled servomotors require a reference signal which is read to determine the desired servo position. This reference signal is compared with a feedback signal from a feedback sensor to determine if the servomotor is correctly positioned or needs adjustment. The servomotors used for the actuators, discussed here, read a PWM signal as the reference signal. To understand the operation of a PWM signal controlled servomotor, an understanding PWM signals is required.

Pulse-width modulation refers to modulation of the pulse duration in a signal of rectangular waveform. The signal could be either of current or voltage. Voltage signals are more commonly used and are what is used for servomotor control. Figure 3.1 on the following page shows a PWM signal of high signal period T_{ON} and low signal period of T_{OFF}. An important characteristic of PWM is that the high and low signal levels are constant and switching of signal level is performed between these levels only. The period of a given cycle, T_{CYCLE}, is the sum of both high and low times within that cycle. Commonly T_{CYCLE} is kept constant and the *duty cycle* of the signal is varied by controlling the T_{ON} time. Thus, T_{OFF} is the remainder of T_{CYCLE} after T_{ON} has elapsed. This scheme defines T_{ON} and T_{CYCLE} the controlled variables of the waveform.

The PWM signal read by the servomotors discussed here has high and low signal levels of five and zero volts, respectively. T_{CYCLE} is kept constant and T_{ON} is varied to give the desired position information the servo requires. Each rising slope

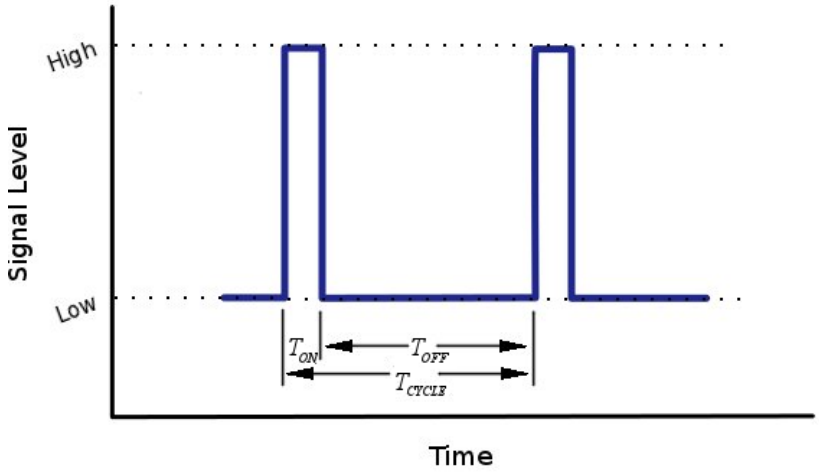

Figure 3.1: *Description of a pulse-width modulation signal: signal level can be either the signal current or voltage. Each cycle is comprised of a high and low portion of durations T_{ON} and T_{OFF}.*

is interpreted as a new data event by the servo, which triggers measurement of the duration, T_{ON}. This duration is interpreted as a positional value to be compared with the positional value from the feedback sensor. Any difference between these two signals creates an error signal. The servo attempts to minimize this error signal by adjusting the position of the servo output. With each new high pulse, a new T_{ON} is read and servo output adjusted for accordingly.

Among PWM controlled servomotors there is an accepted range for T_{ON} durations for reasons of compatibility. A T_{ON} duration of 1500 microseconds corresponds with the centre position of the servo output. A deviation from this T_{ON} value, within limit, will result in a positioning of the servo to either side of the centre position. The limits of motion are commonly between 1000 and 2000 microseconds, however these vary between manufacturers and servo models. For example, digital servomotors from a leading manufacturer, Hitec RCD USA Inc., use the pulse duration limits of 900-2100 microseconds.

The last variable of the PWM signal is T_{CYCLE}. This period determines the frequency of pulses in the signal. The shorter T_{CYCLE}, the quicker the pulse frequency; which corresponds with a higher temporal resolution of the reference signal. The frequency at which pulses are delivered is known as the frame rate of the reference signal.

A commonly used value for T_{CYCLE} is 20 milliseconds, which corresponds with a frame rate of 50 Hz. This rate is often used since for the vast applications of PWM controlled servomotors it creates a reference signal of sufficiently high temporal resolution. When quick response of the servomotor is required, the frame rate can

be limiting if not quick enough. Thus some servomotors are capable of accepting higher rates to mitigate these restrictions.

Now with this basis of understanding of servomotor operation and PWM signal theory, the discussion can be continued on the performance of the actuators.

Chapter 4

Performance Characterization

Performance of the actuators was based on their ability to produce the desired sinusoidal waveform, and the uniformity of actuation from one to another. The actuators' performance was analyzed both quantitatively and qualitatively. Qualitative analysis of actuator motion was carried out by review of plots created using a Linear Variable Differential Transformer (LVDT) for measurement of the actuator motion. Quantitative analysis was performed on this LVDT measured actuator output data using three methods: a percent Total Harmonic Distortion (% THD) based upon amplitudes as shown in Equation 4.1, normalized actuation amplitude ($\bar{A}$) shown in Equation 4.2, and their performance relative to one another measured as normalized absolute deviation ($\bar{D}_i$), Equation 4.4

$$\%THD = 100 \times \frac{\sqrt{\alpha_2^2 + \alpha_3^2 + \cdots + \alpha_n^2}}{\alpha_1} \tag{4.1}$$

$$\bar{A} = \frac{A_{\text{mean}}}{A_{\text{theor}}} \tag{4.2}$$

$$A_{\text{theor}} = C_{\text{amp}} A_{\text{RS}} \tag{4.3}$$

$$\bar{D}_i = \frac{|A_{\text{CumulativeMean}} - a_i|}{A_{\text{theor}}} \tag{4.4}$$

Where: $\alpha_1 \cdots \alpha_n$ – amplitude of the $1^{\text{st}} \cdots n^{\text{th}}$ harmonic [mm]

A_{mean} – arithmetic mean of LVDT measured actuator output amplitudes [mm]

A_{theor} – theoretical actuator output amplitude based upon calibration [mm]

C_{amp} – calibration constant [mm/μs]

A_{RS} – reference signal amplitude [μs]

$A_{\text{CumulativeMean}}$ – cumulative arithmetic mean of all LVDT measured actuator output amplitudes [mm]

a_i – i^{th} LVDT measured actuator output amplitude [mm]

Total harmonic distortion is a good measure of closeness the output waveform has to a pure sinusoid. For a pure sinusoidal signal, the measured THD would equal zero, as $\alpha_2 \cdots \alpha_n$ would all be zero. If the value is larger than zero, this indicates other frequencies are present in the output signal other than desired.

To measure if the output amplitude is of desired magnitude, a normalized actuation amplitude was used. Normalized actuation amplitude is the ratio of measured output amplitude with a theoretical amplitude. As discussed in the review of PWM controlled servomotor operation, Chapter 3, the reference signal read by the servo does not have much meaning in terms of a physical quantity. Thus, a calibration constant, C_{amp} , was calculated from a calibration of measured servo movement verses servo reference signal amplitude (PWM amplitude) to convert the reference signal amplitude into a physical value. A step motion was used for this calibration, since during a step the actuator has time to settle in the positions commanded by the reference signal. Thus, an accurate calibration can be acquired. This calibration constant was then used to calculate the theoretical actuator output amplitude for a given reference signal amplitude.

There was a slight non-linearity of the actuator output motion observed for small amplitude step motions. For step motions of reference signal approximately less than 20 μs the measured calibration constant was measured as $C_{\text{amp}} = 0.018$ mm/μs. For larger forcing amplitudes the output motion followed the reference signal linearly with a calibration constant of $C_{\text{amp}} = 0.022$ mm/μs. This can be seen in Figure 4.1 which shows the calculated calibration constant for varying step motion amplitudes in μs. Due to the non-linearity being small and for low amplitudes only, the later calibration constant is used for calculating the theoretical actuator output amplitude.

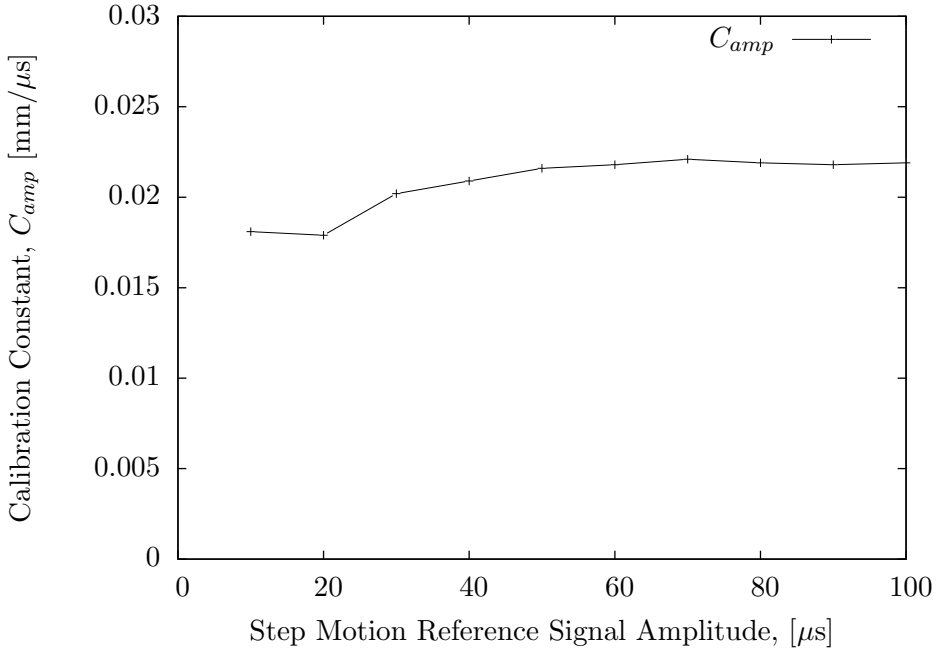

Figure 4.1: *Calibration constant (C_{amp}) as a function of varying step motion reference signal amplitudes [μs].*

The third measurement, algebraically akin to a standard deviation, is a normalized absolute deviation, $\bar{D}_i$. It is the absolute amount of difference between an actuator's output amplitude from the cumulative mean of all measured actuators. When plotted, for each actuation case (reference signal frequency and amplitude), the maximum calculated deviation, $\bar{D}_{\max}$, is used.

These three measurements, along with qualitative analysis of the output waveforms, will give insight of the actuators' performance. This will help with deciding which areas of the actuators are of need of improvement, which will be discussed in following sections.

Chapter 5

Actuator Board Alpha

The initial actuator board based on Stuart Gilbert's (2007) prototype design was constructed and further refined by MSc student Aaron Baugh (2010). Baugh was the first to use this actuator board for his experimental research which will be discussed in Part II of this thesis. Here only select details of his constructed actuator will be discussed as they pertain to the performance. More in depth details on his construction can be found in his Masters Thesis (Baugh 2010).

The actuator board originally consisted of 22 actuators spaced approximately 4 inches apart on a 3/4 inch thick plywood sheet. Each actuator used a Hitec hobby HS-225MG servomotor to control the motion of a syringe plunger via a mechanical connection.

An overview of actuator board Alpha can be seen in Figure 5.1 on the next page. It depicts the basic components which will be further discussed in more detail in the following sections.

5.1 Electrical Connections

The servomotors were powered by a Kepo JQE 6-22M DC variable power supply with a max current output of 22 Amps. The power was routed in parallel to each of the servomotors by a single pair of 18 AWG (American Wire Gauge) wire. As can be seen in Figure 5.2, at the location of each servomotor the power was spliced from the main power line to the motor using crimp connectors. All power connections were elevated above the actuator board using a rail system to prevent short circuiting in the event of a water leak.

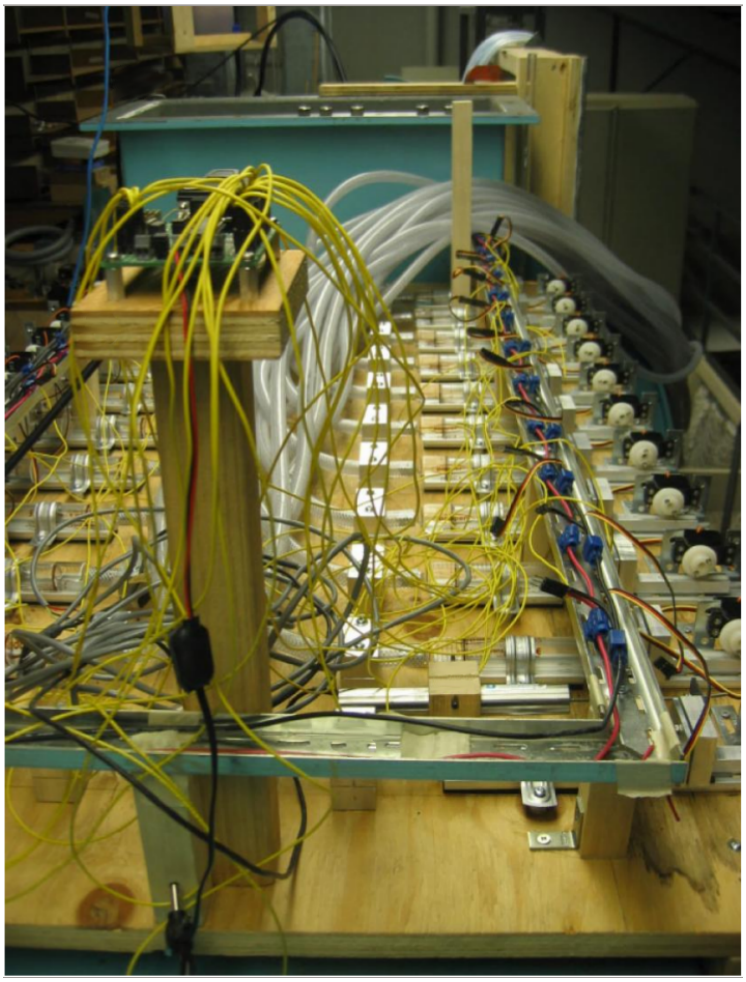

Figure 5.1: *Overview of actuator Alpha as used by Baugh (2010). Shows the entire actuator board positioned on top of the water tunnel. Image reproduced with permission from A. Baugh.*

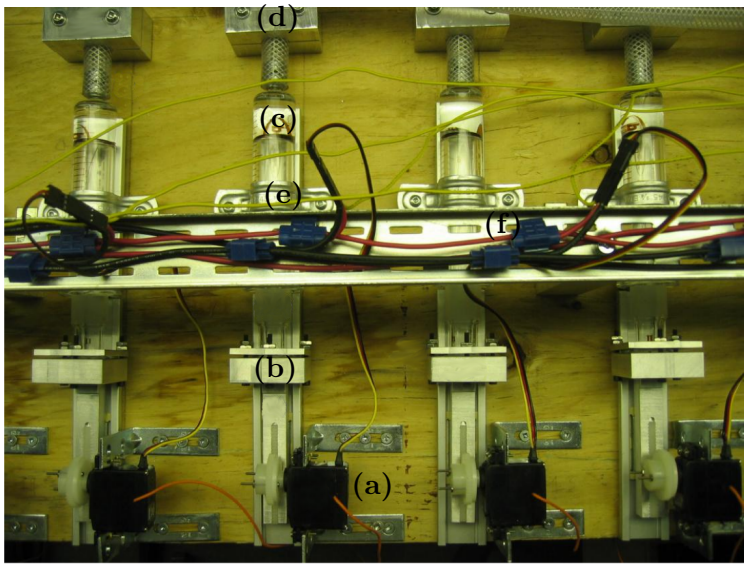

Figure 5.2: *close up view of actuator Alpha. The labelled items are: HS-225MG servo motor mounted above slider(a), plate mounting system to hold plunger at end of rack (b), syringe barrel (c), Baugh fabricated tube clamp(d), conduit clamp(e), power and reference signal routing (f). Image reproduced with permission from A. Baugh.*

5.2 Reference Signals

Each of the 22 actuators were designed to receive a unique reference signal, so each actuator could output a unique actuation waveform. This was achieved by using a National Instrument LabVIEW program developed by Baugh running on a PC which would send formatted ASCII instruction packets at 20 ms intervals to a Lynxmotion SSC-32 servo controller. The LabVIEW generated instructions were created by sampling at 20 ms intervals a sinusoidal waveform of a unique amplitude, frequency, and phase for each actuator. This data would be compiled into the ASCII packets to be sent to the Lynxmotion controller. The Lynxmotion servo controller would convert the instructions sent from LabVIEW into 22 unique PWM reference signals, which would in turn be read by the servomotors. The final result being a sinusoidal motion of the actuators. Figure 5.3 shows a block diagram of this process.

5.3 Mechanical Connections

The servomotor output motion was transferred to the syringe plunger using a rack and pinion force transmission system. A pinion mounted on the output of servo meshed with a rack. The rack was mounted on top a low friction PTFE slider which was intended to restrict the motion of the rack in line with the central axis of the syringe. At the end of the rack, a plate mounting system secured the plunger onto

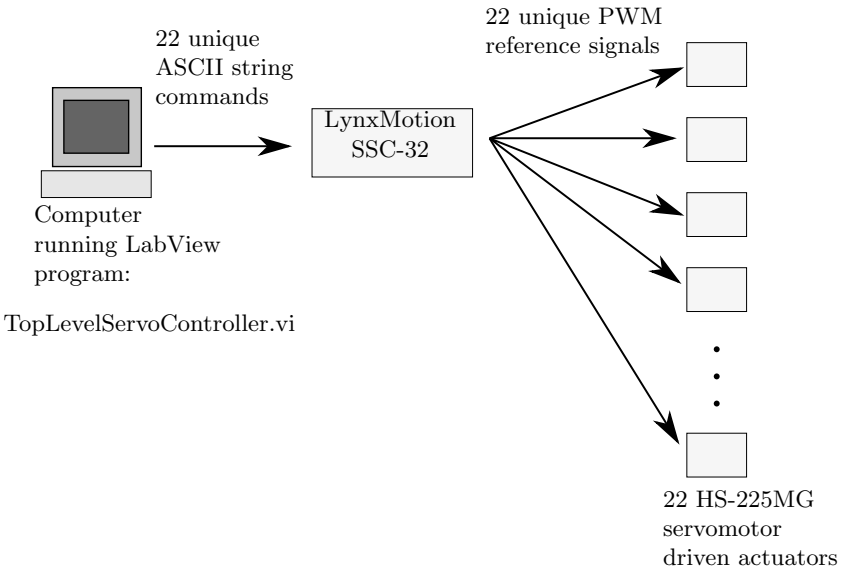

Figure 5.3: *Block diagram showing Alpha reference signal generation.*

the rack to couple their motion. This allowed the servomotor to push and pull on the syringe plunger giving the blowing-suction type actuation desired. Referring to Figure 5.2 on the preceding page, the servomotors were mounted above the slider using two steel L-mounting brackets. They are suspended such to allow proper meshing of the pinion and rack.

The syringe barrels were securely fixed to the plywood board inline with the sliders. Mounting of the barrels was done using conduit clamps around their mid-length and fabricated tube clamps holding the tubes fitted over their lure locks. Thus, as the servo would move the rack, the plunger would displace water within the syringe barrel.

Chapter 6

Actuator Alpha Performance

6.1 LVDT Output Measurement: Actuator Alpha

Figure 6.1, page 22, shows the measured output plots for actuator Alpha created from a LVDT sampling the movement of the actuator output. Specifics on LVDT measurement can be seen in Appendix C. The LVDT signal was converted to a digital signal using a National Instrument USB-6229 Multifunction Data Acquisition Module (DAQ) sampling at a 2 kHz rate. Before digital conversion, the LVDT signal was filtered using an analog 2nd order passive RC filter with a cutoff frequency of 200 Hz. This would help prevent aliasing of unwanted higher frequencies cause by noise. For each case the servomotors were driven by a reference signal of one hertz sinusoidal waveform with PWM amplitudes of 10, 50, and 100 microseconds. The actuators were capable of producing actuation amplitudes larger than this. However, for the purpose of performance measurement, 100 μs was used as the maximum amplitude tested.

Before analyzing their performance using the more quantitative measurements, let us examine these plots. In Figure 6.1(a) the reference signal amplitude is of 10 μs, this corresponds to desired actuator displacement amplitude of 0.22 mm. From the plot it is difficult to discern an output amplitude due to the poor performance resulting in a non-periodic motion. If one measures from the highest point to lowest point of the motion during the 20 s period of the Figure, an amplitude of 0.12 mm is observed; half of the desired amplitude. Figure 6.1(b) shows an improvement in tracking of the control signal which is apparent from the more periodic motion of the actuator. The desired amplitude for this waveform is 1.1 mm which is still larger then the actuator output. Figure 6.1(c) shows the best performance of the three. The desired amplitude for this waveform is 2.2 mm, the output is again shy of this amplitude.

One can also observe that at the peaks of the actuator output, the waveform

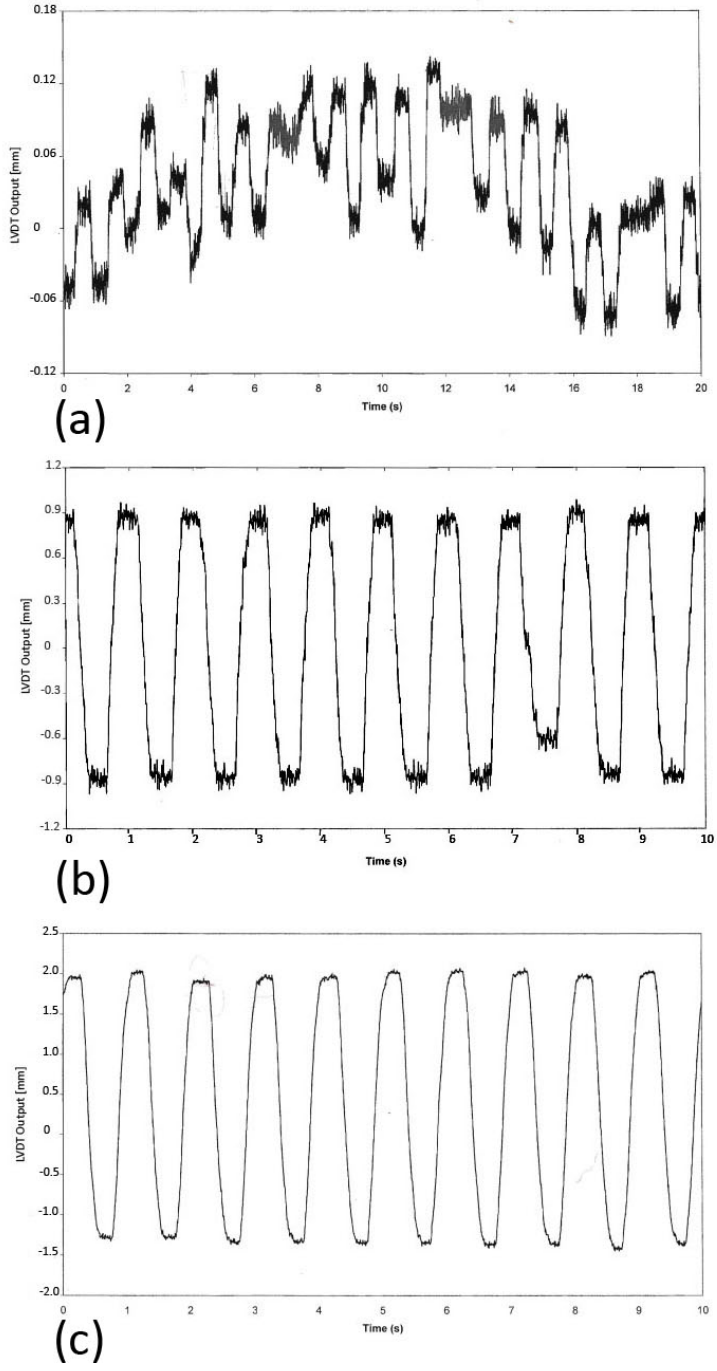

Figure 6.1: *LVDT output from actuator Alpha performance measurement. Each reference signal is of a sinusoidal waveform for PWM amplitudes 10 μs (a), 50 μs (b), and 100 μs (c). NOTE: 20 second period for Figure (a), and 10 second period for figures (b), and (c).*

appears more flat than a sinusoidal waveform should be. This flatness could be attributed to "sticking" of the actuator due to insufficient torque to fulfil the small motion near the peaks. Another contributor to the flatness could be due to the selection of an improper servomotor feedback location. The feedback location for actuator Alpha is internal to the servomotor; a radial potentiometer measures the angular position of the servomotor's output which is directly connected with the pinion. This feedback measurement is meant to emulate the motion of the actuator at the syringe plunger. Any form of mechanical error in the coupling between pinion to plunger will cause an error in the feedback measurement and actuator output. Sources of mechanical error can be backlash in the meshing of pinion and rack and deformation of any of the structural components.

6.2 Quantitative Performance Analysis: Actuator Alpha

Figures 6.2 through 6.4 Give qualitative results of the Alpha actuator performance. These results are formed from a population of 5 actuators with three measurement trials per actuator. The raw data can be viewed in Appendix A on page 111. This data was generated from LVDT measured actuator motion, similar, however not identical to, the data seen in Figure 6.1. Some improvements were made to the Alpha Actuator after recording Figure 6.1, and the data presented in Figures 6.2 to 6.4 represents the highest performance attained from the Alpha actuators.

Figure 6.2 shows a trend of improving %THD with increasing actuation amplitude ranging from 40% to 5%. This trend is in agreement with the LVDT output in Figure 6.1; at the highest amplitude forcing, the actuator output is most resembling a sinusoid out of the three cases. This %THD level is higher than desired. Ideally the %THD value should be as low as possible. During an experiment a select frequency is chosen to analyze its effect on the flow, thus other frequencies are unwanted.

Figure 6.3 shows that the actuators are not reaching the desired actuation amplitudes for any cases. There is a trend of improvement with increasing actuation amplitude. But even at the best case the actuator output amplitude is only approximately 75% of the desired amplitude.

This could be an indication that the servomotors have insufficient torque for achieving the desired amplitude, or the feedback sensor is not properly representing the motion of the plunger. The feedback is intended to give the position of actuator output. If there is error present in the system which is not detected by feedback, the servomotor has no way to correct for it. One could potentially ameliorate this actuation amplitude deficit by means of calibration: increasing the control signal amplitude until the desired output amplitude is achieved. However, this large error

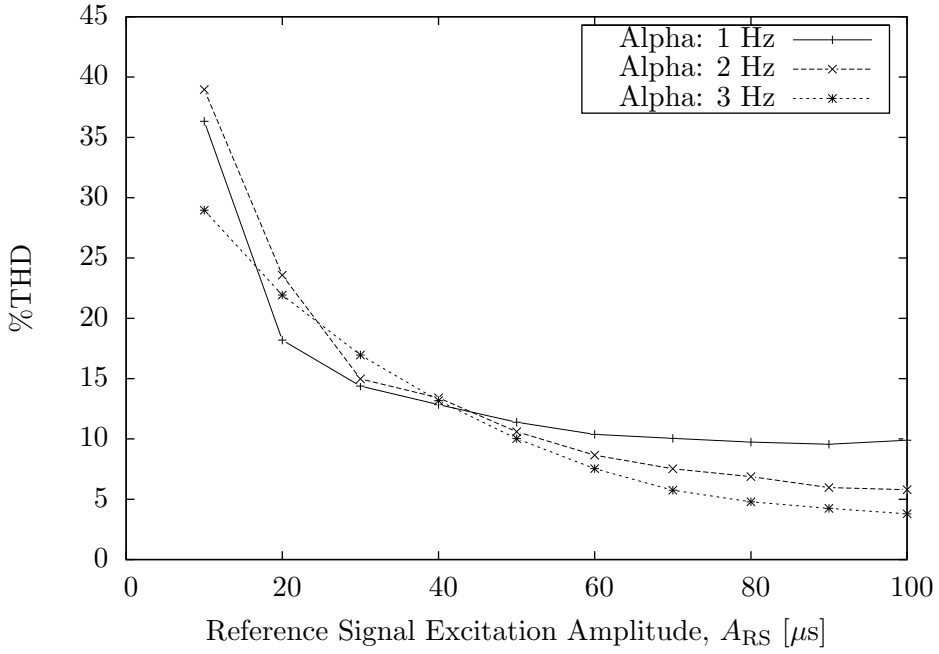

Figure 6.2: *Percent total harmonic distortion of actuator Alpha output,* %THD *as a function of excitation amplitude of the reference signal,* A_{RS}

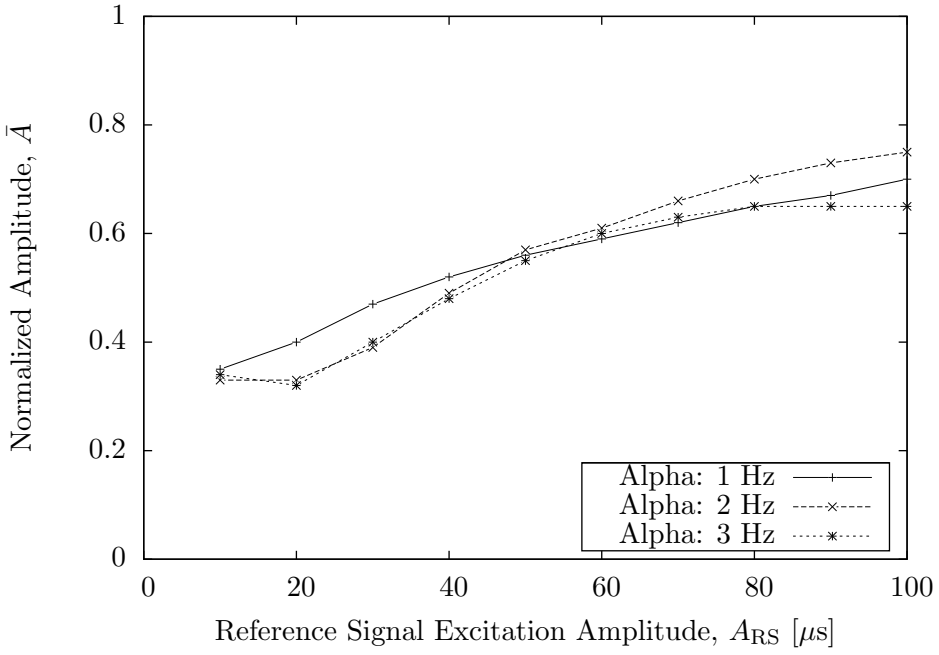

Figure 6.3: *Actuator Alpha output normalized amplitude,* $\bar{A}$ *as a function of excitation amplitude of the reference signal,* A_{RS}.

in amplitude is indicating that there is an underlying problem which should not be ignored or covered up with a calibration.

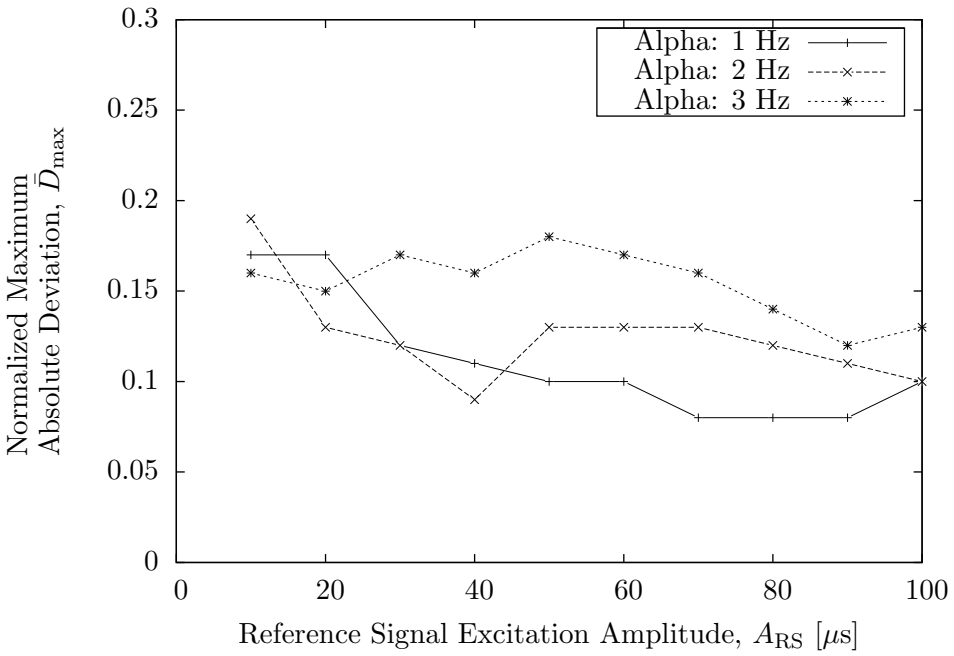

Figure 6.4: *Actuator Alpha output maximum normalized absolute deviation, $\bar{D}_{max}$ as a function of excitation amplitude of the reference signal, A_{RS}.*

Figure 6.4 depicts that the maximum deviation between servos varies from 20% of the desired amplitude to 8% at the best case. This error is an example as to why a calibration to compensate for the lack of actuation amplitude as seen in Figure 6.3 would be a poor solution. There is too much uncertainty of the actuation amplitude between actuators.

A suspect cause of this large deviation is a combined effect of insufficient torque and variance of mechanical impedance between individual actuators. As previously cited, the servomotors may have insufficient torque for proper actuation. Actuation amplitude is thus being limited by how far the labouring servomotor is able to move the plunger and therefore is sensitive to the mechanical impedance the actuator is experiencing. Lessen the impedance and the closer the actuation amplitude becomes to the desired amplitude. Hence, a deviation in impedance among actuators will create a deviation in output amplitude.

From this analysis it is determined that the Alpha actuator performance is more dependant upon actuation amplitude than frequency. In the amplitude region of 0 to 40 μs, the %THD and $\bar{A}$ is most sensitive. $\bar{D}_{max}$ showed less improvement with increasing actuation amplitude than the other two quantities; however, a slight improvement was observed. For actuation amplitudes tested larger than 40 μs the Al-

pha performance is at its best. This indicates that the results from the experiments of Baugh (2010) should have the least error due to actuation error for actuation amplitudes greater than 40 and less than 100 μs. It is probable that the upper limit could be larger than 100 μs, however no data of the Alpha performance was available for amplitudes larger than this. Part II addresses this problem to find a more accurate upper limit.

Chapter 7

Actuator Beta: Improvements to Actuator Design

The poorer than desired performance of the actuators made it necessary for an investigation of the design. The most important issue which required improvement was the large deviation in output amplitude observed. It is of utmost importance for a well posed experiment that the actuators are performing uniformly. To follow will be the discussion of the most prominent improvements, leading to the Beta actuator design.

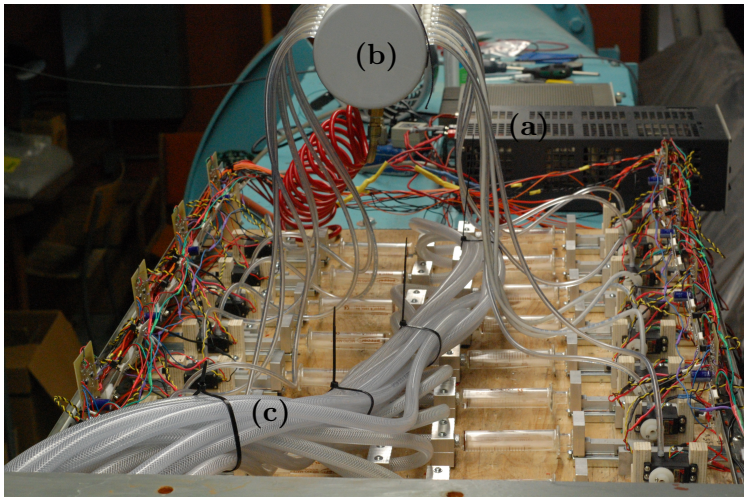

Figure 7.1: *Actuator Beta overview. Labelled items are: actuator power supply (a), servo cooling air supply (b), large diameter tubes to transport actuation to backward-facing step (c).*

Figure 7.1 shows an overview of the final actuator board Beta positioned above the water tunnel. Actuator board Beta consisted of 16 actuators instead of the 22 of actuator board Alpha. There was two causes for reducing the total number of actuators. First, during the experiments of Baugh (2010), the 22 actuators were

never used. All the experiments performed by Baugh used only 16 of the 22. The cost and maintenance required to upkeep the actuator board was dependent on the number of actuators. Since the need for all 22 actuators was not earnest, the cost of updating all 22 actuators with the improvements, which will be discussed in the following sections, was not justified. Thus, the total number of actuators was reduced to 16.

7.1 HS-7965MG Servomotor

The original HS-225MG servomotor used for actuator board Alpha was selected upon its output torque and speed which was deemed theoretically sufficient at the time (Gilbert 2007). It was observed during performance analysis that these servos were not performing as well as expected. As discussed in the previous actuator Alpha performance sections, it is suspected that a lack in torque was a contributing culprit.

Several servomotors were tested and compared with the HS-225MG based on performance and price. The selected replacement is a premium digital servomotor HS-7965MG from from Hitec RCD USA Inc. Table 7.1 gives a comparison of the two servomotors. The HS-7965MG has over twice the available output torque at a maximum of 10 Kg·cm, lower dead-band width which helps small motion response, and faster maximum speed. These enhancements come at a cost of $70 per servo, $40 more than the HS-225MG. This extra cost was deemed acceptable in order to achieve the improvements necessary for proper actuation.

Table 7.1: *Comparison of HS-225MG and HS-7965MG servomotors*

Parameter	**HS-225MG**	**HS-7965MG**
Price	$30	$70
Speed [s/$\frac{\pi}{3}$ rad]	0.11	0.10
Torque [kg·cm]	4.8	10.0

7.2 Actuator Feedback

Servomotors fall in the category of a closed-loop control system. All closed-loop control systems require measurement of the actuator output and have this data fed back (feedback signal) to the controller which compares it with the desired output (reference signal). The difference between the two signals is an error signal, which

the controller tries to minimize by adjusting the output of the actuator to equal that of the reference signal. It is therefore imperative, along with all other components of the control loop, that the feedback is working correctly and measuring the desired motion of the actuator.

The hobby servomotors come stock with an internal radial potentiometer for the purpose of servomotor output radial position feedback. This feedback location does an adequate job for the original design purpose of that servomotor. However, in our case the hobby servomotor is now an integral part of the actuator, and the desired output is no longer the radial position of the servo output, but the transverse position of syringe plunger. Theoretically the two feedback locations are proportional due to the linearity of the system, so using the stock feedback of the servomotor should be sufficient. Unfortunately this proved to be invalid due to unwanted mechanical error in the system connecting the two feedback locations.

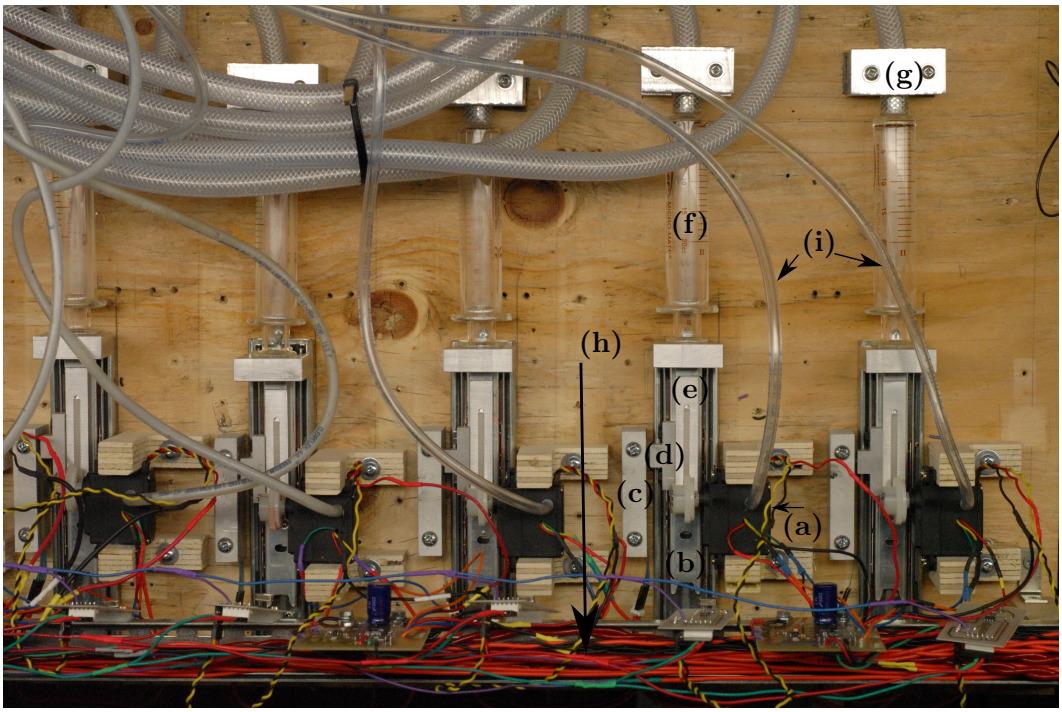

Figure 7.2: *Overhead view of actuator Beta. Labelled items are: HS-7965MG servo motor (a), slider (b), external potentiometer mounting plate (c), external potentiometer slider (d), actuator-rack (e), Syringe (f), tube clamp (g), Power and reference signal wiring (h), servo cooling air lines (i).*

To fix the feedback problem, installation of a new feedback source measuring the plunger position was used. Figure 7.2 and 7.3 on the following page show the feedback location and how it is mounted to the actuator board. Linear potentiometers were mounted to aluminium back supports to run parallel the central axis of the syringe. The potentiometers used, manufactured by Spectra Symbol, are called

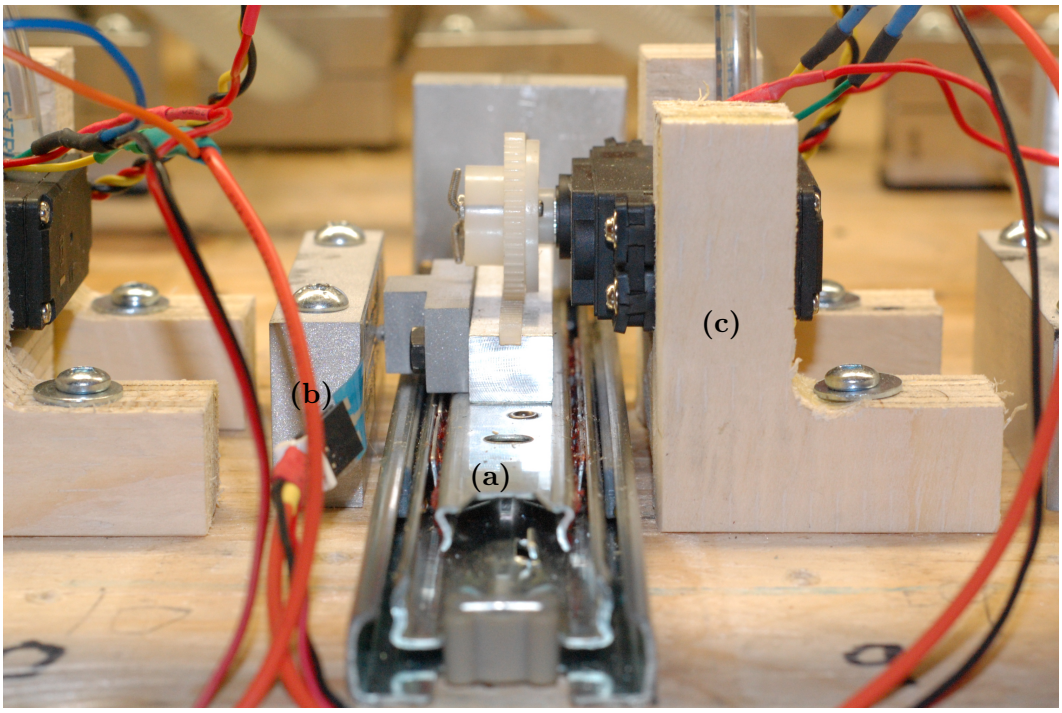

Figure 7.3: *Close up of actuator Beta. Labelled items are: new slider resembling a linear bearing (a), mounting of external potentiometer (b), servo support (c)*

Softpot (short for soft potentiometer). These types of potentiometers are a relatively new design. Apposed to older designs where a mechanical wiper slides over the resistive element, these Softpots contain the resistive element fully enclosed from the ambient environment and no mechanical wipers directly slide over the resistive element. Instead the wiper is external to the potentiometer and presses down a conductive element on top of the resistive element. This is an improvement since the earlier potentiometers were susceptible to wear and dirt collection on the resistive element which can cause error in the measurement. Figure 7.4 shows the schematic of the Softpot. It contains of a lower resistive layer and an upper conductive layer (collector) thinly separated by an adhesive spacer. A non-conducting wiper external to the potentiometer presses down on the Softpot causing the collector and resistive elements to come in contact closing the circuit. The wiper used has a low friction Delrin tip. To ensure proper operation of the potentiometer, it is kept in contact with about 1-3 Newtons of force with the Softpot by use of a spring.

Now with the feedback measurement relocated to the slider, plunger translational position can be directly measured and mechanical error in the system can be compensated for by the servo. This aids in improving all aspects of output performance.

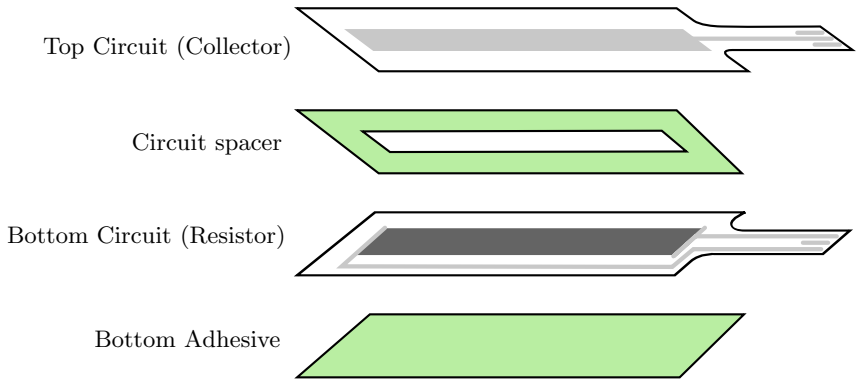

Figure 7.4: *Layers of the Softpot. A top conductive layer separated by a thin adhesive spacer and a lower resistive layer.*

7.3 Amelioration of Mechanical Faults

7.3.1 Slider

The slider is intended to secured the rack-plunger coupling assembly to motion only in a transverse direction parallel to the syringe centre line. The sliders used for actuator Alpha were drawer sliders comprised of aluminium tracks which guided a low friction plastic (PTFE) coated insert. The plastic coated insert is what is mounted to the actuator rack. This slider exhibited unwanted free play since the fit of the plastic insert into the aluminium track was not precise. This had contributed to mechanical error in the system. To mitigate this error, the sliders were replaced with higher quality drawer sliders resembling linear bearings. The new sliders, purchased from Lee Valley Tools,significantly reduced free play and lowered sliding friction.

The reduced free play was also paramount for the proper operation of the external feedback since any wiggle around the vertical axis (perpendicular to the actuator board) would be amplified by the motion of the wiper along the potentiometer and could cause faulty operation of the actuator. The new sliders with the more precise linear bearing action and wide contact area have eliminated the free play.

7.3.2 Servomotor Support

During operation of actuator board Alpha, it was observed that the hardware L-bracket supports where not rigid enough to securely hold the servomotors during actuation; the supports would flex under load. When the feedback location was

internal to the servomotor, this flex could not be detected by the feedback loop and would result in a significant error in the output of the actuator. With the use of the external potentiometer, this flex would be detected and compensated for by the servomotor. However, it would increase the work the servomotor would have to perform in order to produce the desired output. With little effort a proper servomotor support was designed. The new servomotor supports used for actuator Beta can be seen in Figure 7.3. They were constructed from 3/4 inch plywood and securely support the servomotors, eliminating flex in the system.

7.3.3 Syringe Impedance

One of the most troublesome observations from actuator Alpha performance was the large deviation between output amplitudes from one actuator to another. Previously, in the sections discussing the performance of actuator Alpha, it was noted that variance in impedance actuators experienced was the likely cause of this error. Therefore it was of interest to reduce this impedance, or more importantly equalize it to become consistent among all actuators.

Throughout the use of actuator Alpha, it was observed that the impedance experienced by each actuator was highly dependent on the alignment of the syringes with the slider. If the alignment was not exact, the syringe plunger would exhibit a moment load onto the syringe housing. Due to the poor lubricating properties of water which filled the interstice between the plunger and housing, the plunger would bind and create large and fluctuating impedance throughout its motion. This proved to inhibit the performance of the actuator, creating deviation of the impedance each actuator experienced. To alleviate this binding two methods were sought: improvement of slider-syringe alignment, and replacement of the interstitial fluid with a proper lubricating fluid.

To explicitly correct the alignment by adjustment of component position was close to impossible since the holding bracket for the syringe housing and plunger were simply screwed into the actuator board base (a sheet of 3/4 inch plywood). In order to improve upon the alignment, an aligning apparatus would have to be designed and built which would be costly and time consuming. Instead of securely constraining the syringe from each direction of movement, the syringe was released from secure constraint in the plane perpendicular to the slider motion to allow it to float and align itself. This was done by removing the conduit bracket holding the syringe housing altogether, allowing it to be only held in place by the tube clamps at their luer lock ends and the plunger. The plunger itself needed relief from constraint. This was done by removing the plate holding the plunger flush with the slider and instead adhering the plunger to the slider using a 3M high density double sided

1/8 thick foam tape. These changes allowed the two plunger and housing to align themselves while constraining them to the motion of actuation along their central axis.

Improvement of alignment had a measurable improvement on performance, but performance could yet be further improved with the use of a proper lubricating fluid. The interstice where the fluid was required was of large surface area, so the lubricating fluid had to be of low viscosity. The oil chosen was a light weight machine oil (UVINIS Extra machine oil). The viscosity of this oil was of twice the order of water, increasing viscous friction by approximately ten times. However, it prevented binding altogether. With the help of this better alignment method and lubricating oil, consistent impedance experienced by all actuators was achieved.

7.4 Servo Cooling System

Original design intent of the hobby servomotor's was for intermittent use in recreational remote controlled vehicles. They would commonly be used for positioning of the vehicle's directional control surfaces and so forth. Not for performing continuous work at high levels such as they are being used for our actuators. They are not by stock equipped with any cooling mechanism and operate within a confined, unventilated case. During actuation for extended periods of time the servomotors would begin to overheat which has caused failure and premature wear. A cooling system was constructed shown in Figure 7.5 to allow the servomotors to perform the work without overheating.

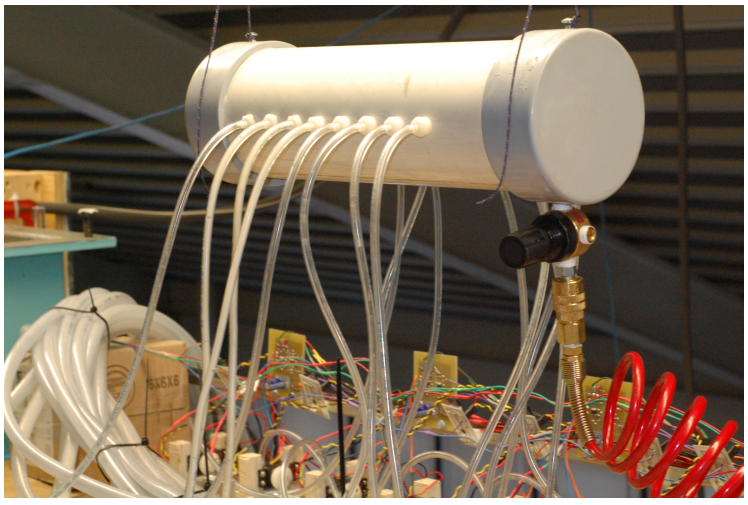

Figure 7.5: *Actuator Beta cooling system. A PVC manifold pressurized with dry air supplied by red hose divides servo cooling air between 16 small diameter tubes. A pressure regulator (black knob connecting red hose with manifold) is used to control cooling air flow rate.*

The cooling system is comprised of a main PVC manifold which is fed with dry compressed air. The air is directed to each servomotor via small diameter tubing which mount to a nipple installed on the side of the servomotor housing. The air injected into the housing would exit the other side through a hole. This simple cooling system keeps the servomotors well ventilated and maintains them at a cool operating temperature.

7.5 Wiring and Current Flow

During large amplitude actuation, some of the actuators would occasionally act sporadic. The first item investigated for insight into the problem was the voltage supplied at the location of each servo. An oscilloscope measuring supply voltage at the servo location during actuator operation revealed that the voltage was significantly lower than the six volts at the power supply and fluctuated drastically. These fluctuations corresponded with fluctuating current draw of the servomotors; each time the reference signal was updated a surge of current was required to move to the commanded position. Since they would all receive updates simultaneously, the current draw from the power supply fluctuated correspondingly and could have a peak as high as 20 amperes.

The original power routing to all Alpha actuators consisted of a single pair of 18 gauge wire running the length from the power supply to all the actuators. At the location of each actuator the power was spliced to that given actuator using crimp connectors. By the time the main power line had reached the last servomotor it ran a total distance of 3 meters. This power routing proved to be inadequate to handle the current draw without significant voltage loss across the line. By the time the power reached the last few servomotors in line, the voltage supply would fluctuate below their minimum operating voltage resulting in erratic operation.

A new power routing used a hierarchy of splices which routed the power more efficiently instead of using a single power line. As well, all connections were properly soldered instead of using crimp connections. The routing hierarchy started from the power supply with a 0.2 meter section of 10 AWG which then split into two pairs of 12 AWG, each of which would supply eight of the sixteen servomotors. The 12 gauge wires then spliced into four pairs of 16 AWG which would each carry the power the remaining distance for two actuators. At the end of each 16 AWG pair 2200 μF capacitance was inserted, as well as at the power supply output, 0.5 F of capacitance was added to the power lines to help alleviate the fluctuation current demand from the power supply. With the added capacitance and more efficient routing of power, the voltage supplied to each actuator was stabilized at the proper operating voltage of 6 volts.

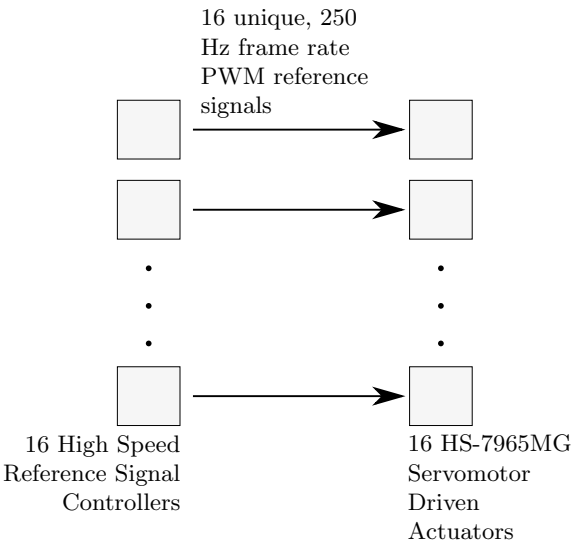

Figure 7.6: *Block diagram showing Beta reference signal generation.*

7.6 Servomotor Control

The original Alpha actuator board controlled the servomotors using a Lynxmotion SSC-32 servo controller (Figure 5.3). The SSC-32 would send each actuator a unique PWM signal at a 20 ms interval, corresponding with a 50 Hz frame rate. When the SSC-32 would receive a command generated in LabVIEW on a PC, it would maintain the PWM outputs constant corresponding to the command it received, until a new command from LabView was sent which would override the previous one. Thus by LabView sending a new command to the SSC-32 every 20 ms, the PWM signals would be updated each time the SSC-32 would send a new pulse to the servomotors.

There were two problems with this control scheme. The first problem was LabVIEW wasn't always able to output a new command to the SSC-32 precisely at the prescribed 20 ms period. It had some difficulty in keeping up with the real-time operation. This would result in an occasional late command being sent out which wouldn't be updated at the SSC-32 output until the following pulse. Thus the SSC-32 output reference signal would "hang", sending the same pulse to the servomotors twice in a row which would result in choppy operation of the servomotors. The second problem was that the 50 Hz frame rate was not adjustable, it was a fixed rate of the SSC-32. For most applications this rate is quick enough, and is a standard among PWM controlled servomotors. However, if one wants to improve the time resolution of the reference signal, the refresh rate would have to be increased.

The HS-7965MG digital servos can accept a frame rate as high as 250 Hz. To take advantage of this higher frame rate, a new servo reference signal controller was

needed, capable of creating a PWM signal at this higher rate. There exists endless options for designing a new controller to create 16 reference signals at this refresh rate. One could use a similar design to the SSC-32 card. It uses a microcontroller to update shift registers which hold the desired PWM signal outputs. However, at this higher refresh rate, using this method can be quite difficult in creating this many unique PWM signals. A field-programmable gate array (FPGA) could be used in place of the microprocessor which could be programmed to create the sixteen PWM signals much more efficiently than a microcontroller ever could. Another option is to use sixteen individual microprocessors in lieu of the FPGA. Each of the 16 microprocessors would perform the task of controlling just one of the 16 servomotors. This is a less elegant solution than using a FPGA, but just as functional nonetheless. Due to time constraints, the later design option was selected. Sixteen individual servo controllers for each servomotor were created. Figure 7.6 shows a block diagram of reference signal generation, and Figure 7.7 shows two servo controllers positioned adjacent their respective servos.

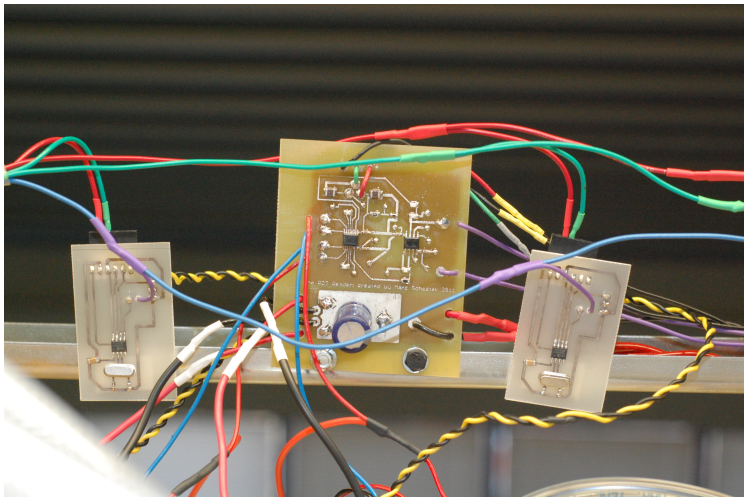

Figure 7.7: *Actuator Beta servo controller and potentiometer reader. The potentiometer reader is the larger of the three circuits, and the two smaller circuits are each a high speed servo controller.*

Details on the operation of the Beta actuator can be seen in Appendix D, as well, schematics of the designed servo controller can be seen in Appendix E along with the code used to program the PIC12F629 microcontroller. The design is relatively simple, the microcontroller is programmed with the desired waveform in program memory. When powered it cycles through the waveform in memory and runs as an embedded system without any input from the computer. This provides a very stable output with no hanging and with proper real-time operation. As well, it is now capable of a time resolution in the reference signal five times higher than

previously.

There is one drawback of the new servo controller design. Previously if one wanted to change the forcing frequency or amplitude of the actuators, this could be done effortlessly and quickly by updating a few numbers in the LabVIEW code. With the new controllers, to change the actuation waveform one needs to update the code programed on the PIC microcontrollers. To perform a reprogram of all 16 servo controllers, an average of 5 minutes is required. It was deemed that this extra time required was worth the improved performance the new controllers provide.

7.7 Potentiometer Reader

The modification of the potentiometer (pot) reader was not for the improvement of actuator performance, but for the ability to have live measurement of each actuators motion. This was used as a check to be certain that all the actuators were operating as expected before an experiment was carried out. The larger circuit in Figure 7.7 is the pot reader used to measure the motion of two adjacent actuators. The aluminium electrolytic capacitor near the bottom of the circuit is the 2200 μF capacitor used for the smoothing of the power supply as discussed in section 7.5. Schematics of the circuit are in Appendix F.

The pot reader was required as the signal from the potentiometers could not be used directly. This was due to a large amount of common mode noise imposed on the potentiometer signal created internally by the Hitec servomotor. Essentially the pot reader would remove the common mode noise on the potentiometer signal with the use of an instrumentation amplifier. This cleaned signal could then be directly read by LabVIEW using a National Instrument USB-6229 Multifunction Data Acquisition Module (DAQ). Before an experiment is carried out, the motion of each actuator can be quickly checked to be certain they are working as expected.

Chapter 8

Actuator Beta Performance

8.1 LVDT Output Measurement: Actuator Beta

Figures 8.1 through 8.3 show the measured output plots for actuator Beta created from a LVDT sampling the movement of the actuator output. Details on the hookup and use of the LVDT can be seen in Appendix C. The LVDT signal was converted to a digital signal using a National Instrument USB-6229 Multifunction Data Acquisition Module (DAQ) sampling at a 2 kHz rate. Before digital conversion, the LVDT signal was filtered using an analog 2nd order passive RC filter with a cutoff frequency of 200 Hz. For the Beta actuator output figures, the servomotors were driven by a reference signal of 1, 2, and 3 Hz sinusoidal waveform with PWM amplitudes of 10, 50, and 100 μs. Before analyzing their performance using the more quantitative measurements, let us examine these plots.

Unlike actuator Alpha output waveforms (Figure 6.1, page 22), it is now visually discernible from the measured output that the actuator output is intended to be of sinusoidal form, even for the low (10 μs) amplitude case. In the low amplitude case, the actuator is still lacking in performance to produce a pure sinusoid; there is an apparent jaggedness of the output. Nonetheless, the output is no longer erratic and now of periodic form. Being periodic, this actuator output is acceptable for experimental use at the low amplitude case.

As the amplitude is increased there is a significant increase in performance. The actuator amplitudes are much closer to the desired amplitudes and for the large amplitude case the output appears to be a smooth, pure sinusoid. From these qualitative observations, there is an apparent significant improvement in performance. Next the performance using the same quantitative measurements as used for actuator Alpha will be discussed.

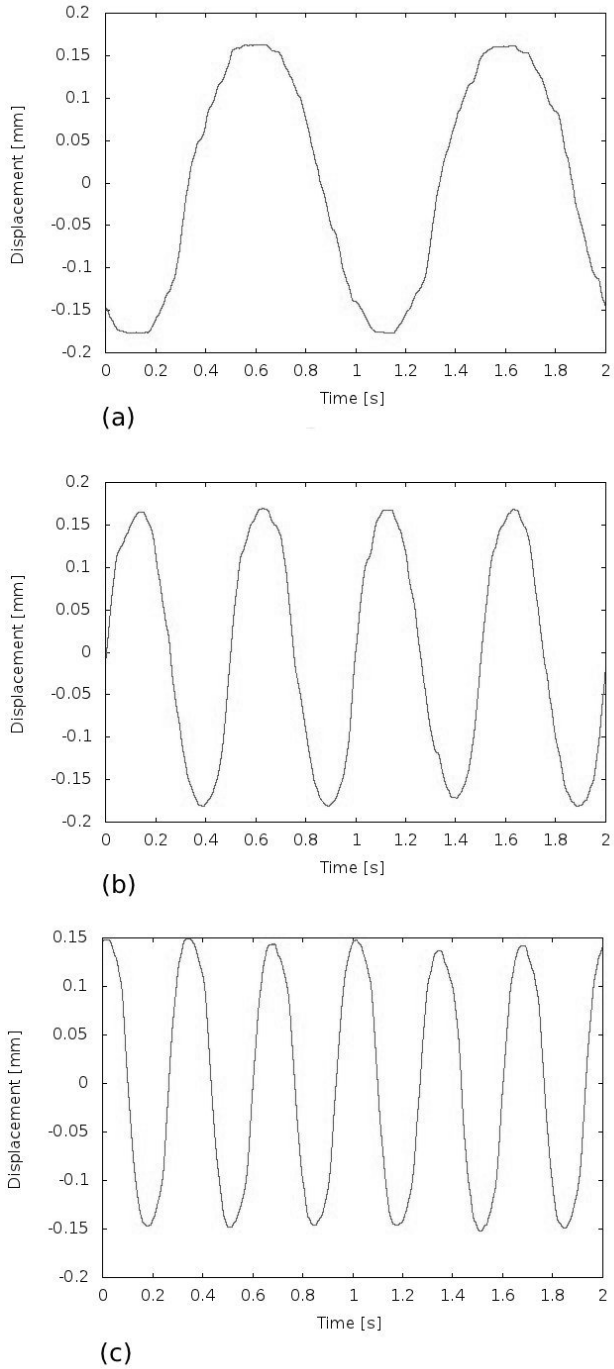

Figure 8.1: *Actuator Beta output waveform measurement using LVDT for 10 μs amplitude sinusoidal reference signal at (a) 1 Hz (b) 2 Hz (c) 3 Hz*

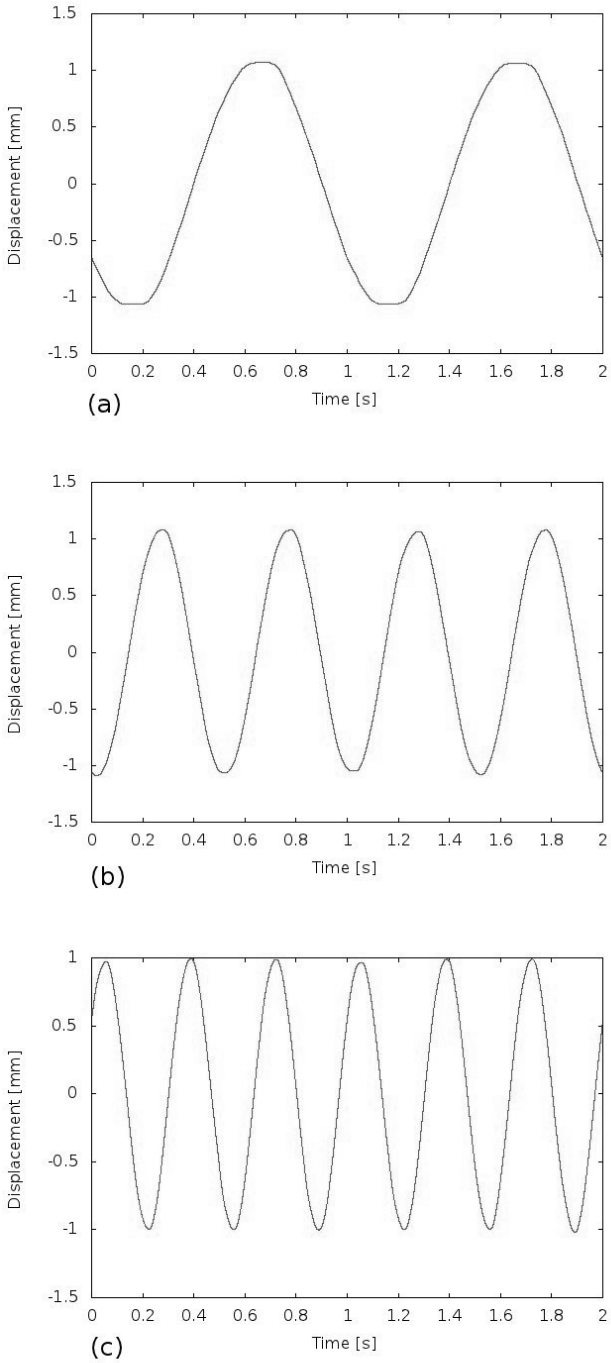

Figure 8.2: *Actuator Beta output waveform measurement using LVDT for 50 μs amplitude sinusoidal reference signal at (a) 1 Hz (b) 2 Hz (c) 3 Hz*

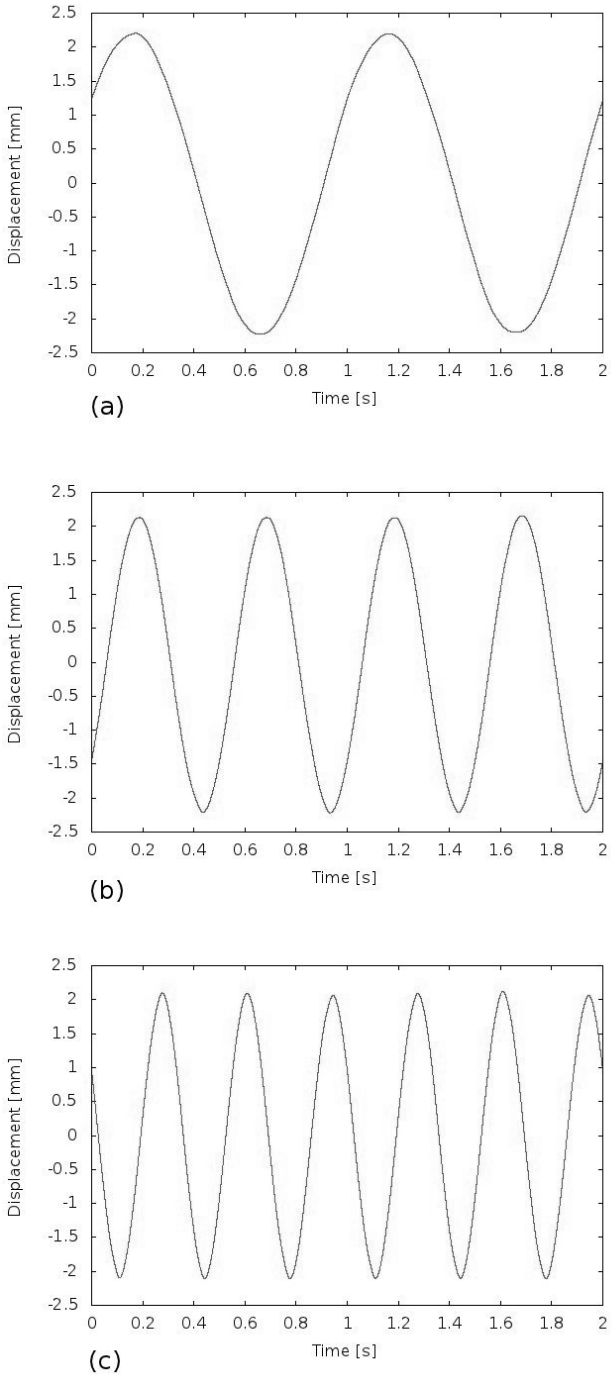

Figure 8.3: *Actuator Beta output waveform measurement using LVDT for 100 μs amplitude sinusoidal reference signal at (a) 1 Hz (b) 2 Hz (c) 3 Hz*

8.2 Quantitative Performance Analysis: Actuator Beta

Figures 8.4- 8.6 on the next page show quantitative results of actuator Beta performance. These results are formed from a population of three actuators with three measurement trials per actuator. The raw data can be viewed in Appendix B on page 124. Figure 8.4 plots the total harmonic distortion of the actuator output, Figure 8.5 plots normalized amplitude, and Figure 8.6 shows the normalized absolute deviation among the measured actuators.

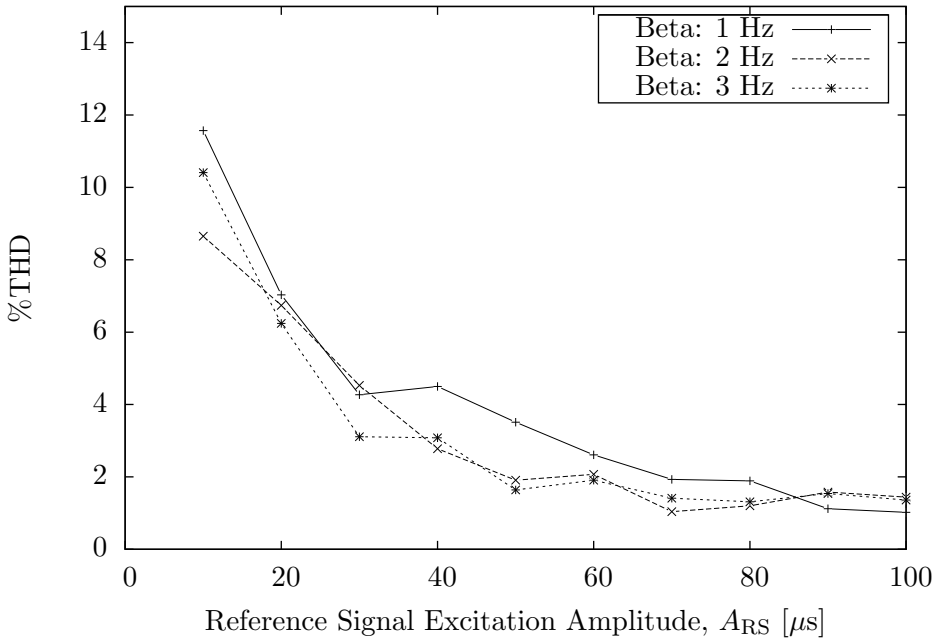

Figure 8.4: *actuator Beta output total harmonic distortion,* %THD *as a function of excitation amplitude of reference signal,* A_{RS}.

A smaller population of three was used for actuator Beta performance data, apposed to five actuators as used for actuator Alpha measurements. This smaller population was chosen as the deviation among actuators Beta were much lower than with the actuator Alpha measurements. Thus, a smaller population is required to give an acceptable representation of the mean.

Figure 8.4 depicts a trend of improving THD with increasing excitation amplitude. At the lowest amplitude, %THD values of approximately 11.5 to 9 percent were measured. %THD quickly decreases to as low as one percent by the largest amplitude.

Figure 8.5 shows that normalized amplitude reaches unity at around an excitation amplitude of 50 μs up to 100 μs. Below 50 μs amplitude, the actuators are not producing an expected output amplitude. At the lowest excitation amplitude, the

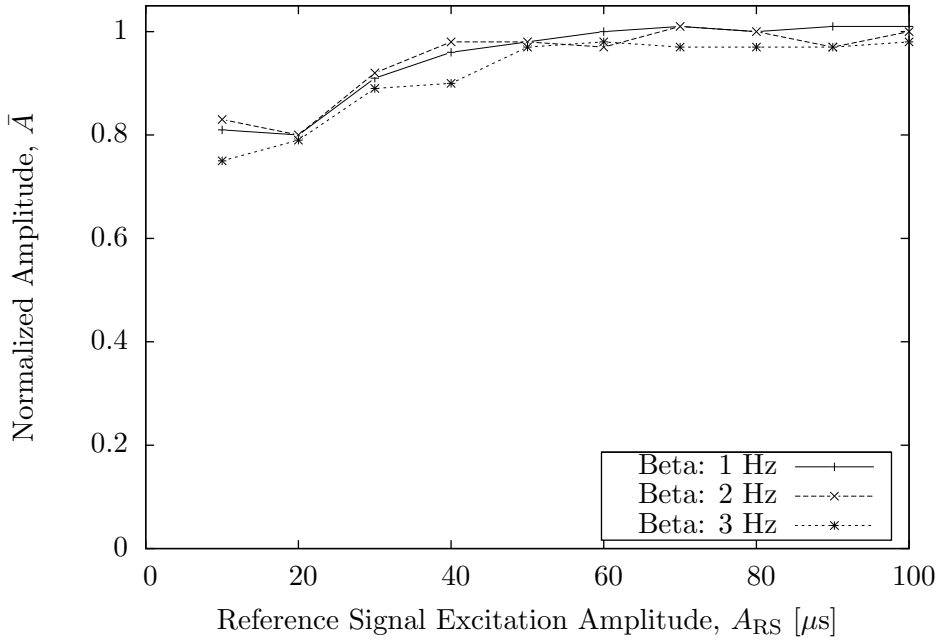

Figure 8.5: *actuator Beta output normalized amplitude, $\bar{A}$ as a function of excitation amplitude of reference signal, A_{RS}.*

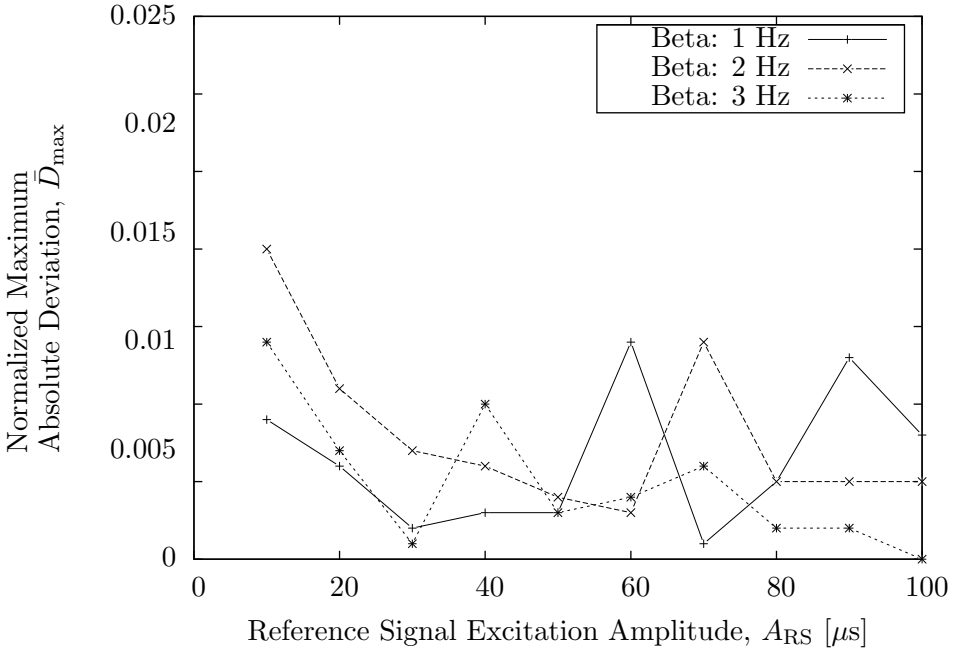

Figure 8.6: *actuator Beta output normalized maximum absolute deviation, $\bar{D}_i$ as a function of excitation amplitude of reference signal, A_{RS}*

output amplitude is approximately 80% of the expected value.

Figure 8.6 shows some of the most interesting results. The deviation between actuators is at the worst case 0.02%. These results are exciting because they indicate that the actuators are operating reliably and uniformly. Thus, using a calibration to compensate for the lack of expected excitation amplitude, as shown in Figure 8.5, is feasible. The calibration of actuator Beta will be discussed in section 8.5.

8.3 Comparison of Servo Reference Signal Controllers

This section gives a brief comparison of actuator Beta performance with the original 50 Hz frame rate Lynxmotion SSC-32 servo controller and the new high speed servo controller. Section 7.6 discussed the design of a high speed servo controller which is capable of a 250 Hz frame rate. This higher frame rate creates a servo reference signal with better temporal resolution which would improve the actuator response, especially at higher actuation frequencies. Figure 8.7 shows the LVDT measured output of these two cases. The choppy operation of 8.7(a) is due to a lack of temporal resolution from the 50 Hz frame rate of the lynxmotion SSC-32 servo controller. Especially near the peaks, the effects of lower temporal resolution is visible. Figure 8.7(b) shows the same output waveform, except now the reference signal is generated using the high speed controller. A marked improvement in output smoothness is visible. These Figures give evidence that the high speed servo controller significantly helps the actuator follow the step curvature at the waveform peaks at higher actuation frequencies to produce smooth operation.

Not only does actuator Beta improve performance, but it expands the perturbation parameter space available. Figure 8.8 shows an example of actuator Beta output for a 1 hertz large amplitude sine wave with a 10 hertz low amplitude sine wave superimpose. This multiple frequency actuation would not be possible without the use of the high speed servo controller. The waveform shows excellent repeatability of the actuator output indicating precise actuation. Actuator Beta is capable of more than double the actuation frequency range of actuator Alpha, and allows the possibility of multiple frequency actuation. As well, perturbation amplitudes in the range of 50 mm/s were never attainable with the actuator Alpha design. Thus, attainable amplitudes has also been expanded. This is largely due to the greater torque available with actuator Beta.

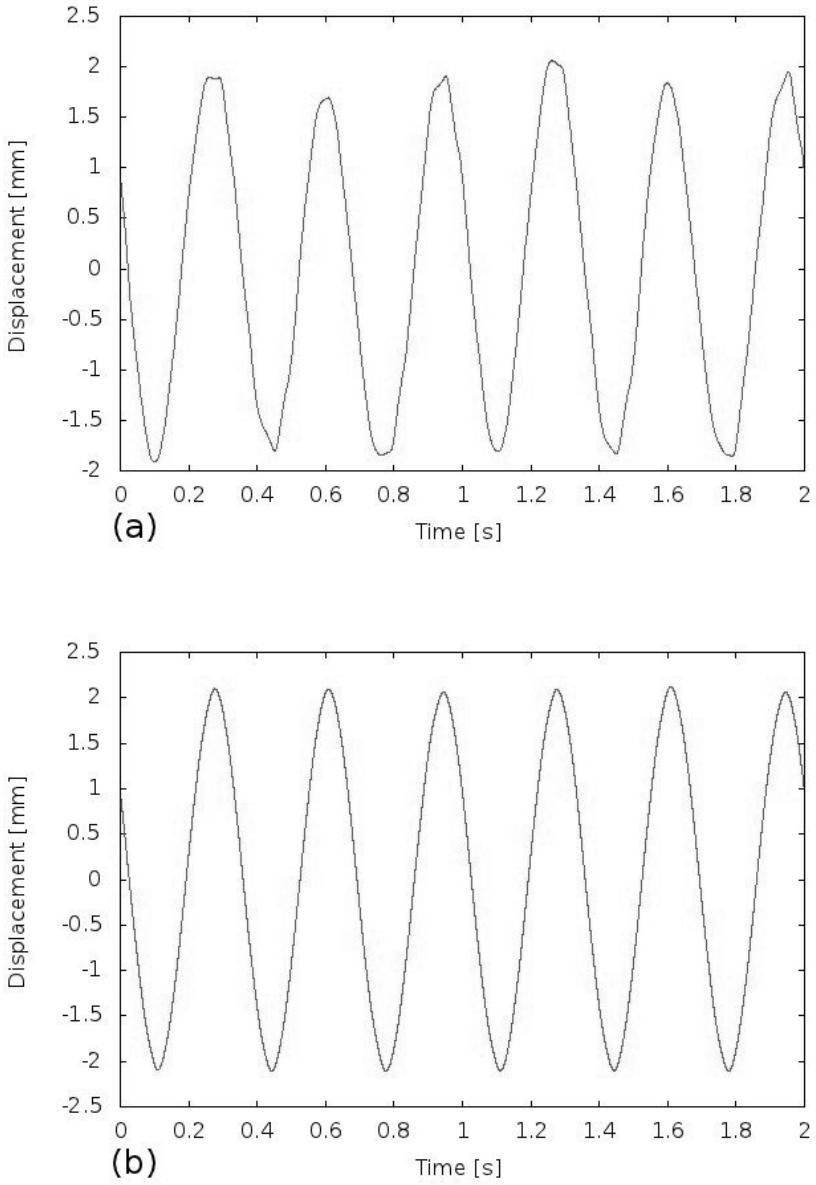

Figure 8.7: *Actuator Beta output measurement using LVDT. Comparison of servo reference signal controllers for 100 μs, 3 hz waveform. Plot (a) controlled using Lynxmotion servo controller at 50 Hz frame rate, Plot (b) controlled using high speed servo controller at 250 Hz frame rate.*

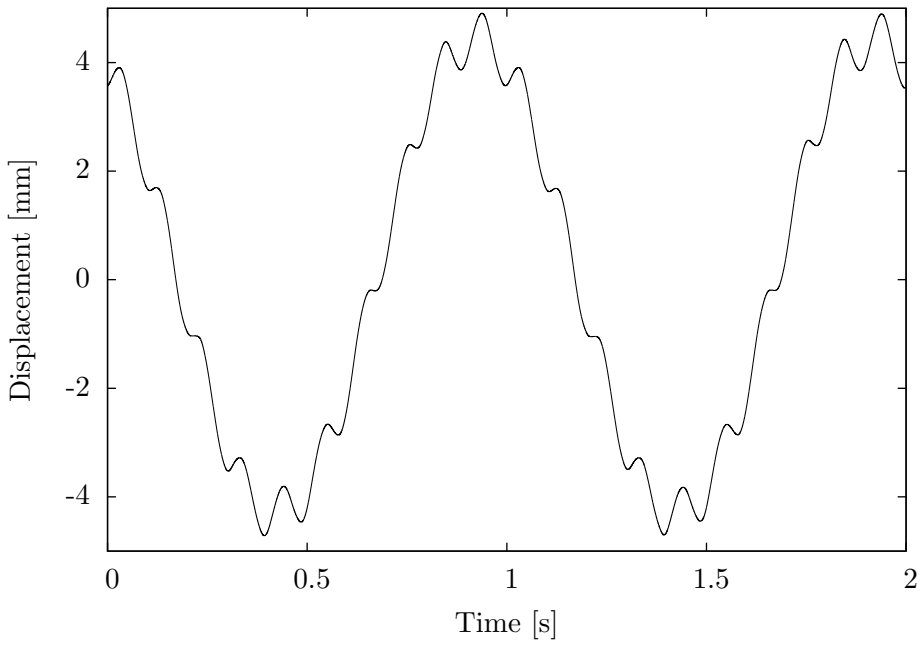

Figure 8.8: *Actuator Beta output measurement using LVDT. Example of multiple frequency forcing; 1 Hz, 200 μs base waveform with 10 Hz, 40 μs superimposed.*

8.4 Comparison of Actuator Performance: Alpha VS Beta

The following figures compare the quantitative data for actuators Alpha and Beta presented in sections 6.2 and 8.2. Comparison is made for %THD, Figure 8.9, normalized actuator output amplitude, Figure 8.10, and maximum normalized absolute deviation, Figure 8.11. All three comparisons show a significant improvement in each case of frequency and amplitude tested.

On average the total harmonic distortion has reduced by 74%, absolute deviation by 95%, and normalized amplitude has reached unity at forcing amplitudes larger than 50 microseconds. The most important factor of improvement is the large decrease in deviation. This indicates that there is little uncertainty of the output of actuator Beta; a necessity for a well posed experiment.

With the now consistent actuator output, a reliable calibration can be attained between output amplitude and reference signal amplitude. Such a calibration will give a more precise actuation, eliminating error due to any non-unity of normalized actuation amplitude seen in Figure 8.10.

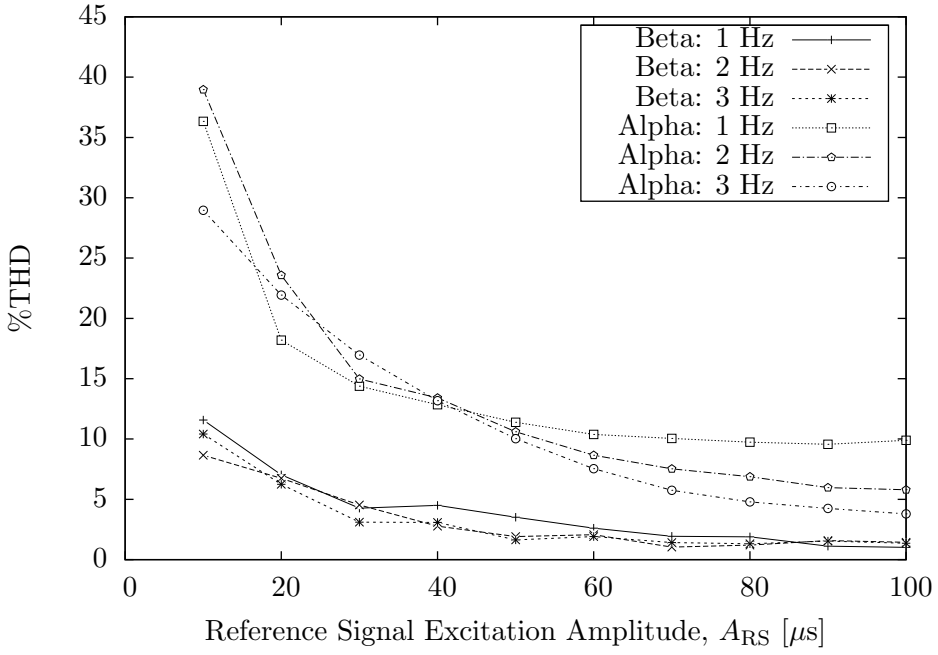

Figure 8.9: *Comparison of total harmonic distortion for actuators Alpha and Beta*

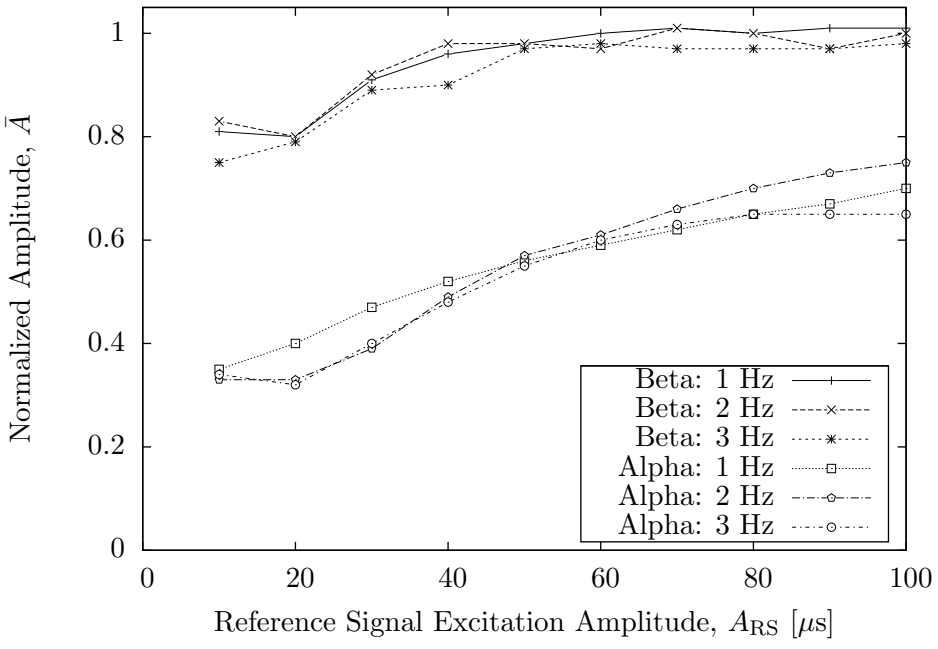

Figure 8.10: *Comparison of normalized amplitude for actuators Alpha and Beta*

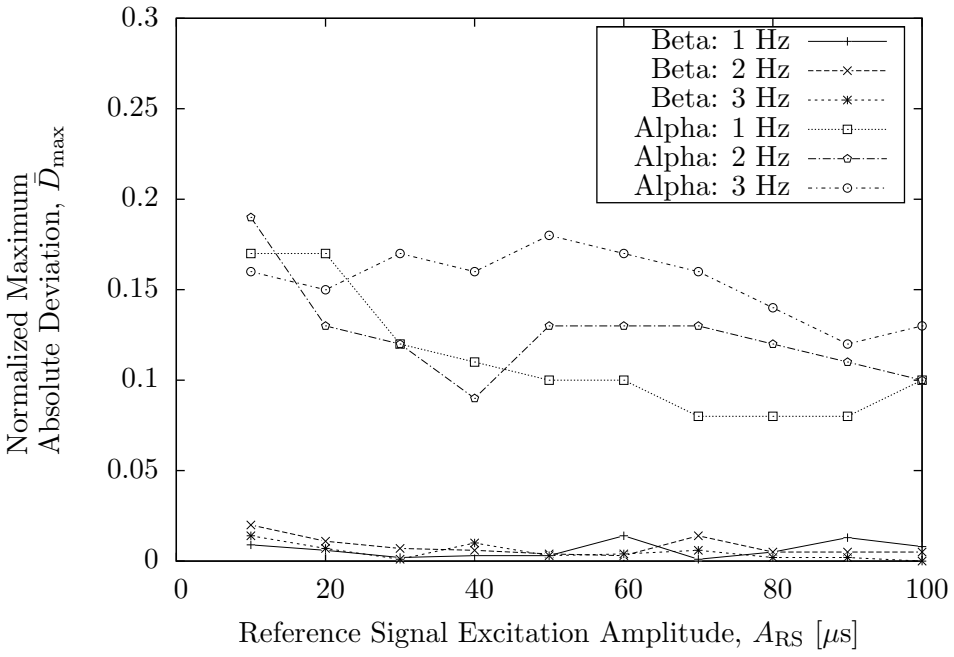

Figure 8.11: *Comparison of normalized maximum absolute deviation for actuators Alpha and Beta*

8.5 Actuator Beta Calibration

One of the experimental variables used in the tests performed for Part II of this thesis is peak excitation velocity u'. Hence the calibration of interest is the relation of servo reference signal amplitude and frequency to peak actuator output velocity. Measurement of actuator output velocity was performed by sampling positional data of the actuator output over a twenty second period using a LVDT, and then numerically differentiating that data in Labview to calculate the velocity of the actuator. As before, the LVDT data sampled using a 2 KHz sample rate was filtered before digital conversion with a 200 Hz cutoff, 2nd order, analog RC filter. After differentiation of the signal, a quadratic mean (RMS) velocity was calculated for each of the measurement cases. The RMS velocity was calculated rather than using peak velocity values, as it mitigates error introduced from the numerical differentiation due to noise, giving a more accurate representation of the excitation velocity.

In order to calculate an RMS velocity from the sampled data, the data set used for the calculation must be of a whole number of actuation cycles. Since all excitation frequencies to be used in experiments are multiples of 1/2 Hz, any measurement period of an even number of seconds will contain a whole number of cycles. The twenty second measurement period will thus always hold a whole number of cycles, and is large enough to give an accurate calculation.

It was predicted that the output velocity should ideally follow a linear trend. To verify the linearity of the actuator output, it was normalized with a theoretical RMS velocity, $V_{\mathrm{RMS}theor}$, based on the calibration constant, C_{amp} (see Chapter 4 for definition of C_{amp}). Equations 8.1 and 8.2 show the calculation of theoretical RMS velocity, and normalized velocity, $\bar{V}$.

$$V_{\mathrm{RMS}theor} = \pi\sqrt{2}C_{\mathrm{amp}}A_{\mathrm{RS}}f_{\mathrm{excitation}} \tag{8.1}$$

$$\bar{V} = \frac{V_{\mathrm{RMS}actuator}}{V_{\mathrm{RMS}theor}} \tag{8.2}$$

Where: $f_{\mathrm{excitation}}$ – excitation frequency [Hz]

$V_{\mathrm{RMS}actuator}$ – actuator output RMS velocity calculated from derivative of sampled LVDT position data [mm/s]

Figure 8.12 shows calibration curves for three excitation frequencies. A close to linear relation for excitation amplitudes 50-150 microseconds can be observed. This linear relation for intermediate excitation amplitudes is more apparent in Figure 8.13. At lower and higher amplitudes, the output velocity becomes less than the linear prediction.

Through experience from using the actuators, it was noted that relying on the calibration curves for determining the excitation amplitudes for experimental purposes provided mediocre values. To attain a more accurate excitation amplitude for experimental use, these curves or in some cases the theoretical RMS velocity calculation was easier to use for an initial guess of the excitation amplitudes to be used. Then for each amplitude-frequency case to be used for an experiment, the actuator output RMS velocity was measured using the LVDT, and through iterative process a more accurate excitation amplitude was found. This process would require a few minutes to calibrate for each forcing case, thus an entire experiment's parameter space could be properly calibrated in only an few hours' work.

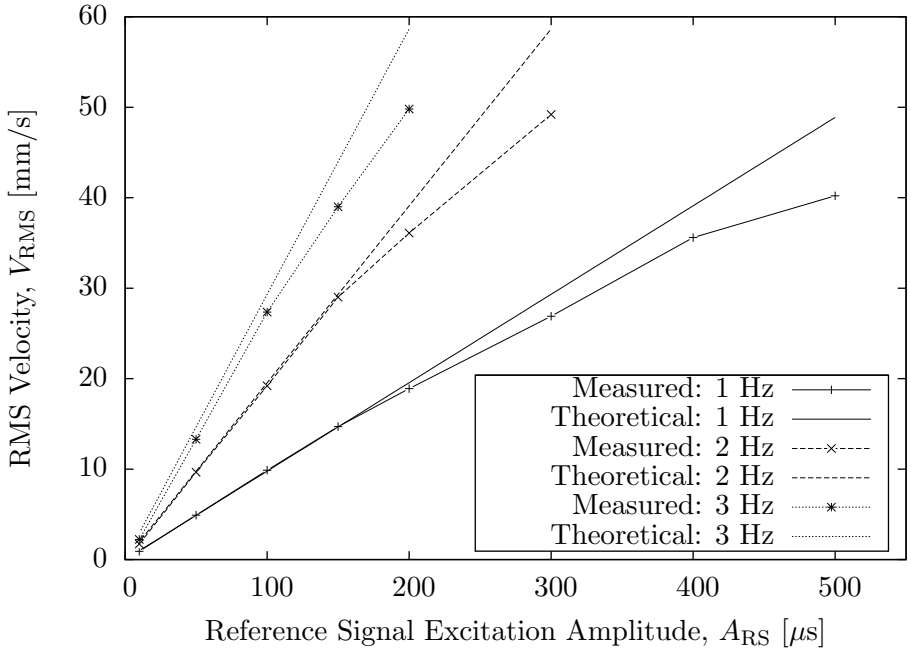

Figure 8.12: *Measured actuator RMS velocity output calibration curves for frequencies 1,2, and 3 hertz and their corresponding theoretical linear plots.*

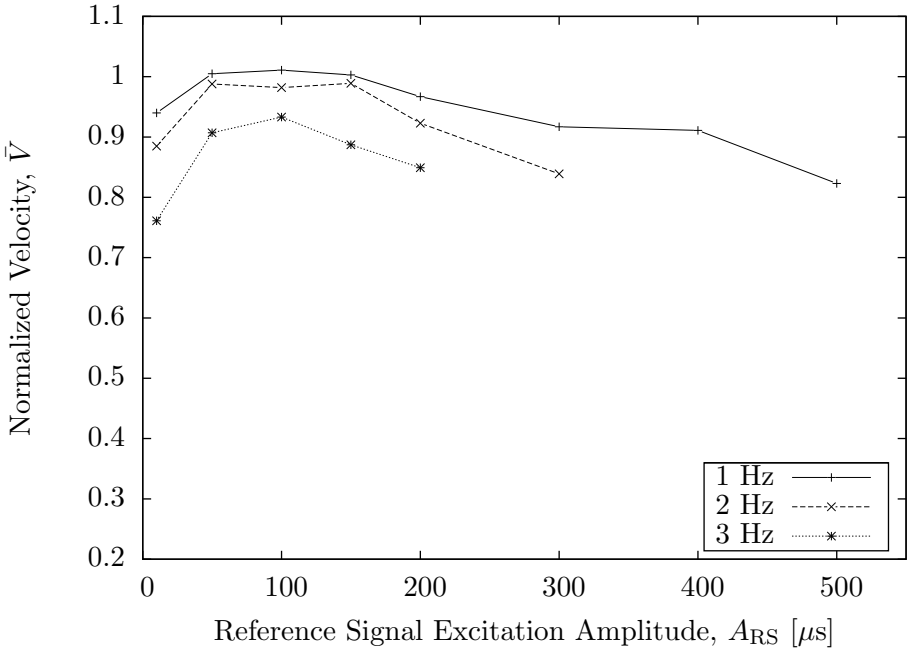

Figure 8.13: *Normalized actuator RMS velocity output calibration curves for frequencies 1,2, and 3 hertz.*

Chapter 9

Part I Summary and Conclusions

Many improvements to the flow actuator have been discussed. These improvements resulted from experience gained about the performance of the original Alpha actuators used in experiment by Baugh. Baugh had noted some difficulty with using the actuators and potential problems which resulted in the detailed performance analysis presented in Part I. Here is a summary highlighting the major changes:

- The selection of the HS-7965MG servomotor. A more suitable servomotor with improved torque, speed, and is compatible with higher frame rates than the original HS-225MG servomotor.
- Improvement of the feedback signal. Originally the actuator feedback came from a radial potentiometer internal to the servomotor. Since the desired motion of the actuator was of the syringe piston, any mechanical error in the coupling of servomotor output to piston motion would not be detected by the feedback loop. Improvement to the feedback loop was achieved by replacing the internal radial potentiometer with a linear potentiometer which directly measured the motion of the syringe piston.
- Amelioration of mechanical faults: the majority of the mechanical aspects of the original actuators were either replaced or improved upon to reduce free-play and flex within the system.
- Developed a servomotor cooling system which eliminated the problem of over-heating in the original design.
- Re-routed the wiring for actuator power. The 16 actuators required a smooth power supply of substantial and fluctuating current demand. The original

power routing was insufficient for efficient power supply resulting in large fluctuations in supplied voltage. Thicker gauge wiring and better connections along with added capacitance to the lines removed the voltage fluctuations.

- A new servo reference signal controller was designed as an embeded system which allowed for a 250 Hz frame rate, 5 times faster then the previous rate. This allowed for a finer temporal resolution of the reference signal, significantly improving the actuator performance. As well, being an embedded system it maintained real-time operation which the original reference signal system could not do.

Through these modifications, the performance of the actuators has been improved to a level which will better experimental results. The major performance enhancements were 74% reduction of actuation total harmonic distortion, and a 95% reduction of absolute deviation between actuators. The large reduction in deviation shows that the actuators are acting reliably and with the use of calibration, a desired actuation amplitude is attainable.

Apart from improved performance, the parameter space accessible has been expanded. Excitation frequencies of 10 Hz or higher are now possible, more than doubling the excitation frequency range. This is only possible with the use of the designed high speed servo controller. There was also a dramatic increase in accessible excitation amplitude due to the increased torque of actuator Beta. With these improvements, multiple frequency actuation is now also feasible.

One of the objectives of the performance analysis was to determine the actuation cases for which the Alpha actuator had the most actuation error. From this analysis it was concluded that the Alpha actuator performance is more dependant upon actuation amplitude than frequency. In the amplitude region of 0 to 40 μs, the %THD and $\bar{A}$ is most sensitive. $\bar{D}_{max}$ showed less improvement with increasing actuation amplitude than the other two quantities; however, a slight improvement was observed. For actuation amplitudes tested larger than 40 μs the Alpha performance is at its best. This indicates that the results from the experiments of Baugh (2010) should have the least error due to actuation error for actuation amplitudes above 40 and less than 100 μs. It is probable that the upper limit could be larger than 100 μs, however no data of the Alpha performance was available for amplitudes larger than this. Part II addresses this problem to find a more accurate upper limit.

The experience gained from this investigation shows that the performance of the control system is defined by the collective performance of each component. For example, the servo supports used for actuator Alpha did not sufficiently restrain the servo in place; they would flex under load introducing error into the output motion

of the actuator. It is therefore important to not treat these seemingly simple components trivially. Even aspects of an actuator which at first seem to be insignificant can have significant influence on the performance of the actuator as a whole. As well, the design of a control system is case dependant. If a design works for one application, it is not guaranteed to work if a outside variable (load, temperature...) is changed. Thus each design application requires careful consideration.

Part II

The Flow Control of a Turbulent Reattaching Shear Layer behind a Backward-Facing Step

Chapter 10

Part II Objectives and Overview

Part II starts with a theoretical investigation of the properties of the boundary layer at the point of separation. As will be discussed, our unforced reattachment length $X_{r_\circ}$ is approximately 20-30% shorter than expected from the results of other unforced BFS experiments. Baugh (2010) gives discussion in his thesis for the possible causes, but does not ascertain a definitive answer. This is largely due to the lack of knowledge of the boundary layer properties at separation. No measurements of boundary layer turbulence or shape/thickness was available at the time of writing, thus the theoretical investigation of boundary layer properties was the only means to gain more knowledge and insight of the cause of our shorter $X_{r_\circ}$.

After the discussion of the boundary layer, the experimental apparatus is discussed as a whole. The apparatus is comprised of three main components, the "RoboStep", Beta actuator board, and hydro-tuft array. The RoboStep is the BFS insert positioned within the test section. The Beta actuator board is what creates the velocity fluctuations for controlling the flow, which are transported to the RoboStep via a network of hydraulic connections. The tuft array, for the purpose of reattachment location measurement, is an array of 989 hydro-tufts. Detail on the design of the novel hydro-tuft is given. Photographing the tuft array captured an instantaneous reattachment line. With the use of a MATLAB program developed by David Breakey, multiple tuft array photographs were averaged to attain a time-averaged reattachment line.

The experiments performed for Part II of this thesis have two main objectives; to compare results using the improved Beta actuator design with the results of Baugh (2010), and an investigation of the effect of large amplitude forcing on the flow.

Part I showed that the Alpha actuator, used for the experiments of Baugh (2010), exhibited deficient performance which increased experimental error due to actuation error. To gain insight into the amount of actuation error present in the results of Baugh (2010), and at which actuation cases the error is least, a select experiment

performed by Baugh is carried out using the improved Beta actuator so the results can be compared.

In the literature, previous backward-facing step experiments give little attention to the effect of forcing amplitude on the flow. They focused mostly on the effect of forcing frequency, and most use a single forcing amplitude for all experiments performed. Our actuators have the capability of producing perturbation amplitudes up to $u'/U_\infty = 2$, much higher than those used by others. The current experiments will explore more in-depth the effect of forcing amplitude on the flow to give more insight into this topic.

Chapter 11

Separating Boundary Layer Approximation

This chapter gives an investigation of the boundary layer characteristics at the point of separation (at the backward-facing step edge). It has been shown in many experimental results that boundary layer properties have a significant impact on reattachment behind the backward-facing step (example: Eaton & Johnston 1980; Oster & Wygnanski 1982; Westphal et al. 1984). Thus, it is of importance to have some understanding of the boundary layer properties at separation. No experimental data of the boundary layer properties was attainable during the time preceding writing, thus all values presented are approximate based upon calculations assuming Blasius and Falkner-Skan boundary layer solutions. A flow velocity at separation of $U_\infty = 0.45$ m/s was used for calculating the boundary layer, as this is the tunnel velocity at which all experiments presented in this thesis were performed. All calculations discussed here can be seen in entirety in Appendix H on page 153

The surface along which the boundary layer (BL) was calculated is shown in Figure 11.1 on the following page. It depicts the profile of the step-side tunnel wall, starting in the settling chamber just after the last turbulence screen and ending at the backward-facing step. Along the initial two meter section in the settling chamber, from x_0 to x_1, it is assumed a Blasius type BL develops. Within the settling chamber, the free-stream velocity is 0.074 m/s corresponding with the $U_\infty = 0.45$ m/s at separation. Using 0.074 m/s as the BL external velocity, U_e, and kinematic viscosity of $\nu = 1.005\text{E}^{-6}$ m^2/s, the Blasius momentum thickness at x_1 is equal to:

$$\delta_\theta(x_1) = 0.664\sqrt{\frac{\nu x_1}{U_e}} = 0.00346 \text{ m} \tag{11.1}$$

It should be noted that at x_1 the Reynolds number based on displacement thickness is equal to $Re_{\delta^*} = 664$. This is greater than the Tollmien-Schlichting wave

critical Reynolds number of 520 for a Blasius boundary layer, which indicates that the boundary layer is becoming unstable and could potentially be in an early transitional stage. However, due to the large favorable pressure gradient throughout the contraction, any instabilities are likely to be suppressed and the boundary layer relaminarized through the contraction.

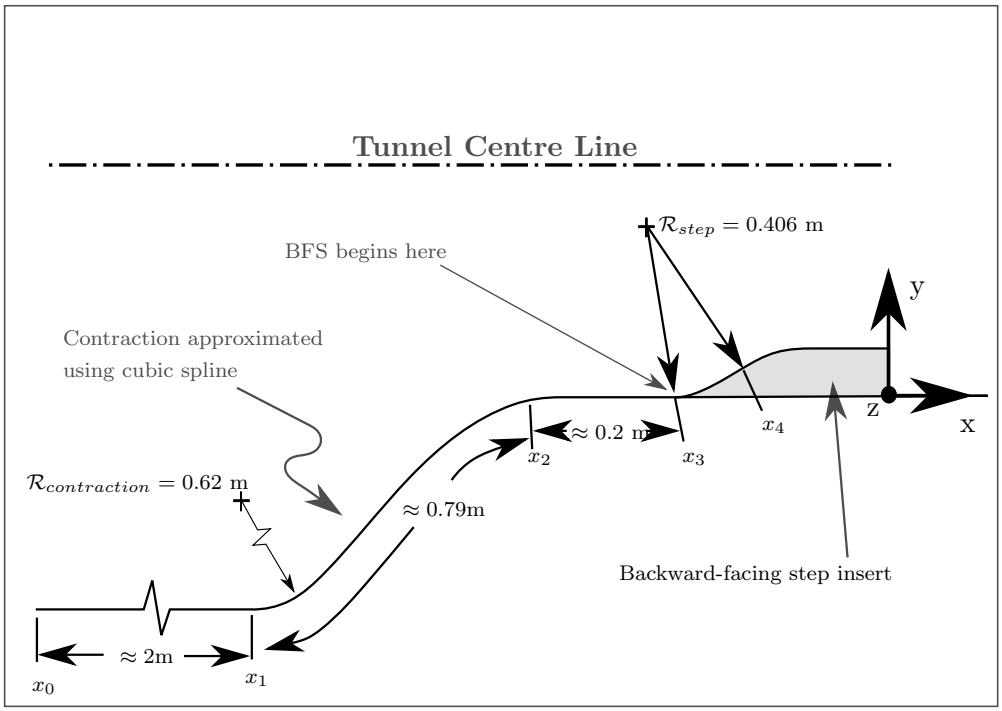

Figure 11.1: *Geometry used for approximation of boundary layer at separation. First two meters are within the tunnel settling chamber. Flow from left to right. (Image not to scale.)*

The tunnel contraction beginning at x_1 has a reduction ratio of 4.78 increasing the mean flow speed from 0.074 m/s to 0.36 m/s. Its profile was estimated using a spline consisting of two cubic functions constrained by position and slope at three points: x_1, the point of inflection along the wall, and x_2. The distance and location of the three points relative to each other was determined from a photograph showing the side profile of the contraction. The profiles of the perpendicular walls were calculated using the same method and assuming similarity in geometry. With the contraction geometry defined and using conservation of mass and Bernoulli's principle, the velocity and pressure gradient along the centerline of the water tunnel was calculated. Figure 11.2 on the next page shows the velocity profile and pressure gradient through the contraction. It should be noted that this calculated velocity profile along the tunnel centerline is not equal to, but intended to approximate the velocity external to the BL.

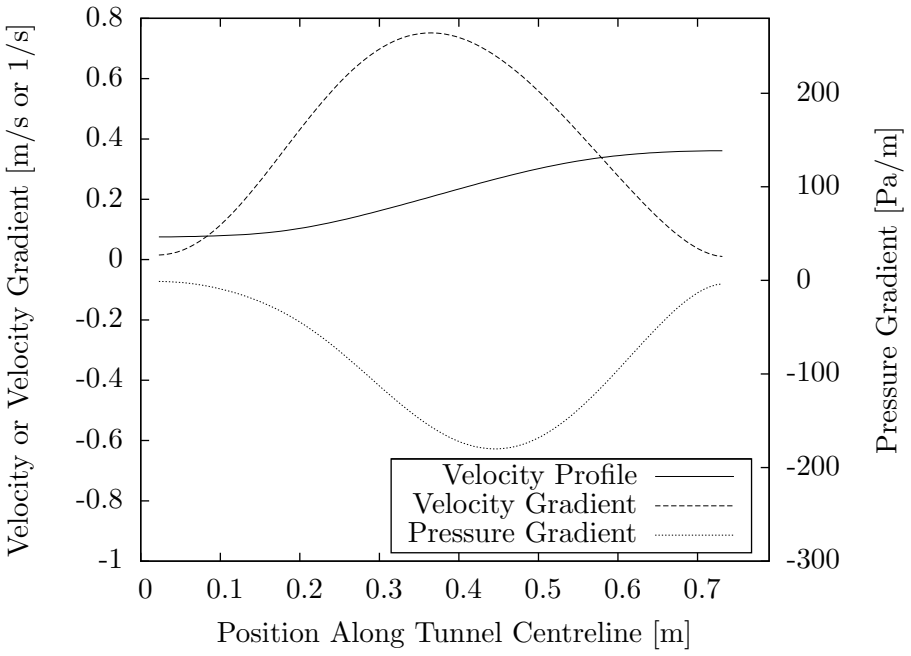

Figure 11.2: *Velocity profile and pressure gradient through tunnel contraction along the tunnel centerline (starting at x_1 and ending at x_2).*

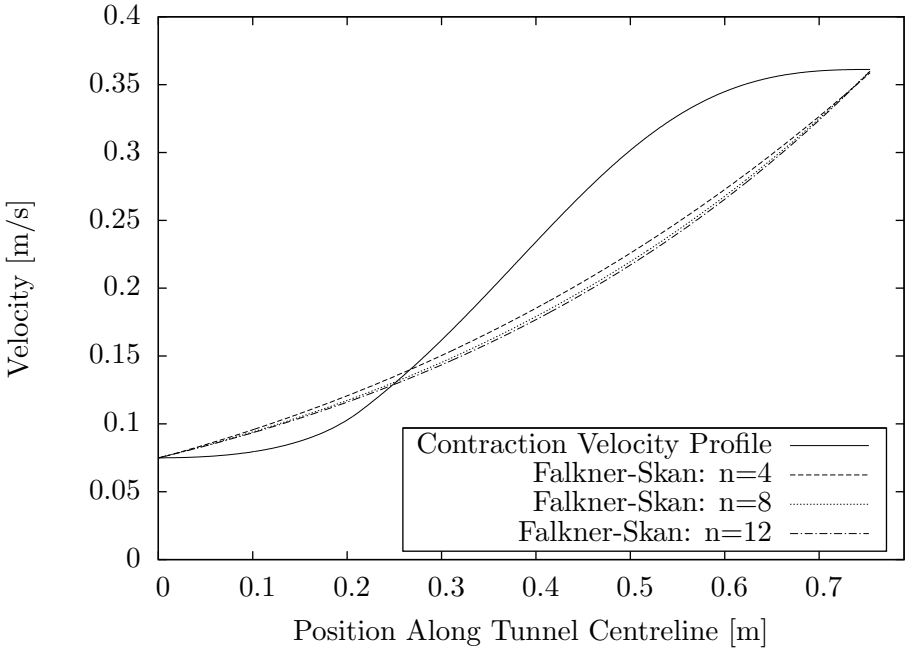

Figure 11.3: *Contraction velocity profile and Falkner-Skan velocity profiles meant to approximate the contraction velocity profile.*

For continuing the calculation of boundary layer growth through the contraction, a Falkner-Skan (FS) solution was chosen. Figure 11.3 shows a few velocity profiles of the Falkner-Skan form $U_{FS}(x) = a(x+b)^n$ used to approximate the calculated velocity profile along the tunnel centerline. Constants a and b are found by constraining the velocity at x_1 and x_2 to that of the calculated velocity profile at the corresponding points. The value b can be thought of a virtual starting point of the FS boundary layer. It can be seen that the FS velocity profiles are continually speeding-up up to the location x_2, unlike the actual flow which begins lessen in acceleration at approximately the halfway point. Since the FS velocity profile for $n > 0$ is continually increasing in acceleration, it will always have a smaller BL thickness than the actual flow.

The idea of using the Falkner-Skan BL solution is that for a particular FS velocity profile constrained to the velocity x-dependence at x_1 and x_2, its solution will have the same momentum thickness at the x_1 location as the incoming Blausius BL. Thus, the Falkner-Skan solution could be used to define a lower limit of the BL growth through the contraction.

To calculate the FS boundary layer thickness, a relation similar to equation 11.1 was required. After an in-depth search of literature, no data could be found giving the required relationship. This lead to the next option of numerically deriving the relation. The solution of the Falkner-Skan equation in its similarity form (11.2 & 11.3) was numerically solved for varying power n and the solutions integrated to give the coefficients for calculating boundary layer thickness. Some of the calculated values are listed in Table 11.1 on the following page. For the case where $n = 0$, which corresponds with a Blasius type boundary layer, the calculated coefficients agree very well with the accepted values of 4.9, 1.72, and 0.664. Full details on the solution can be seen in Appendix H.3 on page 156

$$f(\eta)''' + \frac{n+1}{2} f(\eta) f(\eta)'' - n f(\eta)'^2 + n = 0 \tag{11.2}$$

$$f(0) = 0,\ f'(0) = 0,\ f'(\infty) = 1 \tag{11.3}$$

Where: $\eta = \frac{y}{x}\sqrt{Re_x} = y\sqrt{\frac{U_{FS}(x)}{\nu x}}$

To calculate the desired boundary layer thickness, equation 11.4 on page 62 is used with a corresponding coefficient, a few of which are listed in Table 11.1. Where $U_{FS}(x) = a(x+b)^n$ is the velocity external to the boundary layer. This boundary layer equation is only valid for an external velocity profile of this form. For the case where b=0, the relation simplifies to the form in equation 11.5.

Table 11.1: *Numerical results: Falkner-Skan boundary layer coefficients for* $u/U = 0.99$ *thickness* ($\mathbf{C}_{\delta_{\mathbf{0.99}}}$)*, displacement thickness* ($\mathbf{C}_{\delta^*}$)*, and momentum thickness* ($\mathbf{C}_{\delta_\theta}$)

Power, n	$\mathbf{C}_{\delta_{0.99}}$	$\mathbf{C}_{\delta^*}$	$\mathbf{C}_{\delta_\theta}$
-0.0904	7.05	3.43	0.869
0	4.92	1.72	0.664
$\frac{1}{9}$	4.17	1.32	0.548
$\frac{1}{3}$	3.38	0.985	0.429
$\frac{1}{2}$	3.03	0.855	0.379
1	2.39	0.648	0.292
2	1.89	0.477	0.218
3	1.52	0.395	0.181
4	1.34	0.344	0.158
5	1.21	0.309	0.143
10	0.87	0.221	0.102
20	0.63	0.157	0.0725

$$\delta = (\mathbf{C}_\delta)\sqrt{\frac{\nu x}{U_{FS}(x)}} \tag{11.4}$$

$$\delta = (\mathbf{C}_\delta)\sqrt{\frac{\nu}{a x^{(n-1)}}} \tag{11.5}$$

It was initally hoped that a certain FS solution would give the same boundary layer thickness at x_1 as the incoming Blasius boundary layer from the settling chamber ($\delta_\theta = 0.00346$ m). Figure 11.4 shows a plot of FS momentum thickness at the contraction entrance and exit for varying power n. It shows that no FS solution will give the desired momentum thickness at x_1. Nevertheless, since the BL at x_1 is thinner than the incoming Blasius BL, these results are still able to define a minimum limit of BL thickness at the end of the contraction. It appears that the BL thickness follows an asymptotic behaviour with increasing n. The converging value at x_2 with increasing power n is approximately $\delta_{\theta^{asym}}(x_2) \cong 0.0004$ m. $\delta_{\theta^{asym}}(x_2)$ will be an acceptable lower limit as the actual boundary layer will certainly be of greater thickness.

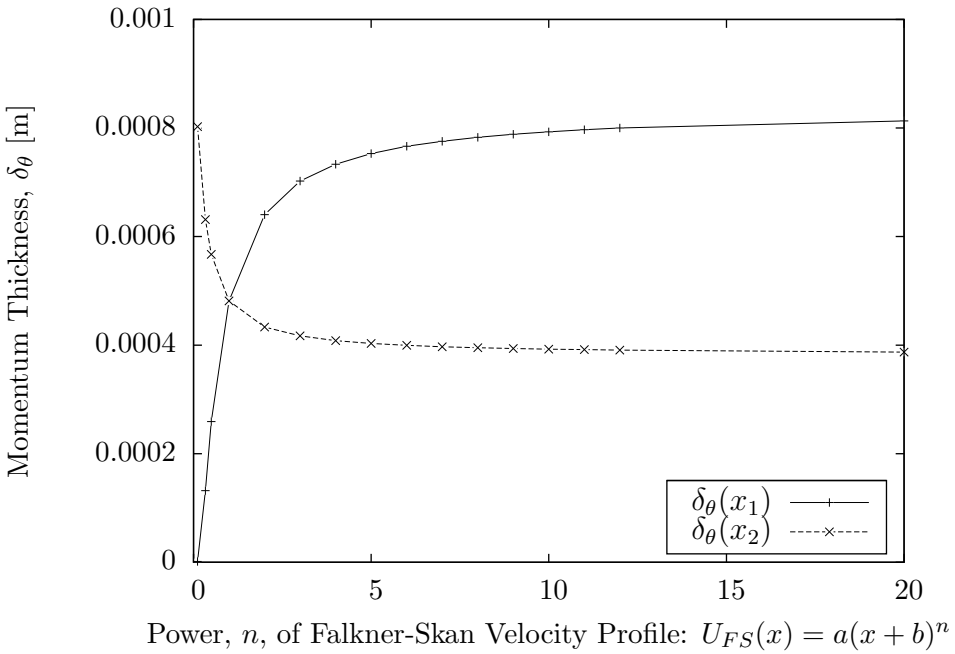

Figure 11.4: *Momentum thickness of the Falkner-Skan solutions at entry and exit of the contraction, x_1 and x_2, for varying power $\frac{1}{9} \leq n \leq 20$. NOTE: Falkner-Skan Velocity profiles are constrained by the free-stream velocity at the two locations x_1 and x_2.*

To define an upper limit of the BL thickness at x_2, the incoming BL thickness from the settling chamber can be used as long as the BL remains laminar through the

contraction. As previously discussed, due to the large favourable pressure gradient throughout the contraction, the BL will likely remain laminar. Thus, the momentum thickness at x_2 confined by the limits is:

$$0.0004 \text{ m} < \delta_\theta(x_2) < 0.00346\text{m}.$$

After the contraction, there is a 0.2m straight section before the beginning of the backward-facing step. The BL limits at x_2 can be extrapolated to give the limits expected at x_3. Using $U_e = 0.36$ m/s and defining virtual starting points for each limit which allow for a Blasius type BL to grow the same thickness at x_2, the limits at x_3 become:

$$0.00064 \text{ m} < \delta_\theta(x_3) < 0.00353 \text{ m}.$$

11.1 Görtler Instability

Before any further discussion on the growth of the laminar boundary layer, let us discuss the possibility of a Görtler instability and its impact on boundary layers. It is a boundary-layer instability which can lead the flow though a transition to turbulence where it would otherwise have been laminar. Its presence is found in curved flows and is driven by an adverse gradient in angular momentum, where the *centrifugal* forces overcome viscous forces. The word centrifugal is emphasized above as to remind that it is not a real force and only used here to help understanding of the apparent forces within a Lagrangian frame of reference.

The Görtler instability is part of a family of three similar instabilities which are driven by the same mechanism, but all vary in flow geometry. The result of these instabilities produces counter rotating streamwise vortices. The first of the family discovered is named after Geoffrey Ingram Taylor. The Taylor problem examines the source of the instability observed in a rotating Couette flow. Whenever the inner cylinder has a larger angular velocity than the outer, there is an adverse gradient of angular momentum. Albeit that the flow problem is name after Taylor, it was first considered by Rayleigh in 1888 (Kundu 2008). Rayleigh examined the source of instability neglecting viscosity. To explain Rayleigh's findings an explaination adopted from Kundu (2008) will be given here. Consider two fluid rings of equal mass at r_1 and r_2 ($> r_1$). Their angular momentum will be proportional to the product of their velocity and radius: $\Omega \propto rU_\theta$. If the two fluid rings interchange radial positions, they will maintain their angular momentum. This can be verified by the well known principle of conservation of momentum. Since momentum is conserved, U_θ must change during the interchange. U_θ is also proportional to the

kinetic energy of the fluid ring, thus the kinetic energy must also change. If the sum of the kinetic energy of the two rings before and after the interchange is compared:

$$KE \propto \frac{U_\theta^2}{2} = \frac{1}{2}\frac{\Omega^2}{r^2}$$
$$KE_{initial} \propto \frac{1}{2}\left[\frac{\Omega_1^2}{r_1^2} + \frac{\Omega_2^2}{r_2^2}\right]$$
$$KE_{final} \propto \frac{1}{2}\left[\frac{\Omega_1^2}{r_2^2} + \frac{\Omega_2^2}{r_1^2}\right]$$

Taking the difference in kinetic energy:

$$\begin{aligned}\Delta KE &= \frac{1}{2}\left[\left(\frac{\Omega_1^2}{r_2^2} + \frac{\Omega_2^2}{r_1^2}\right) - \left(\frac{\Omega_1^2}{r_1^2} + \frac{\Omega_2^2}{r_2^2}\right)\right] \\ &= \frac{1}{2}\left(\Omega_1^2 - \Omega_2^2\right)\left(\frac{1}{r_2^2} - \frac{1}{r_1^2}\right)\end{aligned}$$

Since r_2 was defined as larger than r_1, the sign of ΔKE is dependent upon the difference in angular momentum term. Observe that if Ω_1 is less than Ω_2, the change in kinetic energy is positive. This implies that an external source of energy is required for the interchange to occur. Under this condition interchange will not occur spontaneously, and the flow is stable. However, if Ω_1 is larger than Ω_2, the interchange will result in energy released. In this condition spontaneous interchange can occur as the flow tends to a lower energy state, resulting in an unstable condition. The condition for instability is formally stated as Rayleigh's circulation criterion (Equation 11.6) where circulation Γ is used apposed to angular momentum Ω: ($\Gamma = 2\pi r U_\theta$).

$$\frac{d\Gamma^2}{dr} < 0 \quad \textbf{Unstable} \tag{11.6}$$

With viscosity present, Rayleigh's circulation criterion is only a necessary condition for instability. One could expect stability up to some critical limit with the presence of an adverse angular momentum gradient. Taylor, in 1923, expanded Rayleigh's result in his classic work on the stability of viscous circular Couette flow. In the case of the inner cylinder rotating and the outer fixed, Rayleigh's criterion is satisfied. Due to the presence of viscosity, only at a critical inner cylinder velocity will the first signs of instability show as counter rotating toroidal vortices called Taylor vortices. Taylor's solution indicates that the viscous flow remains stable until a critical Taylor number.

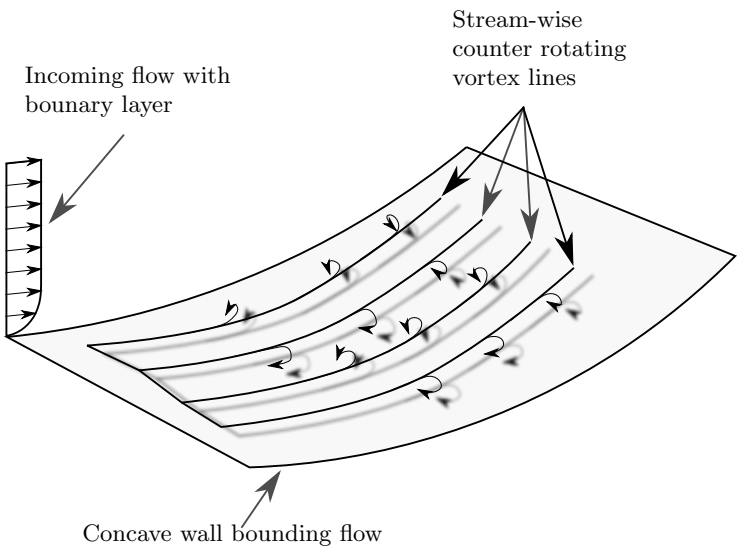

Figure 11.5: *A simplified sketch of Görtler vortices along a concave wall. They form as counter rotating stream-wise vortices within the boundary layer.*

Another instability named the Dean instability is present in a fully developed curved channel flow. Rayleigh's circulation criterion is satisfied within the boundary layer along the outer race of the channel. This type of instability is much closer to the Görtler instability then the Taylor problem, as it occurs due to the presence of a boundary layer. Its difference from the Görtler problem comes from the streamlines of the basic state being parallel. Having parallel streamlines creates a more simplified problem compared to the Görtler problem (Saric 1994).

The Görtler problem is the most intricate of the three. It is similar to the Dean problem, except that the basic state need not have parallel streamlines. It can be thought of as a more general case of the Dean problem and is present when ever a viscous fluid flows along a concave surface. Figure 11.5 shows a simplified sketch of Görtler vorticies along a concave wall. Since the destinction between these flows has not always been clear, the name Taylor has often been associated with all three.

Like the Taylor problem, there is a critical Görtler number which indicates the onset of the Görtler instability. The Görtler number is defined as in equation 11.7:

$$G\ddot{o} = \frac{U_\infty \delta_\theta}{\nu}\sqrt{\frac{\delta_\theta}{\mathcal{R}}} \tag{11.7}$$

Where $\mathcal{R}$ is the radius of curvature of the concave wall.

Since the Görtler problem was first examined by H. Görtler in 1941, there has been many researchers exploring the problem theoretically and experimentally. A recent theoretical study by Kim, Choi, and Yoon (2010) gives a comparison of

previous predicted critical Görtler number with theirs. Table 11.2 below repeats these values. Kim et al. (2010) also compare their results to an experimental study of Hans W. Liepmann (1945). Liepmann's results for a large radius of curvature ($\mathcal{R} = 20$ ft), zero pressure gradient, and low turbulence level (0.06%) give a critical Görtler number of $G\ddot{o} = 7$. This is larger than the theoretical results presented in Table 11.2, but still in reasonable agreeance. Justification of the difference is given by Kim et al.; since linear theory deals with infinitesimal disturbances, it is possible that the difference between theory and experimental results is due to the fact that only finite disturbances are actually observed. The infinitesimal disturbances must grow appreciably before they can be observed.

Table 11.2: *Comparison of critical Görtler numbers from various authors under zero pressure gradient* (Kim, Choi, Yoon, 2010).

Author	**Critical Gö**
Kim, Choi, Yoon 2010	1.738
Lin and Hwang 1999	2.184
H. Görtler 1941	0.3138
G. Hämmerlin 1955	0.1683
Th. Herbert 1976	0.3000
Floryan and Saric 1982	0.2509

These results presented above are for the case of zero pressure gradient. It is well known that pressure gradient strongly affects the position of transition to turbulence of a laminar boundary layer along a flat or convex surface. Under these conditions no adverse angular momentum gradient is present and thus the Tollmien-Schlichting instability is the dominant transition to turbulence mechanism. When the flow is along a concave surface, the Görtler instability along with the TS-instability is present. It can be foreseen that at a low radius of curvature the TS-instability can be of greater influence than the Görtler instability and vice versa.

Liepmann (1945) performed an experimental investigation of the affect pressure gradient has on the critical Görtler number of a laminar boundary layer along a concave surface. He performed these experiments using a radius of curvature of $\mathcal{R} = 2.5$ ft $= 0.762$ m and free-stream turbulence of 0.06%. His results showed no appreciable change with pressure gradient within experimental error. Accordingly, his conclusions stated that the influence of pressure gradient on transition along concave surfaces has zero or small effect and that the dominant mechanism of breakdown to turbulence is the Görtler instability.

11.2 Continuation of the Separating Boundary Layer Approximation

Now with a bit of background and understanding of the driving mechanism of the Görtler instability, let us continue discussion of the boundary layer leading up the backward-facing step. The discussion will continue at the point x_3 with the limits on boundary layer momentum thickness:

$$0.00064 \text{ m} < \delta_\theta(x_3) < 0.00353 \text{ m}.$$

The initial section of the backward-facing step is concave with a radius of curvature of $\mathcal{R}_{step} = 0.406$ m. This radius was calculated from the intersecting lines perpendicular to the beginning and end of the concave section. Using the free-stream velocity $U_\infty = 0.36$ m/s and the two limits of boundary layer thickness, the limits of the Görtler number at the initial concave section of the step are:

$$9.10 < G\ddot{o} < 118$$

Even at the lower limit, the flow is predicted as Görtler unstable. Since the curvature of the ramp leading up to the BFS is greater than in the experiment performed by Liepmann, it can be expected that the Görtler instability is dominant and the "favourable" pressure gradient will have zero or small effect on transition, and will alternatively aid the developement of any recently generated Görtler vortices by stretching. This indicates that the transition to a turbulent boundary layer at the ramp leading up the backward-facing step is probable.

Calculating further growth of the boundary layer over the remaining 0.12 m section along the top of the BFS would not add much to our knowledge of the separating boundary layer at this point: for the momentum thickness to change, the wall needs to "absorb" momentum from the flow. Since this remaining distance is much smaller than the full length over which the boundary layer has developed, it is unlikely that the momentum thickness will grow appreciably. Thus, it would be satisfactory at this point to assume the boundary layer at separation is of a momentum thickness in the order of the preceding limits and embedded with counter rotating Görtler vortices.

$$\boldsymbol{\delta_\theta}|_{\text{separation}} \sim \mathbf{0.003} \text{ m}. \tag{11.8}$$

Chapter 12

Experimental Apparatus

12.1 Overview

All experiments discussed in this thesis were performed in the High-Speed Water Tunnel (HSWT) located in the Mechanical Engineering building at the University of Alberta. Components of the apparatus will be discussed in the following sections. Discussion of the actuator board will be limited to its connection with the experiment. For a detailed discussion of the actuator board see Part I of this thesis.

The HSWT, originally designed to be used as an icing water tunnel in 1974, was recommissioned by Dr. Sigurdson and Coward, A. (2004) to be used as a flow visualization water tunnel. It circumnavigates a two level laboratory on the 5^{th} and 6^{th} floors of the mechanical engineering building. Figure 12.1 shows an overview of the tunnel configuration. The lower level lab holds a 100 horsepower DC motor to power an impeller which drives the water tunnel flow. On the top level is the settling chamber with flow straighteners and turbulence screens for breaking up turbulence into smaller scales. Downstream of the settling chamber, the tunnel contracts into the test section. Here at the upstream portion of the test section the backward-facing step is positioned. The test section has a cross-section of 0.47m high by 0.27m wide, and a length of 2.1m. There are two sets of acrylic windows on the top, bottom , and front, back sides for viewing the flow.

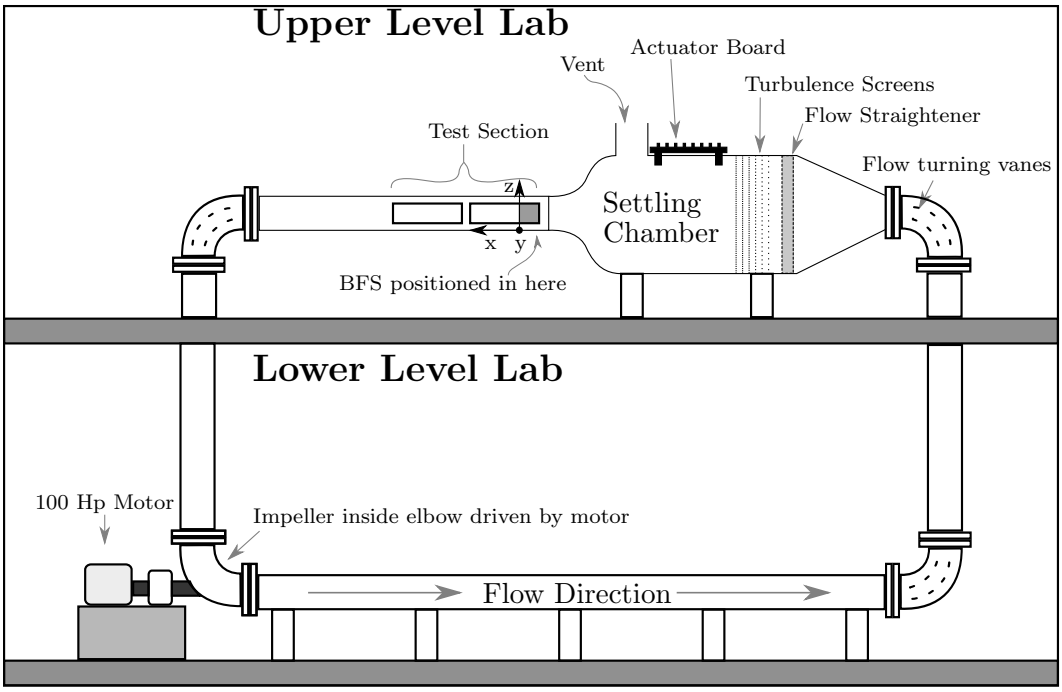

Figure 12.1: *Configuration of high speed water tunnel. The backward-facing step is positioned in the upstream portion of the test section. Note the Cartesian coordinates at the step edge. (Not to scale)*

12.2 Backward-Facing Step Insert

The backward-facing step (BFS) insert, named the "RoboStep", is located inside the test section of the water tunnel. It was designed by Gilbert (2007). Downstream of the RoboStep is where the experimental point of interest lay, as this is where the recirculation zone forms. Figure 12.2 shows the geometry of the step and its orientation in the tunnel. As well, basic flow geometry, actuation port location, and dye injection slit is illustrated. Note the coordinate system which is the same as in Figure 12.1. The step is itself made of three smaller modules. Figure 12.3 shows the full step and the exploded view of the three individual modules; the dye reservoir module (1), the actuator slot module (2), and the step module (3).

A list of the backward-facing step dimensions including the ones shown in Figure 12.2 is given in Table 12.1 on page 72. As will be discussed in Section 12.4, a tuft array located along the base wall of the test section behind the BFS was used for reattachment line measurement. The tuft array base plate has a thickness of 1/8 inches which shortens the step height, h, and test section height, H, when in place. Thus, two columns are listed; one with values adjusted for the tuft array thickness, and the original values without the tuft array in place.

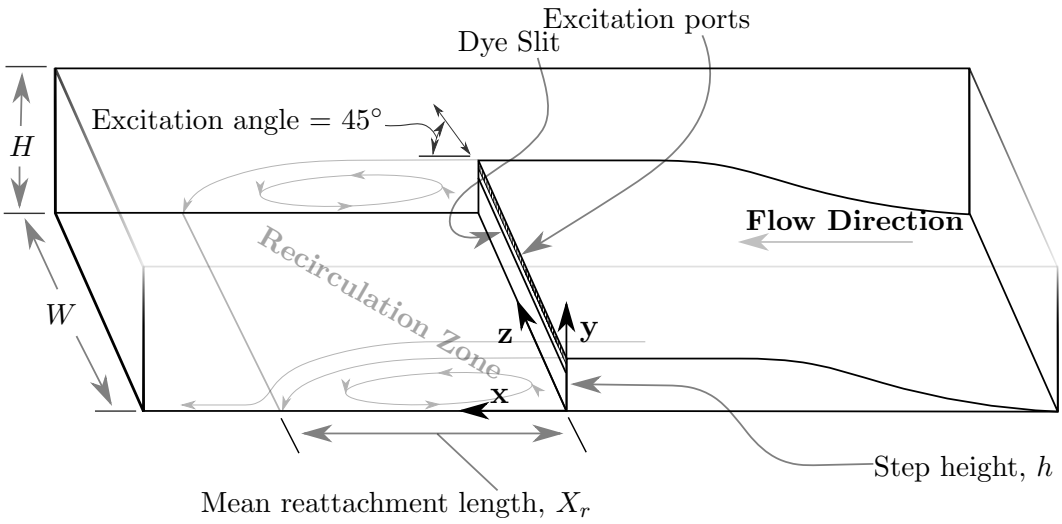

Figure 12.2: *Basic backward-facing step module geometry. Shows configuration of BFS in test section, and basic flow geometry. NOTE: flow is right to left. (Figure not drawn to scale.)*

The actuation ports, arranged evenly along the back side of the step edge, are where the flow perturbations created by the actuator board are introduced into the flow. There are 128 ports along the step edge, all of which have hydraulically independent connections to an actuation source. Thus, actuation can be varied along the span to give a spanwise varying actuation for investigation into forcing the three-dimensional aspects of BFS flow. Since the current Beta actuator board consists of 16 individual actuators, each actuator was connected to eight of the 128 actuation ports. As shown in Figure 12.2, they are orientated such that the perturbations enter the flow along a plan inclined 45° to the flow direction with one axis along the step edge.

There is a dye injection slit located 1.5 mm below the step edge which spans the step width. Here dye enters the flow for flow visualization along the lower side of the free shear layer behind the step. Dye flows first into the dye reservoir module (Figure 12.3(1)), which acts as a buffer to collect dye and help produce even pressure along the dye slit for uniform dye emanation into the flow. The height of the dye slot is approximately 0.4 mm and can be adjusted via 6 set screws. This adjustment capability was a modification made by Baugh from Gilbert's original design which can be used to even the slot width along the span. However, the modification originally came about to fix a leakage between the dye module and actuator module. More detail on the fixing of the leakage problem in given in Baugh's Master's thesis (2010).

The actuator slot module (Figure 12.3(2)) created passage of the perturbation

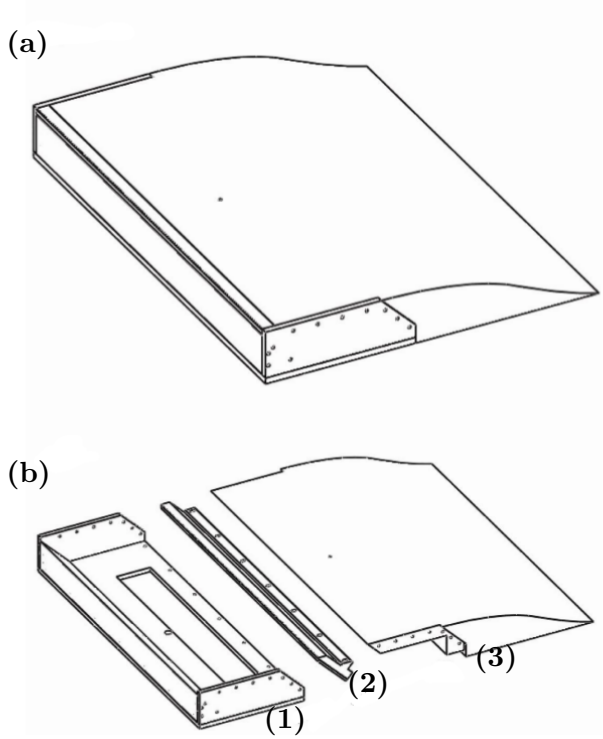

Figure 12.3: *The RoboStep (a), and its modules (b). The exploded view (b) shows the three RoboStep modules: dye reservoir module (1), the actuator slot module (2), and the step module (3). Image courtesy of Baugh (2010).*

flow from the test section wall to the actuation ports at the step edge. Actuation was passed to the actuator slot module via 128 small diameter actuation tubes. For this to happen, all the actuation tubes needed passage through the water tunnel wall. The passages were located at the base of the dye module. Sealing at the wall of the water tunnel test section was done using a 3/16 inch thick soft rubber gasket inserted between the dye module and test section wall. Appropriate holes in the gasket allowed the actuation tubes and dye tube to pass through.

The main step module, module (3) in Figure 12.3, was machined from a single piece of aluminium. It was designed to ensure that the flow leading up to the step edge does not separate (Gilbert 2007). Detailed criteria and design considerations are given in Gilbert's Master's thesis (2007).

Table 12.1: *Pertinent backward-facing step geometry dimensions. Original values shown in the second column and values adjusted for the tuft array base plate thickness in the third column.*

Parameter	**Original Values**	**Adjusted for Tuft Array**
Effective step height, h [cm]	5.54	5.23
Step width, W [cm]	45.72	45.72
Actuation span width, W_a [cm]	44.45	44.45
Step aspect ratio, $AR = \frac{W}{h}$	8.25	8.75
Actuation aspect ration, $AR_a = \frac{W_a}{h}$	8.02	8.51
Test section height, H [cm]	25.4	25.08
Inflow section height, $H_i = H - h$ [cm]	19.86	19.86
Expansion ratio, $ER = \frac{H}{H_i}$	1.28	1.26

12.3 Hydraulic Connections

The hydraulic connections consists of a network of tubes which transport the perturbations created by the actuator board to the backward facing step inside the test section. As seen in Figure 12.1, the actuator board is positioned above the settling chamber. This actuator position is at the same level as the free surface of the water in the water tunnel vent. Thus, the hydrostatic pressure experienced by the actuators is equal with the atmosphere, relieving the actuators of unnecessary load.

The design of the hydraulic connections was proposed by Gilbert (2007). This adaption of this design into a complete system, including establishment of component locations, and design of support structures was undertaken by Baugh (2010).

Figure 12.4 shows an overview of the entire hydraulic connection system. Starting at the actuators, 3/8 inch inner diameter tubing is press fit onto the luer lock fitting of the syringes. These tubes run a length of 244 cm before connecting to individual manifolds (12.4(b)). Each manifold divides the actuation flow from a single actuator into eight branches of 1/8 inch inner diameter tubing creating a total of 128 branches. Each of the 1/8 tubes run a length of 122 cm before connecting with barbed reducing fittings. These fitting were originally designed to connect with a sealing plate at the test section wall where they would pass through to con-

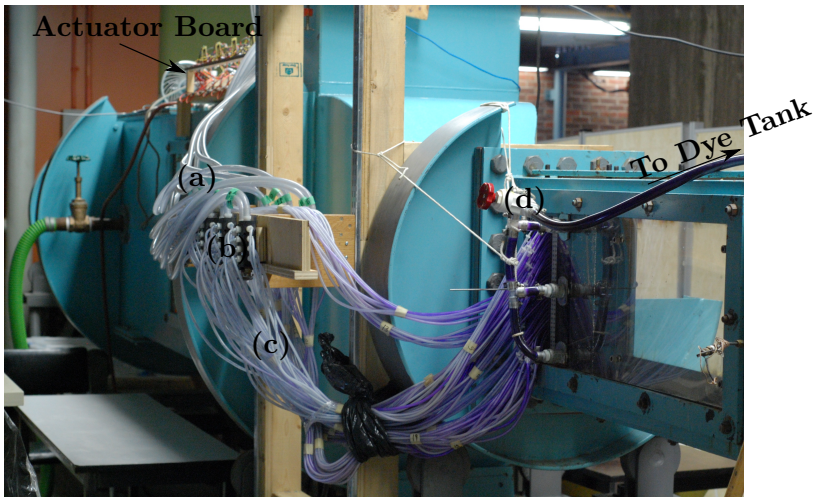

Figure 12.4: *Overview of hydraulic connections: large diameter tubes coming from actuator board (a), manifolds dividing perturbations into smaller diameter tubes (b), smaller diameter tubes traverse remaining distance to actuator slot module (c), valve for controlling dye flow into dye module (d).*

nect with the backward-facing step. However, it was determined that sealing of the water tunnel from the dye module on the inside was sufficient to prevent leakage (Baugh, 2010). The reducing fittings instead connect each 1/8 tube with a 3/32 inch inner diameter tube. These final small diameter tubes run 30.5 cm where they pass through the test section wall and connect with the actuator slot module of the backward facing step. The actuation ports in the actuation module run a length of approximately 5.5 cm before reaching the step edge and are of rectangular cross section, 2.5 mm by 1 mm.

In the original design by Gilbert of the hydraulic system, there existed a "back pressure" reservoir. This reservoir was used for the special actuation cases when 22 actuators were in use. Since the current Beta actuator board has 16 actuators, this back pressure reservoir is no longer used. For more explanation on the use of the reservoir, see Gilbert's Master's thesis (2007).

12.4 Tuft Array

A Tuft, also known as a telltale or yaw string, is commonly used in aeronautical research for visualizing flow direction along a surface. When exposed to a flow, a drag force acts upon the tuft which causes it to yaw into the direction of flow. This property makes an array of tufts an effective tools for visualizing a reattaching flow where the shear stress along the surface is of opposing sign on either side of the reattachment location. Thus an array of tufts was adopted for locating the

reattachment line behind the step, as the reattachment line is defined by the line of zero shear stress (Equation 1.1 on page 2).

For water flows, a suitable tuft has not been found before the innovations presented here. The tuft array design was initially carried out by NSERC Undergraduate Summer Research Assistant Dory Parsonage. It was designed to fill the entire width of the test section step-side wall (453 mm), and starting from the step edge spans a distance of 870 mm $\approx 159h$ downstream. The base plate was constructed of a Transparent 1/8 inch thick polycarbonate sheet. In this plate, a grid of 1 mm diameter hole spaced at 20 by 20 mm was drilled to give placement locations for the tufts. With the tufts mounted into the holes they would protrude into the flow perpendicular to the test section wall, thus eliminating any directional bias which would be present if the tufts were mounted flat to the surface of the plate.

12.4.1 Requirement of the Hydro-Tufts

The demand of performance from the tuft array was of considerable extent. Flow within the reattachment zone has significantly lower velocities than that of the mean flow. In an experimental study done by Eaton & Johnston (1980) on the flow structure behind a backward-facing step, they measured a maximum reverse-flow velocity within the recirculation zone of $0.21U_\infty$, where U_∞ is the free-stream velocity before the step. This is in good agreement with the work done by Yoshioka et al. (2001) who used a PIV measurement and found a maximum reverse flow of 18% U_∞. The free-stream velocity used for all experiments using the tuft array in this thesis was 45 cm/s. This gives a maximum mean reverse-flow velocity of approximately 9.5 cm/s. As the reattachment zone is approached, the mean velocity becomes less.

At these low velocities, the drag force exerted on the tufts becomes considerably small. Thus a material and tuft shape needed to be found which was flexible enough to yield to these small forces. As well, the tuft material had to be able to withstand prolonged use in the aqueous environment.

12.4.2 Hydro-Tuft Design

The aim is to produce 989 tufts constrained to the size limited by the tuft plate grid spacing, and sensitive enough to respond to low velocity flows as described in Section 12.4.1. It proved quite difficult to find a material flexible enough to respond to such a low flow.

Initial research on tuft material was carried out by a NSERC Undergraduate Summer Research Assistant, Dory Parsonage. The extent of his work examined many tuft materials, the most note worthy being: sewing thread, Dacron braided

fly-fishing line, thin strips of both high and low density polyethylene (HDPE & LDPE), thin strips of polyvinylidene chloride (PVdC), and thin latex strips. For the manufacturing of tufts of HDPE, LDPE, PvdC, and latex, Parsonage would cut thin strips out of 0.005-.01 in. thick sheets of the material using two razor blades firmly held together. This method, easy to replicate, would give consistent tuft widths of the same width as one razor blade.

Of all the listed materials above, only the latex tufts were flexible enough to succumb to the flow for adequate use of reattachment measurement. Albeit, his discovery of the latex tufts still had two inherent problem: first being after a day of submersion, the latex would begin to deteriorate, inevitably leading to complete failure of the tuft. Second, installing the 989 tufts in the plate can take an astronomical amount of time! An adhesive with a quick set time to reduce tuft mounting time was preferable. The adhesive selected for this purpose was a cyanoacrylate. This adhesive would alter the latex, making it brittle at the attachment point. A new material was needed with the similar flexibility but with resistance to deterioration in water and chemical resistance to the adhesive. Further exploration was carried out by the author.

A material group which could meet these requirements is silicone rubber. Silicone rubbers can be a very soft material, generally non-reactive, can resist extreme temperatures, and are stable. To produce tufts from this material, it needs to be in a form of a thin sheet so the tuft shapes could be cut from it. However, this proved to be difficult to find a suitable silicone rubber in this form.

The next approach was to look for ways of producing sheets of the desirable rubber. One grade of silicone rubber known as liquid silicone, which is a platinum cure silicone rubber, was just what was needed. It is typically supplied in two liquid parts, one with the platinum catalyst. When the two parts are mixed it cures into a rubber of any shape or form desired. These rubbers are often used in the medical and show biz industries due to their excellent biocompatibility, and realistic flesh appearance and flexibility for making costumes. This ability to form the rubber in a desired form makes it an ideal tuft material candidate.

To produce sheets of the liquid rubber, a press was devised. Figure 12.5 shows the press used to make thin sheets of the rubber. It's comprised of two 900 kg granite slabs (a), two, one inch thick glass plates (b), and a chain hoist to raise and lower the top granite slab. The granite slabs where adopted from an inoperable vibration isolation table. Their mass provided the force for pressing the liquid rubber into a flat sheet. Since the granite surface had some roughness, the two plates of glass were used to produce a smooth sheet. The procedure started by mixing the two parts of the rubber which was then poured onto one of the glass plates. The other glass plate was then placed on top and the top granite slab lowered to compress the

liquid into a thin film.

The resulting rubber sheet thickness was varied by changing the pressure exposed to the liquid rubber mixture. Since the force exerted by the press was constant (the weight of the top granite slab), the pressure was varied by varying the amount of liquid rubber placed between the glass plates; the more rubber applied, the wider it would spread and the less pressure it would encounter resulting in a thicker sheet. After several tests, uniform sheets of four thousands of an inch thick were reliably reproduced. It was observed that sheets thinner than this would not be stable and could easily tear.

The liquid rubber used for the hydro-tuft material is called Dragon Skin®, manufactured by Smooth-on. Figure 12.6 shows the liquid rubber used with the red dye for colouring the rubber(a), and the order of production, starting with a sheet (b), which is cut into stripes as wide as the desired tuft length of 3/4 inch (c), and final tufts (d). To cut the 3/4 inch strips into individual tufts, the technique used by Parsonage with the razor blades was extrapolated. Figure 12.7 shows the die used for cutting the tufts (b). It holds 20 razor blades pressed together which can be used to punch out individual tufts with the blow of a hammer on the backside.

Figure 12.7 shows the apparatus used for installing tufts. The tuft array is supported in a wooden frame which is itself mounted at the back end using a C-clamp so the frame can over hang the work bench, making the tuft plate accessible from both top and bottom sides. When debris or an old tuft needs to be cleared from a tuft hole, tool (a) which is a 1 mm drill bit mounted into a metal handle is used. It needs to be pushed through the hole several times until all is clear.

The easiest method for installing tufts is to insert a tuft through a hole. It needs to be held with one hand on the bottom side so a few millimetres protrude past the top of the tuft plate. With the other free hand, some adhesive is dabbed onto the protruding end and then carefully pulled into the hole so it becomes flush with the top side. The glue will pull the tuft to the inside of the hole by forces of adhesion. As well, due to the forces of adhesion and viscosity of the glue, the tuft can be immediately released without having to hold it in place until the glue dries. This greatly speeds up the installation process.

12.4.3 Performance of Tufts

The new tuft material made of Smooth-On, Dragon Skin® exceed expectations. It has a shore A hardness of 10, which is four times lower than that of the latex used for the previous tufts. This is a substantial reduction in hardness which indicates the silicone rubber should yield easier than the latex tufts, making them more responsive to flow. As well, the rubber is chemical resistant and will not deteriorate in water.

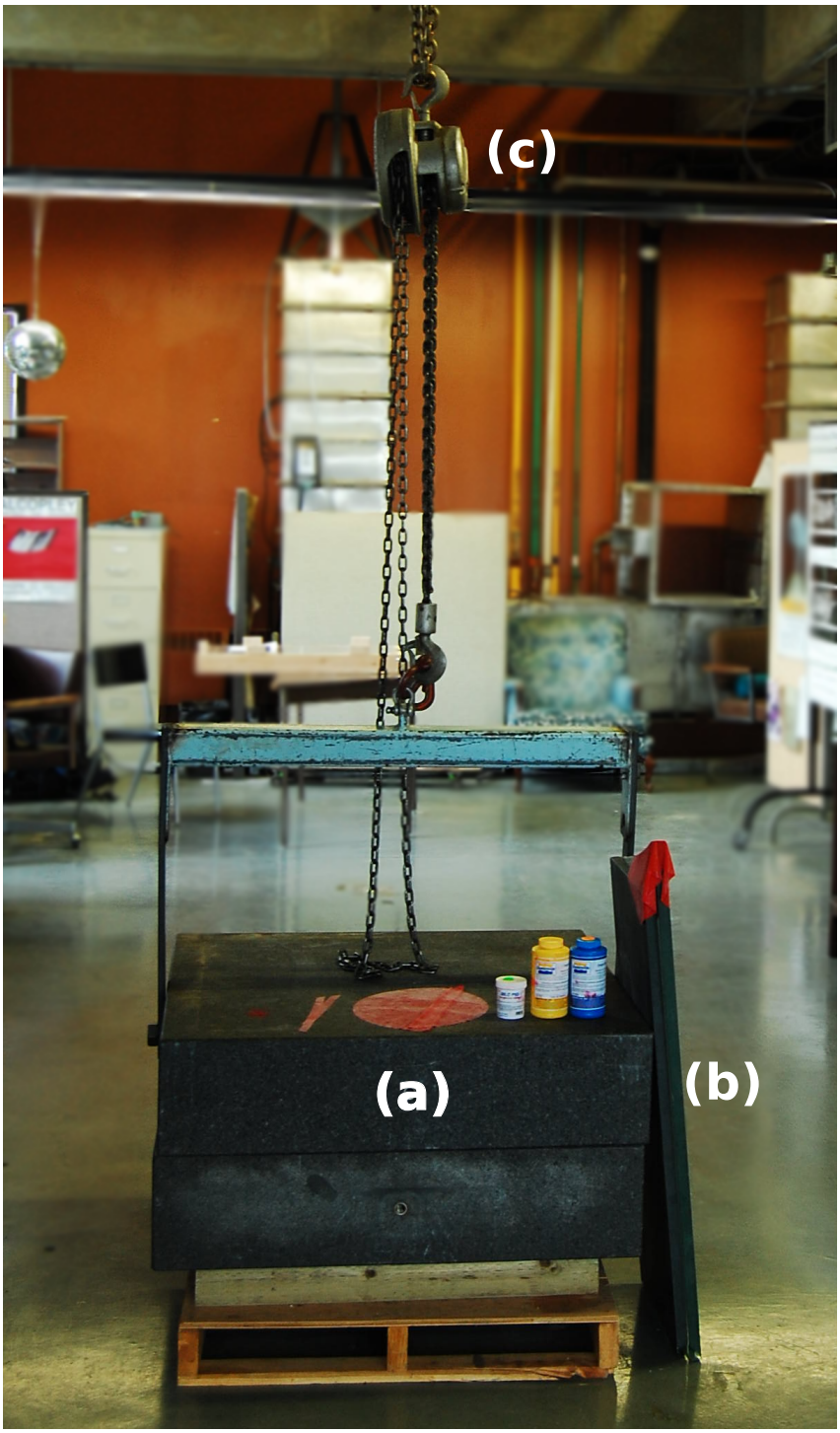

Figure 12.5: *Tuft press: showing the two glass plates (b) leaning on the right side of the granite slabs (a), and the chain hoist (c) for lifting the granite slab.*

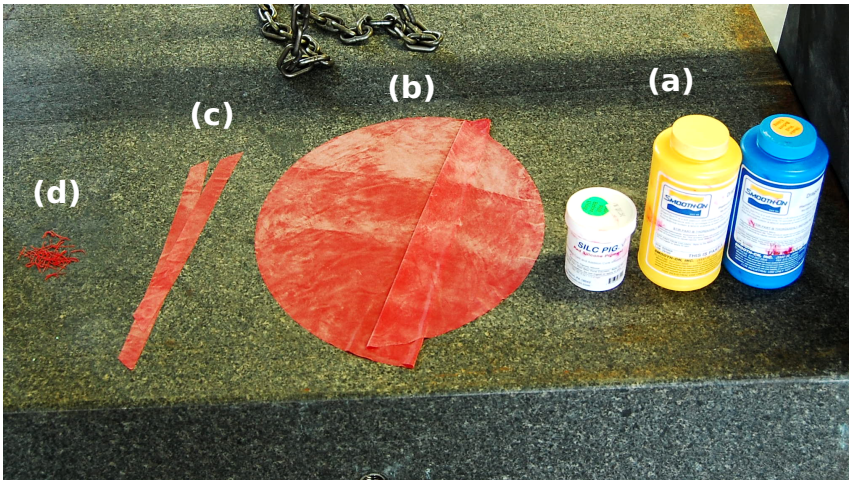

Figure 12.6: *Tuft material and production order. Smooth-on Dragon Skin® liquid rubber (a), 4^{thou} thick silicone rubber sheet (b), 3/4 wide strips (c), and the final tuft (d).*

Only testing the new tuft array will answer whether they are truly an improvement from the previous. During assembly of the tuft array, no signs of deterioration of the rubber was present from reaction with the cyanoacrylate adhesive, as was the case with the latex tufts. As well, to the date of writing, the tuft array has spent approximately 5000 hours submerged in the water tunnel. Over this time it had become stained from rust and other contaminates. Several times it was cleaned using bleach and a calcium rust lime remover which contained: lactic acid, gluconic acid, glycolic acid, sulfamic acid, citric acid, phosphoric acid, and surfactants. Even after all this exposure the tuft array still shows no sign of deterioration.

The other test is to determine the tuft array's functional limit. This limit is the lowest tunnel free-stream velocity to which the tuft array can indicate reattachment. As well, the tuft sensitivity (the lowest flow velocity in the vicinity of a tuft to which it will react and indicate the flow direction) is of interest.

Dean's Research Award student David Sutton (2010) was employed to determine the tuft sensitivity and functional limit of the tuft array. Mr. Sutton noted that in order for the reattachment location to be observed, there is a requirement that a line of tufts are pointing both upstream and downstream on their respective sides of the reattachment line. The minimum tunnel free-stream velocity for this condition to occur was measured by slowly decreasing the tunnel velocity until the reattachment line could no longer be observed. The tuft array functional limit was found to be at a tunnel free-stream velocity 5.8 cm/s, corresponding with $Re_h \approx 3000$. As the flow approached reattachment, it is expected that the flow mean and fluctuating velocities are lower than the free-stream velocity. Thus, the tuft sensitivity will be less than approximately 5 cm/s.

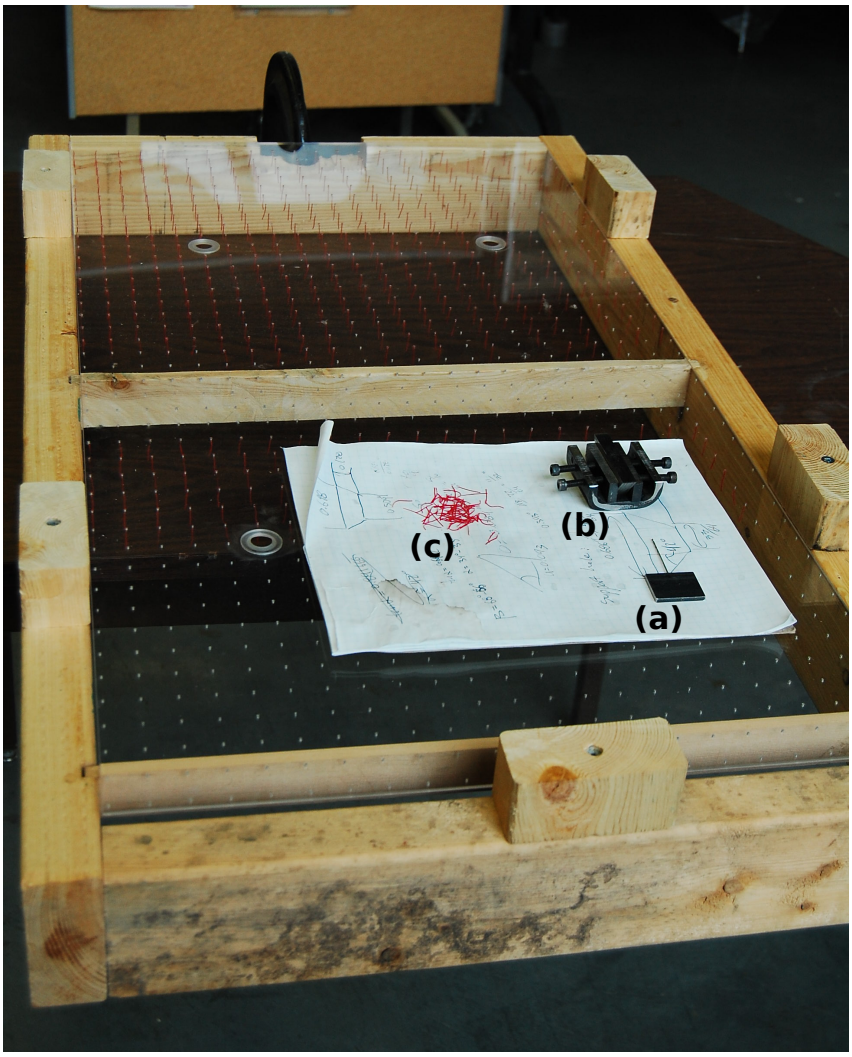

Figure 12.7: *The installation of tufts to create the tuft array. Showing a tool consisting of a 1 mm drill bit and handle (a) for cleaning a hole in the tuft board when a tuft needs to be removed or replaced, tuft cutting dye (b), pile of tufts waiting to be installed (c).*

Chapter 13

Methodology

13.1 Reattachment Location Measurement

All experiments performed for the current study required the measurement of reattachment length, X_r, behind the backward facing step. This length is a key index for the flow characteristics and how forcing introduced at the step edge affects the flow. As described in Section 12.4 on page 73, a tuft array was designed to fulfill this purpose. The array contains over 989 tufts spaced along a twenty by twenty millimetre grid. Data collection for reattachment measurement involved photographing the tuft array during steady state operation of the water tunnel. This was done using a Nikon D1X digital SLR camera with 3008 by 1960 pixel resolution. To minimize distortion in the images, the camera was positioned as far away as possible from the test section. A 60 mm fixed focal length lens was used with the camera 2.5 metres away from the tuft array. Distortion was further corrected by a tuft image processing program, which will be discussed shortly. Figure 13.1 on the next page shows a single unprocessed image taken of the tuft array during an experiment. The width of the tuft image is what was visible through the test section windows: 72% of the backward-facing step span. To help with contrast in the images, the tuft array was back-lit using a light sheet created from a modified drafting table positioned behind the test section.

A single image, such as Figure 13.1, could be used to estimate the instantaneous reattachment location. However, due to the spacing of the tufts, the resolution of the measurement is 20mm. As well, many researchers have observed that the instantaneous reattachment line fluctuates with time (e.g., Eaton & Johnston). For this reason, a time-averaged reattachment line is a more accurate index of the flow.

A virtue of calculating the time-averaged reattachment line will also help improve the resolution of the measurement beyond the 20mm tuft spacing. Eaton and Johnston (1980) defined a time-averaged reattachment location measurement as the

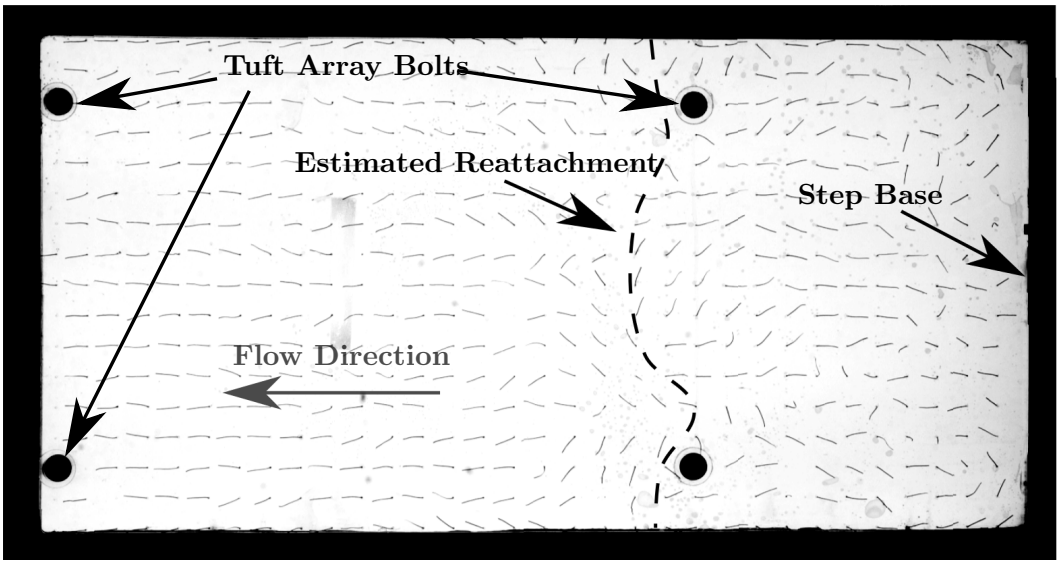

Figure 13.1: *A single unprocessed photograph of the back lit tuft array. The dotted line shows an estimated instantaneous reattachment line from visual inspection.*

point at which the flow, close to the wall along which reattachment occurs, fluctuates between the upstream and downstream direction 50% of the time. This statement is only valid if the reattachment line distribution forms a symmetrical distribution about the mean. Eaton and Johnston showed that this is true; the fluctuating reattachment line forms a symmetrical and continuous distribution about the mean. They used the 50% method for all their reattachment location measurements. For the case of the current study, the amount of fluctuation is greater than the spacing of the tufts. Thus, a time-average results in an improvement of the reattachment measurement.

In order to calculate a time-averaged reattachment line, several images of the tuft array would have to be consecutively captured and then averaged. The frequency of capturing images had to be carefully selected as to avoid aliasing with frequencies within the flow. By manually triggering the camera at an interval of approximately 2-3 seconds, which allowed for random sampling of the reattachment line, aliasing was avoided. If a phase-averaged reattachment line is desired, described in Appendix I, capturing images at a specified phase of the introduced perturbation instead of random sampling would yield this result.

In order to create a time-average, a computational averaging method was required to cope with the large amount of data. David Breakey, a NSERC funded Undergraduate Summer Research Assistant in 2009, was employed to create a method for calculating an average reattachment line from the tuft array image sets. He created a MATLAB program called "tuftImgProApp" for performing this calculation. Here a brief description of averaging methods used and program output will

be given. Details on the use and program information can be found in Mr. Baugh's Master's thesis, (Baugh 2010).

Mr. Breakey's program, tuftImgProApp, would first register each image to determine their coordinate system referenced from the tuft array mounting bolts and step edge. This registration would also help compensate for distortion in the images, as the distance between tuft array mounting bolts and step edge were used for calibration. The program would then isolate each tuft in each image and determine the slope of their orientation using a linear regression method. This would create a vector field of direction vectors for each image.

After the image set had been processed, the calculated set of vector fields would be used to obtain a time-averaged vector field. Three methods could be used for calculating an average: vector-averaging, vector-averaging with normalized magnitudes, and percent fields downstream. Vector-averaging calculates an average direction and magnitude for each tuft from the processed image set. This method allows for the option of normalizing the averaged magnitudes for each vector (vector-averaging with normalized magnitudes). Figure 13.2 on the following page shows an example of the calculated average vector field for both normalized vector option and non-normalized. Their corresponding contour plots of vector x-component magnitude ranging from positive one to negative one can be seen in Figure 13.3 on page 84: a magnitude of positive one indicates tuft average pointing straight downstream, where as a magnitude of negative one indicates fully upstream direction. Inspecting these images one can see that the normalized plots indicate reattachment location with the resolution of the tuft spacing (20 mm grid). The advantage of not normalizing the vector field magnitudes is the reattachment line can be interpolated between the tuft spacing, giving a more accurate reattachment estimation.

The percent fields downstream method calculates a percentage, for each vector within a set of processed tuft images, of how many instances a tuft's x-component was in the downstream direction. If a particular vector points downstream in every image within the set, it will be given a value of 100% downstream and vice versa a value of 0%. Much like Eaton's & Johnston's (1980) method for reattachment location measurement using their thermal tuft, the point where the flow was 50% of the time downstream was deemed the location of reattachment. The contour plot shown in Figure 13.4 on page 85 is an example of a percent fields averaged result.This method was chosen for reattachment line measurement as it did not rely on the vector magnitudes, of which we could not be fully certain. However, it was still reassuring to compare the calculated average reattachment length using the three methods; calculated X_r values differed from each other by a maximum of 0.5% (Baugh, 2010).

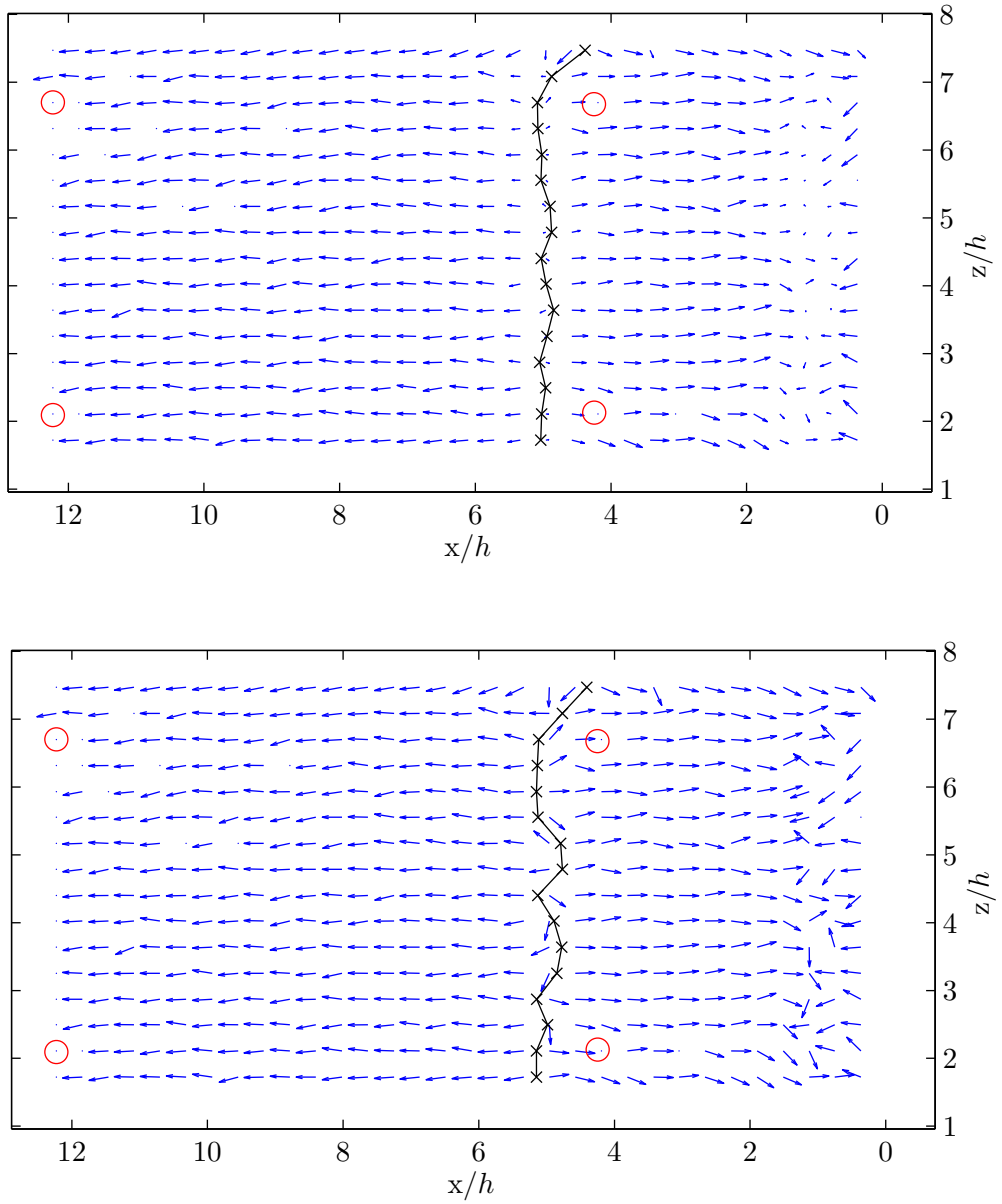

Figure 13.2: *Averaged vector field generated using vector averaging method. Taken from experimental run at a* $Re_h = 24500$ *and natural unforced flow. Top image shows the non-normalized vector field, where as the lower image shows the normalized magnitude vector field. Reattachment line is indicated by black line with Xs at nodes.*

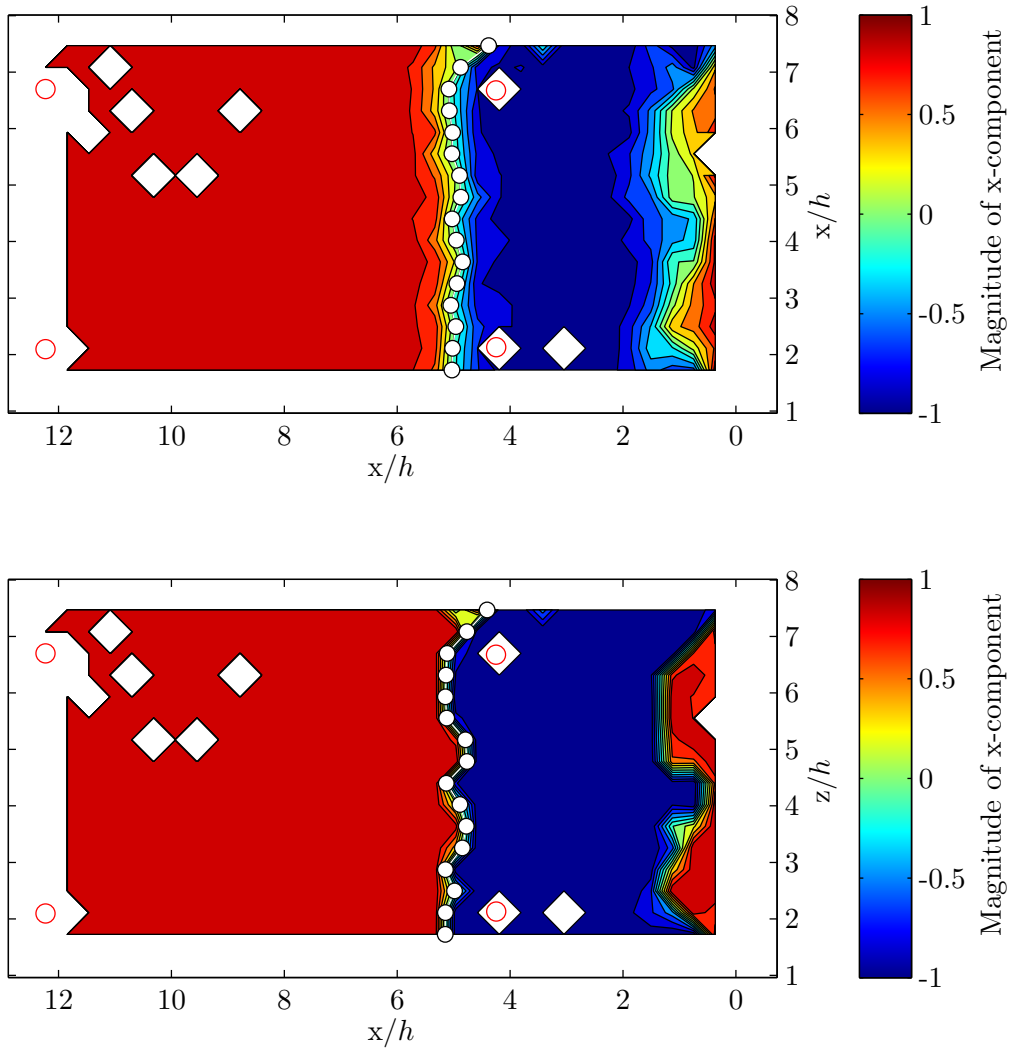

Figure 13.3: *Averaged contour plots generated using vector averaging method. Taken from experimental run at a* $Re_h = 24500$ *and natural unforced flow. Top image shows the contour plot from the non-normalize vector field, where as the lower image shows the contour plot from the normalized magnitude vector field. Reattachment line is indicated by white line with circles at nodes. (A white diamond indicates a tuft is missing in the tuft array.)*

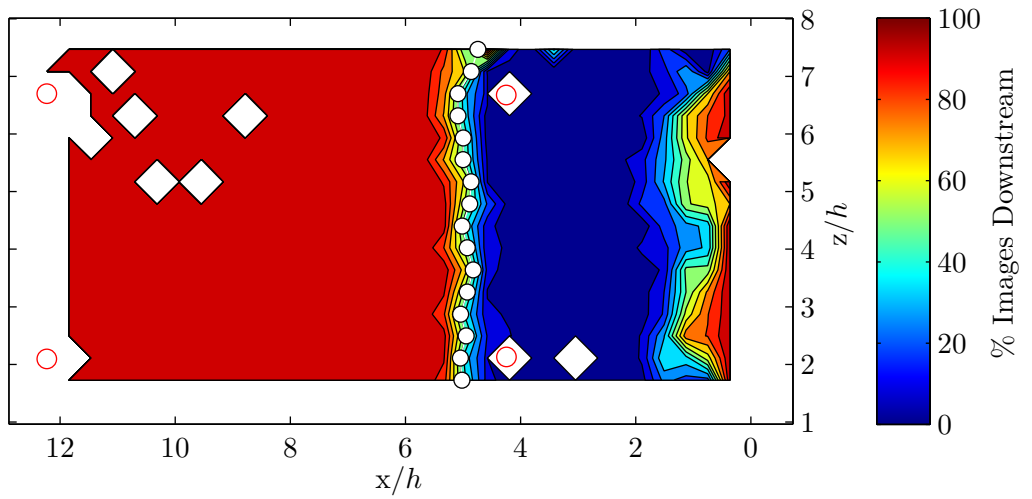

Figure 13.4: *Average reattachment contour plot generated using percent fields downstream averaging method. Taken from experimental run at a* $Re_h = 24500$ *and natural unforced flow. Top image shows the contour plot from the non-normalize vector field, where as the lower image shows the contour plot from the normalized magnitude vector field. Reattachment line is indicated by white line with circles at nodes. (A white diamond indicates a tuft is missing in the tuft array.)*

Baugh (2010) had performed a sensitivity analysis of reattachment length measurement repeatability and image set size. He found that a image set of 50 would be sufficient for reattachment length repeatability of less than 1%. Each image set taken for experiments performed for the current study were of 100 images taken over a time period of approximately 4 minutes.

It should be noted some potential sources of error in reattachment measurement. Notice the top edge of the calculated reattachment line in Figures 13.2, 13.3, and 13.4 has a curvature into the negative x-direction. This is due to an error caused by a single tuft located above the top right tuft mounting bolt which had adhered to the tuft plate and would not yield to the flow. To prevent leakage of water past the mounting bolts, a vacuum sealing grease was applied to their threads. During installation of the tuft array, care was taken to avoid transferring this grease onto the tuft array. However, some had transferred at the top right bolt location, causing some tufts to adhere to the grease creating a false flow measurement. Another source of error was caused by the location of the two right most mounting bolts. During forcing of the flow, the reattachment line would move closer to the step and in certain instances would be in line with these bolts. To eliminate these errors, the reported average reattachment line was calculated using the inner portion of the reattachment line which avoided influence from mounting bolts and faulty tufts.

Another potential experimental problem was caused by the formation of air

bubbles behind the tuft array. When photographs were taken of the tuft array, these bubbles would show up as dark clusters and hinder the ability of tuftImgProApp to process the images. These bubbles arose due to dissolved air in the water coming out of solution. The water tunnel was filled with domestic cold water from the building supply which had to be pumped with high pressure to reach the 6^{th} level lab. Due to this it contained a substantial amount of air in solution. As the water warmed in the tunnel, air would come out of solution. It would require several days for the water to reach thermal equilibrium with the surroundings and excess air come out of solution. If the tuft plate was kept out of the water tunnel until near equilibrium was reached, much fewer bubbles would collect behind the plate. The visibility of these bubbles could be further mitigated by increasing the camera exposure until the bubbles are washed out.

13.2 Unforced Backward-Facing Step Flow

All experiments performed for this thesis were performed at a $Re_h = \frac{U_\infty h}{\nu} = 24500$, where U_∞ is the free-stream velocity at separation. This Reynolds number was chosen to allow for comparison with the high Reynolds number ($Re_h = 24500$) experiments performed by Baugh (2010).

The first experiments performed were of the unforced case. This experiment provided a baseline for reattachment length used in the following forcing experiments. For this experiment and all to follow, before any data was acquired the water tunnel was adjusted to the desired flow rate and left to reach equilibrium for a minimum of thirty minutes. This was done to avoid the possibility of flow pulsations and to make certain that the tunnel was in steady state operation.

With the tunnel in steady state operation, 100 images of the tuft array were captured using the method described in the previous section. Three separate data sets were taken over three days, each one with the water tunnel starting from rest and set into steady state operation. This was always the first experiment performed before any forcing experiments were carried out that day. It was repeated as such over the three days to give independent measurements so they could be used to measure the repeatability of the experiment.

13.3 Large Amplitude Spanwise Invariant Forcing

Spanwise invariant forcing has also been called 2D forcing (Baugh 2010), signifying that the actuation does not vary in the spanwise direction. It is expected that the flow in the wake of the BFS exhibits strong three-dimensionality. As for example,

Sigurdson (1986) observed strong three-dimensionality in the separating and reattaching flow of a forward-facing step. As a result, spanwise *variant* forcing has been called 3D forcing, which is intended to interact with the three-dimensional nature of the flow.

Although the experimental apparatus was designed to have the ability of creating spanwise varying waveforms, all forcing experiments performed for this thesis were of uniform spanwise excitation. It is intended that future work using this apparatus will delve into the spanwise varying realm.

13.3.1 Reattachment Length versus Perturbation Strouhal Number

This experiment is intended as a reproduction of the high Reynolds number, reattachment length vs. Strouhal number as performed by Baugh (2010). The main goal was to compare the results using the improved Beta actuator (described in Part I of this thesis) with that of Baugh. This will help give a limit of which forcing cases (amplitude and frequency) performed by Baugh contained the least amount of error due to actuation error.

All the ports across the step span issued a suction-blowing actuation which varied in time following a sinusoidal waveform as described in Part I of this thesis. The parameter space explored perturbation Strouhal numbers varying from 0.0 to 0.47 and at four different perturbation amplitudes ($\frac{u'}{U_\infty} = 0.1, 0.2, 0.35, 1.08$).

13.3.2 Reattachment Length versus Perturbation Amplitude

Some of the results from the $X_{r_\circ}$ vs. St_h intrigued the author to make a more detailed investigation of perturbation amplitude effect on reattachment length. Perturbation amplitudes were varied from $0.0U_\infty$to$2.0U_\infty$ for two Strouhal numbers of 0.29 and 0.41. In zones of higher rate of $X_{r_\circ}$ change with $\frac{u'}{U_\infty}$, perturbation amplitude was incremented in smaller intervals to help resolve detail in the curve.

Chapter 14

Results and Discussion

This section will begin with an investigation of our shorter than usual reattachment length of $X_{r_\circ}$. Discussion of the forcing experiment results will follow. The complete experimental results can be seen in Appendix G on page 150

14.1 Unforced Backward-Facing Step Flow

Three independent instances of the unforced reattachment length experiment were performed. Each case resulted in a time and spanwise-averaged reattachment length of $X_{r_\circ} = 5.0h$ with 1% variance. Baugh (2010) had performed an experiment of reattachment length versus Reynolds number to determine whether the unforced reattachment length, $X_{r_\circ}$, was Reynolds number independent. He performed the test at Reynolds numbers ranging from $Re_h = 3770$ to $Re_h = 46100$. His results show that our reattachment length was independent of Reynolds number, and like ours $X_{r_\circ} = 26.3cm = 5.0h$. This is lower than expected, as values from other backward-facing step experiments are larger. Based on other BFS experiments, a value within the range $6 \lessapprox X_{r_\circ} \lessapprox 8$ was expected. Baugh investigates possible reasons why our reattachment could be shorter, however little knowledge of the boundary layer at separation was known at the time and his discussion was non conclusive. An abridgement of his discussion will be given here and expanded upon with some new evidence.

For Baugh's investigation of the probable cause for our shorter than usual unforced reattachment length, he examined expansion ratio ER, Re_h, step aspect ratio AR, free-stream turbulence level, and postulates on the possible quality of the boundary layer and its influence. Having verified that the reattachment length was Reynolds number independent, Baugh neglected Re_h as a possible contributing factor.

ER was also dismissed. Experiments performed by Armaly, Durst, Pereira &

Table 14.1: *Unforced reattachment lengths from various authors*

Author	$X_{r_\circ}$	Re_h	ER	AR	$\delta_{0.99}/h$	**BL Condition**
Henning & King (2007)	$7.2h$	25,000	1.27	20	0.68	turbulent
Westphal et al.(1984)	$7.0h$	42,000	1.67	12	0.06	laminar
	$8.0h$	42,000	1.67	12	0.2	turbulent
	$8.6h$	42,000	1.67	12	0.4	turbulent
Chun & Sung (1996)	$7.8h$	33,000	1.5	12.5	0.41	turbulent
	$7.2h$	23,000	1.5	12.5	0.38	turbulent
	$6.8h$	13,000	1.5	12.5	0.28	turbulent
Kim et al. (1980)	7 ± 1	30,000	1.5	24	0.45	turbulent
	7 ± 1	45,000	1.5	16	0.30	turbulent
Adams & Johnston (1988)	$4.9h$	26,000	1.25	11	0.005	laminar
	$6.5h$	26,000	1.25	11	0.2	turbulent
	$6.5h$	26,000	1.25	11	1.7	turbulent

Schönung (1983) showed that as expansion ratios decrease, the reattachment would lessen as well. These results were later assured by Eaton & Johnston (1980) and Ötüngen (1991), the later of whom showed that as ER lessened the shear layer would tend to grow faster, resulting in reduced reattachment lengths. Ötüngen (1991) found that the reduction in reattachment would be of the order of 5% for a 50% reduction in ER. Baugh argued that since our $ER = 1.26$, which is very close with those of Henning & King (2007) ($ER = 1.27$ with a $X_{r_\circ} = 7.2h$), and Bradshaw & Wong (1972) ($ER = 1.25$ with a $X_{r_\circ} = 6h$), of which Henning & King is of comparable Reynolds number, ER could not a significant contributor to our short reattachment length.

Our aspect ratio of 8.25 was a bit suspect as it is less than many of the experimental backward-facing steps used in literature and less than the accepted minimum of 10 to ensure two-dimensionality of the flow in the central region, away from the end walls (de Brederode and Bradshaw 1972). However, as seen in Figure 13.4 on page 85, the time-averaged reattachment line is parallel with the step edge indicating no influence from the end walls. Limited literature is available on the effects of aspect ratio on reattachment length. However, Kim, Kline, and Johnston (1980) performed a backward-facing step experiment using a wind tunnel with step height, h, that could be varied. They gave results for two different step heights giving aspect ratios of 24 and 16 while keeping the free-stream speed constant. For both cases their unforced reattachment lengths were in agreement within experimental error, $X_{r_\circ} = 7 \pm 1$. This is not definitive evidence that our aspect ratio does not affect reattachment since all their reattachment lengths were larger than 10. At this point,

without better evidence, our aspect ratio cannot be excluded as the likely cause of our unusually short $X_{r_\circ}$.

Free-stream turbulence has been reported by many to have significant influence on reattachment length. The free-stream turbulence in our water tunnel was measured to be less than 1% (Gilbert 2007). Experimental results from Hillier and Cherry (1981) on the effect of free-stream turbulence ranging from 1.8% to 7.2% do not account for the amount of deviation of our shorter $X_{r_\circ}$. As well, Isomoto and Honami (1989) measured the effects of free-stream turbulence in the range of 0.25% to 1.3% and observed a reduction for higher turbulence of $0.1h$. Baugh had therefore excluded free-stream turbulence as a suspect.

Thus far all the listed probable causes of our short $X_{r_\circ}$ have been discussed, except for the boundary layer properties. And all of the discussed have been excluded as suspect except for aspect ratio, which was left as unknown. Since no data was available for the boundary layer properties, Baugh wasn't able to comment much on its influence on our $X_{r_\circ}$ in his thesis. In Chapter 11 a theoretical investigation of the boundary layer properties was given in hope to give some enlightenment on this subject. From the analysis, it was discovered that the boundary layer at separation is likely turbulent from the production of Görtler vortices at the ramp leading up the backward-facing step. As well, the estimated boundary layer momentum thickness at separation is $\delta_\theta|_{\text{separation}} \sim 0.003$ m.

With this new knowledge of the boundary layer, its impact on reattachment can be now investigated. It is well known now that any factor which increases shear layer entrainment will increase shear layer growth, resulting in a reduction of reattachment length, X_r (Adams & Johnston 1988). It is also known that the net rate of entrainment is controlled by the speed at which the contortions of the largest scales move into the surrounding fluid (Tennekes & Lumley 1972). Thus the large eddies within the shear layer contribute the most to shortening reattachment. This has been verified and confirmed by many. Westphal et al. (1984) for example used this knowledge to reduce reattachment by 20% by installing vortex generators upstream of the step. The presence of Görtler vortices in the separating boundary layer will have a very similar effect on reattachment as the vortices generated upstream of the step by Westphal et al. (1984). This knowledge makes the presence of counter rotating Görtler vortices a strong suspect.

Baugh had noted that Adams & Johnston (1988) reported a 30% *increase* in reattachment when the separating boundary layer transitioned from laminar to fully turbulent. Without knowledge of our boundary layer, Baugh postulated that our boundary layer could possibly be laminar at separation, and more investigation into our boundary layer would be required. This seems contradictory to our statements in the preceding paragraph, as without careful thought, it could be assumed that a

turbulent separating boundary layer should enhance entrainment. It shall be seen shortly that this is not always the case.

Adams & Johnston changed their boundary layer thicknesses independently of free-stream velocity using a combination of wall suction upstream of the step edge to thin the boundary layer and trips to thicken it. Using this technique they were able to vary the boundary layer thickness in a range of $0.005 \leq \delta_{0.99}/h \leq 1.7$. Thus, they would attain their laminar boundary layer by sucking away the original turbulent one. When they report reattachment reduction for their laminar case, it is important to remember it is laminar because the turbulent boundary layer had been removed by suction and what is remaining is of significant smaller thickness than the original turbulent boundary layer. Their results showed a reattachment length of $X_{r_\circ} \approx 5h$ when $\delta_{0.99}/h \approx 0.005$ and laminar, with a sharp rise in reattachment up to $X_{r_\circ} \approx 6.5h$ when $\delta_{0.99}/h \approx 0.4$ and turbulent. For increasing $\delta_{0.99}/h$ up to their maximum thickness of 1.7, $X_{r_\circ}$ remained approximately constant showing a weak reducing trend. Adams & Johnston concluded that the decrease in reattachment length for their laminar boundary layer at separation (their smallest $\delta_{0.99}/h$ case) resulted from an increase in entrainment of the free shear layer.

These results have been observed by others as well. Westphal et al. (1984) performed an experiment where they varied the boundary layer thickness at separation with constant free-stream velocity by changing the development length along a flat plate upstream of the step. Three values of boundary layer thickness were tested: $\delta_{0.99}/h = 0.06,\ 0.2,\ 0.4$ and $h = 5.08$ cm. The corresponding Reynolds numbers based on momentum thickness were $Re_\theta = 330,\ 850,\ 1500$. The first case of the three was a laminar boundary layer, and the other two were turbulent with the help of a trip upstream of the step. Their results are summarized in Table 14.2. It can be seen that the thinner laminar separating boundary layer results in a reduction in reattachment. They give justification by stating that the thinner separating boundary layers induced more vigorous mixing and higher rates of entrainment within the free shear layer.

Table 14.2: *Results from Westphal et al. (1984): reattachment length as boundary layer thickness varied*

Boundary Layer Condition	$\boldsymbol{\delta_{0.99}/h}$	$\boldsymbol{X_{r_\circ}}$
Thin laminar boundary layer	0.06	7.0
Turbulent boundary layer	0.2	8.0
Turbulent boundary layer	0.4	8.6

From the analysis in Chapter 11, the separating boundary layer has a momentum

thickness in the order of 0.003 m and is permeated with streamwise Görtler vortices. The corresponding $u/U = 0.99$ boundary layer thickness will be $\delta_{0.99} \sim 7\delta_\theta = 0.02$ m. This gives us a $\delta_{0.99}/h \sim 0.4$. Since our step height $h = 5.23$ cm is comparable with that of Westphal et al. (1984), our boundary layer is of similar thickness as their largest. Thus it can be excluded that the separating boundary layer is thin enough to account for the shorter than usual reattachment length.

Having excluded boundary layer thickness as the culprit, the predicted embedded Görtler vortices are becoming the more probable cause for our $X_{r_\circ}$. As cited earlier, Westphal et al. (1984) performed an experiment where they installed vortex generators upstream of the step to fill their separating boundary layer with counter rotating vortices. By doing so they experienced a 20% reduction in reattachment. This is a result of the streamwise vortices enhancing three-dimensional mixing within the free shear layer. The generated counter rotating vortices in their experiment will have a great resemblance to Görtler vortices. Accordingly it can be expected that Görtler vortices can produce the same effect on reattachment.

Thus far, this discussion has been able to assert that Re_h, free-stream turbulence, expansion ratio ER, and δ/h do not result in the shorter than expected unforced reattachment length. The effects of AR has been left as uncertain as there is no definitive supporting data showing it could or could not influence the reattachment length. It is however much less suspect than the influence of the counter rotating Görtler vortices, leaving the presence of counter rotating Görtler vortices in the separating boundary layer as the most feasible explanation.

To be certain that Görtler vortices are producing our shorter unforced reattachment length, either the suspected source of the Görtler vortices needs to be removed or measurement of the separating boundary layer would be in order. Within our water tunnel, measuring boundary layer properties would require the use measurement such as Particle Image Velocimetry (PIV). It would be less difficult, thus more appealing, to remove the Görtler source to determine if the reattachment length increases to a more expected value. This can be accomplished by extending the backward-facing step with a fillet to smoothly connect the space approximately between points x_2 and x_4 (see Figure 11.1 on page 58 for locations of x_2 and x_3) with a convex profile. Since Westphal et al. (1984) reduced reattachment length by 20% with the installation of vortex generators upstream of the step, it would be expected that our unforced reattachment length should increase by approximately 25% with the absence of Görtler vortices. This places our unforced reattachment length within the expected range of $6 \lessapprox X_{r_\circ} \lessapprox 8$.

14.2 Large Amplitude Spanwise Invariant Forcing

This section will discuss results from the two large amplitude spanwise invariant forcing experiments performed for this thesis.

14.2.1 Reattachment Length Versus Perturbation Strouhal Number

Figure 14.1 on the next page plots the spanwise and time-averaged results from our experiment defined in Section 13.3.1. This experiment was intended as a reproduction of an experiment performed by Baugh (2010) using the same facility with the exception of the improved actuator board described in Part I of this thesis.

The experiments of Henning & King (2007) and Chun & Sung (1996) are comparable with this current study. Some of their pertinent experimental parameters can be seen in Table 14.1. The most significant differences between this experiment and theirs are step aspect ratio and unforced reattachment length. As discussed in the previous section, the shorter reattachment length is likely due to the presence of counter rotating Görtler vortices in our separating boundary layer. Regardless, the observed trends in reattachment reduction are similar as those seen by others. Thus, comparisons are made not only with the results of Baugh (2010), but with results from Henning & King (2007) and Chun & Sung (1996) as Baugh did as well. Data from the two authors presenting normalized reattachment length as a function of actuation Strouhal number can be seen in Figures 14.3 and 14.4.

It should be noted for Figure 14.4, the excitation amplitudes for the three curves are reported here as approximate. This is because Chun & Sung reported their forcing amplitude as $A_\circ = (Q_{forced} - Q_{unforced})/U_\infty$. Where Q is the total velocity equal to $\sqrt{(\bar{u}^2 + \bar{v}^2)}$ is the RMS of the time-mean velocity fluctuation components in the x and y directions measured in close proximity to the perturbation source. $Q_{unforced}$ is a measure of the turbulence intensity within the separating boundary layer. Assuming that $Q_{forced} \gg Q_{unforced}$, $A_\circ \approx \frac{1}{\sqrt{2}} u'/U_\infty$. Thus, the reported excitation amplitudes from Chun & Sung: $A_\circ = 0.07,\ 0.05,$ and 0.03 can be compared with our measurement of excitation amplitude as: $u'/U_\infty \approx 0.1,\ 0.07,$ and 0.04. Henning and King reported their excitation amplitudes, $a_\circ$, as a ratio of averaged maximum excitation velocity to the free-stream velocity U_∞. Thus, we were able to make a direct comparison with our excitation amplitudes.

The comparison of the current results and those of Baugh (2010) can be seen in Figure 14.2 on page 95. In this Figure the current results are plotted in bold. The low and high amplitude ($u'/U_\infty = 0.1$ & 1.08) curves show the greatest deviation between the current and Baugh results. To explain this difference, the performance of Alpha actuator board, used in the experiments of Baugh, was worst at these

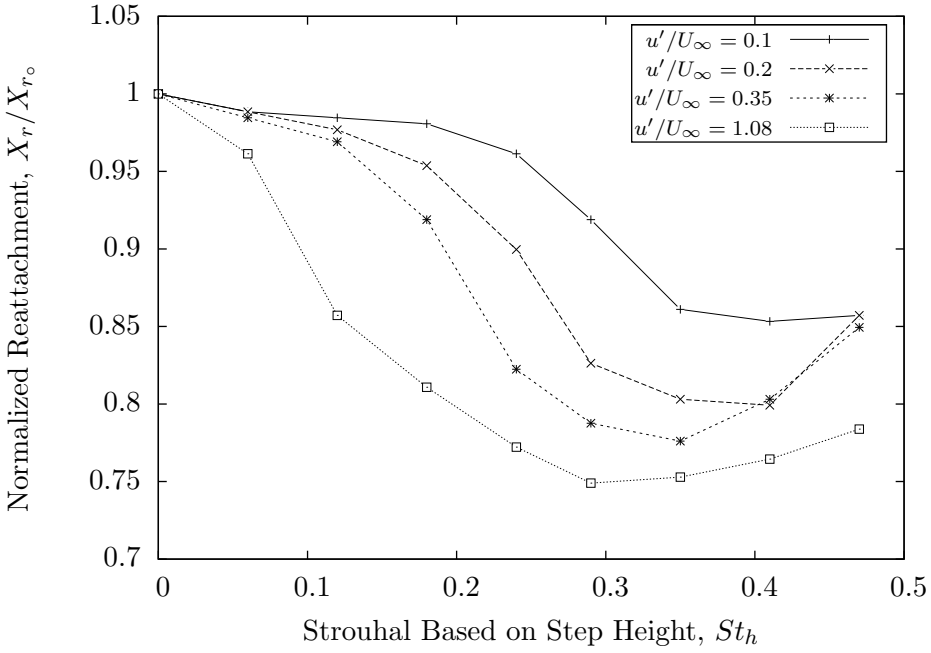

Figure 14.1: *Normalized reattachment length, $X_r/X_{r_\circ}$, as a function of actuation Strouhal number, St_h, for four actuation amplitudes.*

extreme forcing limits as described in Part I. The curves at intermediate excitation amplitudes ($u'/U_\infty = 0.2$ & 0.35) have close resemblance between current and Baugh results, especially for the $u'/U_\infty = 0.35$ case. This is congruent with the previous statement about the poor performance at the extreme limits, as performance of the Alpha actuator was markedly better at the intermediate amplitudes. This same observation was made by Baugh (2010); he noticed that the trend of the curves for low and high excitation amplitudes were not as smooth as that for the intermediate amplitude cases and stated that this could likely be due to the forcing fidelity at the low and high amplitude cases. Thus, it can be concluded that the results of Baugh (2010) are most valid for intermediate forcing amplitudes ($0.2 \lessapprox u'/U_\infty \lessapprox 0.35$), an unfortunate consequence of the poor Alpha actuator operation at the extreme forcing cases.

The general trend of the results agree well with that of Henning & King (2007) and Chun & Sung (1996). However, as seen in Figure 14.5, which compares our lowest excitation amplitude with their results, our reattachment doesn't show as much of a reduction and our minimum occurs at a higher Strouhal number for the same excitation amplitude (our $\frac{X_r}{X_{r_\circ}} = 0.853$ @ $St_h = 0.41$ and Henning & King $\frac{X_r}{X_{r_\circ}} = 0.71$ @ $St_h = 0.29$; Chun & Sung $\frac{X_r}{X_{r_\circ}} = 0.67$ @ $St_h = 0.25$). As mentioned previously, the major difference between the current experiment and that of the other two is the presence of Görtler vortices in our separating boundary

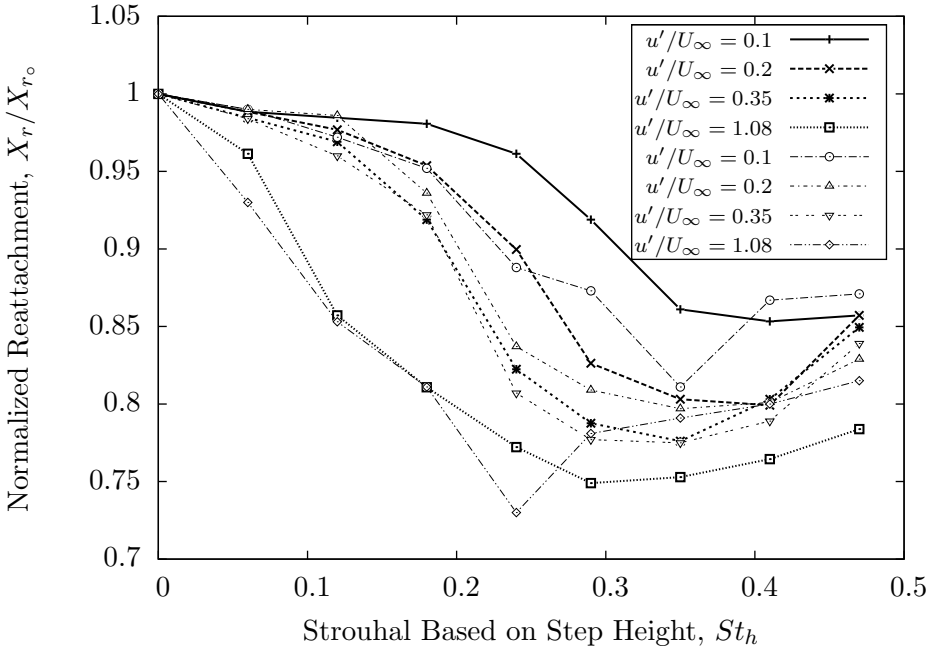

Figure 14.2: *Comparison of current and Baugh (2010) large amplitude forcing data. Current data presented as bold.* Re=24,500

layer. This resulted in a higher entrainment rate of our shear layer and shorter unforced reattachment length. Thus, it is likely that the effect of the introduced perturbations in our experiment is somewhat absorbed by the strong effect of the Görtler vortices.

Each curve in Figure 14.1 shows a discernible minimum which signifies an optimal Strouhal number, except for the lowest amplitude whose minimum is near our maximum forcing frequency. The optimum St_h lay within a range of St_h which provide comparable reduction. Hence, there is not a sharp peak at the optimum St_h, but a range of St_h which provide similar reattachment reduction. This can also be observed in the results of Henning & King and Chun & Sung. It is also clear that the minimum is not independent of excitation amplitude. With increasing excitation amplitude, the minimum shifts to a lower St_h. At $u'/U_\infty = 0.1$ the minimum occurs at $St_h \approx 0.4$ and at $u'/U_\infty = 1.08$ the minimum occurs at $St_h = 0.3$. Henning's and King's results (Figure 14.3) are from two different excitation amplitudes $u'/U_\infty = 0.02$ & 0.08 as a function of St_h. From their data it appears that their optimal Strouhal numbers were also amplitude dependent like ours; there is an apparent slight shift to a lower optimal St_h for their larger excitation amplitude (shift from $St_h = 0.3$ to $St_h =$). However, Henning & King stated that their optimal Strouhal number is amplitude independent. Their conclusion could be due to them only comparing reattachment as a function of St_h for two excitation amplitudes in

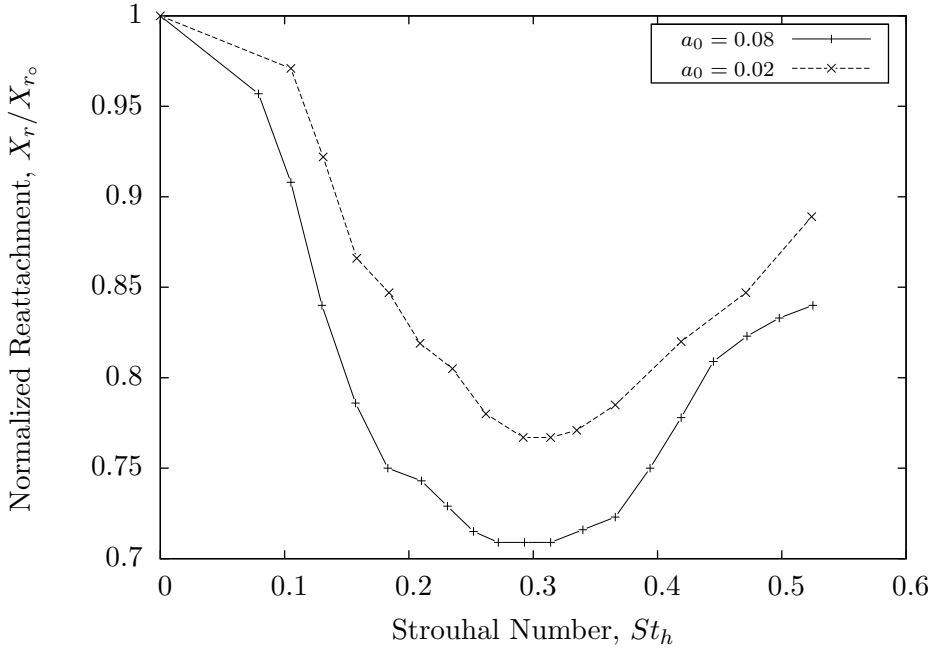

Figure 14.3: *Results from Henning & King (2007) for spanwise invariant forcing. Normalized reattachment length, $X_r/X_{r_\circ}$, as a function of actuation Strouhal number, St_h, for two actuation amplitudes.* $Re_h = 25000$. $a_\circ$ represents the dimensionless actuation amplitude defined by Henning and King. It is the ratio of the phase and spanwise averaged maximum excitation velocity to the free-stream velocity U_∞.

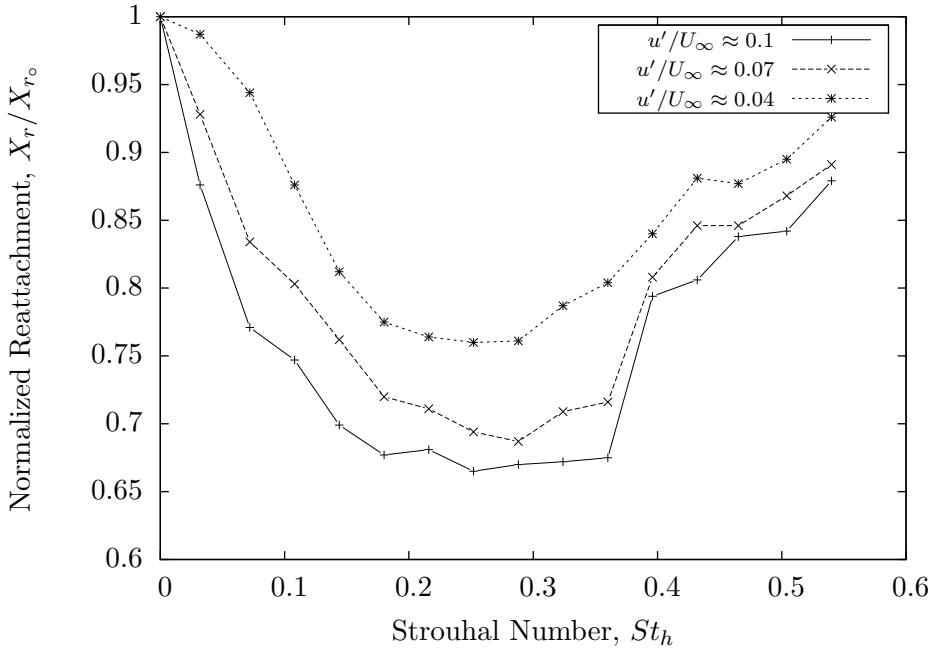

Figure 14.4: *Results from Chun & Sung (1996) for spanwise invariant forcing. Normalized reattachment length, $X_r/X_{r_\circ}$, as a function of actuation Strouhal number, St_h, for three actuation amplitudes.* $Re_h = 23000$.

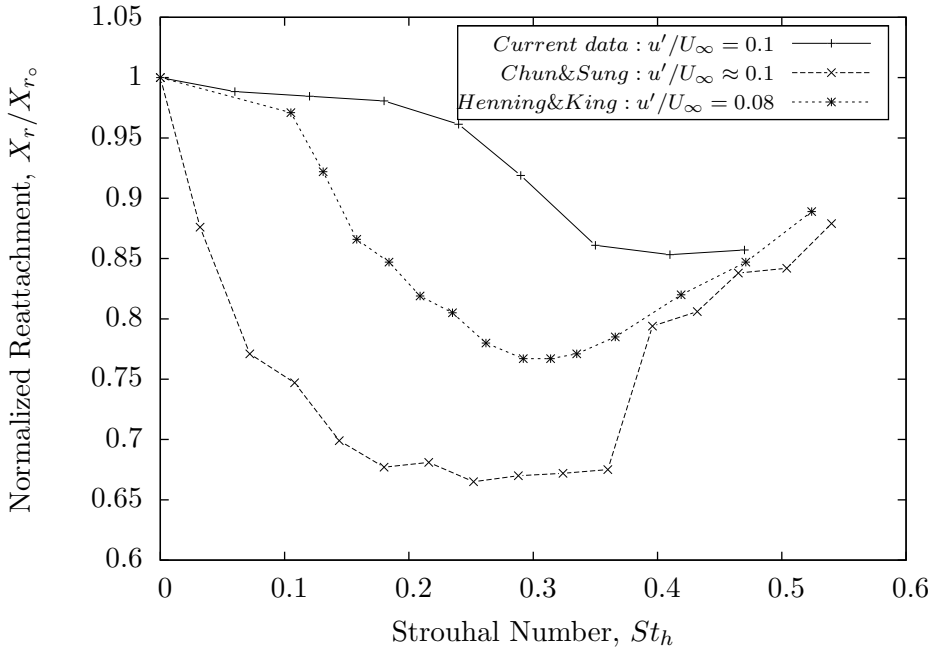

Figure 14.5: *Comparison of current results with Henning & King (2007) and Chun & Sung (1996).* Current $Re_h = 24,500$; Henning & King $Re_h = 25,000$; Chun & Sung $Re_h = 23,000$

close proximity. Thus, the slight observed shift in optimal Strouhal number could have been overseen as within experimental error. They did not give values of experimental error. Thus no certainty can be given whether their shift in St_h is due to error or not. In the results from Chun & Sung (1996) seen in Figure 14.4, no appreciable shift in optimal St_h with excitation amplitude is observed. This could as well be due to the limited space of excitation amplitudes tested.

Forcing amplitude dependence was also observed by Sigurdson (1995) for a separating flow at the leading edge of a blunt-faced cylinder with its axis aligned with the oncoming flow direction. Initially, his forcing Strouhal number was based on cylinder diameter (St_D) and he found that as perturbation amplitude was increased, his optimum St_D would *increase* as a result of the shrinking separation bubble as X_r reduced. When he scaled his forcing Strouhal number on the varying separation bubble height h_{bubble}, the optimal $St_{h_{bubble}}$ would remain constant as X_r was reduced. A possible explanation for our observed decrease in St_h could be that at larger excitation amplitudes the separating shear layer is initially lifted further away from the step side wall, effectively increasing the step height ($h_{effective}$). This would influence the step-mode of vortex shedding (Sigurdson 2011). An increase in $h_{effective}$ would allow larger growth of the spanwise vortices, lowering the Strouhal number.

Another interesting observation is visible in Figure 14.1 at the points of $St_h = 0.41$ and excitation amplitudes $u'/U_\infty = 0.2$ & 0.35. Notice that the trend of reduction in reattachment length with increasing excitation amplitude is broken at this point only. As well, at the next higher tested excitation Strouhal number, $St_h = 0.47$, the differences in reduction between the three lower excitation amplitudes are considerably small with respect to the rest of the data. The data points at $St_h = 0.41$ and excitation amplitudes $u'/U_\infty = 0.2$ & 0.35 were repeated to ensure that the observation was not due to experimental error. For each case, reattachment reduction at $St_h = 0.41$ & $u'/U_\infty = 0.35$ was less than for $St_h = 0.41$ & $u'/U_\infty = 0.2$. This lead the author to perform the experiment which will be discussed in the following Section (14.2.2), to gain more insight into what might cause this deviation from the usual trend.

14.2.2 Reattachment Length Versus Excitation Amplitude

The results presented in Figure 14.6 show spanwise and time-averaged reattachment length as a function of forcing amplitude for two Strouhal numbers. Baugh (2010) had performed a similar experiment for one forcing Strouhal number of a near optimum value of 0.3. A comparison of his and the current results can be seen in Figure 14.7.

Figure 14.6 show that our reattachment reduction does not follow a monotonic trend with increasing actuation amplitude. Reattachment length reaches a pronounced initial minimum at $u'/U_\infty \approx 0.3 - 0.4$, and then rises to a peak at $u'/U_\infty \approx 0.5 - 0.6$. Any larger forcing amplitudes up to our maximum $u'/U_\infty = 2$ results in more reattachment reduction. These initial minimums and peaks are Strouhal dependant. At higher forcing Strouhal numbers they occur at a lower forcing amplitude. For the extreme forcing amplitudes past the peaks ($u'/U_\infty \gtrapprox 0.6$), the trend of reattachment reduction seems to loose most of its dependence on forcing frequency; the curves for $St_h = 0.29$ and $St_h = 0.41$ follow each other closely. Table 14.3 gives a summary of the key points in Figure 14.6

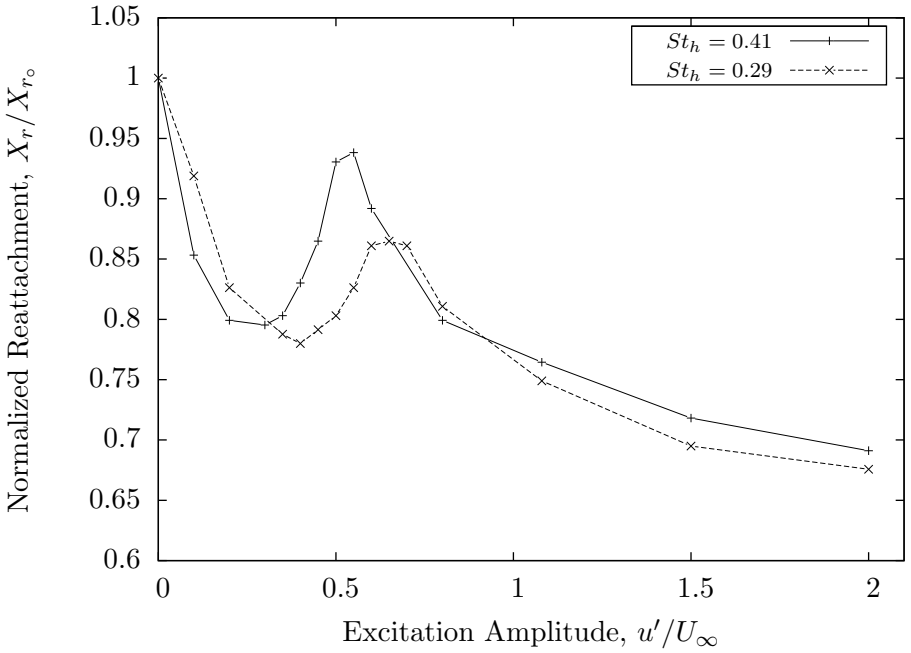

Figure 14.6: *Normalized reattachment length, $X_r/X_{r_\circ}$, as a function of actuation amplitude, u'/U_∞, for two actuation Strouhal numbers.*

Table 14.3: *Summary of reattachment length as a function of actuation amplitude results for $St_h = 0.29$ and $St_h = 0.41$*

Curve Feature	$\boldsymbol{St_h = 0.29}$	$\boldsymbol{St_h = 0.41}$
u'/U_∞ at initial minimums	0.4	0.3
Initial minimum $X_r/X_{r_\circ}$	0.78	0.80
u'/U_∞ at peaks	0.65	0.55
Peak $X_r/X_{r_\circ}$	0.86	0.94
$X_r/X_{r_\circ}$ at $u'/U_\infty = 2$	0.68	0.69

These results are very interesting and have not been reported in literature before. Henning and King (2007) performed a similar experiment of reattachment reduction versus actuation amplitude for Strouhal number of 0.3, however they only tested up to a maximum amplitude of $u'/U_\infty = 0.14$ and did not observe a peak in reattachment reduction as in the current results. Baugh (2010) had also performed a similar experiment, from which the results are compared with ours in Figure 14.7. This comparison shows that Baugh too did see a peak at approximately $u'/U_\infty = 0.6$; however, not as pronounced as in the current results. Baugh had deemed this increase at $u'/U_\infty = 0.6$ to be within experimental error, and was not considered as a significant result.

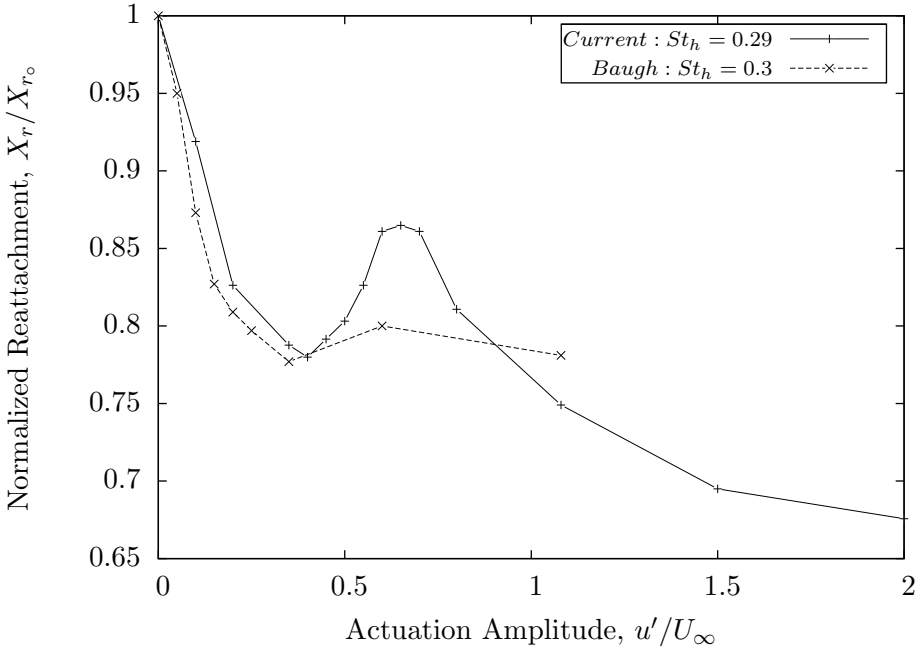

Figure 14.7: *Comparison of Baugh (2010) and current results for normalized reattachment length, $X_r/X_{r_\circ}$, as a function of actuation amplitude, u'/U_∞.*

It appears that two different reattachment reducing mechanisms are at work. The first within the forcing limit of $0 < u'/U_\infty \lessapprox 0.6$ and the second for greater forcing amplitudes. It is unclear what may be the cause, but some thought will be given below. One speculation is that with the presence of counter rotating Görtler vortices, there could be an interaction between these vortices and actuation which is causing the two regimes of reattachment reduction. It is however deemed unlikely that this is the cause. This could be verified by removing the source of Görtler instability as discussed in Section 14.1 and to reperform this experiment without their presence.

A more probable possible cause for this non-monotonic behaviour of the reat-

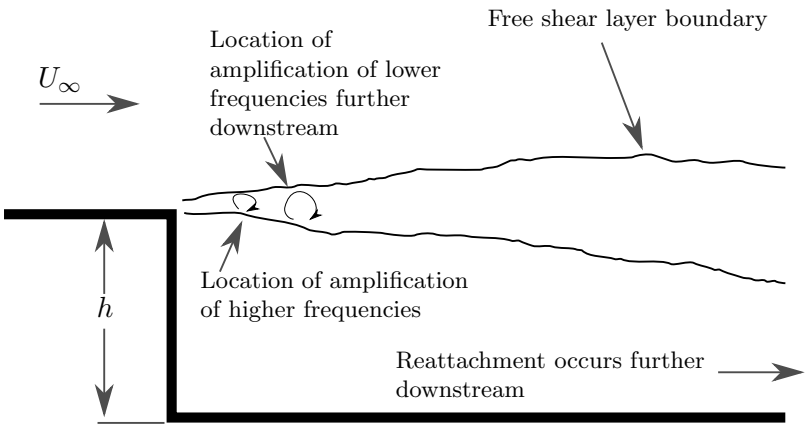

Figure 14.8: *Explanation of possible non-monotonic reattachment mechanism. Boundary of the backward-facing step outlined by thick line.*

tachment length could be a result of how far the forcing "reaches" into the flow. Reference Figure 14.8 for help with explanation. The lowest frequencies amplified by the natural instability within the free shear layer are determined by the largest scale structures within the shear layer. As the shear layer progresses downstream, these structures pair, increasing the thickness of the shear layer. This results in a shift of the instability frequency to a lower frequency further downstream. It is expected that larger forcing amplitudes would produce jets with larger centre velocities further into the flow. Thus, as the forcing amplitude is increased, its effect is transported further into the flow. The initial minimums of Figure 14.6 could be a result of the forcing reaching into the flow at the location where those particular frequencies are amplified the most (Sigurdson 2011). This would explain why the higher forcing frequency, $St_h = 0.41$ produces a minimum at a lower u'/U_∞. As amplitude is further increased, its effect will begin to force past this optimum downstream location within the shear layer and not allow for the amplification to occur until a point later downstream. This would result in the lessening of the reattachment reduction as observed by the peaks.

Now, a discussion on a possible cause for the continuation of reattachment reduction for extreme forcing amplitudes $u'/U_\infty \gtrapprox 0.6$. This could possibly be a result of the forcing becoming so large that it is now defining the flow structure in the wake of the BFS; the forcing is no longer perturbing a regular reattaching flow, but is now creating a new kind of flow. As mentioned for more moderate forcing amplitudes lower than 0.6, the initial instability frequency is determined by the thickness of the

shear layer. The extreme forcing amplitudes could be defining the flow structure, thus it is becoming the dominant source determining which frequencies are to be initially amplified by the flow. This would help explain why the reattachment trend loses St_h dependence for these extreme forcing amplitudes, as it could be that the frequency being amplified is being defined by the forcing at the step edge.

Chapter 15

Part II Conclusions and Future Work

15.1 Summary and Conclusions

An actuator board consisting of 16 individual actuators, as described in Part I of this thesis, was designed and used to introduce velocity perturbations into the separating boundary layer at the edge of the backward-facings step insert (BFS insert named "RoboStep"). Conclusions from Part I are given separately in Chapter 9. The perturbations resulted in enhanced mixing and shorter reattachment lengths in the step wake.

The RoboStep has 128 actuation ports aligned to direct the actuated flow 45° to the free-stream direction at separation. Even though this thesis only investigated the effects of spanwise-invariant forcing, the 128 actuation ports are connected to the 16 separate actuators. This makes the RoboStep unique in terms of the resolution of spanwise actuation profiles it can produce. It can produce any symmetrical periodic waveform with the end walls that can be discretized by a multiple of 16 velocity types. This allows for a largest wave number of 8 along the span.

For reattachment location measurement, a novel hydro-tuft was designed which can indicate flow direction for a flow velocity in the vicinity of the tuft of less than 5 cm/s. An array of 989 of these hydro-tufts was used to capture instantaneous reattachment location measurements. With the use of MATLAB image processing program, developed by David Breakey, multiple images of instantaneous reattachment could be averaged to determine a time-averaged reattachment line and spanwise-averaged reattachment length.

A detailed theoretical investigation of boundary layer growth up to the separation point was performed at our experimental $Re_h = 24500$. It was concluded that our boundary layer remained laminar up the to the leading edge of our backward-facing step insert. The estimated extreme limits of the momentum thickness up

to this point were 0.00064 m$<\ \delta_\theta\ <$ 0.00353 m. At the leading section of the backward-facing step there is a concave wall which allows for a Görtler instability for all boundary layer thicknesses within our determined limits. It is thus concluded that our separating boundary layer is likely permeated with counter rotating Görtler vortices. Due to the unknown growth characteristics for a boundary layer permeated with Görtler vortices, and because the remaining length up to the step edge is comparatively short, it was stated that the momentum thickness should not change appreciably, and at separation is of the order of our limits just upstream of the backward-facing step insert: $\delta_\theta|_{\text{separation}} \sim 0.003$ m.

The results of Baugh (2010) determined that for our test rig the unforced reattachment length $X_{r_\circ} = 5.0$ is independent of Re_h within the range of $3770 \leq Re_h \leq 46100$. This unforced reattachment length was less than those of other backward-facing step experiments with comparable geometry and flow conditions, $6 \lessapprox X_{r_\circ} \lessapprox 8$. It is postulated that this unusual short reattachment length is likely due to the presence of counter rotating Görtler vortices produced upstream of the step along the concave section of our backward-facing step. The presence of Görtler vortices in the separating boundary layer will increase mixing in the free shear layer resulting in a shortening of reattachment length.

One of the objectives of the performing the reattachment length versus perturbation Strouhal number experiment (Section 13.3.1) was to determine which of the forcing cases (amplitude and frequency) for the experiments performed by Baugh contained the least amount actuation error. Some discussion on this was given in Part I. In Part I it was determined that the Alpha actuator performance is more dependant upon actuation amplitude than frequency. For reference signal amplitudes tested larger than 40 μs and less than 100 μs (corresponds with actuation amplitudes of 0.88 mm and 2.2 mm respectively), the Alpha performance was at its best. From the Part I analysis it was unclear whether the 100 μs was the true upper limit or if it was larger. This was due to there not being any data available on the Alpha actuator performance for PWM amplitudes larger than 100 μs. The investigation of Part II agreed with the lower limit and showed that upper limit was in fact larger at approximately a reference signal amplitude of 150 μs (actuation amplitude of 3.3 mm). This was due to the observation that the two curves from Baugh of moderate forcing amplitude, $0.2\ \lessapprox\ u'/U_\infty\ \lessapprox 0.35$ (corresponding with PWM reference signal amplitudes of approximately 40 to 150 μs), followed the current results the closest, indicating the lowest actuation error. From these results it is concluded that the data from Baugh (2010) which contains permissible amounts of actuation error are of velocity amplitudes between $0.2\ \lessapprox\ u'/U_\infty\ \lessapprox 0.35$.

In the course of the performed forcing experiments, two flow response characteristics were discovered that has not been presented in the literature. The spanwise-

invariant forcing experiments examined the effect imposed on reattachment length for varying forcing Strouhal number and forcing amplitude at a Reynolds number of 24,500. Reattachment length was measured as a function of Strouhal number for four different forcing amplitudes. The results show that the optimal Strouhal number (resulting in the shortest reattachment) diminishes with increasing forcing amplitude. For forcing amplitude $u'/U_\infty = 0.1$ the optimal $St_h = 0.4$, and at forcing amplitude $u'/U_\infty = 1.08$ the optimal $St_h = 0.29$. A possible cause for this trend is the lifting of the reattaching shear layer just after separation. This would alter the effective step height, affecting the step mode vortex shedding frequency as indicated by Sigurdson (1995) for a forward-facing step flow. There is also a general trend of reattachment reduction with increasing forcing amplitude.

The effect of varying forcing amplitude on reattachment length was also examined in more detail. Two curves were produced for two different forcing Strouhal numbers. The results show that our reattachment reduction as a function of u'/U_∞ is not monotonic, and has a peak at $u'/U_\infty \approx 0.5 - 0.6$. Thus, it appears that there are two mechanisms acting to reduce reattachment, one at the forcing amplitudes below this peak, and the other at larger amplitudes. One speculation for the cause of this effect is to do with how far the forcing "reaches" into the flow: if the forcing reaches the point within the shear layer where that particular forcing frequency is amplified, it will result in a maximum of reattachment reduction. As forcing amplitude is further increased, it will reach beyond this point where it previously was amplified, halting the process of amplification until a point further downstream. This will result in less shortening of the reattachment length. For extreme forcing amplitudes $u'/U_\infty \gtrapprox 0.6$, it is suspected that the forcing is becoming so large that it is becoming the dominant influence defining the flow structure in the wake of the BFS, and it is observed that the forcing Strouhal dependence lessens.

15.2 Future Work

The flow actuator was designed to allow for variance of forcing in the spanwise direction. The current study did not examine the effects of spanwise-variance of actuation on the flow. Thus the next experiments pending to be performed are those of spanwise-variant actuation. One of the numerical experiments of interest performed by Kang and Choi (2002) studied the effect of a spanwise-varying waveform with constant phase velocity: a sinusoidal waveform which shifts in the spanwise direction at a constant velocity. Although there is great excitement for these experiments to go underway, it would be recommended that a few others should be performed first.

From the theoretical study of the boundary layer properties, it was concluded that the separating boundary layer is likely permeated with counter rotating Görtler

vortices resulting in our shorter than expected reattachment length. One way to determine their presence, and a solution for eliminating them, would be to remove the concave profile at the leading edge of the RoboStep. This can be achieved by extending the RoboStep further upstream with an additional fillet so it connects smoothly with the water tunnel wall within the contraction. This fillet would have to be carefully designed so it does not become dislodged during tunnel operation. If this were to occur, it could block the passage of water resulting in a large pressure rise upstream of the blockage which could be destructive. With the proper fillet, the profile from the contraction up to the BFS edge should remain convex or flat, eliminating the source of Görtler instability. If there is an observed increase in $X_{r_\circ}$ with the fillet in place of the order of 20-30%, this will be definitive evidence that the original RoboStep configuration resulted in the formation of Görtler vortices and that they have been eliminated.

Once the RoboStep fillet is in place, the spanwise-varying actuation experiments and others could be pursued without hindrance. Apart from the spanwise-varying experiments, it would be beneficial to reperform the large amplitude experiments of Section 14.2.2 to confirm whether the observation of a non-monotonic reattachment reduction with increasing forcing amplitude is a result of the interaction of the forcing with the Görtler vortices or not. It could also be beneficial to perform the experiment for a few more forcing Strouhal numbers to verify that the observed trend's dependence on St_h holds.

Having already defined the geometry of the water tunnel wall starting from within the settling chamber up to the BFS (see Appendix H), a computational analysis of the boundary layer growth could be the next progression of understanding of the properties of the separating boundary layer. Or the next level further, some new flow visualization techniques could be used to physically measure the boundary layer at separation. The RoboStep has a port positioned in the middle of the span approximately 4 step heights upstream of the separation point for the installation of a hydrogen bubble wire. Some more designing and work is required to finish the installation, but with this in place, the velocity profile perpendicular the step at the separation point could be measured using an already functioning Image Correlation Velocimetry (ICV) rig. The IVC rig was developed and used by Apps (2001) and details on its use can be seen in his Master's Thesis and Apps, Chen, and Sigurdson (2003).

A Particle Image Velocimetry (PIV) velocity measurement could also potentially be implemented using the ICV rig. Yoshioka et al. (1999) used a PIV method for their velocity measurements in a BFS water flow. They successfully seeded the flow using Nylon12 particles of 60 μm in mean diameter and 1.02 inches in specific gravity. They illuminated the flow field using a Xenon stroboscopic light sheet

similar to the current strobes used for ICV. This method could give more insight into the mechanism of the observed flow phenomena of the current study. For example a working hypothesis was proposed in Section 14.2.1 that the shift of optimal Strouhal number to a lower value with increasing actuation amplitude could be due to the initial lifting of the free shear layer. This could be verified by a PIV measurement.

Another flow measurement which could be implemented with little effort is phase averaging. Described in Appendix I, it could be use in conjunction with the current method of reattachment line measurement to observe a phase-averaged reattachment line apposed to a time-averaged reattachment line. This could be easily implemented by controlling the phase and frequency of captured images of the tuft array with respect to the phase and frequency of actuation. The servomotor reference signal controllers are triggered to initial forcing of each actuator using a common trigger signal. This same trigger signal could trigger a timer to control the sequence of images captured of the tuft array. Phase-averaging could also be performed of the PIV measurements in a similar fashion if PIV measurement of the velocity field is pursued.

For the Beta actuator reference signal generation, a High Speed Servo Controller was designed and constructed. It allowed for versatile control of the actuation waveform and improved actuator performance. However, it adds difficulty to the usability of the system. Another disadvantage of the Beta reference signal generation method is it requires a substantial amount of time (approximately 5 minutes for all 16 actuators) to change the actuation waveform, and the process is not fully automated. This limits the current design to only be used for open-loop control of the BFS flow. It would be beneficial for a new reference signal generation system, capable of a 250 Hz frame rate, which is more transparent and simple to use and allow for the possibility of full computer control of the frequency, amplitude, and phase of each actuator. One possible solution could use a programmable waveform generator such as the AD9833 from Analog Devices as a base building block for such a system.

Bibliography

Adams, E. and Johnston, J.P. 1988. Effects of the separating shear layer on the reattachment flow structure part 2: reattachment length and wall shear stress. *Experiments in Fluids*, 6:493–499.

Apps, C.P. 2001. *a study of synthetic fence jets using I.C.V.* Master's thesis, Department of Mechanical Engineering, University of Alberta.

Apps, C.P., Chen, T., and Sigurdson, L.W. 2003. Image correlation velocimetry applied to discrete smoke-wire streaklines in turbulent pipe flow. *Experiments in Fluids*, 35:288–290.

Armaly, B., Durst, F., Pereira, J., and Schönung, B. 1983. Experimental and theoretical investigation of backward-facing step flow. *J. Fluid Mech.*, 127:473–496.

Baugh, A. 2010. *Active open-loop control of a backward-facing step flow.* Master's thesis, Department of Mechanical Engineering, University of Alberta.

Bhattecharjee, S.B. and Troutt, T. 1986. Modification of vortex interactions in a reattaching separated flow. *AIAA Journal*, 52:113–135.

Bradshaw, P. and Wong, F. 1972. The reattachment and relaxation of a turbulent shear layer. *J. Fluid Mech.*, 52:113–135.

Breakey, D. 2009. Personal communication.

Brown, G. and Roshko, A. 1974. On density effects and large structure in a turbulent mixing layers. *J. Fluid Mech.*, 64:775–816.

Chun, K.B. and Sung, H.J. 1996. Control of turbulent separated flow over a backward-facing step by local forcing. *Experiments in Fluids*, 21:417–426.

Chun, K.B. and Sung, H.J. 1998. Visualization of a locally-forced separated flow over a backward-facing step. *Experiments in Fluids*, 25:133–142.

Chun, K.B. and Sung, H.J. 1999. Effect of spanwise-varing local forcing on turbulent separated flow over a backward-facing step. *Experiments in Fluids*, 26:437–440.

Coward, A. 2004. *Recommissioning an inoperable icing water tunnel as a flow visualization water tunnel.* Master of engineering report, Department of Mechanical Engineering, University of Alberta.

de Brederode, V. and Bradshaw, P. August 1972. Three-dimensional flow in nominally two-dimensional separation bubbles. I. Flow behind a backward-facing step. I.C. Aero Report 72-19, Imperial college of science and technology.

Eaton, J.K. and Johnston, J.P. June 1980. Turbulent flow reattachment: an experimental study of the flow and structure behind a backward-facing step. Technical Report MD-39, Stanford University.

Gilbert, S.K. 2007. *Unsteady spatially varying flow control.* Master's thesis, Department of Mechanical Engineering, University of Alberta.

Hassan, M.A.Z. 1992. The flow over a backward-facing step under controlled perturbations: laminar separation. *J. Fluid Mech.*, 238:73–96.

Henning, L. and King, R. 2007. Robust multivariable closed-loop control of a turbulent backward-facing step flow. *J. Aircraft*, 44(1):201–208.

Hillier, R. and Cherry, N. 1981. the effects of stream turbulence on separation bubbles. *J. Wind Engng and Industrial Aerodynamics*, 8:49–58.

Isomoto, K. and Honami, S. 1989. The effect of inlet turbulence intensity on the reattachment process over a backward-facing step. *J. Fluids Engng*, 111:87–92.

Kang, S. and Choi, H. 2002. Suboptimal feedback control of turbulent flow over a backward-facing step. *J. Fluid Mech.*, 463:201–227.

Kim, J., Kline, S.J., and Johnston, J.P. 1980. Investigation of a reattaching turbulent shear layer: flow over a backward-facing step. *J. Fluids Engng*, 102:302–308.

Kim, M., Choi, C., and Yoon, D. 2010. The onset of Görtler vortices in laminar boundary layer flow over a slightly concave wall. *European J. Mech. B/Fluids*, 29:407–414. Journal homepage: www.elsevier.com/locate/ejmflu.

Kim, S., Choi, H., and Yoo, J.Y. 2007. effect of local forcing on backward-facing step flow with laminar separation. *J. Turb.*, 8(6).

Kundu, P. and Cohen, I. 2008. *Fluid Mechanics.* Elsevier Inc., 4^{th} edition. With contributions by P.S. Ayyaswamy and H.H. Hu.

Lai, J.C.S., Yue, J., and Platzer, M.F. 2002. Control of backward-facing step flow using a flapping foil. *Experiment in Fluids*, 32:44–54.

Liepmann, H.W. 1945. Investigation of boundary layer transition on concave walls. Technical Report 4J28, NACA Wartime Report.

Oster, D. and Wygnanski, I. 1982. The forced mixing layer between parallel streams. *J. Fluid Mech.*, 123:91–130.

Ötügen, M. 1991. Expansion ratio effects on the separated shear layer and reattachment downstream of a backward-facing step. *Experiments in Fluids*, 10(5):273–280.

Roos, F. and Kegelman, J. 1986. Control of coherent structures in reattaching laminar and turbulent shear layers. *AIAA Journal*, 24:1956–1963.

Rothe, P.H. December 1975. *The effects of system rotation on separation, reattachment and performance in two-dimensional diffusers.* Ph.D. thesis, Stanford Univ. CA.

Sakakibara, J. and Anazi, T. June 2001. Chain-link-fence structures produced in a plane jet. *Phys. Fluids*, 13(6):1541–1543.

Saric, W. 1994. Görtler vortices. *Annu. Rev. Fluid Mech.*, 26:379–409.

Sigurdson, L.W. 1986. *The structure and control of a turbulent reattaching flow.* Ph.D. thesis, Caltech.

Sigurdson, L.W. 1995. the structure and control of a turbulent reattaching flow. *J. Fluid Mech.*, 298:139–165.

Sigurdson, L.W. 2011. Personal communication.

Sigurdson, L.W. and Roshko, A. 1984. the large-scale structure of a turbulent reattaching flow. *Bulletin of the American Physical Society*, 29:1542.

Sigurdson, L.W. and Roshko, A. 1985. Controlled unsteady excitation of a reattaching flow. In *AIAA Shear flow control conference*, 85-0552.

Sutton, D. 2010. Personal communication.

Tennekes, H. and Lumley, J.L. 1972. *a first course in turbulence*. the MIT Press.

Uruba, V., Jonáš, P., and Mazur, O. 2007. Control of a channel-flow behind a backward-facing step by suciton/blowing. *Int. J. Heat and Fluid Flow*, 28:665–672.

Westphal, R.V., Johnston, J.P., and Eaton, J.K. 1984. Experimental study of flow reattachment in a single-sided sudden expansion. Technical Report 3765, NASA Contractor Report.

Winant, C.D. and Browand, F.K. 1974. Vortex pairing: the mechanism of turbulent mixing-layer growth at moderate reynolds number. *J. Fluid Mech.*, 63:237–255.

Yanase, S., Kawahara, G., and Kiyama, H. 2001. three-dimensional vortical structures of a backward-facing step flow at moderate Reynolds numbers. *J. Physical Society of Japan*, 70(12):3550–3555.

Yoshioka, S., Obi, S., and Masuda, S. 1999. momentum transfer in the periodically perturbed turbulent separated flow over the backward-facing step. In *Turbulence and Shear Flow Phenomena*, 1. pages 1321–1326.

Yoshioka, S., Obi, S., and Masuda, S. 2001a. Organized vortex motion in periodically perturbed turbulent separated flow over a backward-facing step. *International J. Heat and Fluid Flow*, 22:301–307.

Yoshioka, S., Obi, S., and Masuda, S. January 2001b. Turbulence statistics of periodically perturbed separated flow over backward-facing step. *International J. Heat and Fluid Flow*, 22:391–401.

Appendix A

Actuator Alpha Performance Data

Actuator alpha performance data is presented in the raw. For five of the alpha actuators, three measurement trials were performed of 20 seconds duration for each actuation case. The actuation cases, ranging in excitation amplitude 10-100 μs and excitation frequency 0.5-3.0 Hz, were of a sinusoidal waveform. The motion of the actuators were measured using a 1 inch linear range LVDT attached to the actuator output. This LVDT measurement was digitally recoreded at a 2 kHz sample rate using National Instruments Labview. Before digital conversion of the LVDT data, it was filtered using a 200 Hz cut-off, 2nd order, passive RC analog filter.

Using Labview, the actuator output frequency, output amplitude, and Total Harmonic Distortion (%THD) were calculated. For each acutator, an arithetic mean from the three measurement trials was calculated. The last page shows the actuator performance data calculated from the arithmetic mean of each of the five acutators tested. This performance data is presented in chapter 6 on page 21 of this thesis as %THD, Normalized Actuation Amplitude, and Maximum Absolute Deviation.

Actuator Number 8 Performance Trials LVDT has 1" linear range

10-03-16

LVDT calibration factor: **20.36** **Volts/Inch**

Measurement Trial 1

Excitation Frequency: 0.5 Hz

	Measured Data				
Excitation Amplitude [µs]	Frequency [Hz]	Amplitude [V]	Amplitude [In]	Amplitude [mm]	%THD (10 harmonics)
10	0.099	0.048	0.0024	0.0598	37.7000
20	0.491	0.126	0.0062	0.1572	25.3000
30	0.083	0.202	0.0099	0.2520	17.7000
40	0.496	0.307	0.0151	0.3830	13.1000
50	0.501	0.422	0.0207	0.5265	10.6000
60	0.497	0.537	0.0264	0.6699	9.8300
70	0.496	0.659	0.0324	0.8221	9.5200
80	0.500	0.804	0.0395	1.0030	8.8300
90	0.498	0.913	0.0448	1.1390	9.0000
100	0.498	1.080	0.0530	1.3473	8.0500

Measurement Trial 2

Excitation Frequency: 0.5 Hz

	Measured Data				
Excitation Amplitude [µs]	Frequency [Hz]	Amplitude [V]	Amplitude [In]	Amplitude [mm]	%THD (10 harmonics)
10	nan	0.039	0.0019	0.0482	45.4000
20	0.502	0.124	0.0061	0.1547	15.9000
30	0.500	0.225	0.0111	0.2807	12.6000
40	0.494	0.276	0.0136	0.3443	12.0000
50	0.500	0.418	0.0205	0.5215	10.8000
60	0.500	0.524	0.0257	0.6537	9.3300
70	0.499	0.654	0.0321	0.8159	9.3700
80	0.502	0.772	0.0379	0.9631	9.8000
90	0.500	0.907	0.0445	1.1315	9.2100
100	0.499	1.040	0.0511	1.2974	8.3300

Measurement Trial 1

Excitation Frequency: 1 Hz

	Measured Data				
Excitation Amplitude [µs]	Frequency [Hz]	Amplitude [V]	Amplitude [In]	Amplitude [mm]	%THD (10 harmonics)
10	0.107	0.050	0.0025	0.0626	34.1000
20	0.334	0.098	0.0048	0.1221	17.6000
30	0.998	0.192	0.0094	0.2395	14.3000
40	0.994	0.295	0.0145	0.3680	15.0000
50	1.000	0.427	0.0210	0.5327	13.4000
60	1.000	0.540	0.0265	0.6737	12.5000
70	1.000	0.667	0.0328	0.8321	12.6000
80	1.000	0.796	0.0391	0.9930	12.7000
90	1.010	0.927	0.0455	1.1565	12.2000
100	1.000	1.060	0.0521	1.3224	12.0000

Measurement Trial 2

Excitation Frequency: 1 Hz

	Measured Data				
Excitation Amplitude [µs]	Frequency [Hz]	Amplitude [V]	Amplitude [In]	Amplitude [mm]	%THD (10 harmonics)
10	1.120	0.027	0.0013	0.0331	49.7000
20	nan	0.068	0.0033	0.0842	19.1000
30	1.010	0.188	0.0092	0.2345	14.7000
40	1.000	0.298	0.0146	0.3718	15.7000
50	1.000	0.421	0.0207	0.5252	13.1000
60	0.995	0.549	0.0270	0.6849	12.4000
70	0.998	0.669	0.0329	0.8346	12.1000
80	1.000	0.802	0.0394	1.0005	11.4000
90	1.000	0.918	0.0451	1.1452	10.2000
100	0.998	1.060	0.0521	1.3224	8.7600

Measurement Trial 1

Excitation Frequency: 1.5 Hz

	Measured Data				
Excitation Amplitude [µs]	Frequency [Hz]	Amplitude [V]	Amplitude [In]	Amplitude [mm]	%THD (10 harmonics)
10	nan	0.057	0.0028	0.0712	26.7000
20	0.136	0.118	0.0058	0.1472	20.8000
30	1.500	0.215	0.0106	0.2682	16.5000
40	1.480	0.292	0.0143	0.3643	15.8000
50	1.490	0.428	0.0210	0.5339	13.1000
60	1.500	0.584	0.0287	0.7286	13.6000
70	1.510	0.756	0.0371	0.9431	11.4000
80	1.500	0.902	0.0443	1.1253	10.1000
90	1.500	1.040	0.0511	1.2974	8.4000
100	1.490	1.170	0.0575	1.4596	7.7000

Measurement Trial 2

Excitation Frequency: 1.5 Hz

	Measured Data				
Excitation Amplitude [µs]	Frequency [Hz]	Amplitude [V]	Amplitude [In]	Amplitude [mm]	%THD (10 harmonics)
10	nan	0.051	0.0025	0.0637	32.8000
20	1.500	0.088	0.0043	0.1092	18.7000
30	0.742	0.206	0.0101	0.2570	17.0000
40	1.480	0.309	0.0152	0.3855	16.5000
50	1.500	0.433	0.0213	0.5402	12.9000
60	1.500	0.570	0.0280	0.7111	11.9000
70	1.500	0.720	0.0354	0.8982	10.5000
80	1.500	0.864	0.0424	1.0779	9.0400
90	1.490	1.020	0.0501	1.2725	7.7400
100	1.500	1.220	0.0599	1.5220	7.0400

Measurement Trial 1

Excitation Frequency: 2 Hz

	Measured Data				
Excitation Amplitude [µs]	Frequency [Hz]	Amplitude [V]	Amplitude [In]	Amplitude [mm]	%THD (10 harmonics)
10	0.154	0.059	0.0029	0.0739	21.3000
20	0.069	0.108	0.0053	0.1347	21.9000
30	2.040	0.201	0.0099	0.2508	20.7000
40	1.980	0.300	0.0147	0.3743	20.5000
50	2.010	0.486	0.0239	0.6063	15.7000
60	2.000	0.653	0.0321	0.8146	12.3000
70	2.000	0.785	0.0386	0.9793	9.7100
80	2.000	0.930	0.0457	1.1602	7.6700
90	2.000	1.080	0.0530	1.3473	6.4800
100	2.000	1.250	0.0614	1.5594	6.2700

Measurement Trial 2

Excitation Frequency: 2 Hz

	Measured Data				
Excitation Amplitude [µs]	Frequency [Hz]	Amplitude [V]	Amplitude [In]	Amplitude [mm]	%THD (10 harmonics)
10	0.646	0.055	0.0027	0.0682	23.2000
20	0.125	0.089	0.0044	0.1109	22.8000
30	2.000	0.204	0.0100	0.2545	21.3000
40	1.990	0.304	0.0149	0.3793	19.6000
50	0.400	0.473	0.0232	0.5901	15.6000
60	2.000	0.593	0.0291	0.7398	15.7000
70	2.000	0.810	0.0398	1.0105	12.9000
80	2.010	0.931	0.0457	1.1615	8.2800
90	2.000	1.120	0.0550	1.3972	6.5100
100	2.000	1.250	0.0614	1.5594	6.3900

Measurement Trial 1

Excitation Frequency: 2.5 Hz

	Measured Data				
Excitation Amplitude [µs]	Frequency [Hz]	Amplitude [V]	Amplitude [In]	Amplitude [mm]	%THD (10 harmonics)
10	0.282	0.045	0.0022	0.0566	19.8000
20	0.312	0.094	0.0046	0.1170	26.5000
30	2.510	0.205	0.0101	0.2557	22.3000
40	0.132	0.396	0.0194	0.4940	17.9000
50	2.530	0.529	0.0260	0.6600	14.0000
60	2.500	0.693	0.0340	0.8645	10.3000
70	2.500	0.844	0.0415	1.0529	8.8800
80	2.500	1.040	0.0511	1.2974	7.0500
90	2.510	1.180	0.0580	1.4721	6.5600
100	2.500	1.320	0.0648	1.6468	5.5000

Measurement Trial 2

Excitation Frequency: 2.5 Hz

	Measured Data				
Excitation Amplitude [µs]	Frequency [Hz]	Amplitude [V]	Amplitude [In]	Amplitude [mm]	%THD (10 harmonics)
10	1.200	0.079	0.0039	0.0981	23.4000
20	2.500	0.121	0.0059	0.1510	27.7000
30	2.430	0.208	0.0102	0.2595	21.8000
40	2.490	0.342	0.0168	0.4267	18.8000
50	2.490	0.555	0.0273	0.6924	12.6000
60	2.500	0.704	0.0346	0.8783	9.7900
70	2.510	0.834	0.0410	1.0405	8.5800
80	2.500	0.978	0.0480	1.2201	6.9500
90	2.560	1.140	0.0560	1.4222	5.6400
100	2.510	1.330	0.0653	1.6592	4.7700

Measurement Trial 1

Excitation Frequency: 3 Hz

	Measured Data				
Excitation Amplitude [µs]	Frequency [Hz]	Amplitude [V]	Amplitude [In]	Amplitude [mm]	%THD (10 harmonics)
10	2.900	0.070	0.0034	0.0868	21.1000
20	0.075	0.134	0.0066	0.1672	26.8000
30	2.990	0.286	0.0140	0.3568	17.9000
40	3.020	0.388	0.0191	0.4840	13.7000
50	3.020	0.541	0.0266	0.6749	10.2000
60	3.010	0.735	0.0361	0.9169	8.1600
70	2.980	0.910	0.0447	1.1353	5.8500
80	3.000	1.050	0.0516	1.3099	5.4400
90	3.010	1.140	0.0560	1.4222	3.9200
100	3.000	1.240	0.0609	1.5470	2.8400

Measurement Trial 2

Excitation Frequency: 3 Hz

	Measured Data				
Excitation Amplitude [µs]	Frequency [Hz]	Amplitude [V]	Amplitude [In]	Amplitude [mm]	%THD (10 harmonics)
10	3.100	0.053	0.0026	0.0666	21.1000
20	0.429	0.130	0.0064	0.1622	25.9000
30	3.020	0.261	0.0128	0.3256	18.7000
40	2.990	0.407	0.0200	0.5078	13.9000
50	3.000	0.544	0.0267	0.6787	10.9000
60	3.000	0.736	0.0361	0.9182	8.0900
70	2.990	0.927	0.0455	1.1565	5.7200
80	3.010	1.140	0.0560	1.4222	2.8400
90	3.000	1.250	0.0614	1.5594	3.1100
100	3.020	1.320	0.0648	1.6468	2.7700

Actuator Number 8 Performance Trials

10-03-16

LVDT calibration factor: **20.36** **Volts/Inch**

Measurement Trial 3

Excitation Frequency: 0.5 Hz

	Measured Data				
Excitation Amplitude [µs]	Frequency [Hz]	Amplitude [V]	Amplitude [In]	Amplitude [mm]	%THD (10 harmonics)
10	0.063	0.046	0.0023	0.0573	47.5000
20	0.526	0.120	0.0059	0.1497	25.7000
30	0.166	0.194	0.0095	0.2425	12.9000
40	0.501	0.279	0.0137	0.3481	12.0000
50	0.495	0.424	0.0208	0.5290	10.5000
60	0.499	0.553	0.0272	0.6899	7.9100
70	0.499	0.678	0.0333	0.8458	9.5400
80	0.505	0.804	0.0395	1.0030	9.7700
90	0.498	0.905	0.0444	1.1290	9.0100
100	0.496	1.030	0.0506	1.2850	7.8300

Arithmetic Mean for Actuator 8 Measurement Trials

Excitation Frequency: 0.5 Hz

	Measured Data				
Excitation Amplitude [µs]	Frequency [Hz]	Amplitude [V]	Amplitude [In]	Amplitude [mm]	%THD (10 harmonics)
10	0.081	0.044	0.0022	0.0551	43.533
20	0.506	0.123	0.0061	0.1539	22.300
30	0.250	0.207	0.0102	0.2584	14.400
40	0.497	0.287	0.0141	0.3585	12.367
50	0.499	0.421	0.0207	0.5256	10.633
60	0.499	0.538	0.0264	0.6712	9.023
70	0.498	0.664	0.0326	0.8280	9.477
80	0.502	0.793	0.0390	0.9897	9.467
90	0.499	0.908	0.0446	1.1332	9.073
100	0.498	1.050	0.0516	1.3099	8.070

Measurement Trial 3

Excitation Frequency: 1 Hz

	Measured Data				
Excitation Amplitude [µs]	Frequency [Hz]	Amplitude [V]	Amplitude [In]	Amplitude [mm]	%THD (10 harmonics)
10	nan	0.035	0.0017	0.0435	47.2000
20	1.000	0.077	0.0038	0.0958	23.0000
30	1.030	0.174	0.0085	0.2171	16.2000
40	0.992	0.285	0.0140	0.3556	16.5000
50	1.000	0.406	0.0199	0.5065	13.9000
60	0.995	0.541	0.0266	0.6749	12.4000
70	0.996	0.677	0.0333	0.8446	11.0000
80	1.000	0.817	0.0401	1.0192	10.2000
90	1.000	0.955	0.0469	1.1914	9.5000
100	1.000	1.100	0.0540	1.3723	9.4400

Arithmetic Mean for Actuator 8 Measurement Trials

Excitation Frequency: 1 Hz

	Measured Data				
Excitation Amplitude [µs]	Frequency [Hz]	Amplitude [V]	Amplitude [In]	Amplitude [mm]	%THD (10 harmonics)
10	0.614	0.037	0.0018	0.0464	43.667
20	0.667	0.081	0.0040	0.1007	19.900
30	1.013	0.185	0.0091	0.2304	15.067
40	0.995	0.293	0.0144	0.3651	15.733
50	1.000	0.418	0.0205	0.5215	13.467
60	0.997	0.543	0.0267	0.6778	12.433
70	0.998	0.671	0.0330	0.8371	11.900
80	1.000	0.805	0.0395	1.0043	11.433
90	1.003	0.933	0.0458	1.1644	10.633
100	0.999	1.073	0.0527	1.3390	10.067

Measurement Trial 3

Excitation Frequency: 1.5 Hz

	Measured Data				
Excitation Amplitude [µs]	Frequency [Hz]	Amplitude [V]	Amplitude [In]	Amplitude [mm]	%THD (10 harmonics)
10	nan	0.069	0.0034	0.0858	37.1000
20	0.499	0.083	0.0041	0.1033	20.9000
30	1.470	0.191	0.0094	0.2383	16.6000
40	1.490	0.291	0.0143	0.3630	15.6000
50	1.500	0.417	0.0205	0.5202	13.3000
60	1.480	0.573	0.0281	0.7148	11.9000
70	1.490	0.728	0.0358	0.9082	11.1000
80	1.500	0.884	0.0434	1.1028	8.4100
90	1.500	1.080	0.0530	1.3473	7.4600
100	1.500	1.230	0.0604	1.5345	7.4600

Arithmetic Mean for Actuator 8 Measurement Trials

Excitation Frequency: 1.5 Hz

	Measured Data				
Excitation Amplitude [µs]	Frequency [Hz]	Amplitude [V]	Amplitude [In]	Amplitude [mm]	%THD (10 harmonics)
10	#DIV/0!	0.059	0.0029	0.0736	32.200
20	0.712	0.096	0.0047	0.1199	20.133
30	1.237	0.204	0.0100	0.2545	16.700
40	1.483	0.297	0.0146	0.3709	15.967
50	1.497	0.426	0.0209	0.5315	13.100
60	1.493	0.576	0.0283	0.7182	12.467
70	1.500	0.735	0.0361	0.9165	11.000
80	1.500	0.883	0.0434	1.1020	9.183
90	1.497	1.047	0.0514	1.3058	7.867
100	1.497	1.207	0.0593	1.5054	7.400

Measurement Trial 3

Excitation Frequency: 2 Hz

	Measured Data				
Excitation Amplitude [µs]	Frequency [Hz]	Amplitude [V]	Amplitude [In]	Amplitude [mm]	%THD (10 harmonics)
10	0.665	0.065	0.0032	0.0812	23.5000
20	1.990	0.092	0.0045	0.1144	22.7000
30	2.010	0.208	0.0102	0.2595	21.0000
40	1.990	0.328	0.0161	0.4088	18.8000
50	0.133	0.557	0.0274	0.6949	15.4000
60	2.000	0.664	0.0326	0.8284	11.6000
70	2.000	0.818	0.0402	1.0205	9.9800
80	2.000	0.961	0.0472	1.1989	7.4500
90	2.010	1.100	0.0540	1.3723	6.6400
100	2.000	1.250	0.0614	1.5594	6.6500

Arithmetic Mean for Actuator 8 Measurement Trials

Excitation Frequency: 2 Hz

	Measured Data				
Excitation Amplitude [µs]	Frequency [Hz]	Amplitude [V]	Amplitude [In]	Amplitude [mm]	%THD (10 harmonics)
10	0.488	0.060	0.0029	0.0744	22.667
20	0.728	0.096	0.0047	0.1200	22.467
30	2.017	0.204	0.0100	0.2549	21.000
40	1.987	0.311	0.0153	0.3874	19.633
50	0.848	0.505	0.0248	0.6304	15.567
60	2.000	0.637	0.0313	0.7943	13.200
70	2.000	0.804	0.0395	1.0034	10.863
80	2.003	0.941	0.0462	1.1735	7.800
90	2.003	1.100	0.0540	1.3723	6.543
100	2.000	1.250	0.0614	1.5594	6.437

Measurement Trial 3

Excitation Frequency: 2.5 Hz

	Measured Data				
Excitation Amplitude [µs]	Frequency [Hz]	Amplitude [V]	Amplitude [In]	Amplitude [mm]	%THD (10 harmonics)
10	0.149	0.066	0.0032	0.0820	32.3000
20	2.520	0.110	0.0054	0.1372	25.1000
30	0.833	0.267	0.0131	0.3331	20.7000
40	2.500	0.411	0.0202	0.5127	14.9000
50	2.530	0.552	0.0271	0.6886	10.8000
60	2.510	0.699	0.0343	0.8720	8.4300
70	2.500	0.869	0.0427	1.0841	6.8700
80	2.500	1.000	0.0491	1.2475	5.9000
90	2.480	1.200	0.0589	1.4971	6.0100
100	2.470	1.300	0.0639	1.6218	4.8800

Arithmetic Mean for Actuator 8 Measurement Trials

Excitation Frequency: 2.5 Hz

	Measured Data				
Excitation Amplitude [µs]	Frequency [Hz]	Amplitude [V]	Amplitude [In]	Amplitude [mm]	%THD (10 harmonics)
10	0.544	0.063	0.0031	0.0789	25.167
20	1.777	0.108	0.0053	0.1351	26.433
30	1.924	0.227	0.0111	0.2828	21.600
40	1.707	0.383	0.0188	0.4778	17.200
50	2.517	0.545	0.0268	0.6803	12.467
60	2.503	0.699	0.0343	0.8716	9.507
70	2.503	0.849	0.0417	1.0592	8.110
80	2.500	1.006	0.0494	1.2550	6.633
90	2.517	1.173	0.0576	1.4638	6.070
100	2.493	1.317	0.0647	1.6426	5.050

Measurement Trial 3

Excitation Frequency: 3 Hz

	Measured Data				
Excitation Amplitude [µs]	Frequency [Hz]	Amplitude [V]	Amplitude [In]	Amplitude [mm]	%THD (10 harmonics)
10	0.373	0.066	0.0033	0.0828	22.1000
20	0.176	0.118	0.0058	0.1472	27.6000
30	0.214	0.282	0.0139	0.3518	17.5000
40	2.990	0.415	0.0204	0.5177	13.0000
50	3.010	0.571	0.0280	0.7123	10.3000
60	2.990	0.735	0.0361	0.9169	6.5600
70	3.010	0.837	0.0411	1.0442	6.5500
80	2.990	1.010	0.0496	1.2600	4.7900
90	3.000	1.160	0.0570	1.4472	3.3400
100	3.000	1.250	0.0614	1.5594	2.8700

Arithmetic Mean for Actuator 8 Measurement Trials

Excitation Frequency: 3 Hz

	Measured Data				
Excitation Amplitude [µs]	Frequency [Hz]	Amplitude [V]	Amplitude [In]	Amplitude [mm]	%THD (10 harmonics)
10	2.124	0.063	0.0031	0.0788	21.433
20	0.227	0.127	0.0063	0.1589	26.767
30	2.075	0.276	0.0136	0.3447	18.033
40	3.000	0.403	0.0198	0.5032	13.533
50	3.010	0.552	0.0271	0.6886	10.467
60	3.000	0.735	0.0361	0.9174	7.603
70	2.993	0.891	0.0438	1.1120	6.040
80	3.000	1.067	0.0524	1.3307	4.357
90	3.003	1.183	0.0581	1.4763	3.457
100	3.007	1.270	0.0624	1.5844	2.827

Actuator Number 10 Performance Trials LVDT has 1" linear range

10-03-16

LVDT calibration factor: **20.36** **Volts/Inch**

Measurement Trial 1

Excitation Frequency: 0.5 Hz

	Measured Data				
Excitation Amplitude [µs]	Frequency [Hz]	Amplitude [V]	Amplitude [In]	Amplitude [mm]	%THD (10 harmonics)
10	0.488	0.082	0.0040	0.1018	17.6000
20	0.511	0.205	0.0101	0.2557	11.9000
30	0.501	0.316	0.0155	0.3942	8.7400
40	0.498	0.427	0.0210	0.5327	9.2800
50	0.503	0.560	0.0275	0.6986	6.8300
60	0.498	0.677	0.0333	0.8446	6.9700
70	0.499	0.761	0.0374	0.9494	8.2800
80	0.494	0.895	0.0440	1.1166	7.3600
90	0.498	1.060	0.0521	1.3224	7.0900
100	0.499	1.210	0.0594	1.5095	6.0900

Measurement Trial 2

Excitation Frequency: 0.5 Hz

	Measured Data				
Excitation Amplitude [µs]	Frequency [Hz]	Amplitude [V]	Amplitude [In]	Amplitude [mm]	%THD (10 harmonics)
10	nan	0.067	0.0033	0.0838	17.8000
20	0.497	0.182	0.0089	0.2271	12.6000
30	0.507	0.275	0.0135	0.3431	16.8000
40	0.498	0.369	0.0181	0.4603	10.4000
50	0.496	0.458	0.0225	0.5714	8.0100
60	0.501	0.566	0.0278	0.7061	8.4100
70	0.501	0.688	0.0338	0.8583	8.4700
80	0.501	0.821	0.0403	1.0242	8.3100
90	0.500	0.497	0.0244	0.6200	8.5300
100	0.501	1.100	0.0540	1.3723	7.5600

Measurement Trial 1

Excitation Frequency: 1 Hz

	Measured Data				
Excitation Amplitude [µs]	Frequency [Hz]	Amplitude [V]	Amplitude [In]	Amplitude [mm]	%THD (10 harmonics)
10	0.502	0.087	0.0043	0.1083	19.4000
20	0.969	0.201	0.0099	0.2508	11.9000
30	1.000	0.320	0.0157	0.3992	11.7000
40	1.010	0.430	0.0211	0.5364	10.9000
50	0.999	0.543	0.0267	0.6774	10.5000
60	1.000	0.630	0.0309	0.7860	10.7000
70	1.000	0.791	0.0389	0.9868	9.3300
80	1.000	0.938	0.0461	1.1702	8.5300
90	1.000	1.070	0.0526	1.3349	8.4600
100	1.000	1.210	0.0594	1.5095	8.3200

Measurement Trial 2

Excitation Frequency: 1 Hz

	Measured Data				
Excitation Amplitude [µs]	Frequency [Hz]	Amplitude [V]	Amplitude [In]	Amplitude [mm]	%THD (10 harmonics)
10	0.173	0.042	0.0021	0.0523	34.2000
20	0.251	0.120	0.0059	0.1497	18.4000
30	1.000	0.217	0.0107	0.2707	13.9000
40	1.010	0.336	0.0165	0.4192	12.8000
50	0.999	0.468	0.0230	0.5839	10.1000
60	1.000	0.609	0.0299	0.7598	9.8300
70	0.998	0.720	0.0354	0.8982	10.7000
80	1.000	0.873	0.0429	1.0891	8.6600
90	0.998	0.983	0.0483	1.2263	8.6200
100	1.000	1.130	0.0555	1.4097	9.1200

Measurement Trial 1

Excitation Frequency: 1.5 Hz

	Measured Data				
Excitation Amplitude [µs]	Frequency [Hz]	Amplitude [V]	Amplitude [In]	Amplitude [mm]	%THD (10 harmonics)
10	0.506	0.093	0.0046	0.1163	20.5000
20	1.500	0.198	0.0097	0.2470	12.0000
30	1.500	0.298	0.0146	0.3718	10.6000
40	1.500	0.426	0.0209	0.5315	12.1000
50	1.500	0.576	0.0283	0.7186	10.0000
60	1.500	0.735	0.0361	0.9169	7.4500
70	1.510	0.877	0.0431	1.0941	7.3900
80	1.510	1.000	0.0491	1.2475	6.3000
90	1.500	1.150	0.0565	1.4347	6.2700
100	1.500	1.290	0.0634	1.6093	6.0400

Measurement Trial 2

Excitation Frequency: 1.5 Hz

	Measured Data				
Excitation Amplitude [µs]	Frequency [Hz]	Amplitude [V]	Amplitude [In]	Amplitude [mm]	%THD (10 harmonics)
10	0.167	0.052	0.0025	0.0646	38.5000
20	0.736	0.134	0.0066	0.1672	19.4000
30	1.490	0.231	0.0113	0.2882	13.9000
40	1.510	0.415	0.0204	0.5177	13.2000
50	1.500	0.525	0.0258	0.6550	10.8000
60	1.500	0.650	0.0319	0.8109	10.2000
70	1.490	0.810	0.0398	1.0105	9.3200
80	1.510	0.947	0.0465	1.1814	7.8800
90	1.500	1.110	0.0545	1.3848	6.7200
100	1.500	1.260	0.0619	1.5719	6.6500

Measurement Trial 1

Excitation Frequency: 2 Hz

	Measured Data				
Excitation Amplitude [µs]	Frequency [Hz]	Amplitude [V]	Amplitude [In]	Amplitude [mm]	%THD (10 harmonics)
10	2.100	0.094	0.0046	0.1174	19.1000
20	2.010	0.210	0.0103	0.2620	11.2000
30	2.010	0.313	0.0154	0.3905	13.9000
40	1.970	0.457	0.0224	0.5701	12.1000
50	1.990	0.579	0.0284	0.7223	9.4500
60	2.000	0.729	0.0358	0.9095	7.6600
70	2.000	0.932	0.0458	1.1627	7.0100
80	2.000	1.090	0.0535	1.3598	6.8500
90	2.000	1.260	0.0619	1.5719	5.7700
100	1.990	1.380	0.0678	1.7216	4.6000

Measurement Trial 2

Excitation Frequency: 2 Hz

	Measured Data				
Excitation Amplitude [µs]	Frequency [Hz]	Amplitude [V]	Amplitude [In]	Amplitude [mm]	%THD (10 harmonics)
10	1.000	0.075	0.0037	0.0932	25.0000
20	0.400	0.161	0.0079	0.2009	14.2000
30	1.990	0.262	0.0129	0.3269	17.3000
40	2.000	0.414	0.0203	0.5165	14.5000
50	1.990	0.560	0.0275	0.6986	10.1000
60	1.990	0.720	0.0354	0.8982	8.6000
70	2.000	0.913	0.0448	1.1390	8.2400
80	1.990	1.030	0.0506	1.2850	6.0700
90	2.000	1.200	0.0589	1.4971	5.4800
100	2.000	1.360	0.0668	1.6967	5.3200

Measurement Trial 1

Excitation Frequency: 2.5 Hz

	Measured Data				
Excitation Amplitude [µs]	Frequency [Hz]	Amplitude [V]	Amplitude [In]	Amplitude [mm]	%THD (10 harmonics)
10	0.500	0.089	0.0044	0.1115	21.6000
20	2.500	0.183	0.0090	0.2283	18.3000
30	2.480	0.318	0.0156	0.3967	12.2000
40	2.560	0.471	0.0231	0.5876	10.4000
50	2.500	0.651	0.0320	0.8122	8.0200
60	2.500	0.842	0.0414	1.0504	6.5300
70	2.510	1.020	0.0501	1.2725	5.0500
80	2.540	1.180	0.0580	1.4721	3.9700
90	2.500	1.330	0.0653	1.6592	3.4900
100	2.480	1.440	0.0707	1.7965	3.9900

Measurement Trial 2

Excitation Frequency: 2.5 Hz

	Measured Data				
Excitation Amplitude [µs]	Frequency [Hz]	Amplitude [V]	Amplitude [In]	Amplitude [mm]	%THD (10 harmonics)
10	0.489	0.084	0.0041	0.1050	17.7000
20	2.460	0.172	0.0084	0.2146	18.3000
30	2.480	0.310	0.0152	0.3867	13.4000
40	2.480	0.465	0.0228	0.5801	10.6000
50	2.490	0.609	0.0299	0.7598	8.0900
60	2.520	0.781	0.0384	0.9743	6.2800
70	2.500	0.967	0.0475	1.2064	5.5400
80	2.500	1.140	0.0560	1.4222	3.8300
90	2.500	1.310	0.0643	1.6343	3.5600
100	2.490	1.430	0.0702	1.7840	3.8700

Measurement Trial 1

Excitation Frequency: 3 Hz

	Measured Data				
Excitation Amplitude [µs]	Frequency [Hz]	Amplitude [V]	Amplitude [In]	Amplitude [mm]	%THD (10 harmonics)
10	0.150	0.074	0.0036	0.0921	24.4000
20	0.752	0.202	0.0099	0.2520	17.6000
30	3.000	0.327	0.0161	0.4079	13.2000
40	3.040	0.445	0.0219	0.5552	11.6000
50	3.000	0.684	0.0336	0.8533	8.5300
60	3.020	0.835	0.0410	1.0417	6.1100
70	2.990	1.010	0.0496	1.2600	4.4900
80	2.990	1.120	0.0550	1.3972	4.0700
90	2.990	1.240	0.0609	1.5470	3.8600
100	2.990	1.320	0.0648	1.6468	3.3900

Measurement Trial 2

Excitation Frequency: 3 Hz

	Measured Data				
Excitation Amplitude [µs]	Frequency [Hz]	Amplitude [V]	Amplitude [In]	Amplitude [mm]	%THD (10 harmonics)
10	0.430	0.089	0.0043	0.1104	17.1000
20	2.970	0.181	0.0089	0.2258	15.9000
30	3.020	0.323	0.0159	0.4030	12.7000
40	3.000	0.503	0.0247	0.6275	10.1000
50	3.040	0.676	0.0332	0.8433	6.3600
60	3.000	0.863	0.0424	1.0766	4.6400
70	3.000	1.010	0.0496	1.2600	3.9000
80	3.000	1.130	0.0555	1.4097	3.4000
90	3.010	1.250	0.0614	1.5594	3.1900
100	3.000	1.350	0.0663	1.6842	3.0700

Actuator Number 10 Performance Trials
10-03-16
LVDT calibration factor: **20.36** **Volts/Inch**

Measurement Trial 3
Excitation Frequency: 0.5 Hz

	Measured Data				
Excitation Amplitude [µs]	Frequency [Hz]	Amplitude [V]	Amplitude [In]	Amplitude [mm]	%THD (10 harmonics)
10	0.105	0.043	0.0021	0.0534	17.0000
20	nan	0.055	0.0027	0.0680	26.7000
30	0.493	0.154	0.0076	0.1921	17.1000
40	0.506	0.245	0.0120	0.3056	15.8000
50	0.497	0.370	0.0182	0.4616	13.9000
60	0.496	0.495	0.0243	0.6175	13.5000
70	0.499	0.617	0.0303	0.7697	11.2000
80	0.501	0.755	0.0371	0.9419	11.3000
90	0.493	0.880	0.0432	1.0978	11.0000
100	0.497	1.010	0.0496	1.2600	10.9000

Arithmetic Mean for Actuator 10 Measurement Trials
Excitation Frequency: 0.5 Hz

	Measured Data				
Excitation Amplitude [µs]	Frequency [Hz]	Amplitude [V]	Amplitude [In]	Amplitude [mm]	%THD (10 harmonics)
10	0.297	0.064	0.0031	0.0797	17.467
20	0.504	0.147	0.0072	0.1836	17.067
30	0.500	0.248	0.0122	0.3098	14.213
40	0.501	0.347	0.0170	0.4329	11.827
50	0.499	0.463	0.0227	0.5772	9.580
60	0.498	0.579	0.0285	0.7227	9.627
70	0.500	0.689	0.0338	0.8591	9.317
80	0.499	0.824	0.0405	1.0276	8.990
90	0.497	0.812	0.0399	1.0134	8.873
100	0.499	1.107	0.0544	1.3806	8.183

Measurement Trial 3
Excitation Frequency: 1 Hz

	Measured Data				
Excitation Amplitude [µs]	Frequency [Hz]	Amplitude [V]	Amplitude [In]	Amplitude [mm]	%THD (10 harmonics)
10	0.470	0.028	0.0014	0.0348	29.4000
20	0.922	0.063	0.0031	0.0781	23.0000
30	1.010	0.161	0.0079	0.2009	19.2000
40	1.000	0.264	0.0130	0.3294	16.3000
50	1.000	0.378	0.0186	0.4716	14.9000
60	0.996	0.513	0.0252	0.6400	14.0000
70	1.000	0.635	0.0312	0.7922	14.2000
80	1.000	0.770	0.0378	0.9606	12.7000
90	1.000	0.889	0.0437	1.1091	12.1000
100	1.000	1.070	0.0526	1.3349	10.0000

Arithmetic Mean for Actuator 10 Measurement Trials
Excitation Frequency: 1 Hz

	Measured Data				
Excitation Amplitude [µs]	Frequency [Hz]	Amplitude [V]	Amplitude [In]	Amplitude [mm]	%THD (10 harmonics)
10	0.382	0.052	0.0026	0.0651	27.667
20	0.714	0.128	0.0063	0.1595	17.767
30	1.003	0.233	0.0114	0.2903	14.933
40	1.007	0.343	0.0169	0.4283	13.333
50	0.999	0.463	0.0227	0.5776	11.833
60	0.999	0.584	0.0287	0.7286	11.510
70	0.999	0.715	0.0351	0.8924	11.410
80	1.000	0.860	0.0423	1.0733	9.963
90	0.999	0.981	0.0482	1.2234	9.727
100	1.000	1.137	0.0558	1.4180	9.147

Measurement Trial 3
Excitation Frequency: 1.5 Hz

	Measured Data				
Excitation Amplitude [µs]	Frequency [Hz]	Amplitude [V]	Amplitude [In]	Amplitude [mm]	%THD (10 harmonics)
10	0.128	0.035	0.0017	0.0435	31.4000
20	0.297	0.070	0.0035	0.0878	23.0000
30	1.490	0.177	0.0087	0.2208	19.4000
40	1.500	0.300	0.0147	0.3743	18.0000
50	1.490	0.426	0.0209	0.5315	15.0000
60	1.490	0.556	0.0273	0.6936	14.3000
70	1.500	0.711	0.0349	0.8870	12.8000
80	1.500	0.841	0.0413	1.0492	11.3000
90	1.500	1.000	0.0491	1.2475	9.1200
100	1.490	1.200	0.0589	1.4971	7.0800

Arithmetic Mean for Actuator 10 Measurement Trials
Excitation Frequency: 1.5 Hz

	Measured Data				
Excitation Amplitude [µs]	Frequency [Hz]	Amplitude [V]	Amplitude [In]	Amplitude [mm]	%THD (10 harmonics)
10	0.267	0.060	0.0029	0.0748	30.133
20	0.844	0.134	0.0066	0.1673	18.133
30	1.493	0.235	0.0116	0.2936	14.633
40	1.503	0.380	0.0187	0.4745	14.433
50	1.497	0.509	0.0250	0.6350	11.933
60	1.497	0.647	0.0318	0.8072	10.650
70	1.500	0.799	0.0393	0.9972	9.837
80	1.507	0.929	0.0456	1.1594	8.493
90	1.500	1.087	0.0534	1.3557	7.370
100	1.497	1.250	0.0614	1.5594	6.590

Measurement Trial 3
Excitation Frequency: 2 Hz

	Measured Data				
Excitation Amplitude [µs]	Frequency [Hz]	Amplitude [V]	Amplitude [In]	Amplitude [mm]	%THD (10 harmonics)
10	0.666	0.065	0.0032	0.0816	23.9000
20	2.000	0.105	0.0052	0.1310	27.1000
30	1.990	0.182	0.0089	0.2271	24.6000
40	2.020	0.316	0.0155	0.3942	19.8000
50	2.000	0.517	0.0254	0.6450	15.0000
60	1.990	0.624	0.0306	0.7785	12.7000
70	1.990	0.774	0.0380	0.9656	10.2000
80	2.000	0.936	0.0460	1.1677	8.6600
90	2.000	1.070	0.0526	1.3349	7.2400
100	2.000	1.270	0.0624	1.5844	6.5800

Arithmetic Mean for Actuator 10 Measurement Trials
Excitation Frequency: 2 Hz

	Measured Data				
Excitation Amplitude [µs]	Frequency [Hz]	Amplitude [V]	Amplitude [In]	Amplitude [mm]	%THD (10 harmonics)
10	1.255	0.078	0.0038	0.0974	22.667
20	1.470	0.159	0.0078	0.1979	17.500
30	1.997	0.252	0.0124	0.3148	18.600
40	1.997	0.396	0.0194	0.4936	15.467
50	1.993	0.552	0.0271	0.6886	11.517
60	1.993	0.691	0.0339	0.8621	9.653
70	1.997	0.873	0.0429	1.0891	8.483
80	1.997	1.019	0.0500	1.2708	7.193
90	2.000	1.177	0.0578	1.4679	6.163
100	1.997	1.337	0.0657	1.6676	5.500

Measurement Trial 3
Excitation Frequency: 2.5 Hz

	Measured Data				
Excitation Amplitude [µs]	Frequency [Hz]	Amplitude [V]	Amplitude [In]	Amplitude [mm]	%THD (10 harmonics)
10	0.060	0.049	0.0024	0.0615	20.7000
20	0.228	0.120	0.0059	0.1497	26.8000
30	2.480	0.237	0.0116	0.2957	21.7000
40	2.470	0.322	0.0158	0.4017	21.7000
50	2.500	0.520	0.0255	0.6487	13.9000
60	2.490	0.657	0.0323	0.8196	10.9000
70	2.490	0.814	0.0400	1.0155	9.3400
80	2.500	0.961	0.0472	1.1989	7.5200
90	2.510	1.150	0.0565	1.4347	5.2500
100	2.490	1.340	0.0658	1.6717	5.0800

Arithmetic Mean for Actuator 10 Measurement Trials
Excitation Frequency: 2.5 Hz

	Measured Data				
Excitation Amplitude [µs]	Frequency [Hz]	Amplitude [V]	Amplitude [In]	Amplitude [mm]	%THD (10 harmonics)
10	0.350	0.074	0.0036	0.0927	20.000
20	1.729	0.158	0.0078	0.1975	21.133
30	2.480	0.288	0.0142	0.3597	15.767
40	2.503	0.419	0.0206	0.5231	14.233
50	2.497	0.593	0.0291	0.7402	10.003
60	2.503	0.760	0.0373	0.9481	7.903
70	2.500	0.934	0.0459	1.1648	6.643
80	2.513	1.094	0.0537	1.3644	5.107
90	2.503	1.263	0.0620	1.5761	4.100
100	2.487	1.403	0.0689	1.7507	4.313

Measurement Trial 3
Excitation Frequency: 3 Hz

	Measured Data				
Excitation Amplitude [µs]	Frequency [Hz]	Amplitude [V]	Amplitude [In]	Amplitude [mm]	%THD (10 harmonics)
10	0.112	0.059	0.0029	0.0737	21.0000
20	0.744	0.119	0.0058	0.1485	27.6000
30	0.375	0.249	0.0122	0.3106	20.4000
40	2.970	0.408	0.0200	0.5090	15.0000
50	3.010	0.536	0.0263	0.6687	12.5000
60	3.030	0.687	0.0337	0.8571	9.9400
70	3.010	0.863	0.0424	1.0766	7.0900
80	3.000	1.050	0.0516	1.3099	3.8200
90	2.990	1.150	0.0565	1.4347	3.4800
100	2.990	1.310	0.0643	1.6343	2.3700

Arithmetic Mean for Actuator 10 Measurement Trials
Excitation Frequency: 3 Hz

	Measured Data				
Excitation Amplitude [µs]	Frequency [Hz]	Amplitude [V]	Amplitude [In]	Amplitude [mm]	%THD (10 harmonics)
10	0.231	0.074	0.0036	0.0921	20.833
20	1.489	0.167	0.0082	0.2088	20.367
30	2.132	0.300	0.0147	0.3738	15.433
40	3.003	0.452	0.0222	0.5639	12.233
50	3.017	0.632	0.0310	0.7884	9.130
60	3.017	0.795	0.0390	0.9918	6.897
70	3.000	0.961	0.0472	1.1989	5.160
80	2.997	1.100	0.0540	1.3723	3.763
90	2.997	1.213	0.0596	1.5137	3.510
100	2.993	1.327	0.0652	1.6551	2.943

Actuator Number 12 Performance Trials LVDT has 1" linear range

10-03-12

LVDT calibration factor: **20.36** **Volts/Inch**

Note: Each frequency-amplitude trial case is measured over 20sec period

Measurement Trial 1

Excitation Frequency: 0.5 Hz

	Measured Data				
Excitation Amplitude [µs]	Frequency [Hz]	Amplitude [V]	Amplitude [In]	Amplitude [mm]	%THD (10 harmonics)
10	0.494	0.068	0.0033	0.0848	37.6
20	0.494	0.149	0.0073	0.1859	16.1
30	0.505	0.294	0.0144	0.3668	14.7
40	0.497	0.465	0.0228	0.5801	9.17
50	0.501	0.595	0.0292	0.7423	8.79
60	0.500	0.740	0.0363	0.9232	7.85
70	0.498	0.889	0.0437	1.1091	7.01
80	0.497	1.030	0.0506	1.2850	6.42
90	0.497	1.200	0.0589	1.4971	5.59
100	0.498	1.320	0.0648	1.6468	5.51

Measurement Trial 2

Excitation Frequency: 0.5 Hz

	Measured Data				
Excitation Amplitude [µs]	Frequency [Hz]	Amplitude [V]	Amplitude [In]	Amplitude [mm]	%THD (10 harmonics)
10	0.923	0.024	0.0012	0.0298	38.7
20	0.566	0.027	0.0013	0.0331	40.5
30	0.173	0.035	0.0017	0.0439	22.2
40	0.084	0.352	0.0173	0.4391	21.2
50	0.506	0.529	0.0260	0.6600	12.6
60	0.502	0.693	0.0340	0.8645	12.5
70	0.504	0.853	0.0419	1.0642	11.9
80	0.500	0.998	0.0490	1.2450	8.51
90	0.498	1.140	0.0560	1.4222	8.44
100	0.505	1.310	0.0643	1.6343	7.86

Measurement Trial 1

Excitation Frequency: 1 Hz

	Measured Data				
Excitation Amplitude [µs]	Frequency [Hz]	Amplitude [V]	Amplitude [In]	Amplitude [mm]	%THD (10 harmonics)
10	nan	0.171	0.0084	0.2133	42
20	1.010	0.174	0.0085	0.2171	16.2
30	1.000	0.320	0.0157	0.3992	13.7
40	1.000	0.456	0.0224	0.5689	10.3
50	1.020	0.599	0.0294	0.7473	8.84
60	1.010	0.763	0.0375	0.9519	6.54
70	1.000	0.904	0.0444	1.1278	6.57
80	1.010	1.060	0.0521	1.3224	6.57
90	1.000	1.220	0.0599	1.5220	5.34
100	0.998	1.370	0.0673	1.7091	4.46

Measurement Trial 2

Excitation Frequency: 1 Hz

	Measured Data				
Excitation Amplitude [µs]	Frequency [Hz]	Amplitude [V]	Amplitude [In]	Amplitude [mm]	%THD (10 harmonics)
10	nan	0.064	0.0031	0.0796	46.7
20	0.977	0.134	0.0066	0.1672	22.4
30	1.000	0.286	0.0140	0.3568	12
40	0.980	0.430	0.0211	0.5364	12.9
50	0.992	0.581	0.0285	0.7248	10.9
60	0.995	0.722	0.0355	0.9007	10.7
70	0.998	0.853	0.0419	1.0642	10.7
80	0.999	0.984	0.0483	1.2276	11.3
90	0.989	1.110	0.0545	1.3848	12.6
100	1.000	1.220	0.0599	1.5220	15.3

Measurement Trial 1

Excitation Frequency: 1.5 Hz

	Measured Data				
Excitation Amplitude [µs]	Frequency [Hz]	Amplitude [V]	Amplitude [In]	Amplitude [mm]	%THD (10 harmonics)
10	nan	0.060	0.0029	0.0747	24.9
20	1.540	0.175	0.0086	0.2183	16.3
30	1.530	0.328	0.0161	0.4092	11.4
40	1.510	0.469	0.0230	0.5851	8.45
50	1.490	0.625	0.0307	0.7797	7.29
60	1.500	0.777	0.0382	0.9693	4.17
70	1.510	0.939	0.0461	1.1714	4.38
80	1.500	1.120	0.0550	1.3972	3.63
90	1.500	1.300	0.0639	1.6218	3.01
100	1.500	1.450	0.0712	1.8089	2.88

Measurement Trial 2

Excitation Frequency: 1.5 Hz

	Measured Data				
Excitation Amplitude [µs]	Frequency [Hz]	Amplitude [V]	Amplitude [In]	Amplitude [mm]	%THD (10 harmonics)
10	0.162	0.034	0.0017	0.0427	28.5
20	1.280	0.051	0.0025	0.0641	9.57
30	0.374	0.220	0.0108	0.2745	10.1
40	1.500	0.325	0.0160	0.4055	15.8
50	0.187	0.537	0.0264	0.6699	13.1
60	1.510	0.724	0.0356	0.9032	9.08
70	1.490	0.868	0.0426	1.0829	9.62
80	1.520	1.020	0.0501	1.2725	10
90	1.500	1.170	0.0575	1.4596	12.2
100	1.510	1.330	0.0653	1.6592	16.4

Measurement Trial 1

Excitation Frequency: 2 Hz

	Measured Data				
Excitation Amplitude [µs]	Frequency [Hz]	Amplitude [V]	Amplitude [In]	Amplitude [mm]	%THD (10 harmonics)
10	nan	0.069	0.0034	0.0862	27.3
20	1.930	0.142	0.0070	0.1772	15.3
30	2.000	0.302	0.0148	0.3768	8.16
40	2.000	0.454	0.0223	0.5664	9.28
50	2.000	0.623	0.0306	0.7772	5.73
60	2.000	0.818	0.0402	1.0205	3.91
70	2.000	1.010	0.0496	1.2600	2.87
80	2.000	1.190	0.0584	1.4846	2.43
90	1.990	1.390	0.0683	1.7341	1.91
100	2.000	1.560	0.0766	1.9462	2.5

Measurement Trial 2

Excitation Frequency: 2 Hz

	Measured Data				
Excitation Amplitude [µs]	Frequency [Hz]	Amplitude [V]	Amplitude [In]	Amplitude [mm]	%THD (10 harmonics)
10	0.179	0.030	0.0014	0.0368	33.5
20	0.152	0.032	0.0016	0.0399	13.4
30	0.087	0.049	0.0024	0.0614	8.96
40	0.126	0.239	0.0117	0.2982	16.8
50	0.154	0.554	0.0272	0.6911	14.2
60	1.990	0.742	0.0364	0.9257	6.88
70	1.990	0.907	0.0445	1.1315	6.08
80	2.010	1.090	0.0535	1.3598	6.65
90	2.000	1.250	0.0614	1.5594	6.29
100	1.990	1.400	0.0688	1.7466	7.42

Measurement Trial 1

Excitation Frequency: 2.5 Hz

	Measured Data				
Excitation Amplitude [µs]	Frequency [Hz]	Amplitude [V]	Amplitude [In]	Amplitude [mm]	%THD (10 harmonics)
10	nan	0.229	0.0112	0.2857	47.1
20	2.420	0.129	0.0063	0.1609	16.9
30	2.460	0.292	0.0143	0.3643	11.6
40	2.490	0.463	0.0227	0.5776	7.75
50	2.500	0.649	0.0319	0.8097	4.9
60	2.500	0.849	0.0417	1.0592	3.85
70	2.500	1.040	0.0511	1.2974	2.46
80	2.490	1.220	0.0599	1.5220	1.87
90	2.500	1.360	0.0668	1.6967	2.02
100	2.500	1.530	0.0751	1.9087	2.26

Measurement Trial 2

Excitation Frequency: 2.5 Hz

	Measured Data				
Excitation Amplitude [µs]	Frequency [Hz]	Amplitude [V]	Amplitude [In]	Amplitude [mm]	%THD (10 harmonics)
10	0.356	0.033	0.0016	0.0410	22.5
20	0.495	0.056	0.0027	0.0696	17.5
30	0.829	0.137	0.0067	0.1709	12.9
40	2.480	0.285	0.0140	0.3556	14.2
50	2.480	0.569	0.0279	0.7099	8.41
60	2.470	0.750	0.0368	0.9357	5.78
70	2.490	0.955	0.0469	1.1914	6.37
80	2.500	1.140	0.0560	1.4222	4.34
90	2.490	1.330	0.0653	1.6592	4.27
100	2.510	1.420	0.0697	1.7715	5.17

Measurement Trial 1

Excitation Frequency: 3 Hz

	Measured Data				
Excitation Amplitude [µs]	Frequency [Hz]	Amplitude [V]	Amplitude [In]	Amplitude [mm]	%THD (10 harmonics)
10	nan	0.040	0.0020	0.0498	24.4
20	2.870	0.142	0.0070	0.1772	21.5
30	2.940	0.296	0.0145	0.3693	14.1
40	3.000	0.482	0.0237	0.6013	7.5
50	3.060	0.686	0.0337	0.8558	5.05
60	3.020	0.820	0.0403	1.0230	4.04
70	2.990	0.951	0.0467	1.1864	3.49
80	3.010	1.100	0.0540	1.3723	2.88
90	3.010	1.240	0.0609	1.5470	2.79
100	2.990	1.360	0.0668	1.6967	2.81

Measurement Trial 2

Excitation Frequency: 3 Hz

	Measured Data				
Excitation Amplitude [µs]	Frequency [Hz]	Amplitude [V]	Amplitude [In]	Amplitude [mm]	%THD (10 harmonics)
10	0.510	0.035	0.0017	0.0433	75.6
20	0.375	0.060	0.0029	0.0744	18.7
30	0.097	0.128	0.0063	0.1597	18.4
40	0.429	0.276	0.0136	0.3443	18.1
50	0.300	0.457	0.0224	0.5701	14.6
60	3.010	0.663	0.0326	0.8271	8.16
70	3.010	0.796	0.0391	0.9930	5.45
80	2.990	0.906	0.0445	1.1303	5.57
90	3.010	1.050	0.0516	1.3099	3.84
100	3.000	1.240	0.0609	1.5470	3.36

Actuator Number 12 Performance Trials
10-03-12
LVDT calibration factor: **20.36** **Volts/Inch**

Measurement Trial 3
Excitation Frequency: 0.5 Hz

	Measured Data				
Excitation Amplitude [µs]	Frequency [Hz]	Amplitude [V]	Amplitude [In]	Amplitude [mm]	%THD (10 harmonics)
10	nan	0.033	0.0016	0.0410	158
20	0.495	0.103	0.0051	0.1285	25.3
30	0.497	0.251	0.0123	0.3131	15.4
40	0.502	0.376	0.0185	0.4691	13.1
50	0.495	0.527	0.0259	0.6575	11.7
60	0.502	0.652	0.0320	0.8134	12.5
70	0.498	0.801	0.0393	0.9993	12.2
80	0.497	0.937	0.0460	1.1689	10.2
90	0.498	1.050	0.0516	1.3099	9.61
100	0.498	1.190	0.0584	1.4846	8.79

Arithmetic Mean from Actuator 12 Measurement Trials
Excitation Frequency: 0.5 Hz

	Measured Data				
Excitation Amplitude [µs]	Frequency [Hz]	Amplitude [V]	Amplitude [In]	Amplitude [mm]	%THD (10 harmonics)
10	0.709	0.042	0.0020	0.0519	78.100
20	0.518	0.093	0.0046	0.1158	27.300
30	0.392	0.193	0.0095	0.2413	17.433
40	0.361	0.398	0.0195	0.4961	14.490
50	0.501	0.550	0.0270	0.6866	11.030
60	0.501	0.695	0.0341	0.8670	10.950
70	0.500	0.848	0.0416	1.0575	10.370
80	0.498	0.988	0.0485	1.2330	8.377
90	0.498	1.130	0.0555	1.4097	7.880
100	0.500	1.273	0.0625	1.5885	7.387

Measurement Trial 3
Excitation Frequency: 1 Hz

	Measured Data				
Excitation Amplitude [µs]	Frequency [Hz]	Amplitude [V]	Amplitude [In]	Amplitude [mm]	%THD (10 harmonics)
10	0.345	0.041	0.0020	0.0513	61.8
20	1.000	0.111	0.0055	0.1385	25
30	0.985	0.250	0.0123	0.3119	16.3
40	0.999	0.397	0.0195	0.4953	13.3
50	1.000	0.565	0.0278	0.7049	11.1
60	0.996	0.717	0.0352	0.8945	8.88
70	0.991	0.844	0.0415	1.0529	7.98
80	0.995	1.000	0.0491	1.2475	7.52
90	1.000	1.140	0.0560	1.4222	6.99
100	0.999	1.280	0.0629	1.5969	7.48

Arithmetic Mean from Actuator 12 Measurement Trials
Excitation Frequency: 1 Hz

	Measured Data				
Excitation Amplitude [µs]	Frequency [Hz]	Amplitude [V]	Amplitude [In]	Amplitude [mm]	%THD (10 harmonics)
10	0.345	0.092	0.0045	0.1147	50.167
20	0.996	0.140	0.0069	0.1742	21.200
30	0.995	0.285	0.0140	0.3560	14.000
40	0.993	0.428	0.0210	0.5335	12.167
50	1.004	0.582	0.0286	0.7257	10.280
60	1.000	0.734	0.0361	0.9157	8.707
70	0.996	0.867	0.0426	1.0816	8.417
80	1.001	1.015	0.0498	1.2658	8.463
90	0.996	1.157	0.0568	1.4430	8.310
100	0.999	1.290	0.0634	1.6093	9.080

Measurement Trial 3
Excitation Frequency: 1.5 Hz

	Measured Data				
Excitation Amplitude [µs]	Frequency [Hz]	Amplitude [V]	Amplitude [In]	Amplitude [mm]	%THD (10 harmonics)
10	0.188	0.042	0.0021	0.0524	68
20	0.125	0.104	0.0051	0.1297	14.8
30	1.520	0.260	0.0128	0.3244	12.5
40	1.490	0.416	0.0204	0.5190	11.5
50	1.500	0.578	0.0284	0.7211	8.42
60	1.510	0.736	0.0361	0.9182	7.47
70	1.500	0.891	0.0438	1.1116	6.31
80	1.490	1.050	0.0516	1.3099	6.44
90	1.500	1.210	0.0594	1.5095	5.8
100	1.500	1.370	0.0673	1.7091	5.07

Arithmetic Mean from Actuator 12 Measurement Trials
Excitation Frequency: 1.5 Hz

	Measured Data				
Excitation Amplitude [µs]	Frequency [Hz]	Amplitude [V]	Amplitude [In]	Amplitude [mm]	%THD (10 harmonics)
10	0.175	0.045	0.0022	0.0566	40.467
20	0.982	0.110	0.0054	0.1374	13.557
30	1.141	0.269	0.0132	0.3360	11.333
40	1.500	0.403	0.0198	0.5032	11.917
50	1.059	0.580	0.0285	0.7236	9.603
60	1.507	0.746	0.0366	0.9303	6.907
70	1.500	0.899	0.0442	1.1220	6.770
80	1.503	1.063	0.0522	1.3266	6.690
90	1.500	1.227	0.0602	1.5303	7.003
100	1.503	1.383	0.0679	1.7258	8.117

Measurement Trial 3
Excitation Frequency: 2 Hz

	Measured Data				
Excitation Amplitude [µs]	Frequency [Hz]	Amplitude [V]	Amplitude [In]	Amplitude [mm]	%THD (10 harmonics)
10	0.091	0.046	0.0023	0.0579	25.3
20	1.010	0.068	0.0033	0.0851	13.3
30	0.670	0.263	0.0129	0.3281	11.2
40	2.000	0.459	0.0225	0.5726	9.55
50	2.000	0.660	0.0324	0.8234	6.83
60	1.990	0.786	0.0386	0.9806	6.09
70	2.010	0.988	0.0485	1.2326	5.43
80	2.000	1.200	0.0589	1.4971	6.71
90	2.000	1.350	0.0663	1.6842	4.86
100	2.000	1.510	0.0742	1.8838	5.62

Arithmetic Mean from Actuator 12 Measurement Trials
Excitation Frequency: 2 Hz

	Measured Data				
Excitation Amplitude [µs]	Frequency [Hz]	Amplitude [V]	Amplitude [In]	Amplitude [mm]	%THD (10 harmonics)
10	0.135	0.048	0.0024	0.0603	28.700
20	1.031	0.081	0.0040	0.1007	14.000
30	0.919	0.205	0.0101	0.2554	9.440
40	1.375	0.384	0.0189	0.4791	11.877
50	1.385	0.612	0.0301	0.7639	8.920
60	1.993	0.782	0.0384	0.9756	5.627
70	2.000	0.968	0.0476	1.2080	4.793
80	2.003	1.160	0.0570	1.4472	5.263
90	1.997	1.330	0.0653	1.6592	4.353
100	1.997	1.490	0.0732	1.8588	5.180

Measurement Trial 3
Excitation Frequency: 2.5 Hz

	Measured Data				
Excitation Amplitude [µs]	Frequency [Hz]	Amplitude [V]	Amplitude [In]	Amplitude [mm]	%THD (10 harmonics)
10	2.150	0.072	0.0035	0.0897	31.2
20	0.166	0.107	0.0053	0.1335	23.5
30	0.830	0.259	0.0127	0.3231	16.1
40	2.460	0.480	0.0236	0.5988	8.51
50	2.490	0.649	0.0319	0.8097	6.01
60	2.500	0.860	0.0422	1.0729	3.94
70	2.510	1.050	0.0516	1.3099	2.62
80	2.490	1.230	0.0604	1.5345	2.26
90	2.500	1.380	0.0678	1.7216	2.24
100	2.510	1.570	0.0771	1.9586	2.96

Arithmetic Mean from Actuator 12 Measurement Trials
Excitation Frequency: 2.5 Hz

	Measured Data				
Excitation Amplitude [µs]	Frequency [Hz]	Amplitude [V]	Amplitude [In]	Amplitude [mm]	%THD (10 harmonics)
10	1.253	0.111	0.0055	0.1388	33.600
20	1.027	0.097	0.0048	0.1213	19.300
30	1.373	0.229	0.0113	0.2861	13.533
40	2.477	0.409	0.0201	0.5107	10.153
50	2.490	0.622	0.0306	0.7764	6.440
60	2.490	0.820	0.0403	1.0226	4.523
70	2.500	1.015	0.0499	1.2663	3.817
80	2.493	1.197	0.0588	1.4929	2.823
90	2.497	1.357	0.0666	1.6925	2.843
100	2.507	1.507	0.0740	1.8796	3.463

Measurement Trial 3
Excitation Frequency: 3 Hz

	Measured Data				
Excitation Amplitude [µs]	Frequency [Hz]	Amplitude [V]	Amplitude [In]	Amplitude [mm]	%THD (10 harmonics)
10	3.030	0.074	0.0036	0.0927	23.5
20	1.000	0.139	0.0068	0.1734	23.2
30	0.751	0.308	0.0151	0.3842	15.3
40	0.376	0.546	0.0268	0.6812	7.31
50	3.010	0.745	0.0366	0.9294	3.87
60	3.010	0.910	0.0447	1.1353	3.61
70	2.980	1.070	0.0526	1.3349	3.31
80	3.000	1.210	0.0594	1.5095	3.39
90	2.970	1.320	0.0648	1.6468	3.25
100	3.000	1.440	0.0707	1.7965	3.17

Arithmetic Mean from Actuator 12 Measurement Trials
Excitation Frequency: 3 Hz

	Measured Data				
Excitation Amplitude [µs]	Frequency [Hz]	Amplitude [V]	Amplitude [In]	Amplitude [mm]	%THD (10 harmonics)
10	1.770	0.050	0.0024	0.0619	41.167
20	1.415	0.114	0.0056	0.1416	21.133
30	1.263	0.244	0.0120	0.3044	15.933
40	1.268	0.435	0.0213	0.5423	10.970
50	2.123	0.629	0.0309	0.7851	7.840
60	3.013	0.798	0.0392	0.9951	5.270
70	2.993	0.939	0.0461	1.1714	4.083
80	3.000	1.072	0.0527	1.3374	3.947
90	2.997	1.203	0.0591	1.5012	3.293
100	2.997	1.347	0.0661	1.6800	3.113

Actuator Number 14 Performance Trials LVDT has 1" linear range

10-03-16

LVDT calibration factor: 20.36 Volts/Inch

Measurement Trial 1

Excitation Frequency: 0.5 Hz

	Measured Data				
Excitation Amplitude [µs]	Frequency [Hz]	Amplitude [V]	Amplitude [In]	Amplitude [mm]	%THD (10 harmonics)
10	0.251	0.040	0.0020	0.0504	31.30
20	0.500	0.116	0.0057	0.1447	18.50
30	0.496	0.264	0.0130	0.3294	21.60
40	0.498	0.322	0.0158	0.4017	18.90
50	0.500	0.502	0.0247	0.6263	17.50
60	0.498	0.685	0.0336	0.8546	14.00
70	0.504	0.845	0.0415	1.0542	12.70
80	0.500	1.040	0.0511	1.2974	10.30
90	0.499	1.240	0.0609	1.5470	9.40
100	0.498	1.420	0.0697	1.7715	9.00

Measurement Trial 2

Excitation Frequency: 0.5 Hz

	Measured Data				
Excitation Amplitude [µs]	Frequency [Hz]	Amplitude [V]	Amplitude [In]	Amplitude [mm]	%THD (10 harmonics)
10	1.470	0.020	0.0010	0.0251	129.0000
20	0.250	0.104	0.0051	0.1297	22.3000
30	0.493	0.187	0.0092	0.2333	20.5000
40	0.500	0.255	0.0125	0.3181	19.5000
50	0.502	0.396	0.0194	0.4940	15.3000
60	0.498	0.583	0.0286	0.7273	12.5000
70	0.499	0.736	0.0361	0.9182	12.1000
80	0.498	0.790	0.0388	0.9856	12.0000
90	0.500	0.980	0.0481	1.2226	11.0000
100	0.499	1.180	0.0580	1.4721	11.1000

Measurement Trial 1

Excitation Frequency: 1 Hz

	Measured Data				
Excitation Amplitude [µs]	Frequency [Hz]	Amplitude [V]	Amplitude [In]	Amplitude [mm]	%THD (10 harmonics)
10	0.494	0.059	0.0029	0.0734	27.30
20	0.992	0.198	0.0097	0.2470	13.40
30	1.010	0.332	0.0163	0.4142	11.40
40	1.000	0.455	0.0223	0.5676	11.80
50	1.000	0.608	0.0299	0.7585	10.70
60	0.990	0.762	0.0374	0.9506	8.47
70	1.000	0.927	0.0455	1.1565	8.48
80	0.994	1.080	0.0530	1.3473	8.76
90	1.000	1.220	0.0599	1.5220	9.13
100	1.010	1.390	0.0683	1.7341	9.11

Measurement Trial 2

Excitation Frequency: 1 Hz

	Measured Data				
Excitation Amplitude [µs]	Frequency [Hz]	Amplitude [V]	Amplitude [In]	Amplitude [mm]	%THD (10 harmonics)
10	0.495	0.021	0.0010	0.0266	38.6000
20		0.030	0.0015	0.0373	27.3000
30	0.200	0.097	0.0048	0.1211	28.4
40	1.010	0.248	0.0122	0.3094	20.1000
50	1.000	0.360	0.0177	0.4491	17.6000
60	0.998	0.465	0.0228	0.5801	16.5000
70	0.995	0.594	0.0292	0.7410	14.4000
80	0.995	0.738	0.0362	0.9207	14.9000
90	11.000	0.931	0.0457	1.1615	14.6000
100	0.998	1.090	0.0535	1.3598	14.2000

Measurement Trial 1

Excitation Frequency: 1.5 Hz

	Measured Data				
Excitation Amplitude [µs]	Frequency [Hz]	Amplitude [V]	Amplitude [In]	Amplitude [mm]	%THD (10 harmonics)
10	0.125	0.026	0.0013	0.0322	56.70
20	1.410	0.155	0.0076	0.1934	11.60
30	1.490	0.274	0.0135	0.3418	11.20
40	1.490	0.441	0.0217	0.5502	11.10
50	1.490	0.596	0.0293	0.7435	7.45
60	1.500	0.762	0.0374	0.9506	6.82
70	1.500	0.949	0.0466	1.1839	6.28
80	1.500	1.130	0.0555	1.4097	5.31
90	1.500	1.360	0.0668	1.6967	5.08
100	1.500	1.490	0.0732	1.8588	5.20

Measurement Trial 2

Excitation Frequency: 1.5 Hz

	Measured Data				
Excitation Amplitude [µs]	Frequency [Hz]	Amplitude [V]	Amplitude [In]	Amplitude [mm]	%THD (10 harmonics)
10	1.42	0.213	0.0105	0.2657	97.3000
20	0.841	0.030	0.0015	0.0377	31.3000
30	1.510	0.091	0.0045	0.1134	21.7000
40	1.490	0.204	0.0100	0.2545	18.5000
50	1.490	0.310	0.0152	0.3867	17.4000
60	1.500	0.410	0.0201	0.5115	15.4000
70	1.510	0.548	0.0269	0.6837	13.0000
80	1.500	0.676	0.0332	0.8433	12.0000
90	1.510	0.827	0.0406	1.0317	10.8000
100	1.510	1.020	0.0501	1.2725	10.9000

Measurement Trial 1

Excitation Frequency: 2 Hz

	Measured Data				
Excitation Amplitude [µs]	Frequency [Hz]	Amplitude [V]	Amplitude [In]	Amplitude [mm]	%THD (10 harmonics)
10	0.451	0.024	0.0012	0.0298	79.20
20	0.986	0.096	0.0047	0.1196	19.40
30	2.010	0.217	0.0107	0.2707	14.40
40	2.000	0.405	0.0199	0.5053	11.80
50	2.000	0.565	0.0278	0.7049	8.46
60	2.000	0.736	0.0361	0.9182	6.94
70	2.000	0.986	0.0484	1.2301	5.18
80	2.000	1.160	0.0570	1.4472	4.82
90	2.000	1.340	0.0658	1.6717	4.58
100	2.000	1.510	0.0742	1.8838	4.37

Measurement Trial 2

Excitation Frequency: 2 Hz

	Measured Data				
Excitation Amplitude [µs]	Frequency [Hz]	Amplitude [V]	Amplitude [In]	Amplitude [mm]	%THD (10 harmonics)
10	0.63	0.021	0.0010	0.0266	19.6000
20	1.500	0.022	0.0011	0.0273	102.0000
30	0.144	0.064	0.0032	0.0803	22.7000
40	2.000	0.188	0.0092	0.2345	16.7000
50	2.010	0.276	0.0136	0.3443	16.6
60	2.000	0.381	0.0187	0.4753	13.3000
70	2.000	0.488	0.0240	0.6088	12.7000
80	2.020	0.622	0.0306	0.7760	12.3000
90	2.000	0.755	0.0371	0.9419	11.0000
100	1.990	0.873	0.0429	1.0891	10.1000

Measurement Trial 1

Excitation Frequency: 2.5 Hz

	Measured Data				
Excitation Amplitude [µs]	Frequency [Hz]	Amplitude [V]	Amplitude [In]	Amplitude [mm]	%THD (10 harmonics)
10	0.290	0.030	0.0015	0.0374	42.80
20	0.125	0.085	0.0042	0.1065	21.80
30	2.520	0.249	0.0122	0.3106	16.50
40	2.520	0.443	0.0218	0.5527	11.80
50	2.500	0.612	0.0301	0.7635	6.83
60	2.510	0.742	0.0364	0.9257	6.54
70	2.500	0.943	0.0463	1.1764	5.73
80	2.490	1.020	0.0501	1.2725	5.81
90	2.500	1.270	0.0624	1.5844	4.64
100	2.500	1.400	0.0688	1.7466	3.69

Measurement Trial 2

Excitation Frequency: 2.5 Hz

	Measured Data				
Excitation Amplitude [µs]	Frequency [Hz]	Amplitude [V]	Amplitude [In]	Amplitude [mm]	%THD (10 harmonics)
10	1.860	0.022	0.0011	0.0276	108.0000
20	1.340	0.022	0.0011	0.0279	92.8000
30	0.228	0.068	0.0033	0.0846	23.2000
40	1.250	0.153	0.0075	0.1909	19.7000
50	2.500	0.251	0.0123	0.3131	15.7000
60	2.510	0.343	0.0168	0.4279	14.2000
70	2.500	0.380	0.0187	0.4741	14.4000
80	2.480	0.452	0.0222	0.5639	12.5000
90	2.480	0.619	0.0304	0.7722	11.6000
100	2.500	0.685	0.0336	0.8546	10.6000

Measurement Trial 1

Excitation Frequency: 3 Hz

	Measured Data				
Excitation Amplitude [µs]	Frequency [Hz]	Amplitude [V]	Amplitude [In]	Amplitude [mm]	%THD (10 harmonics)
10	0.120	0.053	0.0026	0.0657	24.90
20	0.598	0.120	0.0059	0.1497	22.00
30	3.000	0.223	0.0110	0.2782	17.40
40	3.030	0.361	0.0177	0.4504	12.90
50	3.000	0.528	0.0259	0.6587	8.12
60	3.020	0.743	0.0365	0.9269	5.81
70	3.000	0.914	0.0449	1.1403	3.43
80	3.000	1.080	0.0530	1.3473	3.66
90	3.080	1.150	0.0565	1.4347	4.11
100	3.000	1.230	0.0604	1.5345	4.01

Measurement Trial 2

Excitation Frequency: 3 Hz

	Measured Data				
Excitation Amplitude [µs]	Frequency [Hz]	Amplitude [V]	Amplitude [In]	Amplitude [mm]	%THD (10 harmonics)
10	0.868	0.022	0.0011	0.0277	15.4000
20	0.876	0.022	0.0011	0.0279	34.8000
30	0.595	0.062	0.0031	0.0776	24.9000
40	0.749	0.141	0.0069	0.1759	19.1000
50	1.000	0.257	0.0126	0.3206	15.0000
60	2.99	0.330	0.0162	0.4117	10.9000
70	3.010	0.442	0.0217	0.5514	9.4200
80	2.950	0.594	0.0292	0.7410	6.8500
90	2.970	0.685	0.0337	0.8551	6.4100
100	3.000	0.777	0.0382	0.9693	5.7600

Actuator Number 14 Performance Trials
10-03-16
LVDT calibration factor: **20.36** **Volts/Inch**

Measurement Trial 3
Excitation Frequency: 0.5 Hz

	Measured Data				
Excitation Amplitude [µs]	Frequency [Hz]	Amplitude [V]	Amplitude [In]	Amplitude [mm]	%THD (10 harmonics)
10	0.507	0.050	0.0024	0.0618	30.7000
20	0.495	0.149	0.0073	0.1859	20.8000
30	0.507	0.199	0.0098	0.2483	22.0000
40	0.498	0.285	0.0140	0.3556	20.5000
50	0.501	0.426	0.0209	0.5315	16.9000
60	0.501	0.553	0.0272	0.6899	15.8000
70	0.499	0.689	0.0338	0.8596	13.9000
80	0.501	0.909	0.0446	1.1340	13.1000
90	0.498	1.070	0.0526	1.3349	12.2000
100	0.501	1.250	0.0614	1.5594	10.9000

Arithmetic Mean for Actuator 14 Measurement Trials
Excitation Frequency: 0.5 Hz

	Measured Data				
Excitation Amplitude [µs]	Frequency [Hz]	Amplitude [V]	Amplitude [In]	Amplitude [mm]	%THD (10 harmonics)
10	0.743	0.037	0.0018	0.0457	63.667
20	0.415	0.123	0.0060	0.1534	20.533
30	0.499	0.217	0.0106	0.2703	21.367
40	0.499	0.287	0.0141	0.3585	19.633
50	0.501	0.441	0.0217	0.5506	16.567
60	0.499	0.607	0.0298	0.7573	14.100
70	0.501	0.757	0.0372	0.9440	12.900
80	0.500	0.913	0.0448	1.1390	11.800
90	0.499	1.097	0.0539	1.3681	10.867
100	0.499	1.283	0.0630	1.6010	10.333

Measurement Trial 3
Excitation Frequency: 1 Hz

	Measured Data				
Excitation Amplitude [µs]	Frequency [Hz]	Amplitude [V]	Amplitude [In]	Amplitude [mm]	%THD (10 harmonics)
10		0.042	0.0020	0.0518	32.0000
20	0.503	0.149	0.0073	0.1859	15.6000
30	1.010	0.247	0.0121	0.3081	11.2000
40	0.996	0.350	0.0172	0.4366	13.6000
50	1.000	0.491	0.0241	0.6125	12.1000
60	0.995	0.621	0.0305	0.7747	11.9000
70	0.999	0.761	0.0374	0.9494	12.1000
80	0.999	0.908	0.0446	1.1324	11.2000
90	0.998	1.080	0.0530	1.3473	10.3000
100	1.000	1.250	0.0614	1.5594	10.5000

Arithmetic Mean for Actuator 14 Measurement Trials
Excitation Frequency: 1 Hz

	Measured Data				
Excitation Amplitude [µs]	Frequency [Hz]	Amplitude [V]	Amplitude [In]	Amplitude [mm]	%THD (10 harmonics)
10	0.495	0.041	0.0020	0.0506	32.633
20	0.748	0.126	0.0062	0.1567	18.767
30	0.740	0.225	0.0111	0.2812	17.000
40	1.002	0.351	0.0172	0.4379	15.167
50	1.000	0.486	0.0239	0.6067	13.467
60	0.994	0.616	0.0303	0.7685	12.290
70	0.998	0.761	0.0374	0.9490	11.660
80	0.996	0.909	0.0446	1.1335	11.620
90	4.333	1.077	0.0529	1.3436	11.343
100	1.003	1.243	0.0611	1.5511	11.270

Measurement Trial 3
Excitation Frequency: 1.5 Hz

	Measured Data				
Excitation Amplitude [µs]	Frequency [Hz]	Amplitude [V]	Amplitude [In]	Amplitude [mm]	%THD (10 harmonics)
10		0.026	0.0013	0.0322	40.4000
20	0.747	0.097	0.0048	0.1213	18.1000
30	1.490	0.228	0.0112	0.2844	11.0000
40	1.500	0.323	0.0159	0.4030	9.2400
50	1.500	0.488	0.0240	0.6088	8.7000
60	1.500	0.609	0.0299	0.7598	8.3800
70	1.500	0.751	0.0369	0.9369	7.9900
80	1.500	0.929	0.0456	1.1590	7.2400
90	1.500	1.080	0.0530	1.3473	7.2200
100	1.500	1.250	0.0614	1.5594	7.6100

Arithmetic Mean for Actuator 14 Measurement Trials
Excitation Frequency: 1.5 Hz

	Measured Data				
Excitation Amplitude [µs]	Frequency [Hz]	Amplitude [V]	Amplitude [In]	Amplitude [mm]	%THD (10 harmonics)
10	0.773	0.088	0.0043	0.1100	64.800
20	0.999	0.094	0.0046	0.1174	20.333
30	1.497	0.198	0.0097	0.2466	14.633
40	1.493	0.323	0.0158	0.4025	12.947
50	1.493	0.465	0.0228	0.5797	11.183
60	1.500	0.594	0.0292	0.7406	10.200
70	1.503	0.749	0.0368	0.9348	9.090
80	1.500	0.912	0.0448	1.1373	8.183
90	1.503	1.089	0.0535	1.3586	7.700
100	1.503	1.253	0.0616	1.5636	7.903

Measurement Trial 3
Excitation Frequency: 2 Hz

	Measured Data				
Excitation Amplitude [µs]	Frequency [Hz]	Amplitude [V]	Amplitude [In]	Amplitude [mm]	%THD (10 harmonics)
10	0.313	0.029	0.0014	0.0364	111.0000
20	0.668	0.086	0.0042	0.1073	19.0000
30	1.970	0.144	0.0071	0.1796	16.4000
40	0.667	0.250	0.0123	0.3119	14.5000
50	2.010	0.403	0.0198	0.5028	11.9000
60	1.980	0.525	0.0258	0.6550	11.1000
70	2	0.681	0.0334	0.8496	9.1000
80	2.000	0.835	0.0410	1.0417	7.8800
90	2.000	1.060	0.0521	1.3224	7.6900
100	1.980	1.160	0.0570	1.4472	7.6500

Arithmetic Mean for Actuator 14 Measurement Trials
Excitation Frequency: 2 Hz

	Measured Data				
Excitation Amplitude [µs]	Frequency [Hz]	Amplitude [V]	Amplitude [In]	Amplitude [mm]	%THD (10 harmonics)
10	0.464	0.025	0.0012	0.0309	69.933
20	1.051	0.068	0.0033	0.0847	46.800
30	1.375	0.142	0.0070	0.1769	17.833
40	1.556	0.281	0.0138	0.3506	14.333
50	2.007	0.415	0.0204	0.5173	12.320
60	1.993	0.547	0.0269	0.6828	10.447
70	2.000	0.718	0.0353	0.8962	8.993
80	2.007	0.872	0.0428	1.0883	8.333
90	2.000	1.052	0.0517	1.3120	7.757
100	1.990	1.181	0.0580	1.4733	7.373

Measurement Trial 3
Excitation Frequency: 2.5 Hz

	Measured Data				
Excitation Amplitude [µs]	Frequency [Hz]	Amplitude [V]	Amplitude [In]	Amplitude [mm]	%THD (10 harmonics)
10	0.552	0.023	0.0011	0.0283	121.0000
20	2.480	0.054	0.0026	0.0672	27.1000
30	0.208	0.129	0.0063	0.1609	18.8000
40	1.250	0.249	0.0122	0.3106	15.2000
50	2.500	0.365	0.0179	0.4554	10.1000
60	2.510	0.493	0.0242	0.6150	9.7800
70	2.520	0.608	0.0299	0.7585	10.2000
80	2.500	0.722	0.0355	0.9007	8.77
90	2.500	0.866	0.0425	1.0804	7.2500
100	2.500	0.970	0.0476	1.2101	7.2400

Arithmetic Mean for Actuator 14 Measurement Trials
Excitation Frequency: 2.5 Hz

	Measured Data				
Excitation Amplitude [µs]	Frequency [Hz]	Amplitude [V]	Amplitude [In]	Amplitude [mm]	%THD (10 harmonics)
10	0.901	0.025	0.0012	0.0311	90.600
20	1.315	0.054	0.0026	0.0672	47.233
30	0.985	0.149	0.0073	0.1854	19.500
40	1.673	0.282	0.0138	0.3514	15.567
50	2.500	0.409	0.0201	0.5107	10.877
60	2.510	0.526	0.0258	0.6562	10.173
70	2.507	0.644	0.0316	0.8030	10.110
80	2.490	0.731	0.0359	0.9124	9.027
90	2.493	0.918	0.0451	1.1457	7.830
100	2.500	1.018	0.0500	1.2704	7.177

Measurement Trial 3
Excitation Frequency: 3 Hz

	Measured Data				
Excitation Amplitude [µs]	Frequency [Hz]	Amplitude [V]	Amplitude [In]	Amplitude [mm]	%THD (10 harmonics)
10		0.022	0.0011	0.0271	46.1000
20	0.748	0.058	0.0028	0.0721	25.7000
30	0.295	0.125	0.0061	0.1559	19.7000
40	2.930	0.197	0.0097	0.2458	14.4000
50	3.000	0.312	0.0153	0.3892	11.9000
60	2.980	0.400	0.0196	0.4990	9.6900
70	2.980	0.514	0.0252	0.6412	6.8400
80	3.070	0.636	0.0312	0.7934	6.2500
90	3.020	0.682	0.0335	0.8508	5.8200
100	3.000	0.755	0.0371	0.9419	5.6900

Arithmetic Mean for Actuator 14 Measurement Trials
Excitation Frequency: 3 Hz

	Measured Data				
Excitation Amplitude [µs]	Frequency [Hz]	Amplitude [V]	Amplitude [In]	Amplitude [mm]	%THD (10 harmonics)
10	0.494	0.032	0.0016	0.0402	28.800
20	0.741	0.067	0.0033	0.0833	27.500
30	1.297	0.137	0.0067	0.1706	20.667
40	2.236	0.233	0.0114	0.2907	15.467
50	2.333	0.366	0.0180	0.4562	11.673
60	3.003	0.491	0.0241	0.6125	8.800
70	2.977	0.623	0.0306	0.7776	6.563
80	3.013	0.770	0.0378	0.9606	5.587
90	3.033	0.839	0.0412	1.0469	5.447
100	3.000	0.921	0.0452	1.1486	5.153

Actuator Number 16 Performance Trials LVDT has 1" linear range

10-03-16

LVDT calibration factor: **20.36** **Volts/Inch**

Measurement Trial 1

Excitation Frequency: 0.5 Hz

	Measured Data				
Excitation Amplitude [µs]	Frequency [Hz]	Amplitude [V]	Amplitude [In]	Amplitude [mm]	%THD (10 harmonics)
10	0.503	0.129	0.0063	0.1609	14.9
20	0.504	0.174	0.0085	0.2171	16.2
30	0.516	0.271	0.0133	0.3381	12.6
40	0.497	0.353	0.0173	0.4404	11.2
50	0.501	0.477	0.0234	0.5951	9.95
60	0.500	0.600	0.0295	0.7485	10.7
70	0.505	0.731	0.0359	0.9120	9.8
80	0.500	0.931	0.0457	1.1615	9.85
90	0.499	1.220	0.0599	1.5220	10.3
100	0.504	1.250	0.0614	1.5594	11.9

Measurement Trial 2

Excitation Frequency: 0.5 Hz

	Measured Data				
Excitation Amplitude [µs]	Frequency [Hz]	Amplitude [V]	Amplitude [In]	Amplitude [mm]	%THD (10 harmonics)
10	0.483	0.048	0.0023	0.0595	35.7000
20	0.507	0.164	0.0081	0.2046	17.2000
30	0.494	0.247	0.0121	0.3081	11.4000
40	0.500	0.328	0.0161	0.4092	10.6000
50	0.501	0.444	0.0218	0.5539	9.6400
60	0.497	0.588	0.0289	0.7336	8.3200
70	0.500	0.734	0.0361	0.9157	8.5000
80	0.501	0.877	0.0431	1.0941	8.5600
90	0.500	1.010	0.0496	1.2600	10.5000
100	0.499	1.210	0.0594	1.5095	14.4400

Measurement Trial 1

Excitation Frequency: 1 Hz

	Measured Data				
Excitation Amplitude [µs]	Frequency [Hz]	Amplitude [V]	Amplitude [In]	Amplitude [mm]	%THD (10 harmonics)
10	0.504	0.057	0.0028	0.0711	38.9
20	0.200	0.177	0.0087	0.2208	20.3
30	0.501	0.262	0.0129	0.3269	14
40	1.010	0.359	0.0176	0.4479	12.8
50	1.000	0.457	0.0224	0.5701	11.1
60	1.000	0.596	0.0293	0.7435	10.8
70	1.000	0.740	0.0363	0.9232	10
80	0.997	0.919	0.0451	1.1465	9.08
90	1.000	1.060	0.0521	1.3224	9.78
100	0.999	1.360	0.0668	1.6967	9.99

Measurement Trial 2

Excitation Frequency: 1 Hz

	Measured Data				
Excitation Amplitude [µs]	Frequency [Hz]	Amplitude [V]	Amplitude [In]	Amplitude [mm]	%THD (10 harmonics)
10	1.040	0.052	0.0025	0.0647	37.5000
20	0.977	0.156	0.0077	0.1946	12.9000
30	0.983	0.217	0.0107	0.2707	11.7000
40	0.992	0.324	0.0159	0.4042	10.4000
50	1.000	0.440	0.0216	0.5489	10.3000
60	1.000	0.563	0.0277	0.7024	8.5400
70	1.000	0.715	0.0351	0.8920	8.2000
80	1.000	0.857	0.0421	1.0691	9.2600
90	1.000	1.050	0.0516	1.3099	8.2100
100	0.995	1.400	0.0688	1.7466	10.7000

Measurement Trial 1

Excitation Frequency: 1.5 Hz

	Measured Data				
Excitation Amplitude [µs]	Frequency [Hz]	Amplitude [V]	Amplitude [In]	Amplitude [mm]	%THD (10 harmonics)
10	1.540	0.082	0.0040	0.1017	31.7
20	1.510	0.167	0.0082	0.2083	15.7
30	1.500	0.257	0.0126	0.3206	12.2
40	1.500	0.353	0.0173	0.4404	13
50	1.500	0.480	0.0236	0.5988	9.67
60	1.500	0.608	0.0299	0.7585	9.39
70	1.500	0.740	0.0363	0.9232	7.85
80	1.500	0.890	0.0437	1.1103	7.86
90	1.500	1.080	0.0530	1.3473	7.05
100	1.500	1.300	0.0639	1.6218	7.1

Measurement Trial 2

Excitation Frequency: 1.5 Hz

	Measured Data				
Excitation Amplitude [µs]	Frequency [Hz]	Amplitude [V]	Amplitude [In]	Amplitude [mm]	%THD (10 harmonics)
10	0.149	0.077	0.0038	0.0958	41.0000
20	0.759	0.156	0.0077	0.1946	13.9000
30	1.520	0.228	0.0112	0.2844	12.0000
40	1.510	0.329	0.0162	0.4104	10.6000
50	1.490	0.460	0.0226	0.5739	8.4800
60	1.510	0.556	0.0273	0.6936	7.8500
70	1.500	0.711	0.0349	0.8870	7.3100
80	1.500	0.856	0.0420	1.0679	6.5800
90	1.500	1.060	0.0521	1.3224	6.1700
100	1.500	1.240	0.0609	1.5470	7.4900

Measurement Trial 1

Excitation Frequency: 2 Hz

	Measured Data				
Excitation Amplitude [µs]	Frequency [Hz]	Amplitude [V]	Amplitude [In]	Amplitude [mm]	%THD (10 harmonics)
10	0.083	0.072	0.0035	0.0893	35.1
20	0.401	0.153	0.0075	0.1909	18.4
30	1.980	0.233	0.0114	0.2907	16.7
40	2.000	0.317	0.0156	0.3955	13.9
50	1.990	0.441	0.0217	0.5502	10.3
60	1.990	0.572	0.0281	0.7136	9.7
70	2.000	0.713	0.0350	0.8895	8.78
80	2.000	0.870	0.0427	1.0854	7.26
90	2.010	1.050	0.0516	1.3099	6.9
100	2.000	1.240	0.0609	1.5470	6.65

Measurement Trial 2

Excitation Frequency: 2 Hz

	Measured Data				
Excitation Amplitude [µs]	Frequency [Hz]	Amplitude [V]	Amplitude [In]	Amplitude [mm]	%THD (10 harmonics)
10	0.666	0.075	0.0037	0.0932	32.8000
20	2.000	0.146	0.0072	0.1821	18.5000
30	2.010	0.231	0.0113	0.2882	14.1000
40	1.980	0.325	0.0160	0.4055	11.8000
50	1.980	0.426	0.0209	0.5315	9.8100
60	2.000	0.573	0.0281	0.7148	8.9400
70	2.000	0.710	0.0349	0.8858	7.4400
80	1.990	0.926	0.0455	1.1552	6.7500
90	2.010	1.140	0.0560	1.4222	5.1800
100	2.010	1.280	0.0629	1.5969	4.4000

Measurement Trial 1

Excitation Frequency: 2.5 Hz

	Measured Data				
Excitation Amplitude [µs]	Frequency [Hz]	Amplitude [V]	Amplitude [In]	Amplitude [mm]	%THD (10 harmonics)
10	2.520	0.062	0.0030	0.0771	39.4
20	2.500	0.127	0.0062	0.1584	20.7
30	2.520	0.207	0.0102	0.2582	17.5
40	2.530	0.287	0.0141	0.3580	15.3
50	2.490	0.401	0.0197	0.5003	11.7
60	2.490	0.523	0.0257	0.6525	8.95
70	2.500	0.688	0.0338	0.8583	7.68
80	2.500	0.850	0.0417	1.0604	5.12
90	2.510	1.020	0.0501	1.2725	4.63
100	2.520	1.120	0.0550	1.3972	4.36

Measurement Trial 2

Excitation Frequency: 2.5 Hz

	Measured Data				
Excitation Amplitude [µs]	Frequency [Hz]	Amplitude [V]	Amplitude [In]	Amplitude [mm]	%THD (10 harmonics)
10	0.069	0.081	0.0040	0.1007	36.9000
20	0.624	0.142	0.0070	0.1772	19.1000
30	2.490	0.210	0.0103	0.2620	15.1000
40	2.490	0.277	0.0136	0.3456	13.8000
50	2.500	0.368	0.0181	0.4591	11.5000
60	2.520	0.540	0.0265	0.6737	8.7600
70	2.500	0.658	0.0323	0.8209	7.1600
80	2.490	0.904	0.0444	1.1278	5.7000
90	2.490	1.090	0.0535	1.3598	3.9100
100	2.490	1.190	0.0584	1.4846	4.1100

Measurement Trial 1

Excitation Frequency: 3 Hz

	Measured Data				
Excitation Amplitude [µs]	Frequency [Hz]	Amplitude [V]	Amplitude [In]	Amplitude [mm]	%THD (10 harmonics)
10	1.470	0.082	0.0040	0.1018	27.6
20	3.050	0.103	0.0051	0.1285	22.2
30	3.020	0.161	0.0079	0.2009	18.6
40	2.990	0.217	0.0107	0.2707	15.9
50	3.010	0.303	0.0149	0.3780	13.2
60	2.990	0.417	0.0205	0.5202	10.8
70	3.020	0.572	0.0281	0.7136	8.14
80	3.030	0.666	0.0327	0.8309	6.3
90	3.000	0.799	0.0392	0.9968	5.24
100	3.010	0.929	0.0456	1.1590	4.36

Measurement Trial 2

Excitation Frequency: 3 Hz

	Measured Data				
Excitation Amplitude [µs]	Frequency [Hz]	Amplitude [V]	Amplitude [In]	Amplitude [mm]	%THD (10 harmonics)
10	2.900	0.073	0.0036	0.0904	26.6000
20	3.000	0.106	0.0052	0.1322	19.4000
30	3.000	0.168	0.0083	0.2096	16.2000
40	3.030	0.228	0.0112	0.2844	14.3000
50	2.990	0.337	0.0166	0.4204	11.4000
60	2.990	0.480	0.0236	0.5988	8.0200
70	3.010	0.613	0.0301	0.7647	6.6200
80	2.990	0.748	0.0367	0.9332	5.7000
90	2.980	0.919	0.0451	1.1465	4.2100
100	3.000	1.030	0.0506	1.2850	3.5000

Actuator Number 16 Performance Trials
10-03-16
LVDT calibration factor: **20.36** **Volts/Inch**

Measurement Trial 3
Excitation Frequency: 0.5 Hz

	Measured Data				
Excitation Amplitude [µs]	Frequency [Hz]	Amplitude [V]	Amplitude [In]	Amplitude [mm]	%THD (10 harmonics)
10	0.243	0.091	0.0044	0.1130	23.2000
20	0.167	0.200	0.0098	0.2495	12.4000
30	0.488	0.312	0.0153	0.3892	8.7700
40	0.497	0.403	0.0198	0.5028	8.4300
50	0.498	0.511	0.0251	0.6375	6.9900
60	0.500	0.655	0.0322	0.8171	7.3900
70	0.498	0.801	0.0393	0.9993	7.4200
80	0.500	0.947	0.0465	1.1814	7.7100
90	0.502	1.080	0.0530	1.3473	9.2700
100	0.509	1.270	0.0624	1.5844	12.6000

Arithmetic Mean for Actuator 16 Measurement Trials
Excitation Frequency: 0.5 Hz

	Measured Data				
Excitation Amplitude [µs]	Frequency [Hz]	Amplitude [V]	Amplitude [In]	Amplitude [mm]	%THD (10 harmonics)
10	0.410	0.089	0.0044	0.1112	24.600
20	0.393	0.179	0.0088	0.2237	15.267
30	0.499	0.277	0.0136	0.3452	10.923
40	0.498	0.361	0.0177	0.4508	10.077
50	0.500	0.477	0.0234	0.5955	8.860
60	0.499	0.614	0.0302	0.7664	8.803
70	0.501	0.755	0.0371	0.9423	8.573
80	0.500	0.918	0.0451	1.1457	8.707
90	0.500	1.103	0.0542	1.3765	10.023
100	0.504	1.243	0.0611	1.5511	12.980

Measurement Trial 3
Excitation Frequency: 1 Hz

	Measured Data				
Excitation Amplitude [µs]	Frequency [Hz]	Amplitude [V]	Amplitude [In]	Amplitude [mm]	%THD (10 harmonics)
10	1.110	0.081	0.0040	0.1011	28.1000
20	1.010	0.182	0.0089	0.2271	12.0000
30	1.010	0.269	0.0132	0.3356	9.0000
40	0.991	0.364	0.0179	0.4541	8.8200
50	0.999	0.463	0.0227	0.5776	8.5800
60	0.997	0.592	0.0291	0.7385	7.6800
70	1.000	0.745	0.0366	0.9294	7.9600
80	0.997	0.891	0.0438	1.1116	8.4200
90	0.993	1.040	0.0511	1.2974	8.5600
100	0.972	1.140	0.0560	1.4222	9.4800

Arithmetic Mean for Actuator 16 Measurement Trials
Excitation Frequency: 1 Hz

	Measured Data				
Excitation Amplitude [µs]	Frequency [Hz]	Amplitude [V]	Amplitude [In]	Amplitude [mm]	%THD (10 harmonics)
10	0.885	0.063	0.0031	0.0790	34.833
20	0.729	0.172	0.0084	0.2142	15.067
30	0.831	0.249	0.0122	0.3111	11.567
40	0.998	0.349	0.0171	0.4354	10.673
50	1.000	0.453	0.0223	0.5656	9.993
60	0.999	0.584	0.0287	0.7281	9.007
70	1.000	0.733	0.0360	0.9149	8.720
80	0.998	0.889	0.0437	1.1091	8.920
90	0.998	1.050	0.0516	1.3099	8.850
100	0.989	1.300	0.0639	1.6218	10.057

Measurement Trial 3
Excitation Frequency: 1.5 Hz

	Measured Data				
Excitation Amplitude [µs]	Frequency [Hz]	Amplitude [V]	Amplitude [In]	Amplitude [mm]	%THD (10 harmonics)
10	0.187	0.086	0.0042	0.1075	41.0000
20	1.470	0.181	0.0089	0.2258	15.3000
30	1.510	0.246	0.0121	0.3069	10.6000
40	1.500	0.333	0.0164	0.4154	9.3100
50	1.490	0.450	0.0221	0.5614	8.5100
60	1.500	0.552	0.0271	0.6886	8.3100
70	1.490	0.704	0.0346	0.8783	7.9000
80	1.510	0.859	0.0422	1.0716	7.3800
90	1.500	1.040	0.0511	1.2974	6.8200
100	1.520	1.310	0.0643	1.6343	6.8300

Arithmetic Mean for Actuator 16 Measurement Trials
Excitation Frequency: 1.5 Hz

	Measured Data				
Excitation Amplitude [µs]	Frequency [Hz]	Amplitude [V]	Amplitude [In]	Amplitude [mm]	%THD (10 harmonics)
10	0.625	0.082	0.0040	0.1017	37.900
20	1.246	0.168	0.0083	0.2096	14.967
30	1.510	0.244	0.0120	0.3040	11.600
40	1.503	0.338	0.0166	0.4221	10.970
50	1.493	0.463	0.0228	0.5780	8.887
60	1.503	0.572	0.0281	0.7136	8.517
70	1.497	0.718	0.0353	0.8962	7.687
80	1.503	0.868	0.0426	1.0833	7.273
90	1.500	1.060	0.0521	1.3224	6.680
100	1.507	1.283	0.0630	1.6010	7.140

Measurement Trial 3
Excitation Frequency: 2 Hz

	Measured Data				
Excitation Amplitude [µs]	Frequency [Hz]	Amplitude [V]	Amplitude [In]	Amplitude [mm]	%THD (10 harmonics)
10	0.117	0.108	0.0053	0.1347	35.8000
20	2.010	0.158	0.0078	0.1971	11.2000
30	2.020	0.226	0.0111	0.2819	11.3000
40	2.000	0.299	0.0147	0.3730	10.2000
50	2.000	0.397	0.0195	0.4953	8.7800
60	2.000	0.551	0.0271	0.6874	8.1200
70	1.980	0.663	0.0326	0.8271	7.2800
80	1.990	0.868	0.0426	1.0829	6.0000
90	2.010	1.060	0.0521	1.3224	4.7500
100	2.000	1.250	0.0614	1.5594	4.3100

Arithmetic Mean for Actuator 16 Measurement Trials
Excitation Frequency: 2 Hz

	Measured Data				
Excitation Amplitude [µs]	Frequency [Hz]	Amplitude [V]	Amplitude [In]	Amplitude [mm]	%THD (10 harmonics)
10	0.289	0.085	0.0042	0.1058	34.567
20	1.470	0.152	0.0075	0.1900	16.033
30	2.003	0.230	0.0113	0.2869	14.033
40	1.993	0.314	0.0154	0.3913	11.967
50	1.990	0.421	0.0207	0.5256	9.630
60	1.997	0.565	0.0278	0.7053	8.920
70	1.993	0.695	0.0342	0.8675	7.833
80	1.993	0.888	0.0436	1.1078	6.670
90	2.010	1.083	0.0532	1.3515	5.610
100	2.003	1.257	0.0617	1.5677	5.120

Measurement Trial 3
Excitation Frequency: 2.5 Hz

	Measured Data				
Excitation Amplitude [µs]	Frequency [Hz]	Amplitude [V]	Amplitude [In]	Amplitude [mm]	%THD (10 harmonics)
10	0.277	0.079	0.0039	0.0988	35.0000
20	2.500	0.133	0.0065	0.1659	19.8000
30	2.560	0.197	0.0097	0.2458	13.6000
40	2.480	0.278	0.0137	0.3468	12.1000
50	2.490	0.365	0.0179	0.4554	10.1000
60	2.490	0.485	0.0238	0.6051	8.8200
70	2.520	0.629	0.0309	0.7847	6.9200
80	2.510	0.759	0.0373	0.9469	6.5500
90	2.510	1.030	0.0506	1.2850	4.6400
100	2.500	1.140	0.0560	1.4222	4.4700

Arithmetic Mean for Actuator 16 Measurement Trials
Excitation Frequency: 2.5 Hz

	Measured Data				
Excitation Amplitude [µs]	Frequency [Hz]	Amplitude [V]	Amplitude [In]	Amplitude [mm]	%THD (10 harmonics)
10	0.955	0.074	0.0036	0.0922	37.100
20	1.875	0.134	0.0066	0.1672	19.867
30	2.523	0.205	0.0101	0.2553	15.400
40	2.500	0.281	0.0138	0.3501	13.733
50	2.493	0.378	0.0186	0.4716	11.100
60	2.500	0.516	0.0253	0.6437	8.843
70	2.507	0.658	0.0323	0.8213	7.253
80	2.500	0.838	0.0411	1.0450	5.790
90	2.503	1.047	0.0514	1.3058	4.393
100	2.503	1.150	0.0565	1.4347	4.313

Measurement Trial 3
Excitation Frequency: 3 Hz

	Measured Data				
Excitation Amplitude [µs]	Frequency [Hz]	Amplitude [V]	Amplitude [In]	Amplitude [mm]	%THD (10 harmonics)
10	0.740	0.095	0.0047	0.1183	20.9000
20	0.273	0.110	0.0054	0.1372	14.6000
30	3.000	0.161	0.0079	0.2009	12.6000
40	3.020	0.233	0.0114	0.2907	12.0000
50	3.000	0.338	0.0166	0.4217	9.8400
60	3.010	0.447	0.0220	0.5577	8.7500
70	2.990	0.554	0.0272	0.6911	6.7900
80	3.010	0.718	0.0353	0.8957	5.6100
90	3.010	0.842	0.0414	1.0504	4.8200
100	2.990	0.987	0.0485	1.2313	4.0400

Arithmetic Mean for Actuator 16 Measurement Trials
Excitation Frequency: 3 Hz

	Measured Data				
Excitation Amplitude [µs]	Frequency [Hz]	Amplitude [V]	Amplitude [In]	Amplitude [mm]	%THD (10 harmonics)
10	1.703	0.083	0.0041	0.1035	25.033
20	2.108	0.106	0.0052	0.1327	18.733
30	3.007	0.163	0.0080	0.2038	15.800
40	3.013	0.226	0.0111	0.2819	14.067
50	3.000	0.326	0.0160	0.4067	11.480
60	2.997	0.448	0.0220	0.5589	9.190
70	3.007	0.580	0.0285	0.7232	7.183
80	3.010	0.711	0.0349	0.8866	5.870
90	2.997	0.853	0.0419	1.0646	4.757
100	3.000	0.982	0.0482	1.2251	3.967

Actuator Alpha Comparison for Actuators: 8,10,12,14,16

10-03-16

20.36

Arithmetic Mean of all Actuators

Excitation Frequency: 0.5 Hz

	Measured Data				
Excitation Amplitude [µs]	Frequency [Hz]	Amplitude [V]	Amplitude [In]	Amplitude [mm]	%THD (10 harmonics)
10	0.539	0.058	0.0028	0.0721	45.958
20	0.458	0.136	0.0067	0.1691	20.042
30	0.473	0.234	0.0115	0.2916	15.984
40	0.465	0.348	0.0171	0.4346	14.007
50	0.500	0.483	0.0237	0.6025	11.509
60	0.499	0.624	0.0306	0.7784	10.870
70	0.500	0.762	0.0374	0.9507	10.290
80	0.499	0.911	0.0447	1.1363	9.468
90	0.499	1.036	0.0509	1.2919	9.411
100	0.501	1.227	0.0602	1.5303	9.721

Arithmetic Mean of all Actuators

Excitation Frequency: 1 Hz

	Measured Data				
Excitation Amplitude [µs]	Frequency [Hz]	Amplitude [V]	Amplitude [In]	Amplitude [mm]	%THD (10 harmonics)
10	0.526	0.062	0.0030	0.0773	36.325
20	0.797	0.141	0.0069	0.1762	18.200
30	0.892	0.248	0.0122	0.3096	14.375
40	1.000	0.368	0.0181	0.4588	12.835
50	1.001	0.496	0.0244	0.6189	11.393
60	0.998	0.629	0.0309	0.7852	10.378
70	0.998	0.769	0.0378	0.9595	10.052
80	0.999	0.918	0.0451	1.1454	9.742
90	1.832	1.066	0.0524	1.3300	9.558
100	0.998	1.243	0.0610	1.5501	9.888

Arithmetic Mean of all Actuators

Excitation Frequency: 1.5 Hz

	Measured Data				
Excitation Amplitude [µs]	Frequency [Hz]	Amplitude [V]	Amplitude [In]	Amplitude [mm]	%THD (10 harmonics)
10	0.460	0.069	0.0034	0.0858	43.325
20	1.018	0.127	0.0062	0.1579	16.748
30	1.410	0.236	0.0116	0.2950	13.050
40	1.500	0.361	0.0177	0.4506	12.567
50	1.386	0.504	0.0248	0.6291	10.402
60	1.502	0.640	0.0314	0.7979	9.068
70	1.500	0.792	0.0389	0.9875	8.346
80	1.503	0.943	0.0463	1.1766	7.660
90	1.501	1.116	0.0548	1.3917	7.188
100	1.503	1.293	0.0635	1.6125	7.438

Actuator Alpha Comparison for Actuators: 8,10,12,14,16

10-03-16

Arithmetic Mean of all Actuators

Excitation Frequency: 2 Hz

	Measured Data				
Excitation Amplitude [µs]	Frequency [Hz]	Amplitude [V]	Amplitude [In]	Amplitude [mm]	%THD (10 harmonics)
10	0.536	0.059	0.0029	0.0736	38.967
20	1.256	0.115	0.0056	0.1434	23.583
30	1.573	0.207	0.0102	0.2585	14.977
40	1.730	0.344	0.0169	0.4286	13.411
50	1.844	0.500	0.0246	0.6239	10.597
60	1.994	0.646	0.0317	0.8064	8.662
70	1.998	0.814	0.0400	1.0152	7.526
80	2.000	0.985	0.0484	1.2285	6.865
90	2.002	1.160	0.0570	1.4477	5.971
100	1.997	1.316	0.0646	1.6419	5.793

Arithmetic Mean of all Actuators

Excitation Frequency: 2.5 Hz

	Measured Data				
Excitation Amplitude [µs]	Frequency [Hz]	Amplitude [V]	Amplitude [In]	Amplitude [mm]	%THD (10 harmonics)
10	0.865	0.071	0.0035	0.0887	45.325
20	1.487	0.111	0.0054	0.1383	26.883
30	1.840	0.218	0.0107	0.2716	16.050
40	2.288	0.348	0.0171	0.4338	13.422
50	2.495	0.501	0.0246	0.6247	9.605
60	2.501	0.655	0.0322	0.8177	7.861
70	2.503	0.813	0.0399	1.0138	6.956
80	2.499	0.965	0.0474	1.2037	5.687
90	2.499	1.146	0.0563	1.4300	4.792
100	2.499	1.270	0.0624	1.5839	4.817

Arithmetic Mean of all Actuators

Excitation Frequency: 3 Hz

	Measured Data				
Excitation Amplitude [µs]	Frequency [Hz]	Amplitude [V]	Amplitude [In]	Amplitude [mm]	%THD (10 harmonics)
10	1.050	0.060	0.0029	0.0744	28.958
20	1.438	0.113	0.0056	0.1416	21.933
30	1.924	0.211	0.0104	0.2631	16.958
40	2.380	0.336	0.0165	0.4197	13.184
50	2.618	0.488	0.0240	0.6091	10.031
60	3.008	0.633	0.0311	0.7896	7.539
70	2.994	0.776	0.0381	0.9678	5.748
80	3.005	0.913	0.0449	1.1392	4.792
90	3.006	1.027	0.0505	1.2816	4.252
100	2.998	1.144	0.0562	1.4272	3.794

Actuator Alpha Comparison for Actuators: 8,10,12,14,16

Normalized Maximum Absolute Deviation
Excitation Frequency: 0.5 Hz

	Measured Data				
Excitation Amplitude [µs]	Frequency [Hz]	Amplitude [V]	Amplitude [In]	Amplitude [mm]	%THD (10 harmonics)
10	0.850	0.541	0.541	0.177	32.142
20	0.142	0.323	0.323	0.124	7.258
30	0.472	0.184	0.184	0.081	5.383
40	0.223	0.175	0.175	0.086	5.627
50	0.003	0.140	0.140	0.076	5.058
60	0.004	0.138	0.138	0.081	3.230
70	0.005	0.129	0.129	0.080	2.610
80	0.006	0.129	0.129	0.083	2.332
90	0.004	0.216	0.216	0.141	1.531
100	0.007	0.144	0.144	0.100	3.259

Normalized Amplitude
Excitation Frequency: 0.5Hz

Excitation Amplitude[µs]	Theoretical Output Amplitude [mm]	Normalized Amplitude [mm]
10	0.22	0.33
20	0.44	0.38
30	0.66	0.44
40	0.88	0.49
50	1.1	0.55
60	1.32	0.59
70	1.54	0.62
80	1.76	0.65
90	1.98	0.65
100	2.2	0.7

Normalized Maximum Absolute Deviation
Excitation Frequency: 1 Hz

	Measured Data				
Excitation Amplitude [µs]	Frequency [Hz]	Amplitude [V]	Amplitude [In]	Amplitude [mm]	%THD (10 harmonics)
10	0.680	0.483	0.483	0.170	8.658
20	0.250	0.428	0.428	0.171	3.133
30	0.171	0.256	0.256	0.120	2.808
40	0.007	0.204	0.204	0.106	2.898
50	0.003	0.173	0.173	0.097	2.073
60	0.004	0.166	0.166	0.099	2.055
70	0.002	0.128	0.128	0.079	1.848
80	0.003	0.123	0.123	0.080	1.692
90	1.366	0.125	0.125	0.084	1.076
100	0.009	0.136	0.136	0.096	0.742

Normalized Amplitude
Excitation Frequency: 1.0Hz

Excitation Amplitude[µs]	Theoretical Output Amplitude [mm]	Normalized Amplitude [mm]
10	0.22	0.35
20	0.44	0.4
30	0.66	0.47
40	0.88	0.52
50	1.1	0.56
60	1.32	0.59
70	1.54	0.62
80	1.76	0.65
90	1.98	0.67
100	2.2	0.7

Normalized Maximum Absolute Deviation
Excitation Frequency: 1.5 Hz

	Measured Data				
Excitation Amplitude [µs]	Frequency [Hz]	Amplitude [V]	Amplitude [In]	Amplitude [mm]	%THD (10 harmonics)
10	#DIV/0!	0.340	0.340	0.133	13.192
20	0.301	0.327	0.327	0.117	3.386
30	0.191	0.164	0.164	0.073	3.650
40	0.011	0.177	0.177	0.090	3.400
50	0.236	0.155	0.155	0.089	2.698
60	0.006	0.166	0.166	0.100	3.398
70	0.002	0.136	0.136	0.087	2.654
80	0.002	0.127	0.127	0.085	1.523
90	0.003	0.100	0.100	0.070	0.678
100	0.004	0.070	0.070	0.052	0.848

Normalized Amplitude
Excitation Frequency: 1.5Hz

Excitation Amplitude[µs]	Theoretical Output Amplitude [mm]	Normalized Amplitude [mm]
10	0.22	0.39
20	0.44	0.36
30	0.66	0.45
40	0.88	0.51
50	1.1	0.57
60	1.32	0.6
70	1.54	0.64
80	1.76	0.67
90	1.98	0.7
100	2.2	0.73

Normalized Maximum Absolute Deviation
Excitation Frequency: 2 Hz

	Measured Data				
Excitation Amplitude [µs]	Frequency [Hz]	Amplitude [V]	Amplitude [In]	Amplitude [mm]	%THD (10 harmonics)
10	1.343	0.580	0.580	0.194	16.300
20	0.420	0.409	0.409	0.133	7.550
30	0.416	0.316	0.316	0.124	6.023
40	0.205	0.182	0.182	0.089	6.223
50	0.540	0.224	0.224	0.127	4.970
60	0.003	0.210	0.210	0.128	4.538
70	0.002	0.190	0.190	0.125	3.338
80	0.003	0.178	0.178	0.124	0.935
90	0.004	0.146	0.146	0.107	0.573
100	0.003	0.132	0.132	0.099	0.673

Normalized Amplitude
Excitation Frequency: 2.0Hz

Excitation Amplitude[µs]	Theoretical Output Amplitude [mm]	Normalized Amplitude [mm]
10	0.22	0.33
20	0.44	0.33
30	0.66	0.39
40	0.88	0.49
50	1.1	0.57
60	1.32	0.61
70	1.54	0.66
80	1.76	0.7
90	1.98	0.73
100	2.2	0.75

Normalized Maximum Absolute Deviation
Excitation Frequency: 2.5 Hz

	Measured Data				
Excitation Amplitude [µs]	Frequency [Hz]	Amplitude [V]	Amplitude [In]	Amplitude [mm]	%THD (10 harmonics)
10	0.596	0.649	0.649	0.262	25.325
20	0.309	0.514	0.514	0.162	7.017
30	0.465	0.324	0.324	0.133	5.550
40	0.269	0.206	0.206	0.101	3.778
50	0.009	0.245	0.245	0.139	2.862
60	0.004	0.251	0.251	0.155	1.646
70	0.001	0.249	0.249	0.164	1.154
80	0.006	0.242	0.242	0.166	0.947
90	0.007	0.199	0.199	0.144	1.278
100	0.005	0.198	0.198	0.142	0.503

Normalized Amplitude
Excitation Frequency: 2.5Hz

Excitation Amplitude[µs]	Theoretical Output Amplitude [mm]	Normalized Amplitude [mm]
10	0.22	0.4
20	0.44	0.31
30	0.66	0.41
40	0.88	0.49
50	1.1	0.57
60	1.32	0.62
70	1.54	0.66
80	1.76	0.68
90	1.98	0.72
100	2.2	0.72

Normalized Maximum Absolute Deviation
Excitation Frequency: 3 Hz

	Measured Data				
Excitation Amplitude [µs]	Frequency [Hz]	Amplitude [V]	Amplitude [In]	Amplitude [mm]	%THD (10 harmonics)
10	1.024	0.460	0.460	0.156	8.125
20	0.842	0.475	0.475	0.153	4.833
30	0.562	0.421	0.421	0.168	1.525
40	0.467	0.344	0.344	0.164	0.951
50	0.189	0.332	0.332	0.184	1.449
60	0.004	0.292	0.292	0.175	1.651
70	0.006	0.253	0.253	0.159	1.436
80	0.003	0.222	0.222	0.144	1.078
90	0.009	0.183	0.183	0.119	0.795
100	0.003	0.195	0.195	0.127	0.968

Normalized Amplitude
Excitation Frequency: 3.0Hz

Excitation Amplitude[µs]	Theoretical Output Amplitude [mm]	Normalized Amplitude [mm]
10	0.22	0.34
20	0.44	0.32
30	0.66	0.4
40	0.88	0.48
50	1.1	0.55
60	1.32	0.6
70	1.54	0.63
80	1.76	0.65
90	1.98	0.65
100	2.2	0.65

Appendix B

Actuator Beta Performance Data

Actuator beta performance data is presented in the raw. For three of the beta actuators, three measurement trials were performed of 20 seconds duration for each actuation case. The actuation cases, ranging in excitation amplitude 10-100 μs and excitation frequency 0.5-3.0 Hz, were of a sinusoidal waveform. The motion of the actuators were measured using a 1 inch linear range LVDT attached to the actuator output. This LVDT measurement was digitally recoreded at a 2 kHz sample rate using National Instruments Labview. Before digital conversion of the LVDT data, it was filtered using a 200 Hz cut-off, 2nd order, passive RC analog filter.

Using Labview, the actuator output frequency, output amplitude, and Total Harmonic Distortion (%THD) were calculated. For each acutator, an arithetic mean from the three measurement trials was calculated. The last page shows the actuator performance data calculated from the arithmetic mean of each of the three acutators tested. This performance data is presented in chapter 8 on page 38 of this thesis as %THD, Normalized Actuation Amplitude, and Maximum Absolute Deviation.

Actuator Number 13 Performance Trials LVDT has 1" linear range

10-03-16

LVDT calibration factor: **20.36** **Volts/Inch**

Note: Each frequency-amplitude run is measured over 20sec period

Measurement Trial 1

Excitation Frequency: 0.5 Hz

	Measured Data				
Excitation Amplitude [µs]	Frequency [Hz]	Amplitude [V]	Amplitude [In]	Amplitude [mm]	%THD (10 harmonics)
10	0.500	0.158	0.0078	0.1973	12.39
20	0.500	0.299	0.0147	0.3735	7.83
30	0.500	0.509	0.0250	0.6352	5.28
40	0.500	0.689	0.0338	0.8593	4.52
50	0.500	0.889	0.0437	1.1089	3.15
60	0.500	1.061	0.0521	1.3231	3.29
70	0.500	1.241	0.0610	1.5486	2.83
80	0.500	1.410	0.0692	1.7587	2.22
90	0.500	1.590	0.0781	1.9832	2.06
100	0.500	1.729	0.0849	2.1572	2.55

Measurement Trial 2

Excitation Frequency: 0.5 Hz

	Measured Data				
Excitation Amplitude [µs]	Frequency [Hz]	Amplitude [V]	Amplitude [In]	Amplitude [mm]	%THD (10 harmonics)
10	0.500	0.138	0.0068	0.1717	14.86
20	0.500	0.278	0.0137	0.3473	7.97
30	0.500	0.493	0.0242	0.6146	4.44
40	0.500	0.671	0.0330	0.8372	4.51
50	0.500	0.881	0.0433	1.0990	2.96
60	0.500	1.050	0.0516	1.3094	3.66
70	0.500	1.242	0.0610	1.5490	3.22
80	0.500	1.387	0.0681	1.7307	2.9
90	0.500	1.591	0.0781	1.9847	2.04
100	0.500	1.748	0.0859	2.1812	1.75

Measurement Trial 1

Excitation Frequency: 1 Hz

	Measured Data				
Excitation Amplitude [µs]	Frequency [Hz]	Amplitude [V]	Amplitude [In]	Amplitude [mm]	%THD (10 harmonics)
10	1.000	0.151	0.0074	0.1884	11.7
20	1.000	0.280	0.0138	0.3495	6.81
30	1.000	0.486	0.0239	0.6068	4.41
40	1.000	0.689	0.0339	0.8600	4.73
50	1.000	0.873	0.0429	1.0890	3.97
60	1.000	1.030	0.0506	1.2847	2.46
70	1.000	1.270	0.0624	1.5843	2.15
80	1.000	1.397	0.0686	1.7434	1.84
90	1.000	1.548	0.0760	1.9312	1.07
100	1.000	1.760	0.0864	2.1952	1.23

Measurement Trial 2

Excitation Frequency: 1 Hz

	Measured Data				
Excitation Amplitude [µs]	Frequency [Hz]	Amplitude [V]	Amplitude [In]	Amplitude [mm]	%THD (10 harmonics)
10	1.000	0.143	0.0070	0.1784	11.56
20	1.000	0.289	0.0142	0.3608	6.32
30	1.000	0.479	0.0235	0.5972	4.2
40	1.000	0.678	0.0333	0.8459	4.38
50	1.000	0.859	0.0422	1.0713	3.14
60	1.000	1.072	0.0526	1.3368	2.56
70	1.000	1.249	0.0613	1.5582	1.72
80	1.000	1.401	0.0688	1.7475	1.72
90	1.000	1.621	0.0796	2.0227	1.01
100	1.000	1.781	0.0875	2.2222	1.16

Measurement Trial 1

Excitation Frequency: 1.5 Hz

	Measured Data				
Excitation Amplitude [µs]	Frequency [Hz]	Amplitude [V]	Amplitude [In]	Amplitude [mm]	%THD (10 harmonics)
10	1.500	0.143	0.0070	0.1785	8.22
20	1.500	0.284	0.0140	0.3544	6.13
30	1.500	0.462	0.0227	0.5761	3.44
40	1.500	0.653	0.0321	0.8147	3.29
50	1.500	0.850	0.0418	1.0606	1.99
60	1.500	1.042	0.0512	1.2996	1.51
70	1.500	1.237	0.0608	1.5434	1.39
80	1.500	1.402	0.0689	1.7489	0.9
90	1.500	1.570	0.0771	1.9582	0.72
100	1.500	1.768	0.0869	2.2061	1.88

Measurement Trial 2

Excitation Frequency: 1.5 Hz

	Measured Data				
Excitation Amplitude [µs]	Frequency [Hz]	Amplitude [V]	Amplitude [In]	Amplitude [mm]	%THD (10 harmonics)
10	1.500	0.158	0.0078	0.1970	8.81
20	1.500	0.299	0.0147	0.3733	6.23
30	1.500	0.505	0.0248	0.6296	3.26
40	1.500	0.691	0.0340	0.8624	3.02
50	1.500	0.872	0.0428	1.0877	2.16
60	1.500	1.081	0.0531	1.3483	1.29
70	1.500	1.250	0.0614	1.5595	0.81
80	1.500	1.427	0.0701	1.7802	0.89
90	1.500	1.588	0.0780	1.9811	1.13
100	1.500	1.719	0.0844	2.1443	1.73

Measurement Trial 1

Excitation Frequency: 2 Hz

	Measured Data				
Excitation Amplitude [µs]	Frequency [Hz]	Amplitude [V]	Amplitude [In]	Amplitude [mm]	%THD (10 harmonics)
10	2.000	0.136	0.0067	0.1694	8.3
20	2.000	0.282	0.0138	0.3512	7.25
30	2.000	0.470	0.0231	0.5860	4.7
40	2.000	0.672	0.0330	0.8388	2.87
50	2.000	0.858	0.0422	1.0710	1.71
60	2.000	1.029	0.0505	1.2834	2
70	2.000	1.200	0.0589	1.4971	1.19
80	2.000	1.368	0.0672	1.7066	1.05
90	2.000	1.538	0.0755	1.9187	2.06
100	2.000	1.717	0.0843	2.1424	1.38

Measurement Trial 2

Excitation Frequency: 2 Hz

	Measured Data				
Excitation Amplitude [µs]	Frequency [Hz]	Amplitude [V]	Amplitude [In]	Amplitude [mm]	%THD (10 harmonics)
10	2.000	0.147	0.0072	0.1838	7.99
20	2.000	0.281	0.0138	0.3509	7.16
30	2.000	0.488	0.0240	0.6089	4.36
40	2.000	0.690	0.0339	0.8603	3.03
50	2.000	0.866	0.0425	1.0800	1.7
60	2.000	1.041	0.0511	1.2990	1.77
70	2.000	1.241	0.0610	1.5488	0.93
80	2.000	1.419	0.0697	1.7697	1.23
90	2.000	1.519	0.0746	1.8945	1.52
100	2.000	1.760	0.0864	2.1958	1.53

Measurement Trial 1

Excitation Frequency: 2.5 Hz

	Measured Data				
Excitation Amplitude [µs]	Frequency [Hz]	Amplitude [V]	Amplitude [In]	Amplitude [mm]	%THD (10 harmonics)
10	2.500	0.143	0.0070	0.1785	8.44
20	2.500	0.284	0.0140	0.3544	5.07
30	2.500	0.462	0.0227	0.5761	3.92
40	2.500	0.653	0.0321	0.8147	2.34
50	2.500	0.850	0.0418	1.0606	2.24
60	2.500	1.042	0.0512	1.2996	1.06
70	2.500	1.237	0.0608	1.5434	0.94
80	2.500	1.402	0.0689	1.7489	1.13
90	2.500	1.570	0.0771	1.9582	1.19
100	2.500	1.768	0.0869	2.2061	0.97

Measurement Trial 2

Excitation Frequency: 2.5 Hz

	Measured Data				
Excitation Amplitude [µs]	Frequency [Hz]	Amplitude [V]	Amplitude [In]	Amplitude [mm]	%THD (10 harmonics)
10	2.500	0.144	0.0071	0.1800	7.92
20	2.500	0.284	0.0139	0.3540	4.93
30	2.500	0.470	0.0231	0.5867	3.37
40	2.500	0.645	0.0317	0.8048	3.1
50	2.500	0.850	0.0418	1.0609	1.11
60	2.500	1.030	0.0506	1.2849	1.8
70	2.500	1.239	0.0608	1.5451	1.1
80	2.500	1.408	0.0691	1.7562	1.08
90	2.500	1.571	0.0772	1.9597	0.93
100	2.500	1.760	0.0864	2.1955	0.91

Measurement Trial 1

Excitation Frequency: 3 Hz

	Measured Data				
Excitation Amplitude [µs]	Frequency [Hz]	Amplitude [V]	Amplitude [In]	Amplitude [mm]	%THD (10 harmonics)
10	3.000	0.136	0.0067	0.1694	10.42
20	3.000	0.282	0.0138	0.3512	5.56
30	3.000	0.470	0.0231	0.5860	3.53
40	3.000	0.641	0.0315	0.7997	3.34
50	3.000	0.858	0.0422	1.0710	1.56
60	3.000	1.029	0.0505	1.2834	1.76
70	3.000	1.181	0.0580	1.4731	1.15
80	3.000	1.368	0.0672	1.7066	1.51
90	3.000	1.538	0.0755	1.9187	1.53
100	3.000	1.717	0.0843	2.1424	1.65

Measurement Trial 2

Excitation Frequency: 3 Hz

	Measured Data				
Excitation Amplitude [µs]	Frequency [Hz]	Amplitude [V]	Amplitude [In]	Amplitude [mm]	%THD (10 harmonics)
10	3.000	0.130	0.0064	0.1622	10.5
20	3.000	0.275	0.0135	0.3430	6.64
30	3.000	0.470	0.0231	0.5858	2.77
40	3.000	0.639	0.0314	0.7972	2.21
50	3.000	0.843	0.0414	1.0511	1.33
60	3.000	1.030	0.0506	1.2849	2.06
70	3.000	1.220	0.0599	1.5218	1.9
80	3.000	1.359	0.0667	1.6950	0.86
90	3.000	1.531	0.0752	1.9105	1.63
100	3.000	1.729	0.0849	2.1570	0.97

Actuator Number 13 Performance Trials
10-03-16
LVDT calibration factor: **20.36** **Volts/Inch**

Measurement Trial 3
Excitation Frequency: 0.5 Hz

	Measured Data				
Excitation Amplitude [µs]	Frequency [Hz]	Amplitude [V]	Amplitude [In]	Amplitude [mm]	%THD (10 harmonics)
10	0.500	0.142	0.0070	0.1771	14.19
20	0.500	0.282	0.0139	0.3521	7.6
30	0.500	0.504	0.0248	0.6293	5.02
40	0.500	0.676	0.0332	0.8435	4.54
50	0.500	0.875	0.0430	1.0919	3.44
60	0.500	1.048	0.0515	1.3076	3.49
70	0.500	1.242	0.0610	1.5490	3.18
80	0.500	1.387	0.0681	1.7309	2.32
90	0.500	1.579	0.0776	1.9699	2.2
100	0.500	1.750	0.0860	2.1838	2.35

Arithmetic Mean for Actuator 13 Measurement Trials
Excitation Frequency: 0.5 Hz

	Measured Data				
Excitation Amplitude [µs]	Frequency [Hz]	Amplitude [V]	Amplitude [In]	Amplitude [mm]	%THD (10 harmonics)
10	0.500	0.146	0.0072	0.1821	13.813
20	0.500	0.287	0.0141	0.3576	7.801
30	0.500	0.502	0.0247	0.6264	4.914
40	0.500	0.679	0.0333	0.8467	4.524
50	0.500	0.882	0.0433	1.0999	3.181
60	0.500	1.053	0.0517	1.3134	3.482
70	0.500	1.242	0.0610	1.5489	3.077
80	0.500	1.395	0.0685	1.7401	2.478
90	0.500	1.587	0.0779	1.9793	2.100
100	0.500	1.743	0.0856	2.1741	2.215

Measurement Trial 3
Excitation Frequency: 1 Hz

	Measured Data				
Excitation Amplitude [µs]	Frequency [Hz]	Amplitude [V]	Amplitude [In]	Amplitude [mm]	%THD (10 harmonics)
10	1.000	0.140	0.0069	0.1747	11.41
20	1.000	0.275	0.0135	0.3431	7.79
30	1.000	0.480	0.0236	0.5988	4.27
40	1.000	0.680	0.0334	0.8483	4.28
50	1.000	0.875	0.0430	1.0916	3.17
60	1.000	1.030	0.0506	1.2850	2.76
70	1.000	1.237	0.0608	1.5432	1.78
80	1.000	1.410	0.0693	1.7590	1.83
90	1.000	1.601	0.0786	1.9973	1.05
100	1.000	1.752	0.0861	2.1857	0.89

Arithmetic Mean for Actuator 13 Measurement Trials
Excitation Frequency: 1 Hz

	Measured Data				
Excitation Amplitude [µs]	Frequency [Hz]	Amplitude [V]	Amplitude [In]	Amplitude [mm]	%THD (10 harmonics)
10	1.000	0.145	0.0071	0.1805	11.556
20	1.000	0.281	0.0138	0.3511	6.974
30	1.000	0.482	0.0237	0.6009	4.293
40	1.000	0.682	0.0335	0.8514	4.462
50	1.000	0.869	0.0427	1.0840	3.424
60	1.000	1.044	0.0513	1.3022	2.594
70	1.000	1.252	0.0615	1.5619	1.885
80	1.000	1.403	0.0689	1.7500	1.796
90	1.000	1.590	0.0781	1.9837	1.043
100	1.000	1.764	0.0867	2.2010	1.094

Measurement Trial 3
Excitation Frequency: 1.5 Hz

	Measured Data				
Excitation Amplitude [µs]	Frequency [Hz]	Amplitude [V]	Amplitude [In]	Amplitude [mm]	%THD (10 harmonics)
10	1.500	0.155	0.0076	0.1938	8.84
20	1.500	0.306	0.0150	0.3812	6.17
30	1.500	0.511	0.0251	0.6371	3.61
40	1.500	0.701	0.0344	0.8743	2.4
50	1.500	0.890	0.0437	1.1098	2.52
60	1.500	1.080	0.0530	1.3474	1.2
70	1.500	1.252	0.0615	1.5619	1.37
80	1.500	1.438	0.0706	1.7939	1.32
90	1.500	1.590	0.0781	1.9830	0.98
100	1.500	1.740	0.0855	2.1706	1.2

Arithmetic Mean for Actuator 13 Measurement Trials
Excitation Frequency: 1.5 Hz

	Measured Data				
Excitation Amplitude [µs]	Frequency [Hz]	Amplitude [V]	Amplitude [In]	Amplitude [mm]	%THD (10 harmonics)
10	1.500	0.152	0.0075	0.1898	8.625
20	1.500	0.296	0.0146	0.3696	6.174
30	1.500	0.492	0.0242	0.6143	3.432
40	1.500	0.682	0.0335	0.8505	2.902
50	1.500	0.871	0.0428	1.0860	2.224
60	1.500	1.068	0.0524	1.3318	1.333
70	1.500	1.246	0.0612	1.5549	1.189
80	1.500	1.422	0.0699	1.7744	1.038
90	1.500	1.582	0.0777	1.9741	0.942
100	1.500	1.742	0.0856	2.1737	1.600

Measurement Trial 3
Excitation Frequency: 2 Hz

	Measured Data				
Excitation Amplitude [µs]	Frequency [Hz]	Amplitude [V]	Amplitude [In]	Amplitude [mm]	%THD (10 harmonics)
10	2.000	0.147	0.0072	0.1830	9.32
20	2.000	0.289	0.0142	0.3602	5.9
30	2.000	0.491	0.0241	0.6127	4.54
40	2.000	0.705	0.0346	0.8789	2.42
50	2.000	0.862	0.0423	1.0752	2.19
60	2.000	1.018	0.0500	1.2702	2.09
70	2.000	1.251	0.0614	1.5608	0.67
80	2.000	1.432	0.0703	1.7864	1.24
90	2.000	1.539	0.0756	1.9196	1.15
100	2.000	1.758	0.0863	2.1931	1.5

Arithmetic Mean for Actuator 13 Measurement Trials
Excitation Frequency: 2 Hz

	Measured Data				
Excitation Amplitude [µs]	Frequency [Hz]	Amplitude [V]	Amplitude [In]	Amplitude [mm]	%THD (10 harmonics)
10	2.000	0.143	0.0070	0.1787	8.536
20	2.000	0.284	0.0139	0.3541	6.767
30	2.000	0.483	0.0237	0.6025	4.534
40	2.000	0.689	0.0338	0.8593	2.773
50	2.000	0.862	0.0423	1.0754	1.862
60	2.000	1.029	0.0506	1.2842	1.957
70	2.000	1.231	0.0605	1.5355	0.930
80	2.000	1.406	0.0691	1.7542	1.172
90	2.000	1.532	0.0752	1.9109	1.578
100	2.000	1.745	0.0857	2.1771	1.468

Measurement Trial 3
Excitation Frequency: 2.5 Hz

	Measured Data				
Excitation Amplitude [µs]	Frequency [Hz]	Amplitude [V]	Amplitude [In]	Amplitude [mm]	%THD (10 harmonics)
10	2.500	0.152	0.0075	0.1900	7.12
20	2.500	0.289	0.0142	0.3603	4.58
30	2.500	0.483	0.0237	0.6025	2.92
40	2.500	0.654	0.0321	0.8153	2.34
50	2.500	0.867	0.0426	1.0816	1.23
60	2.500	1.042	0.0512	1.2996	1.23
70	2.500	1.238	0.0608	1.5446	1.59
80	2.500	1.408	0.0692	1.7568	1.74
90	2.500	1.581	0.0776	1.9720	1.36
100	2.500	1.761	0.0865	2.1964	0.93

Arithmetic Mean for Actuator 13 Measurement Trials
Excitation Frequency: 2.5 Hz

	Measured Data				
Excitation Amplitude [µs]	Frequency [Hz]	Amplitude [V]	Amplitude [In]	Amplitude [mm]	%THD (10 harmonics)
10	2.500	0.147	0.0072	0.1828	7.826
20	2.500	0.286	0.0140	0.3562	4.859
30	2.500	0.472	0.0232	0.5884	3.402
40	2.500	0.651	0.0320	0.8116	2.596
50	2.500	0.856	0.0420	1.0677	1.525
60	2.500	1.038	0.0510	1.2947	1.360
70	2.500	1.238	0.0608	1.5444	1.208
80	2.500	1.406	0.0691	1.7540	1.318
90	2.500	1.574	0.0773	1.9633	1.155
100	2.500	1.763	0.0866	2.1993	0.936

Measurement Trial 3
Excitation Frequency: 3 Hz

	Measured Data				
Excitation Amplitude [µs]	Frequency [Hz]	Amplitude [V]	Amplitude [In]	Amplitude [mm]	%THD (10 harmonics)
10	3.000	0.125	0.0061	0.1559	10.1
20	3.000	0.281	0.0138	0.3506	6.47
30	3.000	0.473	0.0232	0.5895	3.09
40	3.000	0.642	0.0315	0.8009	3.12
50	3.000	0.854	0.0420	1.0657	2.02
60	3.000	1.051	0.0516	1.3112	1.96
70	3.000	1.202	0.0590	1.4989	1.19
80	3.000	1.370	0.0673	1.7091	1.31
90	3.000	1.538	0.0755	1.9181	1.47
100	3.000	1.741	0.0855	2.1720	1.25

Arithmetic Mean for Actuator 13 Measurement Trials
Excitation Frequency: 3 Hz

	Measured Data				
Excitation Amplitude [µs]	Frequency [Hz]	Amplitude [V]	Amplitude [In]	Amplitude [mm]	%THD (10 harmonics)
10	3.000	0.130	0.0064	0.1625	10.340
20	3.000	0.279	0.0137	0.3483	6.222
30	3.000	0.471	0.0231	0.5871	3.130
40	3.000	0.641	0.0315	0.7993	2.888
50	3.000	0.852	0.0418	1.0626	1.635
60	3.000	1.037	0.0509	1.2932	1.927
70	3.000	1.201	0.0590	1.4979	1.415
80	3.000	1.366	0.0671	1.7036	1.228
90	3.000	1.536	0.0754	1.9158	1.543
100	3.000	1.729	0.0849	2.1571	1.289

Actuator Number 14 Performance Trials LVDT has 1" linear range

10-03-16

LVDT calibration factor: **20.36** **Volts/Inch**

Note: Each frequency-amplitude run is measured over 20sec period

Measurement Trial 1

Excitation Frequency: 0.5 Hz

	Measured Data				
Excitation Amplitude [µs]	Frequency [Hz]	Amplitude [V]	Amplitude [In]	Amplitude [mm]	%THD (10 harmonics)
10	0.500	0.142	0.0070	0.1771	14.19
20	0.500	0.282	0.0139	0.3521	7.6
30	0.500	0.504	0.0248	0.6293	5.02
40	0.500	0.676	0.0332	0.8435	4.54
50	0.500	0.875	0.0430	1.0919	3.44
60	0.500	1.048	0.0515	1.3076	3.49
70	0.500	1.242	0.0610	1.5490	3.18
80	0.500	1.387	0.0681	1.7309	2.32
90	0.500	1.579	0.0776	1.9699	2.2
100	0.500	1.750	0.0860	2.1838	2.35

Measurement Trial 2

Excitation Frequency: 0.5 Hz

	Measured Data				
Excitation Amplitude [µs]	Frequency [Hz]	Amplitude [V]	Amplitude [In]	Amplitude [mm]	%THD (10 harmonics)
10	0.500	0.138	0.0068	0.1717	14.86
20	0.500	0.278	0.0137	0.3473	7.97
30	0.500	0.493	0.0242	0.6146	4.44
40	0.500	0.671	0.0330	0.8372	4.51
50	0.500	0.881	0.0433	1.0990	2.96
60	0.500	1.050	0.0516	1.3094	3.66
70	0.500	1.242	0.0610	1.5490	3.22
80	0.500	1.387	0.0681	1.7307	2.9
90	0.500	1.591	0.0781	1.9847	2.04
100	0.500	1.748	0.0859	2.1812	1.75

Measurement Trial 1

Excitation Frequency: 1 Hz

	Measured Data				
Excitation Amplitude [µs]	Frequency [Hz]	Amplitude [V]	Amplitude [In]	Amplitude [mm]	%THD (10 harmonics)
10	1.000	0.143	0.0070	0.1784	11.41
20	1.000	0.283	0.0139	0.3534	7.79
30	1.000	0.485	0.0238	0.6049	4.27
40	1.000	0.682	0.0335	0.8511	4.28
50	1.000	0.879	0.0432	1.0962	3.17
60	1.000	1.048	0.0515	1.3080	2.76
70	1.000	1.250	0.0614	1.5597	1.78
80	1.000	1.419	0.0697	1.7697	1.83
90	1.000	1.638	0.0805	2.0441	1.05
100	1.000	1.779	0.0874	2.2198	0.89

Measurement Trial 2

Excitation Frequency: 1 Hz

	Measured Data				
Excitation Amplitude [µs]	Frequency [Hz]	Amplitude [V]	Amplitude [In]	Amplitude [mm]	%THD (10 harmonics)
10	1.000	0.143	0.0070	0.1784	11.56
20	1.000	0.289	0.0142	0.3608	6.32
30	1.000	0.479	0.0235	0.5972	4.2
40	1.000	0.678	0.0333	0.8459	4.38
50	1.000	0.859	0.0422	1.0713	3.14
60	1.000	1.072	0.0526	1.3368	2.56
70	1.000	1.249	0.0613	1.5582	1.72
80	1.000	1.401	0.0688	1.7475	1.72
90	1.000	1.621	0.0796	2.0227	1.01
100	1.000	1.781	0.0875	2.2222	1.16

Measurement Trial 1

Excitation Frequency: 1.5 Hz

	Measured Data				
Excitation Amplitude [µs]	Frequency [Hz]	Amplitude [V]	Amplitude [In]	Amplitude [mm]	%THD (10 harmonics)
10	1.500	0.155	0.0076	0.1938	8.84
20	1.500	0.306	0.0150	0.3812	6.17
30	1.500	0.511	0.0251	0.6371	3.61
40	1.500	0.701	0.0344	0.8743	2.4
50	1.500	0.890	0.0437	1.1098	2.52
60	1.500	1.080	0.0530	1.3474	1.2
70	1.500	1.252	0.0615	1.5619	1.37
80	1.500	1.438	0.0706	1.7939	1.32
90	1.500	1.590	0.0781	1.9830	0.98
100	1.500	1.740	0.0855	2.1706	1.2

Measurement Trial 2

Excitation Frequency: 1.5 Hz

	Measured Data				
Excitation Amplitude [µs]	Frequency [Hz]	Amplitude [V]	Amplitude [In]	Amplitude [mm]	%THD (10 harmonics)
10	1.500	0.158	0.0078	0.1970	8.81
20	1.500	0.299	0.0147	0.3733	6.23
30	1.500	0.505	0.0248	0.6296	3.26
40	1.500	0.691	0.0340	0.8624	3.02
50	1.500	0.872	0.0428	1.0877	2.16
60	1.500	1.081	0.0531	1.3483	1.29
70	1.500	1.250	0.0614	1.5595	0.81
80	1.500	1.427	0.0701	1.7802	0.89
90	1.500	1.588	0.0780	1.9811	1.13
100	1.500	1.719	0.0844	2.1443	1.73

Measurement Trial 1

Excitation Frequency: 2 Hz

	Measured Data				
Excitation Amplitude [µs]	Frequency [Hz]	Amplitude [V]	Amplitude [In]	Amplitude [mm]	%THD (10 harmonics)
10	2.000	0.147	0.0072	0.1830	9.32
20	2.000	0.289	0.0142	0.3602	5.9
30	2.000	0.491	0.0241	0.6127	4.54
40	2.000	0.705	0.0346	0.8789	2.42
50	2.000	0.862	0.0423	1.0752	2.19
60	2.000	1.018	0.0500	1.2702	2.09
70	2.000	1.251	0.0614	1.5608	0.67
80	2.000	1.432	0.0703	1.7864	1.24
90	2.000	1.539	0.0756	1.9196	1.15
100	2.000	1.758	0.0863	2.1931	1.5

Measurement Trial 2

Excitation Frequency: 2 Hz

	Measured Data				
Excitation Amplitude [µs]	Frequency [Hz]	Amplitude [V]	Amplitude [In]	Amplitude [mm]	%THD (10 harmonics)
10	2.000	0.147	0.0072	0.1838	7.99
20	2.000	0.281	0.0138	0.3509	7.16
30	2.000	0.488	0.0240	0.6089	4.36
40	2.000	0.690	0.0339	0.8603	3.03
50	2.000	0.866	0.0425	1.0800	1.7
60	2.000	1.041	0.0511	1.2990	1.77
70	2.000	1.241	0.0610	1.5488	0.93
80	2.000	1.419	0.0697	1.7697	1.23
90	2.000	1.519	0.0746	1.8945	1.52
100	2.000	1.760	0.0864	2.1958	1.53

Measurement Trial 1

Excitation Frequency: 2.5 Hz

	Measured Data				
Excitation Amplitude [µs]	Frequency [Hz]	Amplitude [V]	Amplitude [In]	Amplitude [mm]	%THD (10 harmonics)
10	2.500	0.152	0.0075	0.1900	7.12
20	2.500	0.289	0.0142	0.3603	4.58
30	2.500	0.483	0.0237	0.6025	2.92
40	2.500	0.654	0.0321	0.8153	2.34
50	2.500	0.867	0.0426	1.0816	1.23
60	2.500	1.042	0.0512	1.2996	1.23
70	2.500	1.238	0.0608	1.5446	1.59
80	2.500	1.408	0.0692	1.7568	1.74
90	2.500	1.581	0.0776	1.9720	1.36
100	2.500	1.761	0.0865	2.1964	0.93

Measurement Trial 2

Excitation Frequency: 2.5 Hz

	Measured Data				
Excitation Amplitude [µs]	Frequency [Hz]	Amplitude [V]	Amplitude [In]	Amplitude [mm]	%THD (10 harmonics)
10	2.500	0.144	0.0071	0.1800	7.92
20	2.500	0.284	0.0139	0.3540	4.93
30	2.500	0.470	0.0231	0.5867	3.37
40	2.500	0.645	0.0317	0.8048	3.1
50	2.500	0.850	0.0418	1.0609	1.11
60	2.500	1.030	0.0506	1.2849	1.8
70	2.500	1.239	0.0608	1.5451	1.1
80	2.500	1.408	0.0691	1.7562	1.08
90	2.500	1.571	0.0772	1.9597	0.93
100	2.500	1.760	0.0864	2.1955	0.91

Measurement Trial 1

Excitation Frequency: 3 Hz

	Measured Data				
Excitation Amplitude [µs]	Frequency [Hz]	Amplitude [V]	Amplitude [In]	Amplitude [mm]	%THD (10 harmonics)
10	3.000	0.128	0.0063	0.1597	10.1
20	3.000	0.281	0.0138	0.3506	6.47
30	3.000	0.473	0.0232	0.5895	3.09
40	3.000	0.643	0.0316	0.8022	3.12
50	3.000	0.854	0.0420	1.0657	2.02
60	3.000	1.031	0.0506	1.2861	1.96
70	3.000	1.202	0.0590	1.4989	1.19
80	3.000	1.370	0.0673	1.7091	1.31
90	3.000	1.538	0.0755	1.9181	1.47
100	3.000	1.741	0.0855	2.1720	1.25

Measurement Trial 2

Excitation Frequency: 3 Hz

	Measured Data				
Excitation Amplitude [µs]	Frequency [Hz]	Amplitude [V]	Amplitude [In]	Amplitude [mm]	%THD (10 harmonics)
10	3.000	0.130	0.0064	0.1622	10.5
20	3.000	0.275	0.0135	0.3430	6.64
30	3.000	0.470	0.0231	0.5858	2.77
40	3.000	0.642	0.0315	0.8009	2.21
50	3.000	0.843	0.0414	1.0511	1.33
60	3.000	1.030	0.0506	1.2849	2.06
70	3.000	1.220	0.0599	1.5218	1.9
80	3.000	1.359	0.0667	1.6950	0.86
90	3.000	1.531	0.0752	1.9105	1.63
100	3.000	1.729	0.0849	2.1570	0.97

Actuator Number 14 Performance Trials
10-03-16

LVDT calibration factor: **20.36** **Volts/Inch**

Measurement Trial 3
Excitation Frequency: 0.5 Hz

	Measured Data				
Excitation Amplitude [µs]	Frequency [Hz]	Amplitude [V]	Amplitude [In]	Amplitude [mm]	%THD (10 harmonics)
10	0.500	0.142	0.0070	0.1772	12.34
20	0.500	0.280	0.0137	0.3487	7.89
30	0.500	0.500	0.0246	0.6243	5.37
40	0.500	0.677	0.0332	0.8444	4.84
50	0.500	0.873	0.0429	1.0890	3.11
60	0.500	1.060	0.0521	1.3224	3.14
70	0.500	1.250	0.0614	1.5594	2.91
80	0.500	1.400	0.0688	1.7466	2.29
90	0.500	1.580	0.0776	1.9711	2.09
100	0.500	1.740	0.0855	2.1707	2.13

Arithmetic Mean for Actuator 14 Measurement Trials
Excitation Frequency: 0.5 Hz

	Measured Data				
Excitation Amplitude [µs]	Frequency [Hz]	Amplitude [V]	Amplitude [In]	Amplitude [mm]	%THD (10 harmonics)
10	0.500	0.141	0.0069	0.1753	13.797
20	0.500	0.280	0.0138	0.3494	7.822
30	0.500	0.499	0.0245	0.6227	4.943
40	0.500	0.675	0.0331	0.8417	4.630
50	0.500	0.876	0.0430	1.0933	3.169
60	0.500	1.053	0.0517	1.3131	3.429
70	0.500	1.244	0.0611	1.5525	3.103
80	0.500	1.392	0.0683	1.7361	2.503
90	0.500	1.583	0.0778	1.9752	2.108
100	0.500	1.746	0.0858	2.1786	2.073

Measurement Trial 3
Excitation Frequency: 1 Hz

	Measured Data				
Excitation Amplitude [µs]	Frequency [Hz]	Amplitude [V]	Amplitude [In]	Amplitude [mm]	%THD (10 harmonics)
10	1.000	0.142	0.0070	0.1777	11.37
20	1.000	0.283	0.0139	0.3526	6.47
30	1.000	0.476	0.0234	0.5941	4.05
40	1.000	0.675	0.0332	0.8423	4.73
50	1.000	0.857	0.0421	1.0696	4.09
60	1.000	1.080	0.0530	1.3473	2.44
70	1.000	1.250	0.0614	1.5594	2.26
80	1.000	1.410	0.0693	1.7590	1.98
90	1.000	1.600	0.0786	1.9961	1.38
100	1.000	1.780	0.0874	2.2206	0.97

Arithmetic Mean for Actuator 14 Measurement Trials
Excitation Frequency: 1 Hz

	Measured Data				
Excitation Amplitude [µs]	Frequency [Hz]	Amplitude [V]	Amplitude [In]	Amplitude [mm]	%THD (10 harmonics)
10	1.000	0.143	0.0070	0.1782	11.447
20	1.000	0.285	0.0140	0.3556	6.860
30	1.000	0.480	0.0236	0.5987	4.172
40	1.000	0.678	0.0333	0.8464	4.462
50	1.000	0.865	0.0425	1.0790	3.466
60	1.000	1.067	0.0524	1.3307	2.586
70	1.000	1.250	0.0614	1.5591	1.921
80	1.000	1.410	0.0692	1.7587	1.844
90	1.000	1.620	0.0796	2.0210	1.145
100	1.000	1.780	0.0874	2.2209	1.005

Measurement Trial 3
Excitation Frequency: 1.5 Hz

	Measured Data				
Excitation Amplitude [µs]	Frequency [Hz]	Amplitude [V]	Amplitude [In]	Amplitude [mm]	%THD (10 harmonics)
10	1.500	0.144	0.0071	0.1796	8.43
20	1.500	0.299	0.0147	0.3728	5.97
30	1.500	0.505	0.0248	0.6302	3.76
40	1.500	0.688	0.0338	0.8579	3.7
50	1.500	0.890	0.0437	1.1108	1.55
60	1.500	1.057	0.0519	1.3190	1.53
70	1.500	1.241	0.0609	1.5479	1.01
80	1.500	1.408	0.0692	1.7568	1.32
90	1.500	1.590	0.0781	1.9836	0.94
100	1.500	1.730	0.0850	2.1578	1.48

Arithmetic Mean for Actuator 14 Measurement Trials
Excitation Frequency: 1.5 Hz

	Measured Data				
Excitation Amplitude [µs]	Frequency [Hz]	Amplitude [V]	Amplitude [In]	Amplitude [mm]	%THD (10 harmonics)
10	1.500	0.152	0.0075	0.1901	8.696
20	1.500	0.301	0.0148	0.3758	6.118
30	1.500	0.507	0.0249	0.6323	3.541
40	1.500	0.693	0.0340	0.8649	3.038
50	1.500	0.884	0.0434	1.1028	2.079
60	1.500	1.073	0.0527	1.3382	1.340
70	1.500	1.248	0.0613	1.5564	1.062
80	1.500	1.424	0.0700	1.7770	1.179
90	1.500	1.589	0.0781	1.9826	1.016
100	1.500	1.729	0.0849	2.1576	1.470

Measurement Trial 3
Excitation Frequency: 2 Hz

	Measured Data				
Excitation Amplitude [µs]	Frequency [Hz]	Amplitude [V]	Amplitude [In]	Amplitude [mm]	%THD (10 harmonics)
10	2.000	0.151	0.0074	0.1885	8.51
20	2.000	0.284	0.0139	0.3541	7.16
30	2.000	0.485	0.0238	0.6045	4.57
40	2.000	0.688	0.0338	0.8579	2.71
50	2.000	0.873	0.0429	1.0888	1.53
60	2.000	1.030	0.0506	1.2846	2.24
70	2.000	1.268	0.0623	1.5820	1.4
80	2.000	1.399	0.0687	1.7447	0.95
90	2.000	1.551	0.0762	1.9355	1.97
100	2.000	1.760	0.0864	2.1953	1.18

Arithmetic Mean for Actuator 14 Measurement Trials
Excitation Frequency: 2 Hz

	Measured Data				
Excitation Amplitude [µs]	Frequency [Hz]	Amplitude [V]	Amplitude [In]	Amplitude [mm]	%THD (10 harmonics)
10	2.000	0.148	0.0073	0.1851	8.607
20	2.000	0.285	0.0140	0.3551	6.739
30	2.000	0.488	0.0240	0.6087	4.491
40	2.000	0.694	0.0341	0.8657	2.719
50	2.000	0.867	0.0426	1.0813	1.802
60	2.000	1.030	0.0506	1.2846	2.036
70	2.000	1.254	0.0616	1.5639	1.000
80	2.000	1.416	0.0696	1.7669	1.140
90	2.000	1.536	0.0755	1.9165	1.547
100	2.000	1.759	0.0864	2.1947	1.401

Measurement Trial 3
Excitation Frequency: 2.5 Hz

	Measured Data				
Excitation Amplitude [µs]	Frequency [Hz]	Amplitude [V]	Amplitude [In]	Amplitude [mm]	%THD (10 harmonics)
10	2.500	0.142	0.0070	0.1775	8.39
20	2.500	0.285	0.0140	0.3550	5.4
30	2.500	0.466	0.0229	0.5812	4.01
40	2.500	0.654	0.0321	0.8156	2.16
50	2.500	0.854	0.0419	1.0651	2.26
60	2.500	1.038	0.0510	1.2954	1.13
70	2.500	1.239	0.0609	1.5461	1.44
80	2.500	1.399	0.0687	1.7457	1.08
90	2.500	1.568	0.0770	1.9565	1.44
100	2.500	1.769	0.0869	2.2073	1.33

Arithmetic Mean for Actuator 14 Measurement Trials
Excitation Frequency: 2.5 Hz

	Measured Data				
Excitation Amplitude [µs]	Frequency [Hz]	Amplitude [V]	Amplitude [In]	Amplitude [mm]	%THD (10 harmonics)
10	2.500	0.146	0.0072	0.1825	7.808
20	2.500	0.286	0.0140	0.3564	4.969
30	2.500	0.473	0.0232	0.5901	3.434
40	2.500	0.651	0.0320	0.8119	2.535
50	2.500	0.857	0.0421	1.0692	1.531
60	2.500	1.037	0.0509	1.2933	1.384
70	2.500	1.239	0.0608	1.5453	1.375
80	2.500	1.405	0.0690	1.7529	1.300
90	2.500	1.573	0.0773	1.9628	1.239
100	2.500	1.763	0.0866	2.1997	1.056

Measurement Trial 3
Excitation Frequency: 3 Hz

	Measured Data				
Excitation Amplitude [µs]	Frequency [Hz]	Amplitude [V]	Amplitude [In]	Amplitude [mm]	%THD (10 harmonics)
10	3.000	0.136	0.0067	0.1695	10.58
20	3.000	0.280	0.0138	0.3493	5.9
30	3.000	0.468	0.0230	0.5835	3.53
40	3.000	0.640	0.0314	0.7984	3.35
50	3.000	0.858	0.0421	1.0705	1.5
60	3.000	1.030	0.0506	1.2844	1.54
70	3.000	1.181	0.0580	1.4740	1.09
80	3.000	1.367	0.0672	1.7057	1.55
90	3.000	1.541	0.0757	1.9221	1.41
100	3.000	1.721	0.0845	2.1464	1.44

Arithmetic Mean for Actuator 14 Measurement Trials
Excitation Frequency: 3 Hz

	Measured Data				
Excitation Amplitude [µs]	Frequency [Hz]	Amplitude [V]	Amplitude [In]	Amplitude [mm]	%THD (10 harmonics)
10	3.000	0.131	0.0064	0.1638	10.394
20	3.000	0.279	0.0137	0.3476	6.335
30	3.000	0.470	0.0231	0.5863	3.131
40	3.000	0.642	0.0315	0.8005	2.893
50	3.000	0.852	0.0418	1.0624	1.615
60	3.000	1.030	0.0506	1.2851	1.855
70	3.000	1.201	0.0590	1.4982	1.393
80	3.000	1.365	0.0671	1.7033	1.240
90	3.000	1.537	0.0755	1.9169	1.504
100	3.000	1.730	0.0850	2.1585	1.220

Actuator Number 15 Performance Trials LVDT has 1" linear range

10-03-16

LVDT calibration factor: **20.36** **Volts/Inch**

Note: Each frequency-amplitude run is measured over 20sec period

Measurement Trial 1

Excitation Frequency: 0.5 Hz

	Measured Data				
Excitation Amplitude [µs]	Frequency [Hz]	Amplitude [V]	Amplitude [In]	Amplitude [mm]	%THD (10 harmonics)
10	0.500	0.142	0.0070	0.1772	12.3
20	0.500	0.280	0.0138	0.3493	8.12
30	0.500	0.499	0.0245	0.6225	5.25
40	0.500	0.675	0.0332	0.8421	4.85
50	0.500	0.875	0.0430	1.0916	3.23
60	0.500	1.060	0.0521	1.3224	3.17
70	0.500	1.250	0.0614	1.5594	3.01
80	0.500	1.400	0.0688	1.7466	2.5
90	0.500	1.580	0.0776	1.9711	2.12
100	0.500	1.740	0.0855	2.1707	2.39

Measurement Trial 2

Excitation Frequency: 0.5 Hz

	Measured Data				
Excitation Amplitude [µs]	Frequency [Hz]	Amplitude [V]	Amplitude [In]	Amplitude [mm]	%THD (10 harmonics)
10	0.500	0.143	0.0070	0.1784	14.2
20	0.500	0.281	0.0138	0.3506	7.83
30	0.500	0.503	0.0247	0.6275	4.71
40	0.500	0.678	0.0333	0.8458	4.74
50	0.500	0.875	0.0430	1.0916	3.19
60	0.500	1.050	0.0516	1.3099	3.6
70	0.500	1.240	0.0609	1.5470	2.83
80	0.500	1.390	0.0683	1.7341	2.55
90	0.500	1.580	0.0776	1.9711	1.94
100	0.500	1.750	0.0860	2.1832	2.06

Measurement Trial 1

Excitation Frequency: 1 Hz

	Measured Data				
Excitation Amplitude [µs]	Frequency [Hz]	Amplitude [V]	Amplitude [In]	Amplitude [mm]	%THD (10 harmonics)
10	1.000	0.141	0.0069	0.1759	11.7
20	1.000	0.285	0.0140	0.3556	6.75
30	1.000	0.479	0.0235	0.5976	4.29
40	1.000	0.674	0.0331	0.8408	4.6
50	1.000	0.859	0.0422	1.0716	4
60	1.000	1.080	0.0530	1.3473	2.55
70	1.000	1.250	0.0614	1.5594	2.12
80	1.000	1.410	0.0693	1.7590	2.02
90	1.000	1.600	0.0786	1.9961	1.39
100	1.000	1.800	0.0884	2.2456	1.18

Measurement Trial 2

Excitation Frequency: 1 Hz

	Measured Data				
Excitation Amplitude [µs]	Frequency [Hz]	Amplitude [V]	Amplitude [In]	Amplitude [mm]	%THD (10 harmonics)
10	1.000	0.143	0.0070	0.1784	11.7
20	1.000	0.283	0.0139	0.3531	7.79
30	1.000	0.485	0.0238	0.6051	4.41
40	1.000	0.685	0.0336	0.8546	4.57
50	1.000	0.878	0.0431	1.0953	3.27
60	1.000	1.050	0.0516	1.3099	2.75
70	1.000	1.250	0.0614	1.5594	1.82
80	1.000	1.420	0.0697	1.7715	2.05
90	1.000	1.640	0.0806	2.0460	0.97
100	1.000	1.780	0.0874	2.2206	0.75

Measurement Trial 1

Excitation Frequency: 1.5 Hz

	Measured Data				
Excitation Amplitude [µs]	Frequency [Hz]	Amplitude [V]	Amplitude [In]	Amplitude [mm]	%THD (10 harmonics)
10	1.500	0.159	0.0078	0.1984	8.32
20	1.500	0.301	0.0148	0.3755	6.1
30	1.500	0.508	0.0250	0.6338	3.63
40	1.500	0.690	0.0339	0.8608	3.6
50	1.500	0.890	0.0437	1.1103	1.93
60	1.500	1.060	0.0521	1.3224	1.75
70	1.500	1.240	0.0609	1.5470	1.21
80	1.500	1.410	0.0693	1.7590	1.27
90	1.500	1.590	0.0781	1.9836	0.99
100	1.500	1.730	0.0850	2.1583	1.74

Measurement Trial 2

Excitation Frequency: 1.5 Hz

	Measured Data				
Excitation Amplitude [µs]	Frequency [Hz]	Amplitude [V]	Amplitude [In]	Amplitude [mm]	%THD (10 harmonics)
10	1.500	0.154	0.0076	0.1921	8.81
20	1.500	0.307	0.0151	0.3830	5.82
30	1.500	0.512	0.0251	0.6387	3.62
40	1.500	0.700	0.0344	0.8733	2.64
50	1.500	0.889	0.0437	1.1091	2.24
60	1.500	1.080	0.0530	1.3473	1.43
70	1.500	1.250	0.0614	1.5594	1.42
80	1.500	1.440	0.0707	1.7965	1.3
90	1.500	1.590	0.0781	1.9836	1.02
100	1.500	1.740	0.0855	2.1707	1.42

Measurement Trial 1

Excitation Frequency: 2 Hz

	Measured Data				
Excitation Amplitude [µs]	Frequency [Hz]	Amplitude [V]	Amplitude [In]	Amplitude [mm]	%THD (10 harmonics)
10	2.000	0.150	0.0074	0.1871	8.38
20	2.000	0.282	0.0139	0.3518	7.25
30	2.000	0.487	0.0239	0.6076	4.78
40	2.000	0.688	0.0338	0.8583	2.99
50	2.000	0.873	0.0429	1.0891	1.85
60	2.000	1.030	0.0506	1.2850	2.18
70	2.000	1.270	0.0624	1.5844	1.45
80	2.000	1.400	0.0688	1.7466	1.06
90	2.000	1.550	0.0761	1.9337	2.13
100	2.000	1.760	0.0864	2.1957	1.46

Measurement Trial 2

Excitation Frequency: 2 Hz

	Measured Data				
Excitation Amplitude [µs]	Frequency [Hz]	Amplitude [V]	Amplitude [In]	Amplitude [mm]	%THD (10 harmonics)
10	2.000	0.147	0.0072	0.1834	9.26
20	2.000	0.275	0.0135	0.3431	6.16
30	2.000	0.490	0.0241	0.6113	4.33
40	2.000	0.706	0.0347	0.8808	2.73
50	2.000	0.862	0.0423	1.0754	2.28
60	2.000	1.020	0.0501	1.2725	2.28
70	2.000	1.250	0.0614	1.5594	0.93
80	2.000	1.430	0.0702	1.7840	1.53
90	2.000	1.540	0.0756	1.9212	1.07
100	2.000	1.760	0.0864	2.1957	1.46

Measurement Trial 1

Excitation Frequency: 2.5 Hz

	Measured Data				
Excitation Amplitude [µs]	Frequency [Hz]	Amplitude [V]	Amplitude [In]	Amplitude [mm]	%THD (10 harmonics)
10	2.500	0.144	0.0071	0.1796	8.4
20	2.500	0.287	0.0141	0.3580	5.21
30	2.500	0.464	0.0228	0.5789	3.92
40	2.500	0.655	0.0322	0.8171	2.17
50	2.500	0.852	0.0418	1.0629	2.15
60	2.500	1.040	0.0511	1.2974	1.26
70	2.500	1.240	0.0609	1.5470	1.26
80	2.500	1.400	0.0688	1.7466	1.34
90	2.500	1.570	0.0771	1.9586	1.27
100	2.500	1.770	0.0869	2.2082	1.19

Measurement Trial 2

Excitation Frequency: 2.5 Hz

	Measured Data				
Excitation Amplitude [µs]	Frequency [Hz]	Amplitude [V]	Amplitude [In]	Amplitude [mm]	%THD (10 harmonics)
10	2.500	0.152	0.0075	0.1896	7.5
20	2.500	0.290	0.0142	0.3618	4.95
30	2.500	0.485	0.0238	0.6051	3.17
40	2.500	0.652	0.0320	0.8134	2.62
50	2.500	0.867	0.0426	1.0816	1.29
60	2.500	1.040	0.0511	1.2974	1.41
70	2.500	1.240	0.0609	1.5470	1.41
80	2.500	1.410	0.0693	1.7590	1.39
90	2.500	1.580	0.0776	1.9711	1.37
100	2.500	1.760	0.0864	2.1957	1.23

Measurement Trial 1

Excitation Frequency: 3 Hz

	Measured Data				
		Amplitude			
Excitation Amplitude [µs]	Frequency [Hz]	Amplitude [V]	Amplitude [In]	Amplitude [mm]	%THD (10 harmonics)
10	3.000	0.136	0.0067	0.1697	10.7
20	3.000	0.282	0.0139	0.3518	5.95
30	3.000	0.468	0.0230	0.5839	3.4
40	3.000	0.638	0.0313	0.7959	3.54
50	3.000	0.858	0.0421	1.0704	1.69
60	3.000	1.030	0.0506	1.2850	1.94
70	3.000	1.180	0.0580	1.4721	1.4
80	3.000	1.370	0.0673	1.7091	1.42
90	3.000	1.540	0.0756	1.9212	1.57
100	3.000	1.720	0.0845	2.1458	1.55

Measurement Trial 2

Excitation Frequency: 3 Hz

	Measured Data				
		Amplitude			
Excitation Amplitude [µs]	Frequency [Hz]	Amplitude [V]	Amplitude [In]	Amplitude [mm]	%THD (10 harmonics)
10	3.000	0.133	0.0065	0.1659	10.3
20	3.000	0.283	0.0139	0.3531	6.37
30	3.000	0.473	0.0232	0.5901	2.73
40	3.000	0.624	0.0306	0.7785	3.38
50	3.000	0.853	0.0419	1.0642	1.66
60	3.000	1.030	0.0506	1.2850	1.97
70	3.000	1.200	0.0589	1.4971	1.47
80	3.000	1.370	0.0673	1.7091	1.51
90	3.000	1.540	0.0756	1.9212	1.57
100	3.000	1.740	0.0855	2.1707	1.59

Actuator Number 15 Performance Trials
10-03-16
LVDT calibration factor: **20.36** **Volts/Inch**

Measurement Trial 3
Excitation Frequency: 0.5 Hz

	Measured Data				
Excitation Amplitude [µs]	Frequency [Hz]	Amplitude [V]	Amplitude [In]	Amplitude [mm]	%THD (10 harmonics)
10	0.500	0.140	0.0069	0.1747	14.7
20	0.500	0.279	0.0137	0.3481	7.91
30	0.500	0.494	0.0243	0.6163	4.65
40	0.500	0.672	0.0330	0.8383	4.82
50	0.500	0.880	0.0432	1.0978	3.22
60	0.500	1.050	0.0516	1.3099	3.45
70	0.500	1.240	0.0609	1.5470	3.01
80	0.500	1.390	0.0683	1.7341	2.81
90	0.500	1.590	0.0781	1.9836	2.03
100	0.500	1.750	0.0860	2.1832	2.03

Arithmetic Mean for Actuator 15 Measurement Trials
Excitation Frequency: 0.5 Hz

	Measured Data				
Excitation Amplitude [µs]	Frequency [Hz]	Amplitude [V]	Amplitude [In]	Amplitude [mm]	%THD (10 harmonics)
10	0.500	0.143	0.0070	0.1778	13.250
20	0.500	0.281	0.0138	0.3499	7.975
30	0.500	0.501	0.0246	0.6250	4.980
40	0.500	0.677	0.0332	0.8440	4.795
50	0.500	0.875	0.0430	1.0916	3.210
60	0.500	1.055	0.0518	1.3162	3.385
70	0.500	1.245	0.0611	1.5532	2.920
80	0.500	1.395	0.0685	1.7403	2.525
90	0.500	1.580	0.0776	1.9711	2.030
100	0.500	1.745	0.0857	2.1770	2.225

Measurement Trial 3
Excitation Frequency: 1 Hz

	Measured Data				
Excitation Amplitude [µs]	Frequency [Hz]	Amplitude [V]	Amplitude [In]	Amplitude [mm]	%THD (10 harmonics)
10	1.000	0.145	0.0071	0.1809	11.5
20	1.000	0.290	0.0142	0.3618	6.55
30	1.000	0.480	0.0236	0.5988	4.52
40	1.000	0.679	0.0333	0.8471	4.6
50	1.000	0.859	0.0422	1.0716	3.26
60	1.000	1.070	0.0526	1.3349	2.86
70	1.000	1.250	0.0614	1.5594	1.87
80	1.000	1.400	0.0688	1.7466	2.05
90	1.000	1.620	0.0796	2.0210	1.07
100	1.000	1.780	0.0874	2.2206	1.4

Arithmetic Mean for Actuator 15 Measurement Trials
Excitation Frequency: 1 Hz

	Measured Data				
Excitation Amplitude [µs]	Frequency [Hz]	Amplitude [V]	Amplitude [In]	Amplitude [mm]	%THD (10 harmonics)
10	1.000	0.142	0.0070	0.1772	11.7
20	1.000	0.284	0.0139	0.3543	7.27
30	1.000	0.482	0.0237	0.6013	4.35
40	1.000	0.680	0.0334	0.8477	4.59
50	1.000	0.869	0.0427	1.0835	3.64
60	1.000	1.065	0.0523	1.3286	2.65
70	1.000	1.250	0.0614	1.5594	1.97
80	1.000	1.415	0.0695	1.7653	2.04
90	1.000	1.620	0.0796	2.0210	1.18
100	1.000	1.790	0.0879	2.2331	0.97

Measurement Trial 3
Excitation Frequency: 1.5 Hz

	Measured Data				
Excitation Amplitude [µs]	Frequency [Hz]	Amplitude [V]	Amplitude [In]	Amplitude [mm]	%THD (10 harmonics)
10	1.500	0.156	0.0077	0.1946	8.96
20	1.500	0.300	0.0147	0.3743	6.18
30	1.500	0.503	0.0247	0.6275	3.46
40	1.500	0.690	0.0339	0.8608	3.08
50	1.500	0.874	0.0429	1.0904	2.32
60	1.500	1.080	0.0530	1.3473	1.63
70	1.500	1.250	0.0614	1.5594	1.06
80	1.500	1.430	0.0702	1.7840	1.27
90	1.500	1.590	0.0781	1.9836	1.18
100	1.500	1.720	0.0845	2.1458	1.66

Arithmetic Mean for Actuator 15 Measurement Trials
Excitation Frequency: 1.5 Hz

	Measured Data				
Excitation Amplitude [µs]	Frequency [Hz]	Amplitude [V]	Amplitude [In]	Amplitude [mm]	%THD (10 harmonics)
10	1.500	0.157	0.0077	0.1952	8.565
20	1.500	0.304	0.0149	0.3793	5.960
30	1.500	0.510	0.0250	0.6362	3.625
40	1.500	0.695	0.0341	0.8670	3.120
50	1.500	0.890	0.0437	1.1097	2.085
60	1.500	1.070	0.0526	1.3349	1.590
70	1.500	1.245	0.0611	1.5532	1.315
80	1.500	1.425	0.0700	1.7778	1.285
90	1.500	1.590	0.0781	1.9836	1.004
100	1.500	1.735	0.0852	2.1645	1.580

Measurement Trial 3
Excitation Frequency: 2 Hz

	Measured Data				
Excitation Amplitude [µs]	Frequency [Hz]	Amplitude [V]	Amplitude [In]	Amplitude [mm]	%THD (10 harmonics)
10	2.000	0.148	0.0073	0.1846	8.21
20	2.000	0.272	0.0134	0.3393	7.5
30	2.000	0.488	0.0240	0.6088	4.61
40	2.000	0.689	0.0338	0.8596	2.89
50	2.000	0.867	0.0426	1.0816	1.57
60	2.000	1.040	0.0511	1.2974	1.66
70	2.000	1.240	0.0609	1.5470	0.96
80	2.000	1.420	0.0697	1.7715	1.35
90	2.000	1.520	0.0747	1.8963	1.74
100	2.000	1.760	0.0864	2.1957	1.47

Arithmetic Mean for Actuator 15 Measurement Trials
Excitation Frequency: 2 Hz

	Measured Data				
Excitation Amplitude [µs]	Frequency [Hz]	Amplitude [V]	Amplitude [In]	Amplitude [mm]	%THD (10 harmonics)
10	2.000	0.149	0.0073	0.1853	8.820
20	2.000	0.279	0.0137	0.3474	6.705
30	2.000	0.489	0.0240	0.6094	4.555
40	2.000	0.697	0.0342	0.8695	2.860
50	2.000	0.868	0.0426	1.0822	2.065
60	2.000	1.025	0.0503	1.2787	2.230
70	2.000	1.260	0.0619	1.5719	1.191
80	2.000	1.415	0.0695	1.7653	1.295
90	2.000	1.545	0.0759	1.9275	1.600
100	2.000	1.760	0.0864	2.1957	1.460

Measurement Trial 3
Excitation Frequency: 2.5 Hz

	Measured Data				
Excitation Amplitude [µs]	Frequency [Hz]	Amplitude [V]	Amplitude [In]	Amplitude [mm]	%THD (10 harmonics)
10	2.500	0.147	0.0072	0.1834	7.92
20	2.500	0.286	0.0140	0.3568	5.23
30	2.500	0.470	0.0231	0.5863	3.68
40	2.500	0.648	0.0318	0.8084	3.08
50	2.500	0.853	0.0419	1.0642	1.31
60	2.500	1.030	0.0506	1.2850	1.64
70	2.500	1.240	0.0609	1.5470	1.39
80	2.500	1.410	0.0693	1.7590	1.25
90	2.500	1.570	0.0771	1.9586	1.29
100	2.500	1.760	0.0864	2.1957	1.22

Arithmetic Mean for Actuator 15 Measurement Trials
Excitation Frequency: 2.5 Hz

	Measured Data				
Excitation Amplitude [µs]	Frequency [Hz]	Amplitude [V]	Amplitude [In]	Amplitude [mm]	%THD (10 harmonics)
10	2.500	0.148	0.0073	0.1846	7.950
20	2.500	0.289	0.0142	0.3599	5.080
30	2.500	0.475	0.0233	0.5920	3.545
40	2.500	0.654	0.0321	0.8153	2.395
50	2.500	0.860	0.0422	1.0723	1.720
60	2.500	1.040	0.0511	1.2974	1.335
70	2.500	1.240	0.0609	1.5470	1.335
80	2.500	1.405	0.0690	1.7528	1.365
90	2.500	1.575	0.0774	1.9649	1.320
100	2.500	1.765	0.0867	2.2019	1.210

Measurement Trial 3
Excitation Frequency: 3 Hz

	Measured Data				
		Amplitude			
Excitation Amplitude [µs]	Frequency [Hz]	Amplitude [V]	Amplitude [In]	Amplitude [mm]	%THD (10 harmonics)
10	3.000	0.131	0.0064	0.1634	10.8
20	3.000	0.273	0.0134	0.3406	6.46
30	3.000	0.471	0.0231	0.5876	2.89
40	3.000	0.631	0.0310	0.7872	2.53
50	3.000	0.844	0.0415	1.0529	1.53
60	3.000	1.030	0.0506	1.2850	1.98
70	3.000	1.220	0.0599	1.5220	1.78
80	3.000	1.360	0.0668	1.6967	0.98
90	3.000	1.530	0.0751	1.9087	1.53
100	3.000	1.730	0.0850	2.1583	1.24

Arithmetic Mean for Actuator 15 Measurement Trials
Excitation Frequency: 3 Hz

	Measured Data				
		Amplitude			
Excitation Amplitude [µs]	Frequency [Hz]	Amplitude [V]	Amplitude [In]	Amplitude [mm]	%THD (10 harmonics)
10	3.000	0.135	0.0066	0.1678	10.500
20	3.000	0.283	0.0139	0.3524	6.160
30	3.000	0.471	0.0231	0.5870	3.065
40	3.000	0.631	0.0310	0.7872	3.460
50	3.000	0.856	0.0420	1.0673	1.675
60	3.000	1.030	0.0506	1.2850	1.955
70	3.000	1.190	0.0584	1.4846	1.435
80	3.000	1.370	0.0673	1.7091	1.465
90	3.000	1.540	0.0756	1.9212	1.570
100	3.000	1.730	0.0850	2.1583	1.570

Actuator Beta Comparison for Actuators: 13,14,15

10-03-16

Arithmetic Mean of all Actuators

Excitation Frequency: 0.5 Hz

	Measured Data				
Excitation Amplitude [µs]	Frequency [Hz]	Amplitude [V]	Amplitude [In]	Amplitude [mm]	%THD (10 harmonics)
10	0.500	0.143	0.007	0.178	13.620
20	0.500	0.282	0.014	0.352	7.866
30	0.500	0.501	0.025	0.625	4.945
40	0.500	0.677	0.033	0.844	4.650
50	0.500	0.878	0.043	1.095	3.187
60	0.500	1.053	0.052	1.314	3.432
70	0.500	1.244	0.061	1.552	3.034
80	0.500	1.394	0.068	1.739	2.502
90	0.500	1.583	0.078	1.975	2.079
100	0.500	1.745	0.086	2.177	2.171

Arithmetic Mean of all Actuators

Excitation Frequency: 1 Hz

	Measured Data				
Excitation Amplitude [µs]	Frequency [Hz]	Amplitude [V]	Amplitude [In]	Amplitude [mm]	%THD (10 harmonics)
10	1.000	0.143	0.007	0.179	11.567
20	1.000	0.284	0.014	0.354	7.035
30	1.000	0.481	0.024	0.600	4.272
40	1.000	0.680	0.033	0.849	4.503
50	1.000	0.867	0.043	1.082	3.508
60	1.000	1.058	0.052	1.321	2.610
70	1.000	1.251	0.061	1.560	1.925
80	1.000	1.409	0.069	1.758	1.892
90	1.000	1.610	0.079	2.009	1.123
100	1.000	1.778	0.087	2.218	1.021

Arithmetic Mean of all Actuators

Excitation Frequency: 1.5 Hz

	Measured Data				
Excitation Amplitude [µs]	Frequency [Hz]	Amplitude [V]	Amplitude [In]	Amplitude [mm]	%THD (10 harmonics)
10	1.500	0.154	0.008	0.192	8.629
20	1.500	0.300	0.015	0.375	6.084
30	1.500	0.503	0.025	0.628	3.533
40	1.500	0.690	0.034	0.861	3.020
50	1.500	0.881	0.043	1.099	2.129
60	1.500	1.070	0.053	1.335	1.421
70	1.500	1.246	0.061	1.555	1.189
80	1.500	1.424	0.070	1.776	1.168
90	1.500	1.587	0.078	1.980	0.987
100	1.500	1.736	0.085	2.165	1.550

Arithmetic Mean of all Actuators

Excitation Frequency: 2 Hz

	Measured Data				
Excitation Amplitude [µs]	Frequency [Hz]	Amplitude [V]	Amplitude [In]	Amplitude [mm]	%THD (10 harmonics)
10	2.000	0.147	0.007	0.183	8.654
20	2.000	0.282	0.014	0.352	6.737
30	2.000	0.486	0.024	0.607	4.527
40	2.000	0.693	0.034	0.865	2.784
50	2.000	0.865	0.043	1.080	1.910
60	2.000	1.028	0.050	1.283	2.074
70	2.000	1.248	0.061	1.557	1.040
80	2.000	1.412	0.069	1.762	1.202
90	2.000	1.538	0.076	1.918	1.575
100	2.000	1.755	0.086	2.189	1.443

Arithmetic Mean of all Actuators

Excitation Frequency: 2.5 Hz

	Measured Data				
Excitation Amplitude [µs]	Frequency [Hz]	Amplitude [V]	Amplitude [In]	Amplitude [mm]	%THD (10 harmonics)
10	2.500	0.147	0.007	0.183	7.861
20	2.500	0.287	0.014	0.358	4.969
30	2.500	0.473	0.023	0.590	3.460
40	2.500	0.652	0.032	0.813	2.508
50	2.500	0.857	0.042	1.070	1.592
60	2.500	1.038	0.051	1.295	1.360
70	2.500	1.239	0.061	1.546	1.306
80	2.500	1.405	0.069	1.753	1.328
90	2.500	1.574	0.077	1.964	1.238
100	2.500	1.764	0.087	2.200	1.067

Arithmetic Mean of all Actuators

Excitation Frequency: 3 Hz

	Measured Data				
Excitation Amplitude [µs]	Frequency [Hz]	Amplitude [V]	Amplitude [In]	Amplitude [mm]	%THD (10 harmonics)
10	3.000	0.132	0.006	0.165	10.411
20	3.000	0.280	0.014	0.349	6.239
30	3.000	0.470	0.023	0.587	3.109
40	3.000	0.638	0.031	0.796	3.080
50	3.000	0.853	0.042	1.064	1.642
60	3.000	1.032	0.051	1.288	1.912
70	3.000	1.197	0.059	1.494	1.414
80	3.000	1.367	0.067	1.705	1.311
90	3.000	1.537	0.076	1.918	1.539
100	3.000	1.730	0.085	2.158	1.360

Actuator Beta Comparison for Actuators: 13,14,15

Normalized Maximum Absolute Deviation
Excitation Frequency: 0.5 Hz

	Measured Data				
Excitation Amplitude [µs]	Frequency [Hz]	Amplitude [V]	Amplitude [In]	Amplitude [mm]	%THD (10 harmonics)
10		0.021	0.021	0.017	0.370
20		0.015	0.015	0.012	0.109
30		0.003	0.003	0.003	0.035
40		0.003	0.003	0.003	0.145
50		0.005	0.005	0.005	0.023
60		0.001	0.001	0.001	0.050
70		0.002	0.002	0.002	0.114
80		0.002	0.002	0.002	0.024
90		0.002	0.002	0.002	0.049
100		0.001	0.001	0.001	0.098

Normalized Amplitude
Excitation Frequency: 0.5Hz

Excitation Amplitude[µs]	Theoretical Output Amplitude [mm]	Normalized Amplitude [mm]
10	0.22	0.81
20	0.44	0.8
30	0.66	0.95
40	0.88	0.96
50	1.1	1
60	1.32	1
70	1.54	1.01
80	1.76	0.99
90	1.98	1
100	2.2	0.99

Normalized Maximum Absolute Deviation
Excitation Frequency: 1 Hz

	Measured Data				
Excitation Amplitude [µs]	Frequency [Hz]	Amplitude [V]	Amplitude [In]	Amplitude [mm]	%THD (10 harmonics)
10		0.011	0.011	0.009	0.133
20		0.007	0.007	0.006	0.235
30		0.003	0.003	0.002	0.100
40		0.003	0.003	0.003	0.082
50		0.003	0.003	0.003	0.127
60		0.014	0.014	0.014	0.040
70		0.001	0.001	0.001	0.045
80		0.005	0.005	0.005	0.143
90		0.012	0.012	0.013	0.079
100		0.008	0.008	0.008	0.073

Normalized Amplitude
Excitation Frequency: 1.0Hz

Excitation Amplitude[µs]	Theoretical Output Amplitude [mm]	Normalized Amplitude [mm]
10	0.22	0.81
20	0.44	0.8
30	0.66	0.91
40	0.88	0.96
50	1.1	0.98
60	1.32	1
70	1.54	1.01
80	1.76	1
90	1.98	1.01
100	2.2	1.01

Normalized Maximum Absolute Deviation
Excitation Frequency: 1.5 Hz

	Measured Data				
Excitation Amplitude [µs]	Frequency [Hz]	Amplitude [V]	Amplitude [In]	Amplitude [mm]	%THD (10 harmonics)
10		0.018	0.018	0.016	0.067
20		0.014	0.014	0.012	0.124
30		0.021	0.021	0.020	0.101
40		0.012	0.012	0.012	0.118
50		0.012	0.012	0.012	0.094
60		0.002	0.002	0.002	0.169
70		0.001	0.001	0.001	0.127
80		0.001	0.001	0.001	0.129
90		0.003	0.003	0.003	0.045
100		0.004	0.004	0.004	0.080

Normalized Amplitude
Excitation Frequency: 1.5Hz

Excitation Amplitude[µs]	Theoretical Output Amplitude [mm]	Normalized Amplitude [mm]
10	0.22	0.87
20	0.44	0.85
30	0.66	0.95
40	0.88	0.98
50	1.1	1
60	1.32	1.01
70	1.54	1.01
80	1.76	1.01
90	1.98	1
100	2.2	0.98

Normalized Maximum Absolute Deviation
Excitation Frequency: 2 Hz

	Measured Data				
Excitation Amplitude [µs]	Frequency [Hz]	Amplitude [V]	Amplitude [In]	Amplitude [mm]	%THD (10 harmonics)
10		0.024	0.024	0.020	0.166
20		0.014	0.014	0.011	0.032
30		0.007	0.007	0.007	0.036
40		0.006	0.006	0.006	0.076
50		0.004	0.004	0.004	0.155
60		0.003	0.003	0.003	0.156
70		0.014	0.014	0.014	0.151
80		0.004	0.004	0.005	0.093
90		0.005	0.005	0.005	0.028
100		0.006	0.006	0.005	0.042

Normalized Amplitude
Excitation Frequency: 2.0Hz

Excitation Amplitude[µs]	Theoretical Output Amplitude [mm]	Normalized Amplitude [mm]
10	0.22	0.83
20	0.44	0.8
30	0.66	0.92
40	0.88	0.98
50	1.1	0.98
60	1.32	0.97
70	1.54	1.01
80	1.76	1
90	1.98	0.97
100	2.2	1

Normalized Maximum Absolute Deviation
Excitation Frequency: 2.5 Hz

	Measured Data				
Excitation Amplitude [µs]	Frequency [Hz]	Amplitude [V]	Amplitude [In]	Amplitude [mm]	%THD (10 harmonics)
10		0.007	0.007	0.006	0.089
20		0.007	0.007	0.005	0.111
30		0.003	0.003	0.003	0.085
40		0.003	0.003	0.003	0.113
50		0.002	0.002	0.002	0.128
60		0.002	0.002	0.002	0.025
70		0.001	0.001	0.001	0.098
80		0.000	0.000	0.000	0.037
90		0.001	0.001	0.001	0.083
100		0.001	0.001	0.001	0.143

Normalized Amplitude
Excitation Frequency: 2.5Hz

Excitation Amplitude[µs]	Theoretical Output Amplitude [mm]	Normalized Amplitude [mm]
10	0.22	0.83
20	0.44	0.81
30	0.66	0.89
40	0.88	0.92
50	1.1	0.97
60	1.32	0.98
70	1.54	1
80	1.76	1
90	1.98	0.99
100	2.2	1

Normalized Maximum Absolute Deviation
Excitation Frequency: 3 Hz

	Measured Data				
Excitation Amplitude [µs]	Frequency [Hz]	Amplitude [V]	Amplitude [In]	Amplitude [mm]	%THD (10 harmonics)
10		0.019	0.019	0.014	0.089
20		0.009	0.009	0.007	0.096
30		0.001	0.001	0.001	0.044
40		0.011	0.011	0.010	0.380
50		0.003	0.003	0.003	0.033
60		0.004	0.004	0.004	0.058
70		0.006	0.006	0.006	0.022
80		0.002	0.002	0.002	0.154
90		0.002	0.002	0.002	0.035
100		0.000	0.000	0.000	0.210

Normalized Amplitude
Excitation Frequency: 3.0Hz

Excitation Amplitude[µs]	Theoretical Output Amplitude [mm]	Normalized Amplitude [mm]
10	0.22	0.75
20	0.44	0.79
30	0.66	0.89
40	0.88	0.9
50	1.1	0.97
60	1.32	0.98
70	1.54	0.97
80	1.76	0.97
90	1.98	0.97
100	2.2	0.98

Appendix C

Linear Variable Differential Transformer Hookup and Use

A Schaevitz DC-EC-500 series LVDT was used for measuring actuator output motion. This LVDT has a ±0.5 inch linear range and 0.25 % linearity of the full scale range. It was connected to measure the motion of syringe plunger. Figure C.1 shows the LVDT and linkage used for the measurement. Figure C.2 shows a block diagram of how the LVDT was connected to an actuator. A wooden piece with a cut out notch was press fit onto the neck of the syringe plunger. This press fit was secure. A stainless steel threaded rod connected the LVDT nickle-iron core to the wooden piece. The LVDT housing itself was held by a wooden support. Using shims, the LVDT housing was positioned so the core could move freely within and was centred. Then a weight was placed on top of the LVDT wooden support to friction lock it in place. This hook-up method allowed for the LVDT to quickly and securely attached to an actuator.

The LVDT signal was converted to a digital signal using a National Instrument USB-6229 Multifunction Data Acquisition Module (DAQ) sampling at a 2 kHz rate. Before digital conversion, the LVDT signal was filtered using an analog 2nd order passive RC filter with a cutoff frequency of 200 Hz. The analog filter prior to digital conversion mitigated aliasing of high frequency noise in the signal during digital conversion.

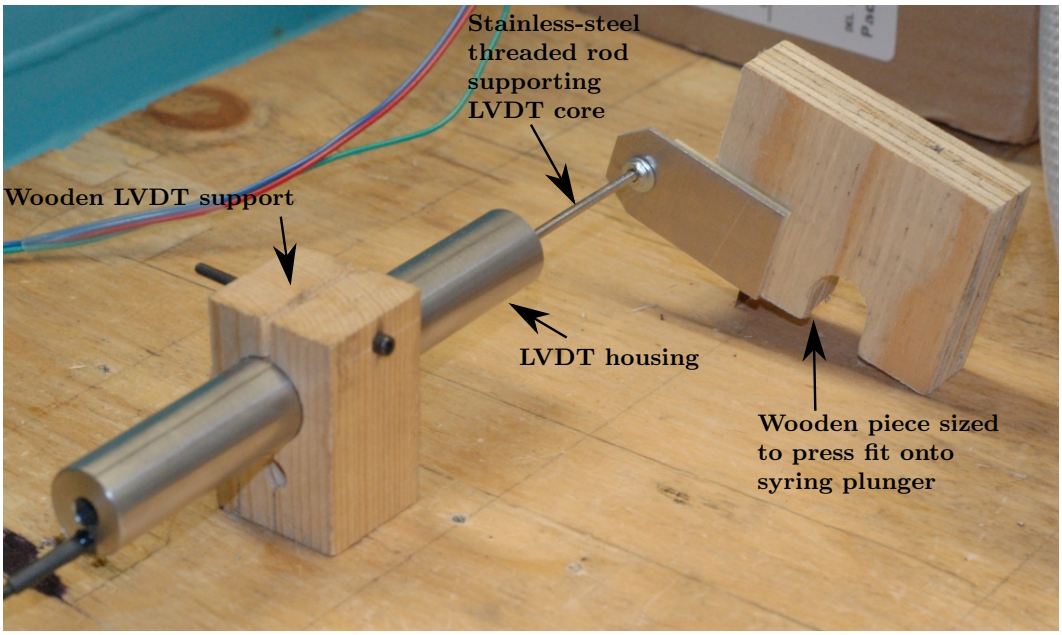

Figure C.1: *LVDT support, linkage, and wooden mounting piece for connecting with syringe plunger.*

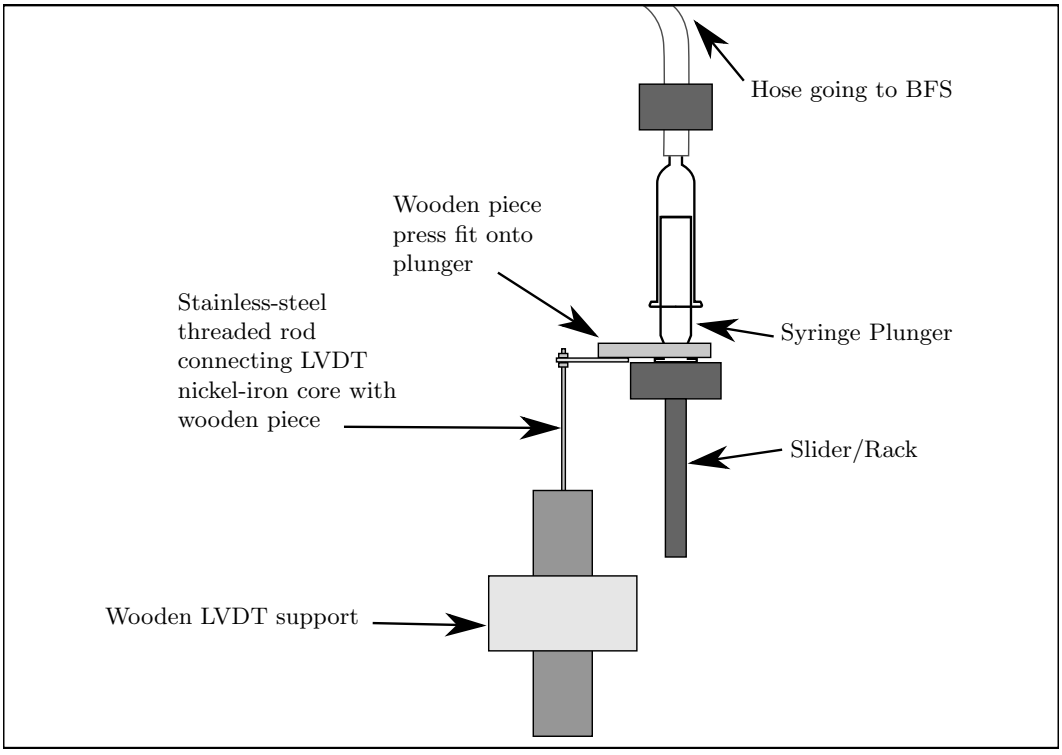

Figure C.2: *LVDT hook up diagram for measurement of syringe plunger motion.*

Appendix D

Beta Actuator Operation

The Beta Actuators are controlled by a reference signal generated from the High Speed Servo Controller (HSSC) (Appendix E). Each of the HSSCs needs to be programed with the desired waveform. The waveform can be of any arbitrary shape, frequency, and phase. The microprocessor used on the HSSC is a midrange PIC 12f629. To program the PIC microprocessor, a PICkit^{TM}3 programmer and Microchips MPLAB integrated development environment installed on a Windows machine are required. Detailed documentation on the MPLAB environment and PICkit programmer can be found at: http://www.microchip.com/

The assembly code which is used to program the PIC 12f629 is given in Appendix E.1. To updated the code for a new waveform, the main body of this code needs no editing. There is a look up table at the end of the code which only needs updating for changing the actuation waveform. This is a table listing the duration of each of the PWM pulses within the reference signal in binary numeral system. A excel spread sheet document (PulseWidthCalculator.xls) was created for easily generating a new look up table for a given sinusoidal waveform. Using the excel file, only frequency, phase, and amplitude needs to be input and the look up table is generated. This excel generated look up table need only be copied and pasted into the assembly code, replacing the previous look up table. Below is an excerpt from the code showing where the look up table needs to be swapped with the newly generated look up table:

```
;****************** Look Up Table*******************************

SINE_TABLE CODE
sine movwf PCL


    !!Replace Look up table from below here!!


;Table Size Variables
retlw .250
retlw .6


;Start Lower Byte Data
retlw b'11011100'
retlw b'11011111'
retlw b'11100001'
retlw b'11100100'
```

.
.
.
retlw b'11100100'

!!to here!!

;THE

END

With the new code compiled, it is loaded onto the PIC 12f629 using the PICkit which connects with the HSSC using the 6 pin header. After all the HSSCs have been loaded with the desired waveform, the actuator board is ready for operation.

The sequence of powering up the components is important. First the ±15 volt supply for the potentiometer readers needs to be powered. With out the potentiometer readers powered, the servos will not operate properly. It is important that a split power supply is used set to ±15 volts. (If the voltage exceeds ±18 volts, damage will result to the potentiometer readers.) If uncertain of the current voltage setting of the power supply, first unplug the potentiometer power routing wires from the power supply. Then turn it on to adjust the voltage to the desired ±15 volts.

After the potentiometer readers are powered, the servomotor power can be turned on. They require a single sided 6 volts power supply capable of supplying at least 20 amperes of current. Next the black push button for powering the HSSCs can be switched on. If the power is on, a orange LED near the button will light and the servos will begin to operate.

Due to a slight variance in start up time of the HSSCs, a trigger signal is used to synchronize all the HSSCs so they are operating with the correct phase relative to one another. (This process is not entirely necessary, as the variance in start up time is small relative the period of the forcing frequencies used: 1 to 10 hertz). However, it is a good idea and recommended that the HSSCs are synchronize. To do this a LabView program (ServoSync.vi) is used to control the trigger signal.

Appendix E

High Speed Servo Controller

E.1 High Speed Servo Controller Assembly Code

```
;*************************************************************************************************
;       SERVO CONTROLLER                                                                         *
;               Uses look up table to output pulse signals for servo control                     *
;               Look up table generated from OpenDocument spread sheet file: PulseDataCalculator.ods  *
;               Updates Servo Signal at 250Hz                                                    *
;                                                                                                *
;               20 MHz clock                                                                     *
;               Written by Marc Schostek June 14 2011                                            *
;*************************************************************************************************


        list      p=12f629           ; list directive to define processor
        #include <p12f629.inc>       ; processor specific variable definitions

        errorlevel  -302             ; suppress message 302 from list file

        ; configuration bits
        __CONFIG   _CP_OFF & _CPD_OFF & _BODEN_OFF & _MCLRE_OFF & _WDT_OFF & _PWRTE_ON & _HS_OSC


;***** Variable Definitions
INTERUPT                UDATA_SHR               ; variables used for temperary storing during ISR

        W_temp          res     1
        STATUS_temp     res     1

GENVAR                  UDATA_SHR               ; general variables

        end4ms                  res 1           ; Bit zero is used to know if the end of a 4 ms period has been reached
        dataValueL              res 1           ; variable used to store current lower byte data value
                                                        ;retrieved from lookup table
        dataValueU              res 1           ; variable used to store current upper byte data value
                                                        ;retrieved from lookup table
        dataSampleL             res 1           ; used to store current data value position to be retrieved
                                                        ;from lookup table for the lower byte
        dataSampleU             res 1           ; used to store current data value position to be retrieved
                                                        ;from lookup table for the upper byte
        dly_upper               res 1           ; Used for delay_upper loop
        dly_lower               res 1           ; for delay_lower loop
        dly_innerU              res 1           ; Used for delay_upper loop
        tableSize               res 1           ; Is the length of the table (number of data samples in Look;
                                                        ;up Table). Used for the correct offset to look up upper
                                                        ;byte (dataSampleU)
        tableEnd                res 1           ; Used for testing when to reset dataSampleL and dataSampleU
                                                        ;variables so code can loop through the look up table
                                                        ;( 256 - table length)




;*********************************************************************
RESET   CODE    0X000                           ; reset vector
                pagesel start                   ; jump to main code
                goto    start

;***** Iterrupt service routine
ISR             CODE    0X004

        bcf     INTCON,GIE                      ; disable interrupts
        movwf   W_temp                          ; save W
        movf    STATUS,w
        movwf   STATUS_temp                     ; save status

        banksel PIR1
        btfsc   PIR1,TMR1IF                     ; If Timer1 interrupt
        goto    Timer1ISR                       ;       Then goto Timer1 ISR
        goto    GP2ISR                          ; Else goto GP2 ISR

MainISR

        movf    STATUS_temp,w                   ; restore STATUS and WORKING registers
        movwf   STATUS
        swapf   W_temp,f
        swapf   W_temp,w
        bsf     INTCON,GIE                      ; re-enable interrupts
        retfie

Timer1ISR

        movlw   .256-.32-.2     ;offset timer1 low byte
        banksel TMR1L           ;for over flow after 4000 us [ (32 + 78*256) * 0.2 us = 4000 us)
                                        ;use this timing for 1.0Hz and faster forcing
        movwf   TMR1L           ;For over flow after 8000 us [ (64 + 156*256) * 0.2 us = 8000 us)
                                        ;use this timing for 0.5Hz forcing
        movlw   .256-.78-.1     ;(after inital TMR1L count, timer high counts 256*78 or 256*156)
        movwf   TMR1H
        banksel PIR1
        bcf     PIR1,TMR1IF     ; clear timer1 interrupt flag in PERIPHERAL INTERRUPT REGISTER
```

```
91          bsf     end4ms,0        ; set bit zero to signify that timer1 overflowed
92                                  ;(used in wait loop at bottom of Main code)
93          goto    MainISR
94
95  GP2ISR
96          clrf    dataSampleL
97          clrf    dataSampleU             ; clear dataSample variables so after GP2 interrupt we start from bottom of lookup table
98
99  waitGP2low                              ; and wait until GPIO pin switch back low
100         btfsc   GPIO,GP2
101         goto waitGP2low
102
103         bcf     INTCON,INTF             ; clear GP2 interrupt flag
104         bcf     INTCON,INTE             ; dissable GP2 interrupts so can only trigger once
105         goto    MainISR
106
107 ;***** MAIN PROGRAM ***********************************
108 MAIN    CODE
109 start
110
111 ;*****  initialization
112
113
114         ;Initialize TRISIO
115         movlw   b'00111101'             ; configure GP1 as output & rest as input
116         banksel TRISIO
117         movwf   TRISIO
118
119         ; configure OPTION_REG
120         movlw   b'1100000'
121                         ; 1-------      ; pull ups disabled
122                         ; -1------      ; GP2 interrupt on rising edge
123         banksel OPTION_REG
124         movwf   OPTION_REG
125
126
127         ; configure Timer1
128         movlw   b'00000001'
129                         ;--------1      ; timer 1 on
130         banksel T1CON
131         movwf   T1CON
132
133         clrf    TMR1H                   ; good idea to clear Timer1 pair and interrupt flags before enabling interrupts
134         clrf    TMR1L
135         bcf             PIR1,TMR1IF     ; clear Timer1 interrupt flag
136
137         ; configure interrupt
138         movlw   b'11010000'
139                         ; 1-------      ; enable global interrupts
140                         ; -1------      ; enalbe Peripheral Interrupt for timer1 interrupt
141                         ; ---1----      ; enalbe GP2 interrupt
142         movwf   INTCON
143         movlw   b'00000001'             ; enalbe Timer1 over flow interrupt in PERIPHERAL INTERRUPT ENABLE REGISTER 1
144         banksel PIE1
145         movwf   PIE1
146
147         banksel GPIO
148         clrf    GPIO                    ; start with Servo Signal Off
149
150         clrf    dataSampleL             ; start at first lower datasample in lookup table
151         clrf    dataSampleU             ; start at first upper datasample in loopup table
152         clrf    dly_innerU
153         clrf    end4ms                  ; start cleared
154
155         ;initialize look up table size variables
156         movlw   HIGH sine               ; load high bits of sine table base address
157         movwf   PCLATH                  ;       into PCLATH
158         movlw   LOW     sine            ; move location of tableSize Variable to W
159         addlw   .1
160         btfsc   STATUS,C                ; if overflow
161         incf    PCLATH,f                ;       increment PCLATH
162         call    sine                    ; look up tableSize offset value
163         banksel tableSize
164         movwf   tableSize
165
166         movlw   HIGH sine               ; load high bits of sine table base address
167         movwf   PCLATH                  ;       into PCLATH
168         movlw   LOW     sine            ; move location of tableEnd Variable to W
169         addlw   .2
170         btfsc   STATUS,C                ; if overflow
171         incf    PCLATH,f                ;       increment PCLATH
172         call    sine                    ; look up tableSize offset value
173         banksel tableEnd
174         movwf   tableEnd
175
176 ;***** Main Loop
177 main_loop
178
179                 bcf             INTCON,GIE      ; temporairly disable global interrupts until pulse has finished
180
```

```
                ;Perform table lookup for lower byte
                movlw   HIGH sine               ; load high bits of sine table base address
                movwf   PCLATH                  ;       into PCLATH
                movlw   LOW     sine
                banksel dataSampleL
                addwf   dataSampleL,w           ; add look up offset
                btfsc   STATUS,C                ; if overflow
                incf    PCLATH,f                ;       increment PCLATH
                addlw   .3                      ;       add offset to skip table size variables
                btfsc   STATUS,C                ; if overflow
                incf    PCLATH,f                ;       increment PCLATH
                call    sine                    ; look up data sample
                movwf   dataValueL              ; and load into dataValue
                incf    dataSampleL
                movf    dataSampleL,w
                addwf   tableEnd,w
                btfsc   STATUS,Z        ; if dataSample + tableEnd is greater than 255, then dataSampleL should
                                                ;be reset to zero to start from beginning of look uptable again
                clrf    dataSampleL

                ;Perform table lookup for upper byte
                movlw   HIGH sine               ; load high bits of sine table base address
                movwf   PCLATH                  ;       into PCLATH
                movlw   LOW     sine
                addwf   dataSampleU,w   ; add look up offset
                btfsc   STATUS,C                ; if overflow
                incf    PCLATH,f                ;       increment PCLATH
                addwf   tableSize,w             ; add offset for upper bytes
                btfsc   STATUS,C                ; if overflow
                incf    PCLATH,f                ;       increment PCLATH
                addlw   .3
                btfsc   STATUS,C                ; if overflow
                incf    PCLATH,f                ;       increment PCLATH
                call    sine                    ; look up data sample
                movwf   dataValueU              ; and load into dataValue
                incf    dataSampleU
                movf    dataSampleU,w
                addwf   tableEnd,w
                btfsc   STATUS,Z        ; if dataSample + tableEnd is greater than 255, then dataSampleU should
                                                ;be reset to zero so next look up at beginning of look up table
                clrf    dataSampleU


                banksel GPIO
                bsf             GPIO,GP1                ; turn on servo signal

                ; Upper byte delay first
delay_Upper                                             ; delay_Upper [ (256 us + 3 us) * dataValueU = 259 us * dataValueU

                ; dly_inner is cleared durring initialization to main loop

dly1    nop                                             ; Inner loop [ 1us * 256  = 256 us ]
                nop
                decfsz  dly_innerU
                goto    dly1

                decfsz  dataValueU
                goto    delay_Upper


                ; Test if lower byte is zero and turn off signal if true
                banksel GPIO
                movf    dataValueL,f            ; move dataValueL into itself to test if it is zero
                btfsc   STATUS,Z
                bcf     GPIO,GP1                ; turn off servo signal only if dataValueL is zero. Use this
                                                   ;rather than jump to after loop since if dataValueL is zero,
                ; we want the signal to turn off immediatly. (as long as signal is off, we don't
                        ; care if delay_Lower runs through)

                ; Now lower byte delay
delay_Lower                                     ; delay_Lower [ 1us * dataValueL ]
                nop
                nop
                decfsz  dataValueL
                goto    delay_Lower

                banksel GPIO
                bcf     GPIO,GP1                ; turn off servo signal

                bsf     INTCON,GIE              ; re-enable global interrupts now that signal is low


wait    ; now all we have to do is wait until end of 4ms period
                btfss   end4ms,0
                goto    wait

                bcf     end4ms,0                ; clear bit to rest for next loop

                ;repeat forever
                goto    main_loop
```

```
271
272
273
274 ;****************** Look Up Table ***************************************************************
275
276 SINE_TABLE      CODE
277 sine    movwf   PCL
278
279 ;Table Size Variables
280       retlw      .250
281       retlw      .6
282 ;Start Lower Byte Data
283       retlw      b'11011100'
284       retlw      b'11011111'
285       retlw      b'11100001'
286       retlw      b'11100100'
287       retlw      b'11100110'
288       retlw      b'11101001'
289       retlw      b'11101011'
290       retlw      b'11101110'
291       retlw      b'11110000'
292       retlw      b'11110010'
293       retlw      b'11110101'
294       retlw      b'11110111'
295       retlw      b'11111010'
296       retlw      b'11111100'
297       retlw      b'11111110'
298       retlw      b'00000001'
299       retlw      b'00000011'
300       retlw      b'00000101'
301       retlw      b'00001000'
302       retlw      b'00001010'
303       retlw      b'00001100'
304       retlw      b'00001110'
305       retlw      b'00010001'
306       retlw      b'00010011'
307       retlw      b'00010101'
308       retlw      b'00010111'
309       retlw      b'00011001'
310       retlw      b'00011011'
311       retlw      b'00011101'
312       retlw      b'00011111'
313       retlw      b'00100000'
314       retlw      b'00100010'
315       retlw      b'00100100'
316       retlw      b'00100110'
317       retlw      b'00100111'
318       retlw      b'00101001'
319       retlw      b'00101011'
320       retlw      b'00101100'
321       retlw      b'00101110'
322       retlw      b'00101111'
323       retlw      b'00110000'
324       retlw      b'00110010'
325       retlw      b'00110011'
326       retlw      b'00110100'
327       retlw      b'00110101'
328       retlw      b'00110110'
329       retlw      b'00111000'
330       retlw      b'00111001'
331       retlw      b'00111001'
332       retlw      b'00111010'
333       retlw      b'00111011'
334       retlw      b'00111100'
335       retlw      b'00111101'
336       retlw      b'00111101'
337       retlw      b'00111110'
338       retlw      b'00111110'
339       retlw      b'00111111'
340       retlw      b'00111111'
341       retlw      b'00111111'
342       retlw      b'01000000'
343       retlw      b'01000000'
344       retlw      b'01000000'
345       retlw      b'01000000'
346       retlw      b'01000000'
347       retlw      b'01000000'
348       retlw      b'01000000'
349       retlw      b'01000000'
350       retlw      b'00111111'
351       retlw      b'00111111'
352       retlw      b'00111111'
353       retlw      b'00111110'
354       retlw      b'00111110'
355       retlw      b'00111101'
356       retlw      b'00111101'
357       retlw      b'00111100'
358       retlw      b'00111011'
359       retlw      b'00111010'
360       retlw      b'00111001'
```

```
        retlw      b'00111001'
        retlw      b'00111000'
        retlw      b'00110110'
        retlw      b'00110101'
        retlw      b'00110100'
        retlw      b'00110011'
        retlw      b'00110010'
        retlw      b'00110000'
        retlw      b'00101111'
        retlw      b'00101110'
        retlw      b'00101100'
        retlw      b'00101011'
        retlw      b'00101001'
        retlw      b'00100111'
        retlw      b'00100110'
        retlw      b'00100100'
        retlw      b'00100010'
        retlw      b'00100000'
        retlw      b'00011111'
        retlw      b'00011101'
        retlw      b'00011011'
        retlw      b'00011001'
        retlw      b'00010111'
        retlw      b'00010101'
        retlw      b'00010011'
        retlw      b'00010001'
        retlw      b'00001110'
        retlw      b'00001100'
        retlw      b'00001010'
        retlw      b'00001000'
        retlw      b'00000101'
        retlw      b'00000011'
        retlw      b'00000001'
        retlw      b'11111110'
        retlw      b'11111100'
        retlw      b'11111010'
        retlw      b'11110111'
        retlw      b'11110101'
        retlw      b'11110010'
        retlw      b'11110000'
        retlw      b'11101110'
        retlw      b'11101011'
        retlw      b'11101001'
        retlw      b'11100110'
        retlw      b'11100100'
        retlw      b'11100001'
        retlw      b'11011111'
        retlw      b'11011100'
        retlw      b'11011001'
        retlw      b'11010111'
        retlw      b'11010100'
        retlw      b'11010010'
        retlw      b'11001111'
        retlw      b'11001101'
        retlw      b'11001010'
        retlw      b'11001000'
        retlw      b'11000110'
        retlw      b'11000011'
        retlw      b'11000001'
        retlw      b'10111110'
        retlw      b'10111100'
        retlw      b'10111010'
        retlw      b'10110111'
        retlw      b'10110101'
        retlw      b'10110011'
        retlw      b'10110000'
        retlw      b'10101110'
        retlw      b'10101100'
        retlw      b'10101010'
        retlw      b'10100111'
        retlw      b'10100101'
        retlw      b'10100011'
        retlw      b'10100001'
        retlw      b'10011111'
        retlw      b'10011101'
        retlw      b'10011011'
        retlw      b'10011001'
        retlw      b'10011000'
        retlw      b'10010110'
        retlw      b'10010100'
        retlw      b'10010010'
        retlw      b'10010001'
        retlw      b'10001111'
        retlw      b'10001101'
        retlw      b'10001100'
        retlw      b'10001010'
        retlw      b'10001001'
        retlw      b'10001000'
        retlw      b'10000110'
        retlw      b'10000101'
```

```
        retlw      b'10000100'
        retlw      b'10000011'
        retlw      b'10000010'
        retlw      b'10000000'
        retlw      b'01111111'
        retlw      b'01111111'
        retlw      b'01111110'
        retlw      b'01111101'
        retlw      b'01111100'
        retlw      b'01111011'
        retlw      b'01111011'
        retlw      b'01111010'
        retlw      b'01111010'
        retlw      b'01111001'
        retlw      b'01111001'
        retlw      b'01111001'
        retlw      b'01111000'
        retlw      b'01111000'
        retlw      b'01111000'
        retlw      b'01111000'
        retlw      b'01111000'
        retlw      b'01111000'
        retlw      b'01111000'
        retlw      b'01111000'
        retlw      b'01111001'
        retlw      b'01111001'
        retlw      b'01111001'
        retlw      b'01111010'
        retlw      b'01111010'
        retlw      b'01111011'
        retlw      b'01111011'
        retlw      b'01111100'
        retlw      b'01111101'
        retlw      b'01111110'
        retlw      b'01111111'
        retlw      b'01111111'
        retlw      b'10000000'
        retlw      b'10000010'
        retlw      b'10000011'
        retlw      b'10000100'
        retlw      b'10000101'
        retlw      b'10000110'
        retlw      b'10001000'
        retlw      b'10001001'
        retlw      b'10001010'
        retlw      b'10001100'
        retlw      b'10001101'
        retlw      b'10001111'
        retlw      b'10010001'
        retlw      b'10010010'
        retlw      b'10010100'
        retlw      b'10010110'
        retlw      b'10011000'
        retlw      b'10011001'
        retlw      b'10011011'
        retlw      b'10011101'
        retlw      b'10011111'
        retlw      b'10100001'
        retlw      b'10100011'
        retlw      b'10100101'
        retlw      b'10100111'
        retlw      b'10101010'
        retlw      b'10101100'
        retlw      b'10101110'
        retlw      b'10110000'
        retlw      b'10110011'
        retlw      b'10110101'
        retlw      b'10110111'
        retlw      b'10111010'
        retlw      b'10111100'
        retlw      b'10111110'
        retlw      b'11000001'
        retlw      b'11000011'
        retlw      b'11000110'
        retlw      b'11001000'
        retlw      b'11001010'
        retlw      b'11001101'
        retlw      b'11001111'
        retlw      b'11010010'
        retlw      b'11010100'
        retlw      b'11010111'
        retlw      b'11011001'
        ; Start Upper Byte Signal Data
        retlw      b'00000101'
        retlw      b'00000101'
        retlw      b'00000101'
        retlw      b'00000101'
        retlw      b'00000101'
        retlw      b'00000101'
        retlw      b'00000101'
```

```
        retlw   b'00000101'
        retlw   b'00000101'
        retlw   b'00000101'
        retlw   b'00000101'
        retlw   b'00000101'
        retlw   b'00000101'
        retlw   b'00000101'
        retlw   b'00000101'
        retlw   b'00000110'
        retlw   b'00000110'
        retlw   b'00000110'
        retlw   b'00000110'
        retlw   b'00000110'
        retlw   b'00000110'
        retlw   b'00000110'
        retlw   b'00000110'
        retlw   b'00000110'
        retlw   b'00000110'
        retlw   b'00000110'
        retlw   b'00000110'
        retlw   b'00000110'
        retlw   b'00000110'
        retlw   b'00000110'
        retlw   b'00000110'
        retlw   b'00000110'
        retlw   b'00000110'
        retlw   b'00000110'
        retlw   b'00000110'
        retlw   b'00000110'
        retlw   b'00000110'
        retlw   b'00000110'
        retlw   b'00000110'
        retlw   b'00000110'
        retlw   b'00000110'
        retlw   b'00000110'
        retlw   b'00000110'
        retlw   b'00000110'
        retlw   b'00000110'
        retlw   b'00000110'
        retlw   b'00000110'
        retlw   b'00000110'
        retlw   b'00000110'
        retlw   b'00000110'
        retlw   b'00000110'
        retlw   b'00000110'
        retlw   b'00000110'
        retlw   b'00000110'
        retlw   b'00000110'
        retlw   b'00000110'
        retlw   b'00000110'
        retlw   b'00000110'
        retlw   b'00000110'
        retlw   b'00000110'
        retlw   b'00000110'
        retlw   b'00000110'
        retlw   b'00000110'
        retlw   b'00000110'
        retlw   b'00000110'
        retlw   b'00000110'
        retlw   b'00000110'
        retlw   b'00000110'
        retlw   b'00000110'
        retlw   b'00000110'
        retlw   b'00000110'
        retlw   b'00000110'
        retlw   b'00000110'
        retlw   b'00000110'
        retlw   b'00000110'
        retlw   b'00000110'
        retlw   b'00000110'
        retlw   b'00000110'
        retlw   b'00000110'
        retlw   b'00000110'
        retlw   b'00000110'
        retlw   b'00000110'
        retlw   b'00000110'
        retlw   b'00000110'
        retlw   b'00000110'
        retlw   b'00000110'
        retlw   b'00000110'
        retlw   b'00000110'
        retlw   b'00000110'
        retlw   b'00000110'
        retlw   b'00000110'
        retlw   b'00000110'
        retlw   b'00000110'
        retlw   b'00000110'
        retlw   b'00000110'
        retlw   b'00000110'
        retlw   b'00000110'
```

```
631         retlw      b'00000110'
632         retlw      b'00000110'
633         retlw      b'00000110'
634         retlw      b'00000110'
635         retlw      b'00000110'
636         retlw      b'00000110'
637         retlw      b'00000110'
638         retlw      b'00000110'
639         retlw      b'00000110'
640         retlw      b'00000110'
641         retlw      b'00000110'
642         retlw      b'00000110'
643         retlw      b'00000110'
644         retlw      b'00000110'
645         retlw      b'00000101'
646         retlw      b'00000101'
647         retlw      b'00000101'
648         retlw      b'00000101'
649         retlw      b'00000101'
650         retlw      b'00000101'
651         retlw      b'00000101'
652         retlw      b'00000101'
653         retlw      b'00000101'
654         retlw      b'00000101'
655         retlw      b'00000101'
656         retlw      b'00000101'
657         retlw      b'00000101'
658         retlw      b'00000101'
659         retlw      b'00000101'
660         retlw      b'00000101'
661         retlw      b'00000101'
662         retlw      b'00000101'
663         retlw      b'00000101'
664         retlw      b'00000101'
665         retlw      b'00000101'
666         retlw      b'00000101'
667         retlw      b'00000101'
668         retlw      b'00000101'
669         retlw      b'00000101'
670         retlw      b'00000101'
671         retlw      b'00000101'
672         retlw      b'00000101'
673         retlw      b'00000101'
674         retlw      b'00000101'
675         retlw      b'00000101'
676         retlw      b'00000101'
677         retlw      b'00000101'
678         retlw      b'00000101'
679         retlw      b'00000101'
680         retlw      b'00000101'
681         retlw      b'00000101'
682         retlw      b'00000101'
683         retlw      b'00000101'
684         retlw      b'00000101'
685         retlw      b'00000101'
686         retlw      b'00000101'
687         retlw      b'00000101'
688         retlw      b'00000101'
689         retlw      b'00000101'
690         retlw      b'00000101'
691         retlw      b'00000101'
692         retlw      b'00000101'
693         retlw      b'00000101'
694         retlw      b'00000101'
695         retlw      b'00000101'
696         retlw      b'00000101'
697         retlw      b'00000101'
698         retlw      b'00000101'
699         retlw      b'00000101'
700         retlw      b'00000101'
701         retlw      b'00000101'
702         retlw      b'00000101'
703         retlw      b'00000101'
704         retlw      b'00000101'
705         retlw      b'00000101'
706         retlw      b'00000101'
707         retlw      b'00000101'
708         retlw      b'00000101'
709         retlw      b'00000101'
710         retlw      b'00000101'
711         retlw      b'00000101'
712         retlw      b'00000101'
713         retlw      b'00000101'
714         retlw      b'00000101'
715         retlw      b'00000101'
716         retlw      b'00000101'
717         retlw      b'00000101'
718         retlw      b'00000101'
719         retlw      b'00000101'
720         retlw      b'00000101'
```

```
        retlw   b'00000101'
        retlw   b'00000101'
        retlw   b'00000101'
        retlw   b'00000101'
        retlw   b'00000101'
        retlw   b'00000101'
        retlw   b'00000101'
        retlw   b'00000101'
        retlw   b'00000101'
        retlw   b'00000101'
        retlw   b'00000101'
        retlw   b'00000101'
        retlw   b'00000101'
        retlw   b'00000101'
        retlw   b'00000101'
        retlw   b'00000101'
        retlw   b'00000101'
        retlw   b'00000101'
        retlw   b'00000101'
        retlw   b'00000101'
        retlw   b'00000101'
        retlw   b'00000101'
        retlw   b'00000101'
        retlw   b'00000101'
        retlw   b'00000101'
        retlw   b'00000101'
        retlw   b'00000101'
        retlw   b'00000101'
        retlw   b'00000101'
        retlw   b'00000101'
        retlw   b'00000101'
        retlw   b'00000101'
        retlw   b'00000101'
        retlw   b'00000101'
        retlw   b'00000101'
        retlw   b'00000101'
        retlw   b'00000101'
        retlw   b'00000101'
        retlw   b'00000101'
        retlw   b'00000101'
        retlw   b'00000101'
        retlw   b'00000101'
        retlw   b'00000101'
        retlw   b'00000101'
        retlw   b'00000101'
        retlw   b'00000101'
        retlw   b'00000101'
        retlw   b'00000101'
        retlw   b'00000101'
        retlw   b'00000101'
        retlw   b'00000101'
        retlw   b'00000101'
        retlw   b'00000101'
        retlw   b'00000101'
        retlw   b'00000101'
        retlw   b'00000101'
        retlw   b'00000101'
        retlw   b'00000101'
        retlw   b'00000101'
        retlw   b'00000101'
        retlw   b'00000101'
        retlw   b'00000101'
        retlw   b'00000101'

;THE
                END

```

This is the program installed on the PIC12F629 for creating the high speed PWM servo control signal. It is written in assembly. Pages 1-3 are the main program and initialization. Pages 4-9 are the look up table used to store the pulse widths for one full actuator cycle. Each pulse width data point is stored in two bytes. The corresponding lower and upper byte is read to determine the duration of each pulse for the generated PWM signal.

E.2 Servo Controller Schematics

Presented here is the high speed servo controller schematics. It is simply a single PIC12F629 microcontroller with 20 MHz oscillator. The 6 pin PROGRAM/POWER header is for supplying the PIC power during operation and attaching a PICkit programmer/debugger for programing the PIC with the desired servo waveform. SERVO-HEADER is a 3 pin header for connecting with the servo control signal communication line.

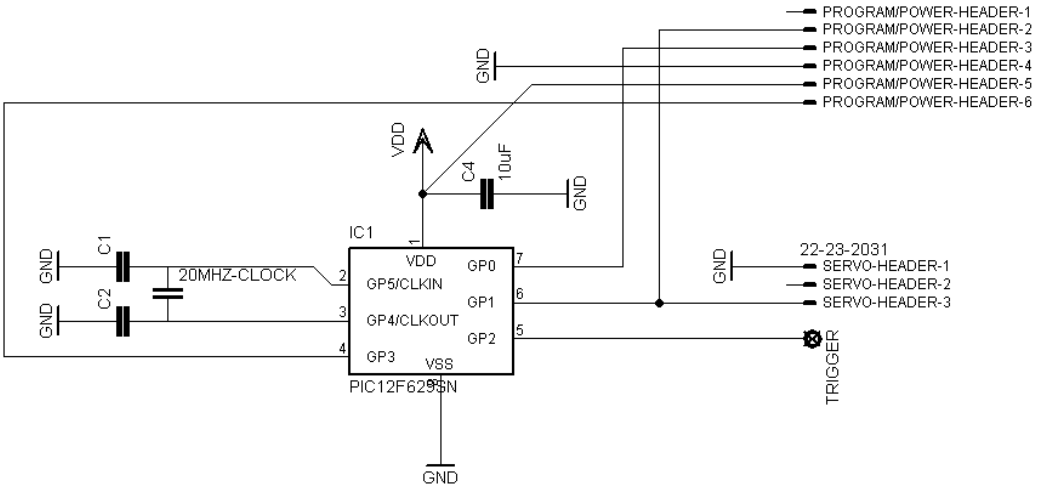

Appendix F

Potentiometer Reader

The pot reader is used for quickly checking the output of each actuator before an experiment. It is needed because there is a large amount of common-mode noise present on the servo potentiometers. Using a dual package, INA2126 instrumentation amplifier from Burr-Brown, the common-mode noise in cancelled to give a clean signal. The servo potentiometer signal ranges between 0.5–1.5 V during operation. With a voltage gain of 5, the instrumentation amplifier output ranges between 1–15 V. A dual package LM358 Operational amplifier is used to subtract 5 volts (I could have chosen a better offset voltage like 8 volts) from the INA2126 output signal. This shifts the potentiometer signal voltage range to −4–10 V. This is done so the potentiometer signals fall within the useful input voltage of the NI USB-6229 DAQ used for digital conversion of −10–10 volts. A ±15 volt split power supply is required to power the Pot Reader.

There is also a separate Servo Power Supply Buffer circuit displayed in the schematics. This is included here as it was printed on the same circuit board as the pot reader as can be seen in figure 7.7 on page 36. This circuit splits the power supplied between two adjacent servos and includes a 2200 μF capacitor to help smooth the supplied power.

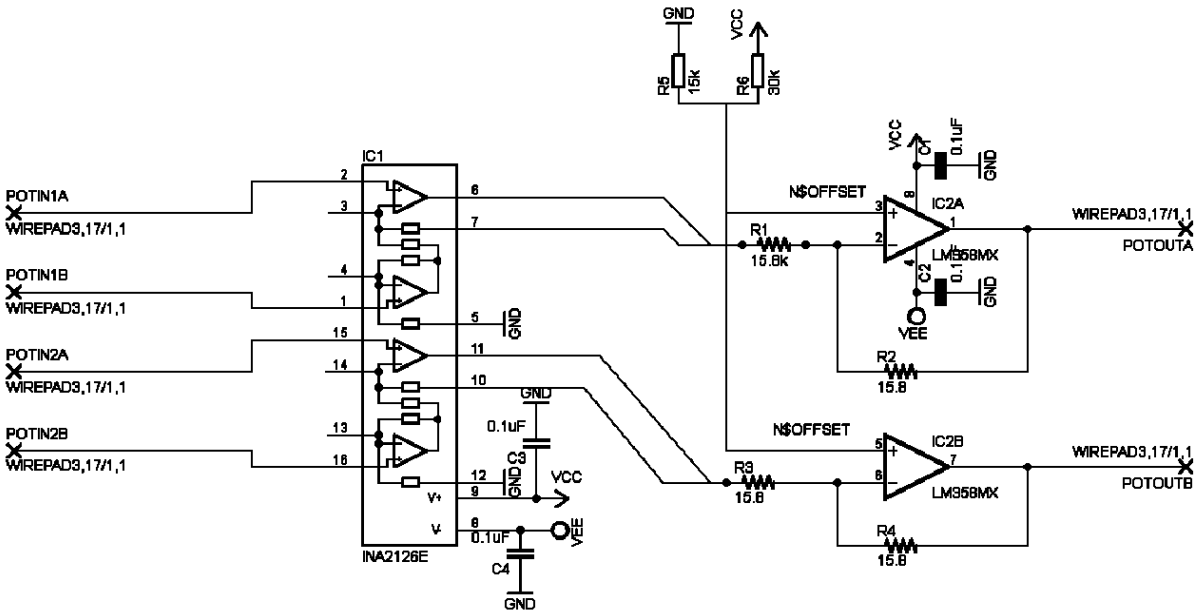

Servo Power with 2200 μF buffer capacitor

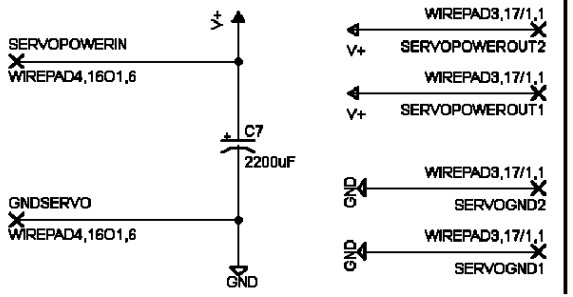

PotReader Power ($\pm$ 15 V)

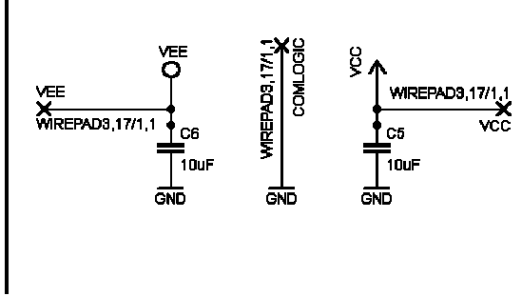

Appendix G

Experimental Data

G.1 Large Amplitude Spanwise Invariant Forcing

Table G.1 presents a summary of the reattachment length verses forcing Strouhal number experiment as well as the unforced experiment. Both experimental conditions and results are given. Figure 14.1 on page 94 gives a plot of this data. The % DownstreamxxXX X_r/h column shows the calculated spanwise and time-averaged reattachment length using the % downstream method from the MATLAB code, TuftImpProApp. 100 images were used for each measurement. The Visually Observed X_r/h column presents the reattachment length based on visual inspection by the author. This is intended as a reference to pick out any obvious error with the calculated reattachment lengths.

Table G.2 presents a summary of the reattachment length verses forcing amplitude experiment. Both experimental conditions and results are given. Figure 14.6 on page 99 gives a plot of this data. The % Downstream X_r/h column shows the calculated spanwise and time-averaged reattachment length using the % downstream method from the MATLAB code, TuftImpProApp. 100 images were used for each measurement. The Visually Observed X_r/h column presents the reattachment length based on visual inspection by the author. This is intended as a reference to pick out any obvious error with the calculated reattachment lengths.

Table G.1: *Reattachment length verses perturbation Strouhal number experimental data*

Pump RPM	U_∞ **[cm/s]**	**Water Temperature [C°]**	Re_h	u'/U_∞	**Calibrated Forcing Amplitude [μs]**	f **[Hz]**	St_h	**Visually Observed** X_r/h	**% Downstream** X_r/h
65.8	45	24	2.45×10^4	Unforced	0	n/a	n/a	5.0	4.95
65.8	45	24	2.45×10^4	0.1	39	0.5	0.06	5.0	4.89
					20	1.0	0.12	4.8	4.88
					14	1.5	0.18	4.8	4.86
					11	2.0	0.24	4.8	4.76
					9	2.5	0.29	4.6	4.55
					9	3.0	0.35	4.4	4.26
					7	3.5	0.41	4.4	4.23
					7	4.0	0.47	4.2	4.24
65.8	45	24	2.45×10^4	0.2	79	0.5	0.06	4.8	4.89
					40	1.0	0.12	4.8	4.84
					28	1.5	0.18	4.8	4.72
					23	2.0	0.24	4.6	4.46
					19	2.5	0.29	4.2	4.09
					17	3.0	0.35	4.0	3.98
					15	3.5	0.41	4.0	3.96
					14	4.0	0.47	4.2	4.24
65.8	45	24	2.45×10^4	0.35	158	0.5	0.06	4.8	4.88
					72	1.0	0.12	4.8	4.80
					50	1.5	0.18	4.6	4.55
					39	2.0	0.24	4.2	4.07
					32	2.5	0.29	4.0	3.90
					28	3.0	0.35	3.8	3.84
					26	3.5	0.41	4.0	3.98
					25	4.0	0.47	4.3	4.21
65.8	45	24	2.45×10^4	1.08	488	0.5	0.06	4.8	4.76
					244	1.0	0.12	4.3	4.24
					163	1.5	0.18	4.0	4.02
					121	2.0	0.24	3.8	3.82
					94	2.5	0.29	3.8	3.71
					83	3.0	0.35	3.8	3.73
					75	3.5	0.41	3.8	3.79
					72	4.0	0.47	4.0	3.88

Table G.2: *Reattachment Length Verses Excitation Amplitude experimental data*

Pump RPM	U_∞ [cm/s]	**Water Temperature** [C°]	Re_h	St_h	u'/U_∞	**Calibrated Forcing Amplitude** [μs]	**Visually Observed** X_r/h	**% Downstream** X_r/h
65.8	45	24	2.45×10^4	0.29	0.1	9	4.6	4.55
					0.2	19	4.0	4.09
					0.35	32	4.0	3.90
					0.4	35	4.0	3.86
					0.45	40	4.0	3.92
					0.5	44	4.0	3.98
					0.55	48	4.0	4.09
					0.6	52	4.2	4.26
					0.65	56	4.2	4.28
					0.7	60	4.2	4.26
					0.8	69	4.0	4.02
					1.08	94	3.8	3.71
					1.5	131	3.6	3.44
					2.0	180	3.4	3.35
65.8	45	24	2.45×10^4	0.41	0.1	7	4.0	4.23
					0.2	15	3.0	3.96
					0.3	22	4.0	3.94
					0.35	26	4.0	3.98
					0.4	29	4.0	4.11
					0.45	31	4.2	4.28
					0.5	36	4.6	4.61
					0.55	38	4.6	4.65
					0.6	42	4.4	4.42
					0.8	56	4.0	3.96
					1.08	75	3.8	3.79
					1.5	105	3.6	3.56
					2.0	144	3.5	3.42

Appendix H

Separating Boundary Layer Calculations

H.1 Calculation of Contraction Geometry

The geometry of the contraction was approximated using two cubic splines for the purpose of calculating the speed up of the flow through the contraction. The contraction has a narrowing, rectangular cross-sectional area and apposing sides of the contraction have identical profiles.

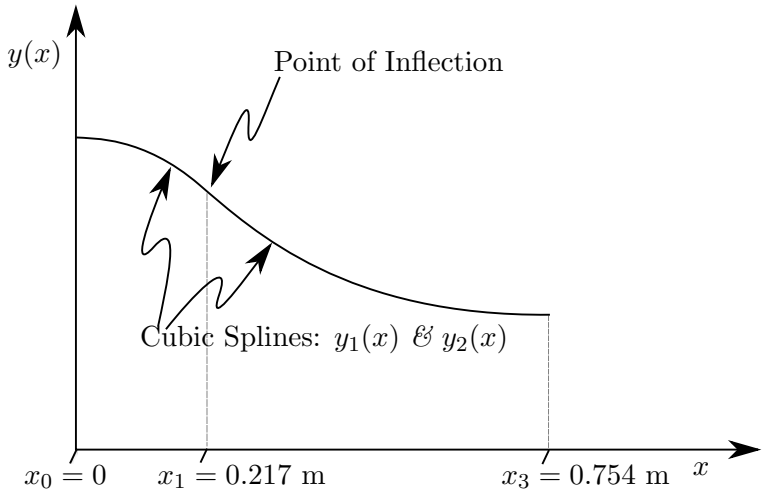

Two cubic splines were used:

$$y(x) = \begin{cases} y_1 = ax^3 + bx^2 + cx + d & : 0 \leq x \leq 0.217 \\ y_2 = ex^3 + fx^2 + gx + h & : 0.217 \leq x \leq 0.754 \end{cases}$$

The step-side and step-side apposing walls have the following values at the points $x_0,\ x_1,\ \&\ x_2$:

$$\begin{aligned} y_1(0) &= 0.455 \\ y_1(0.217) = y_2(0.217) &= 0.382 \\ y_2(0.754) &= 0.229 \end{aligned} \quad \& \quad \begin{aligned} \dot{y_1}(0) &= 0 \\ \dot{y_1}(0.217) = \dot{y_2}(0.217) &= -0.828 \\ \dot{y_2}(0.754) &= 0 \end{aligned}$$

The two end walls (adjacent to step-side wall) have the following values at the points $x_0,\ x_1,\ \&\ x_2$:

$$\begin{aligned} y_1(0) &= 0.305 \\ y_1(0.217) = y_2(0.217) &= 0.248 \\ y_2(0.754) &= 0.127 \end{aligned} \quad \& \quad \begin{aligned} \dot{y_1}(0) &= 0 \\ \dot{y_1}(0.217) = \dot{y_2}(0.217) &= -0.652 \\ \dot{y_2}(0.754) &= 0 \end{aligned}$$

Using these values, the following equation coefficients (a *to* h) can be solved for:
Step-Side Wall:
for coefficients a *to* d:

$$\left[\begin{array}{cccc|c} x_2^3 & x_2^2 & x_2 & 1 & 0.382 \\ 3x_2^2 & 2x_2 & 1 & 0 & -0.828 \\ 3x_1^2 & 2x_1 & 1 & 0 & 0 \\ x_1^3 & x_1^2 & x_1 & 1 & 0.455 \end{array}\right] \Rightarrow \left[\begin{array}{cccc|c} 0.0102 & 0.047 & 0.217 & 1 & 0.382 \\ 0.141 & 0.434 & 1 & 0 & -0.828 \\ 0 & 0 & 1 & 0 & 0 \\ 0 & 0 & 0 & 1 & 0.455 \end{array}\right]$$

and coefficients e *to* h:

$$\left[\begin{array}{cccc|c} x_2^3 & x_2^2 & x_2 & 1 & 0.382 \\ 3x_2^2 & 2x_2 & 1 & 0 & -0.828 \\ 3x_3^2 & 2x_3 & 1 & 0 & 0 \\ x_3^3 & x_3^2 & x_3 & 1 & 0.229 \end{array}\right] \Rightarrow \left[\begin{array}{cccc|c} 0.0102 & 0.047 & 0.217 & 1 & 0.382 \\ 0.141 & 0.434 & 1 & 0 & -0.828 \\ 1.71 & 1.51 & 1 & 0 & 0 \\ 0.429 & 0.569 & 0.754 & 1 & 0.229 \end{array}\right]$$

The solved matrices yield:

$$\begin{bmatrix} a \\ b \\ c \\ d \end{bmatrix} = \begin{bmatrix} -3.2956 \\ -0.8351 \\ 0 \\ 0.455 \end{bmatrix} \& \begin{bmatrix} e \\ f \\ g \\ h \end{bmatrix} = \begin{bmatrix} -0.8953 \\ 2.0749 \\ -1.602 \\ 0.6411 \end{bmatrix}$$

Similarly for the end wall profiles, the corresponding cubic spline coefficients are,
End Walls:

$$\begin{bmatrix} a \\ b \\ c \\ d \end{bmatrix} = \begin{bmatrix} -2.594 \\ -0.6582 \\ 0 \\ 0.305 \end{bmatrix} \& \begin{bmatrix} e \\ f \\ g \\ h \end{bmatrix} = \begin{bmatrix} -0.7050 \\ 1.6341 \\ -1.267 \\ 0.4515 \end{bmatrix}$$

H.2 Calculation of Tunnel Contraction Velocity Profile

Using the contraction profiles, acceleration of the flow as a function of x can be calculated. Using conservation of mass we have the following piecewise velocity profile:

FOR: $0 \leq x \leq 0.217$ m

where : $v_\circ \equiv$ the free-stream velocity before the contraction

$A_\circ \equiv$ the cross-sectional area of the water tunnel before the contraction

$$v_1(x) = \frac{v_\circ A_\circ}{A_1(x)}$$

$$v_1(x) = \frac{v_\circ}{62.83x^6 + 31.87x^5 + 4.040x^4 - 16.06x^3 - 4.073x^2 + 1}$$

FOR: $0.217 \leq x \leq 0.754$ m

$$v_2(x) = \frac{Cv_\circ A_\circ}{A_1(x)}$$

$$v_2(x) = \frac{Cv_\circ}{2.180x^6 - 10.107x^5 + 19.52x^4 - 21.05x^3 + 13.84x^2 - 5.293x + 1}$$

And

$$v_1(0.217) = v_2(0.217)$$

$$1.4817v_\circ = \frac{Cv_\circ}{0.3266} \Rightarrow C = 0.4839$$

The complete velocity profile for $0 \leq x \leq 0.754$ can be seen in figure 11.2 on page 59.

H.3 Falkner-Skan Solution

The following Falkner-Skan boundary layer equations were solved using a developed MATLAB code (section H.3.1). Figure H.1 shows the results for various powers of n.

$$f'''(\eta) + \frac{n+1}{2} f(\eta) f''(\eta) - n f'(\eta)^2 + n = 0$$
$$f(0) = 0,\ f'(0) = 0,\ f'(\infty) = 1$$

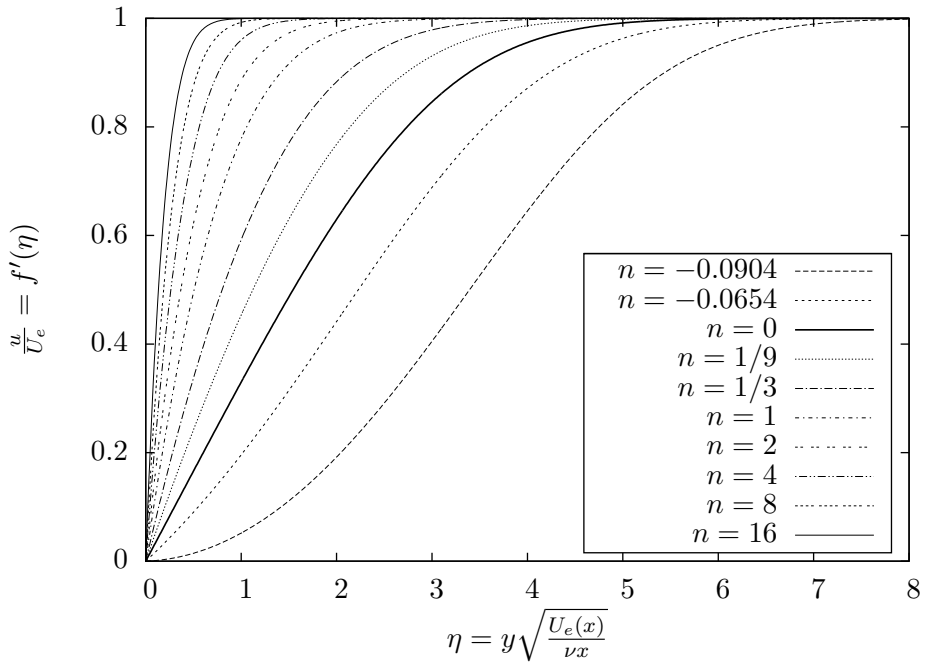

Figure H.1: *Falkner-Skan boundary layer velocity profiles.* $U_e(x) = ax^n$*, where a is constant.*

H.3.1 MATLAB Code

MATLAB comes equipped with a suite of initial value problem solvers. They compute the solution for a system of coupled first order ODEs. In order to use these solvers in solving the Falkner-Skan (FS) third order boundary value problem, the FS problem had to be transformed into a system of first order ODEs, and the boundary values transformed into initial values.

Transforming the third order ODE into a set of first order ODEs was straight forward. First the ODE is rewritten so that the highest derivative is on the left hand side alone. Then the lower order derivatives are replaced with new functions, defined as subsequent derivatives of the original function. For our case, the third order ODE was reduced as follows:

$$f'''(\eta) + \frac{n+1}{2} f(\eta) f''(\eta) - n f'(\eta)^2 + n = 0$$

$$\downarrow$$

$$f'''(\eta) = n f'^2 - \frac{n+1}{2} f(\eta) f''(\eta) - n$$

$$\Downarrow$$

$$y_1' = y_2$$
$$y_2' = y_3$$
$$y_3' = n(y_2^2 - 1) - \frac{n+1}{2} y_1 y_3$$

Where $y_1 = f$, $y_2 = f'$, and $y_3 = f''$.

The original problem's boundary values are:

$$f(0) = 0,\ f'(0) = 0,\ f'(\infty) = 1$$

The first two are already suitable as initial conditions. They become:

$$y_1(0) = 0,\ y_2(0) = 0$$

In deciding how to transform the remaining boundary value at infinity to an initial condition, it was realized that for the solution to converge to 1 at infinity, there is a unique slope of the function at zero. Thus if this slope was known, it could replace the condition at infinity with an initial condition:

$$f'(\infty) = 1 \Rrightarrow f''(0) = \mathcal{U}niqueConstant$$

This new initial condition becomes the initial condition needed for y_3:

$$y_3(0) = \mathcal{U}niqueConstant$$

The unique slope constant was calculated using an iterative process; an initial guess was chosen based on an ad hoc empirical relation. The solution of the equations using this guess for initial condition would then be calculated. Based on the result, the slope constant was adjusted to give a closer convergence to 1 at the maximum domain value.

With the solution converged to 1 at the maximum domain, the solution could be integrated to give constants for calculating displacement, and momentum thickness. A brief description of how the solution was integrated will be given.

Displacement thickness is defined as:

$$\delta^*(x) = \int_0^\infty \left(1 - \frac{u(y,x)}{U}\right) dy.$$

Since,

$$\lim_{y \to \infty} \frac{u(x,y)}{U} = 1$$

converges quickly, choosing an upper limit $y < \infty$ at which $\frac{u}{U}$ is sufficiently close to 1 will be an adequate integration limit:

$$\delta^*(x) = \int_0^\infty \left(1 - \frac{u(y,x)}{U}\right) dy \cong \int_0^y \left(1 - \frac{u(y,x)}{U}\right) dy.$$

Now we need to represent this integral in terms of the none dimensional variable eta, η, used in the Falkner-Skan solution. Eta is defined as:

$$\eta = \frac{y}{x}\sqrt{Re_x} = y\sqrt{\frac{U_{FS}(x)}{\nu x}} = y\sqrt{\frac{ax^{n-1}}{\nu}}$$

where $U_{FS}(x) = ax^n$ is the Falkner-Skan boundary layer external velocity and a is a constant. Rearranging and taking the derivative with respect to y we get:

$$dy = \frac{\partial y}{\partial \eta}d\eta + \frac{\partial y}{\partial x}dx = \sqrt{\frac{\nu x}{U(x)}}d\eta.$$

The second term, $(\frac{\partial y}{\partial x})$, is zero since y and x are independent variables. (It is important to remember that the definition of η does not provide a relation of y to x.)

According to the FS equations, the function $\frac{u}{U}$ is equal to $f'(\eta)$. Knowing this we can now redefine the displacement thickness integral:

$$\delta^*(x) \cong \int_0^y \left(1 - \frac{u(y,x)}{U}\right) dy = \sqrt{\frac{\nu x}{U(x)}} \int_0^\eta \left(1 - f'(\eta)\right) d\eta$$

This is valid if the limit of integration, η is chosen such that:

$$f'(\eta) \cong 1$$

The integral $\int_0^\eta (1 - f'(\eta))\, d\eta$ is performed by the MATLAB code and yields a constant, $\mathcal{C}_{\delta^*}$. This constant is then used to calculate the displacement thickness at any given location x within the region where the FS solution is valid. (Where the boundary layer becomes self-similar.)

$$\boldsymbol{\delta^* \cong \mathcal{C}_{\delta^*}\sqrt{\frac{\nu x}{U(x)}}}$$

The momentum thickness is calculated in a similar fashion.

```
function Solution=FalknerSkanSolutionNextGen(m,initDomain)
%-------------------------------------------------------------------------
% Created by Marc Schostek November 2011
% email: mschostek@gmail.com
%
% Calculate the solution of Falkner-Skan equation. The two input arguments
% and calculted solution are described below. FalknerSkanSolution should be
% run first only using the m argument. Defining initDomain is only
% necessary if the solution is unstable.
%
% m:
% m is power of the velocity profile of the boundary layer external flow
%       U_e = a*x^m; a is a constant
%
% initDomain:
% initDomain is the size of the initial eta domain over which to calculate
% the initial solution. The convergence of the solution is highly dependent
% on proper selection of an initial domain. The initial domain to be
% used for calculating the solution will be automatically selected if
% initDomain arrgument is not used. For most cases this provides a good
% solution. However, if the solution is difficult to find, initDomain can
% be defined by the user.
%
% Solution:
% The output solution contains the following in the the corresponding order:
% X and Y coordinates from the Falkner-Skan boundary layer profile
% Boundary layer thickness coefficient (for u/U=0.99)
% Displacement thickness coefficient
% Momentum thickness coefficient
% slope at the wall (du/dy). Useful for calculating the wall shear drag


%% DefineNested Functions
%the reduced first-order set of ODE equations
    function dydx=falknerskan(t,y)

        %reduced firt order ODE equations representing Falkner-Skan ODE
        dydx =[y(2)
               y(3)
               m*(y(2)^2-1)-(m+1)/2*y(1)*y(3)];

    end
%% initialization

if nargin == 0
    error('Error: need alteast one input arg. See help FalknerSkanSolution')
elseif nargin == 1 %determine the initial eta domain size for calculating solution.
    if  -0.091 <= m && m <= -0.03
            initDomain = 50;
    elseif -0.03 < m && m <= 1
            initDomain = 3;
    elseif 1 < m && m <= 2
            initDomain = 2;
    elseif 2 < m && m <= 5
            initDomain = 1;
    elseif 5 < m && m <= 8
            initDomain = 0.7;
    elseif  8 < m && m <= 18;
            initDomain = 0.3;
    elseif 18 < m
            initDomain = 0.1;
    else
            error('Error: m value not accepted or need to select initial Domain size manually. See help ↙
FalknerSkanSolution')
    end
end

step = 2;
```

```
maxEta = initDomain + (10*step);
Domain = initDomain;
res = 100;
%% Begin Convergence
tic %start stop watch
%Calculate initail Solution from initial condition
Slope = m^(.465)+0.3321; % an adhoc initial guess of the slope (based on experience with this equation)
initCond=[0 0 Slope];
[eta,Y]=ode113(@falknerskan,[0 initDomain],initCond);


%initial convergence of anwer at eta=initDomain+1
%  If initial guess of initSlope too high, first while loop will
%  run through else the second while loop.
while Y(end,2) >= 1
    Slope = Slope - 1e-2;
    initCond = [0 0 Slope];
    [eta,Y]=ode113(@falknerskan,[0 initDomain+1],initCond);
end
while Y(end,2) <= 1
    Slope = Slope + 1e-2;
    initCond = [0 0 Slope];
    [eta,Y]=ode113(@falknerskan,[0 initDomain+1],initCond);
end
disp('done 1st level of convergence');
%% Next level of super convergence
waslow = 0;
SlopeA = Slope;

% Stepping through Domain to larger eta increases stability and improves
% convergence apposed to solving for the largest Domain only.
while Domain < maxEta
    Domain = Domain + step;
    inc = 100000*eps(SlopeA);
    if Domain < maxEta
        convCond = 10000*eps(SlopeA);
    else
        convCond = eps(SlopeA);
    end

    while inc > convCond
        [eta,Y]=ode113(@falknerskan,[0 Domain],initCond);
        holdEta = eta;
        holdY = Y;
        YA = Y(end,2);
        SlopeB = SlopeA - inc;
        initCond = [0 0 SlopeB];
        [eta,Y]=ode113(@falknerskan,[0 Domain],initCond);
        YB = Y(end,2);
        %fprintf('Yb = %.16f\n',Yb);

        if YA == YB
            break
        end

        if YB < 1 % test if we over shot our desired value 1 and reset
            inc = inc/10;
            eta = holdEta;
            Y = holdY;
            waslow = 1;
        else
            if ~waslow
                %calculate the reduction factor, reduc.
                %Then calculate new increment value, inc, which would have
                %reuduced the difference of Ya-1 by approx 1/6. I found that if
                %you try to use a faster convergence (1/2), the convergence
                %slows down as it oversoots and Yb has to climb up above 1
                %before the fast convergence can continue. 1/6 is still an
```

```
137             %aggressive convergence factor.
138             reduc = (YA-YB)/(YA-1);
139             if reduc <=0
140                 reduc=1;
141             end
142              inc = inc/(6*reduc);
143             %set new Slope to continue with convergence
144             SlopeA = SlopeB;
145         else
146             waslow = 0;
147             SlopeA = SlopeB;
148              inc = 0.9*inc;
149         end
150       end
151    end
152     fprintf('Done convergence at Domain = %.5g \n',Domain);
153 end
154 Slope = SlopeA;
155
156 %% Convergence Done! Now calculate a more refined solution
157
158 sol = ode113(@falknerskan,[0 maxEta],initCond);
159 etaSpace = linspace(0,maxEta,res*maxEta)';
160 Y = deval(sol,etaSpace)';
161
162 %Determine first location of Y(:,2) which has larger value than 1;
163 %ind will be upper bound for integration of boundary layer thickness as
164 %integrating past this point will not be valuable to the accuracy of the
165 %result.
166 lsthanone = zeros(maxEta*res);
167 for i = (1:maxEta*res)
168     lsthanone(i) = Y(i,2) > 1;
169 end
170 ind = find(lsthanone,1,'first');
171 ind = ind-1;
172
173 %incase there were no values in the solution greater than one, use maximum
174 %in solution as upper integration limit.
175 if isempty(ind)
176     [uVal,ind] = max(Y(:,2));
177 else
178     uVal = Y(ind,2);
179 end
180
181
182 %find eta value at which u/U=0.99
183 findDelta99 = zeros(maxEta*res);
184 for i = (1:maxEta*res)
185     findDelta99(i) = (Y(i,2) > 0.99)*Y(i,2);
186 end
187 delta99 = find(findDelta99,1,'first');
188 delta99 = delta99/res;
189
190 %calculate displacement and momentum thickness
191 deltaStar = trapz(etaSpace(1:ind),1.-Y(1:ind,2));
192 momentum = trapz(etaSpace(1:ind),Y(1:ind,2).*(1.-Y(1:ind,2)));
193
194 %print results
195 elapsedTime = toc/60;
196 fprintf('   Execution time: %.5g minutes\n',elapsedTime);
197 fprintf('   u/U(%.3g) = %.16g\n\n',ind/res,uVal);
198 fprintf('\nFalkner-Skan Solution for m=%.3g:\n',m);
199 fprintf('        u/U = 0.99 thickness = %.5g\n',delta99);
200 fprintf('      Displacement thickness = %.5g\n',deltaStar);
201 fprintf('          Momentum thickness = %.5g\n',momentum);
202 fprintf('              du/d(eta)@wall = %.5g\n\n',Slope);
203
204
205 %plot Calculated profile
```

```
206 hold on
207 asymp= linspace(0,ind/res,maxEta*res);
208 plot(asymp,1,'k−')
209 plot(etaSpace(1:ind),Y(1:ind,2),'b')
210 title(sprintf('Falkner−Skan Solution for m= %.2g',m))
211
212
213 %output Solution
214 Solution = {etaSpace(1:ind) Y(1:ind,2) delta99 deltaStar momentum Slope};
215
216 end
```

Appendix I

Phase Averaging

This section will describe the method of phase-averaging as it will be used in discussion within some sections of this thesis. This is meant to be a quick introduction on the topic.

Hussain and Reynolds (1970) proposed a method of three-level decomposition of the instantaneous flow velocity for analyzing turbulent flows with an associated oscillatory motion (organized wave) of known frequency. The decomposition of the velocity vector u is as follows:

$$u(\mathbf{x},t) = \bar{u}(\mathbf{x}) + \tilde{u}(\mathbf{x},t) + u'(\mathbf{x},t), \tag{I.1}$$

where $\bar{u}$ is the time-mean, $\tilde{u}$ is the contribution from the organized oscillatory wave in the flow, and u' is the random turbulence. Figure I.1 on the next page gives visualization of these quantities relative to a turbulent velocity signal. The time-mean is given by equation I.2:

$$\bar{u}(\mathbf{x}) = \lim_{T\to\infty} \frac{1}{T} \int_0^T u(\mathbf{x},t)dt; \tag{I.2}$$

and the *phase average* is defined by equation I.3:

$$\langle u(\mathbf{x},t)\rangle = \lim_{N\to\infty} \frac{1}{N} \sum_{n=0}^{N} u(\mathbf{x},t+n\tau), \tag{I.3}$$

where τ is the period of the introduced perturbation as described in figure I.1. This phase average is thus the average at any point in space, $\mathbf{x}$, realized at a prescribed phase, ϕ, of the introduced perturbation. The organized component $\tilde{u}$ is then found by subtracting the time average from the phase average:

$$\tilde{u}(\mathbf{x},t) = \langle u(\mathbf{x},t)\rangle - \bar{u}(\mathbf{x}), \tag{I.4}$$

and then $u'(\mathbf{x},t)$ follows from equation I.1. Hence, by appropriate signal analysis, the three velocity components can be determined.

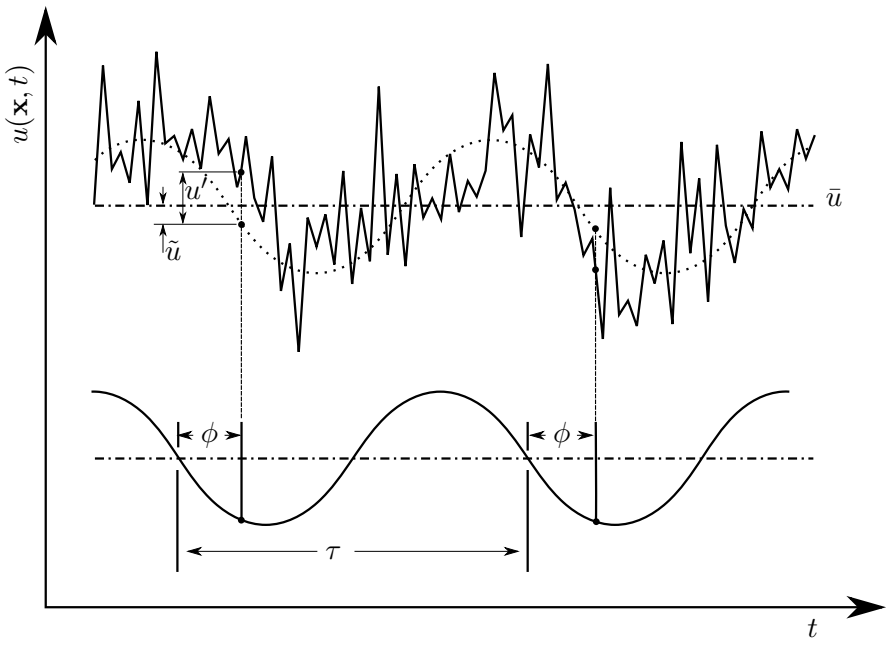

Figure I.1: *depicts procedure for obtaining time and phase averages of a random velocity signal (upper curve) with a weak organized wave of same frequency of introduced perturbation at phase ϕ of the introduced perturbation (lower curve)*